UNIVERSITY OF SOUTHAMPTON

EFFECT OF RADIO-FREQUENCY ELECTROMAGNETIC FIELDS ON NERVOUS TISSUE.

Jacqueline Kim Deans

Doctor of Philosophy

Division of Clinical Neurosciences

June 2003

This thesis was submitted for examination in June 2003.
It does not necessarily represent the final form of the thesis as deposited in the University after examination.

DECLARATION

I, Jacqueline Kim Deans, declare that I am the sole author of this thesis.
The work presented here is original work, completed by me during the period of registration as a postgraduate student candidate. The only exception to the above statement relates to Luxtron temperature measurements in chapter 3 which were completed by my supervisor, Dr J.E.H. Tattersall. Unless stated to the contrary, I have consulted all the references cited in this report.

JACQUELINE K DEANS

June 2003

UNIVERSITY OF SOUTHAMPTON

ABSTRACT

FACULTY OF MEDICINE HEALTH AND BIOLOGICAL SCIENCE

DIVISION of CLINICAL NEUROSCIENCES

Doctor of Philosophy

EFFECTS OF RADIO-FREQUENCY ELECTROMAGNETIC FIELDS ON NERVOUS TISSUE.

by

Jacqueline Kim Deans

Current safety guidelines are based on well-established thermal effects of radiofrequency radiation (RF). The presence of non-thermal biological effects could undermine the basis of these standards, particularly for pulses with high peak fields but low average power.

This work has confirmed previous observations that exposure to low intensity RF fields can affect simple evoked responses in brain tissue slices *in vitro*. The effects were seen at specific absorption rates (SAR) up to 4.4mW.kg^{-1} and were therefore not associated with heating.

Direct dosimetric measurement of the SAR within a brain tissue slice was not quantifiable by micro-thermocouple probe, due to perturbation of the E-field by the metal thermocouple. Non-perturbing temperature probe and thermal imaging camera measurements could not discern any measurable temperature rise during RF exposure due to inadequate resolution.

Studies of physiological mechanisms suggested that RF exposure reduced the effectiveness of inhibitory mechanisms in the brain tissue, whilst having little effect on the excitability of nerve cells. The reduction in inhibition showed no signs of recovery up to 15 minutes after the end of the exposure period.

Pharmacological experiments indicated that NMDA receptors and gap junctions may be involved in the RF-induced effects; suggestions are made for further experiments to help resolve this issue.

RF exposure potentiated the expression of stress-induced heat shock proteins at 41°C in organotypic hippocampal slice cultures. This effect was similar to that previously reported in nematode worms and indicates that similar effects can occur in mammalian brain tissue.

Recommendations are made for further studies to determine the potential significance of these effects of low intensity RF fields for human health.

CONTENTS

LIST OF ILLUSTRATIONS

LIST OF ILLUSTRATIONS (continued).

LIST OF TABLES

ACKNOWLEDGEMENTS

I would like to thank my supervisors, Dr John EH Tattersall and Dr Lars E Sundström for their valued guidance, encouragement and commendable patience. I am deeply indebted to them for their knowledge, input and constructive feedback. It's fair to say that I'd procrastinate for Scotland when it came to writing this work and would've given up long ago without their un-ending support and perseverance.

I express my gratitude to everyone in Clinical Neurological Sciences at Southampton University for making me feel part of their 'family', they supported and encouraged me when I felt disillusioned and were genuinely pleased at my successes. I've made many friendships at Southampton and I'll treasure many happy memories of my time there. In particular, I would like to acknowledge Maureen Gatherer for her help with the 2-D electrophoresis gels, Judy Mepham for assistance with the staining protocols for HSP72 and C-fos immunoreactivity and Geraldine Cole, who could always be counted upon to brighten up my day.

I would also like to thank Nicola Mifsud for help with the CUSUM analysis, Ian, Chris, Patrick and Bob at [Dstl], Porton Down for encouragement and Dr Andrei Pakhomov of Brooks Air Force Base, Texas, USA for assistance in making the micro-thermocouples used in this study.

Finally, I would like to thank my family for their love and support; to my daughter Rachael for her understanding at being up-rooted from the home and friends she loved in Scotland, and to my father Duncan Deans, for always being there when I needed someone to talk to and for believing in me.

I dedicate this work to the memory of my mother Kathleen Deans, who died before I started University. My mum would be immensely proud of the daughter who was told at primary school that she was 'not smart enough to pass an O'level exam'. She taught me to persevere and to never give up, and for that I am eternally grateful.

As a final footnote I would just like to say, 'Well John, I finally managed to eat the whole damn elephant'.

ABBREVIATIONS

μ	Micro (10^{-6})
λ	Wavelength
°C	Degrees Celsius
μm	Micrometer (10^{-6} meters)
μV	Micro Volts (10^{-6} Volts)
4-AP	4-amino pyridine
A	Ampere
$A.m^{-1}$	Amperes per meter
ACh	Acetylcholine
AChE	Acetylcholinesterase
ACPD	1-aminocyclopentane-1,3-dicarboxylic acid
ACSF	Artificial cerebrospinal fluid
AMPA	α-amino-3-hydroxy-5-methyl-4-isoxazolepropionate
AP3	α-amino-3-phosophonopropionate
AP5	α-amino-5-phosphonovalerate
AP7	2-amino-7-phosphonoheptanoic acid
ATP	Adenosine tri phosphate
c	Speed of light ($3x10^{8}$ $m.s^{-1}$)
C	Tissue specific heat (J/kg/°C)
CA	Cornu ammonis
CA1	Cornu ammonis area 1
CA3	Cornu ammonis area 3
Carbenoxolone	3β-Hydroxy-11-oxoolean-12-en-30-oic acid 3-hemisuccinate
CB	Citizens band
CDMA	Code-division multiple access
CGS 19755	Selfotel
CNQX	6-cyano-7-nitroquinoxaline-2,3-dione
CPP	3-(2-carboxypirizin-4-yl)-propyl-1-phosphonic acid
CTA	Conditioned taste aversion
CW	Continuous wave
Cx	Connexin
DAB	Diaminobenzidine tetrachloride
dB	Decibel
D-APV	2-amino-5-phosphonovaleric acid
DECT	Digital enhanced cordless telecommunications
DG	Dentate gyrus
DMSO	Dimethyl sulfoxide
dT	Change in temperature (°C)
dt	Change in time (seconds)
E	Electric field strength
EC	Entorhinal cortex
E-field	Electric field
EHPP	Extremely high peak power
E_m	Resting membrane potential
EMF	Electromagnetic field
EPSP	Excitatory postsynaptic potential
E-S ratio	EPSP - PS ratio
f	Frequency
ff	Fimbria fornix
FDD	Frequency division duplex

FDTD	Finite difference time domain
fEPSP	Field excitatory postsynaptic potential
g	gram
GABA	γ-Amino butyric acid
GABA-T	GABA-transaminase
GAD	Glutamic acid decarboxylase
GHz	Giga Hertz (10^9 Hertz)
GSM	Global standard for mobile communications
H	Magnetic field strength
HBSS	Hank's balanced salt solution
H-field	Magnetic field
HFS	High-frequency stimulation
HSE	Heat shock element
HSF	Heat shock factor
HSP	Heat shock protein
Hz	Hertz
kHz	kilo Hertz (10^3 Hertz)
MHz	Mega Hertz (10^6 Hertz)
GABA	γ-amino butyric acid
GHz	Giga Hertz (10^9 Hertz)
I/O	Input divided by output
ICNIRP	International Commission on Non-Ionising Radiation Protection
IEG	Immediate early genes
IEGMP	Independent Experts Group on Mobile Phones
IPI	Inter-pulse interval
IPSP	Inhibitory postsynaptic potential
ISI	Inter-stimulus interval
J	Joule (Newton's per meter)
KA	Kainic acid
kg	kilogram (10^3 grams)
kHz	kilo Hertz (10^3 Hertz)
kW	kilo Watt (10^3 Watts)
l	Litre
LFS	Low-frequency stimulation
LTD	Long-term depression
LTP	Long-term potentiation
m	milli (10^{-3})
M	Mega (10^6)
mf	Mossy fibre
MΩ	Mega Ohms (10^6 Ohms)
$m.s^{-1}$	metres per second
MCPG	α-Methly-4-carboxyphenylglycine
MEM	Minimum essential medium
mGluR	Metabotropic glutamate receptor
MHz	Mega Hertz (10^6 Hertz)
min	minute
MK801	5R,10S)-(+)-5-Methyl-10,11-dihydro-5H-dibenzo[a,d]cyclohepten-5,10-imine hydrogen maleate
mM	millimolar (10^{-3} Moles)
mm	millimeter
MPE	Maximum permitted exposure
mT	Milli Tesia (10^{-3} Tesla)

MTC	Micro thermocouple
mW	milli Watt (10^{-3} Watts)
MW	Mega Watt (10^{9} Watts)
NBQX	2,3-Dihydro-6-nitro-7-sulphamoyl-benzoquinoxaline
Nifedipine	1,4-Dihydro-2,6-dimethyl-4-2(2-nitrophenyl)-3,5-pyridinedicarboxylic acid dimethyl ester
NMDA	N-Methyl-d-aspartate
NMDAR	N-Methyl-d-aspartate receptor
NRPB	National Radiological Protection Board
p	Pico (10^{-9})
P	Input power (Watts)
PBS	Phosphate buffered saline
PFA	Para formaldehyde
pp	Perforant path
PPF	Paired-pulse facilitation
PPI	Paired-pulse inhibition
PS	Population spike
PSA	Population spike amplitude
PTX	Picrotoxin
RADAR	Radio Detecting And Ranging
RAM	Radiation absorbent material
RF	Radiofrequency
RFR	Radiofrequency radiation
RO	Reverse osmosis
s	Second
S	Subiculum
s.c.	Schaffer collaterals
S.D.	Standard deviation
S.E.	Standard error
SAR	Specific absorption rate
SLM	Stratum lacunosum-moleculare
SMA	Sub-miniature coaxial connector, type A
SO	Stratum oriens
SP	Stratum pyramidale
SR	Stratum radiatum
SRC	Stimulus response curve
T	Tesla
T/C	Test response divided by conditioning response
TACS	Total access communications system
TBS	Tris buffered saline
TD-CDMA	Time division – Code-division multiple access
TDMA	Time division multiple access
TEM	Transverse electromagnetic
TETRA	Terrestrial trunked radio
UMTS	Universal Mobile Telecommunication Service
UWB	Ultra-wide band
V	Volts
$V.m^{-1}$	Volts per meter
VDU	Visual display unit
VSWR	Voltage standing wave ratio
VDCC	Voltage-dependent calcium channel
W	Watt

W-CDMA	Wideband -Code division multiple access
$W.kg^{-1}$	Watts per kilogram
WAP	Wireless application protocol
$W.cm^{-2}$	Watts per centimetre^2
$W.m^{-2}$	Watts per metre^2

1 GENERAL INTRODUCTION

Electromagnetic radiation consists of a series of waves of energy composed of oscillating electric (E) and magnetic (H) fields orientated perpendicular to each other and which travel through space at the speed of light. (Figure 1.1) Taken together, all forms of electromagnetic energy are collectively referred to as the electromagnetic spectrum. Radiofrequency radiation (RFR) is a form of non-ionising electromagnetic energy in the frequency range 30kHz to 300GHz in the electromagnetic spectrum (Figure 1.2).

Figure 1.1 Image from Federal Communications Commission (www.fcc.gov).

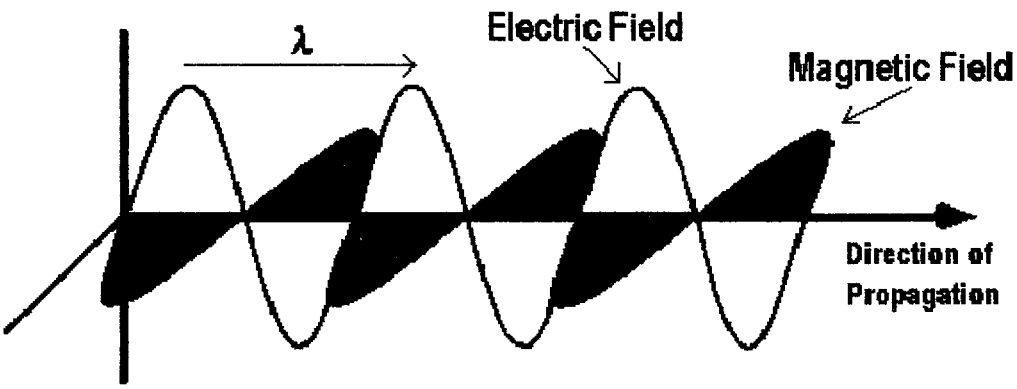

The frequency of electromagnetic (EM) wave propagation (*f*) relates to the number of complete cycles of an EM wave in one second (units hertz (Hz)) and is related to wavelength (λ) by the simple formula $f = c/\lambda$ where c is the speed of light ($3x10^8$ m/s).

One of the most important uses for RF energy is in the telecommunications industry. Radio and television broadcasting, mobile telephones, pagers, cordless telephones, radio communications for the emergency services, amateur radio and satellite communications are some of the many applications of RF energy. Non-communications uses include heating and sealing apparatus, wireless burglar alarms, car door openers and laser pens. Microwave ovens use RF energy to cook food by transfer of energy to water and fat molecules in the food. RF radiation is also used in medical applications for example, diathermy and electro-surgery and military applications including radar and telemetry.

Figure 1.2. The electromagnetic spectrum.

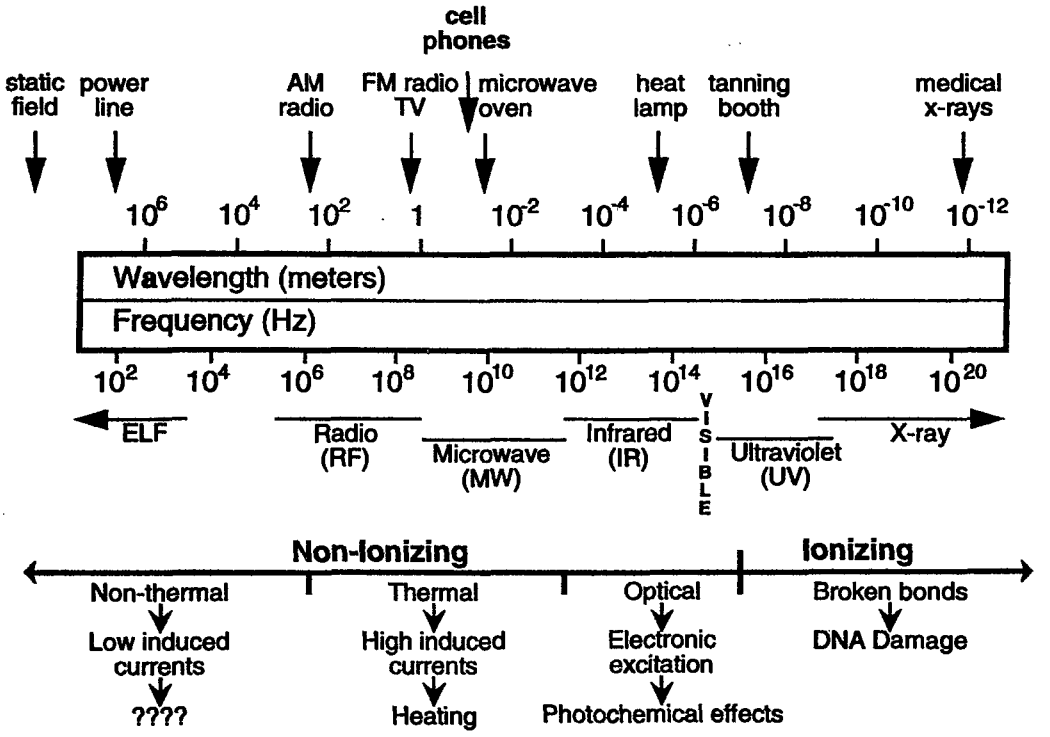

From www.aph.gov.au/senate/committee/ecita_ctte/Emr/contents.htm

1.1 Current Safety Guidelines.

The current safety guidelines on exposure to radiofrequency radiation differ from country to country. In the UK, the National Radiological Protection Board (NRPB) determined national guidelines for the safe exposure to RFR (NRPB, 1993). These guidelines have been superseded by those of International Commission on Non-Ionising Radiation Protection (ICNIRP). The ICNIRP guidelines (ICNIRP, 1998) are similar to those established by NRPB in 1993 but include a five-fold reduction in specific absorption rate limits for exposure of the public to RF fields (Table 1.1).

Safety standards make use of a quantity called the specific absorption rate (SAR) to determine the maximum safe exposure to RF fields. SAR is defined as: the amount of energy absorbed by an object (per unit time per unit mass) exposed to a radiofrequency electromagnetic field (units of SAR = $W.kg^{-1}$).

Biological effects resulting from heating of tissue by RF energy are referred to as thermal effects. Biological effects are dependant on the frequency and intensity of the

field and upon the orientation of the body with respect to the E-field (Durney et al., 1986). As the frequency increases from approximately 100 kHz to 10 MHz the dominant effect of exposure to high-intensity EMF changes from nerve and muscle stimulation to heating (ICNIRP, 1998; Sienkiewicz, 1998). At frequencies from 10MHz to 300 GHz the major effect of RF exposure is heating (ICNIRP, 1998). Exposure to high intensity RF fields (above maximum permitted exposures (MPE)) can result in heating of biological tissue and an increase in body temperature. Body temperature rises of more than 1-2 °C can cause heat exhaustion and heat stroke (ICNIRP, 1998). Tissue damage in humans could occur during exposure to high RF levels because of the body's inability to cope with or dissipate the excessive heat that could be generated.

The two areas of the body particularly vulnerable to RF heating are the eyes (retina and iris) (ICNIRP, 1998; Sienkiewicz, 1998) and the testes (Michaelson, 1991; Sienkiewicz, 1998). The relatively poor blood flow in these areas is thought to be insufficient to dissipate the thermal load caused by RF exposure. It is known that a whole body specific absorption rate of 4 $W.kg^{-1}$ is sufficient to cause thermal heating of body tissues. Consequently, ICNIRP guidelines for the maximum allowable exposure to RF fields have been arbitrarily set at a specific absorption rate of $0.4W.kg^{-1}$ for whole body exposure, giving a safety factor of times 10 (see table 1.1). At SAR rates less than the 0.4 $W.kg^{-1}$ maximum whole body exposure limit, thermal effects are unlikely to occur.

The Independent Experts Group on Mobile Phones (IEGMP, 2000) advised the UK government that in line with its precautionary approach, the ICNIRP (1998) guidelines for public exposure should be adopted for use in the UK rather than the NRPB (1993) guidelines. The IEGMP position is that this would bring the UK 'into line with other countries in the European Union and accord with the Recommendations of the House of Commons Select Committee on Science and Technology Report on Mobile Phones and Health (1999)'.

Table 1.1 *Safety guidelines for exposure to RFR in the frequency range 10MHz to 10GHz.*

Guideline authority	*Body region*	*Average mass (g)*	*Average time (minutes)*	*SAR ($W.kg^{-1}$)*
ICNIRP (1998)	Whole body	n/a	6	0.4 (0.08)
	Head, trunk	10	6	10 (2)
	Limbs	10	6	20 (4)
NRPB (1993)	Whole body	n/a	15	0.4
	Head, foetus	10	6	10
	Neck, trunk	100	6	10
	Limbs	100	6	20

ICNIRP guidelines quote a five-fold lower SAR value for public exposure (brackets) to RF than occupationally exposed workers. Members of the public may be subjected to long-term exposure to RF whereas employees are normally healthy adults, trained to be aware of the potential risks of RF and whose exposure is limited to specific periods under controlled conditions. (NRPB, 1993; ICNIRP, 1998)

Table 1.2

ICNIRP guidelines for exposure to RFR at mobile telecommunications frequencies.

Frequency MHz	*E-field strength ($V.m^{-1}$)*	*H-field strength ($A.m^{-1}$)*	*Power density ($W.m^{-2}$)*
400 – 2000	$1.375 f^{1/2}$	$0.0037 f^{1/2}$	$f / 200$
2000 - 3000	61	0.16	10

The letter *f* is the frequency in MHz. Taken from IEGMP, (2000).

1.2 Radiofrequency radiation and communications.

The current interest in radiofrequency electromagnetic radiation dates back to the pioneering work of Guglielmo Marconi who, in 1895 discovered that it was possible to use electromagnetic radiation to connect transmitting and receiving antennas. In December 1901, Marconi demonstrated that radio waves could be used to transmit information over great distances. A signal, sent from Poldhu, Cornwall was received in Newfoundland, USA a distance of over 3,500 kilometres.

The extensive use of mobile telephones is a recent event; they were first introduced in the UK in the mid 1980's and users slowly but steadily increased into the early 1990's as services expanded (IEGMP, 2000). The number of UK mobile phone users has been growing at a phenomenal rate. In April 2000, the Independent Experts Group on Mobile Phones (IEGMP) reported that there were approximately 25 million phones in circulation (IEGMP, 2000). More recently, a BBC News article in January 2001, estimated that 40 million people in the UK, owned a mobile telephone (http://news.bbc.co.uk/).

Recent advances in technology have meant that mobile phones are routinely used to send and receive text messages; 943 million messages were sent in the UK during May 2001 (http://www.mda-mobiledata.org/). Additionally, wireless application protocol (WAP) phones offer instant access to the Internet. However, the unprecedented increase in mobile telephone numbers has not been achieved without widespread concern about the possibility that exposure to radiofrequency radiation emitted by communications devices could affect the health of susceptible individuals.

1.3 Cellular Communications.

Cellular telephones in the UK operate in the frequency ranges 872-960MHz and 1710-1875MHz. (IEGMP, 2000). There are four main systems using these frequencies, they are:

1.3.1 TACS (analogue).

The Total Access Communication System (TACS) was the first cellular system used in the UK. TACS uses continuous wave (CW) radiofrequency signals at around 900MHz. The nominal power output of analogue phones is 0.63W (IEGMP, 2000). This system uses frequency modulation to deliver its signals to and from the phone. The frequency of the carrier signal is varied by an amount proportional to the size of the modulating signal such that only small changes in the amplitude of the carrier wave occur (Figure 1.3).

Figure 1.3 *Amplitude modulation of a carrier wave.* From IEGMP, (2000)

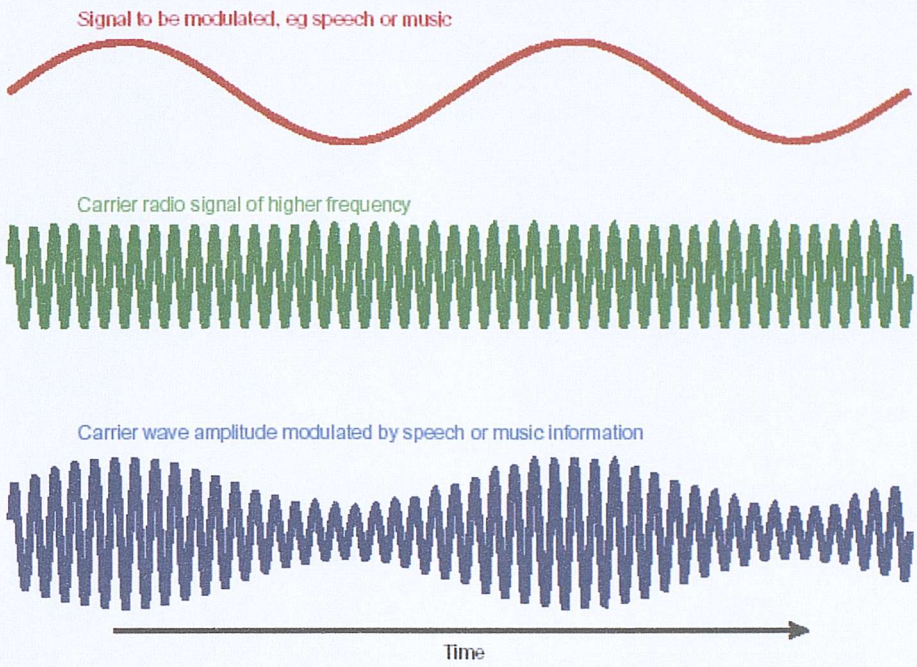

1.3.2 GSM (digital).

The European digital standard for mobile phones is the *Global System for Mobile Communications* or *Groupe Spéciale Mobile* (GSM). This system operates in the frequency ranges 872-960MHz or 1710-1875MHz. (IEGMP, 2000) and uses 217Hz pulse-modulated RF signals. Digital phones use phase modulation to deliver the signals. Phase modulation results in very small changes in the amplitude of the carrier wave as each digit that is transmitted causes a phase change in the carrier wave.

The maximum powers that GSM phones are allowed to transmit according to current standards are 2W for 900MHz bandwidth phones and 1W for phones operating in the 1800MHz bandwidth (IEGMP, 2000). However, the average power transmitted by a GSM phone is at most one-eighth of these values (i.e. 0.25W and 0.125W respectively). The reduction in power is achieved by time division multiple access (TDMA). In essence, TDMA allows each 200 kHz channel to be used by up to eight mobile telephones at one time. TDMA compresses each 4.6ms segment of information to be transmitted into a pulse 0.58ms long so that the phone and base station transmit for 0.58ms every 4.6ms. The GSM system has 548 channels (each of 200kHz) at each base station. Of these channels, 174 are in the 900MHz bandwidth and 374 are in the 1800MHz band.

1.3.3 DECT (digital).

Modern cordless telephones use the *Digital Enhanced Cordless Telecommunications* (DECT) system for communication at frequencies around 1850MHz (similar to those of the GSM cellular mobile phone system). The DECT system uses ten channels, each of which has a bandwidth of 1.728 MHz. Each channel has 24 time slots within a 10 ms time frame. The transmission within a slot uses a form of frequency modulation so that a particular phone emits a pulse every 10 ms (100 Hz). Since the maximum power emitted is 250 mW, the average power emitted by a DECT phone is approximately 10mW (IEGMP, 2000).

1.3.4 TErrestrial Trunked RAdio (TETRA).

TETRA is a digital system used extensively by the emergency services, military personnel and closed user groups such as utilities providers and security services. In Europe, 380-383 MHz and 390-393MHz bandwidth frequencies have been designated for use by the emergency services. TETRA uses TDMA technology to divide each 25 kHz band into four frequency channels. Each frequency channel is pulsed at 17.6 Hz. (IEGMP, 2000).

1.3.5 UMTS (digital).

The new, so-called third generation (3G) mobile telephones currently under development will encompass broadband multi-media mobile telecommunications technology. UMTS (Universal Mobile Telecommunication Service) or IMT-2000, UMTS was developed mainly for countries with GSM networks. UMTS will be delivered in stages, firstly using FDD (Frequency Division Duplex)(W-CDMA) at frequencies between 1920-1980 and 2110-2170 MHz (5MHz channel spacing, 200kHz raster) and later TDD (Time Division Duplex) (TD/CDMA), 1920-1980 and 2110-2170 MHz (5MHz channel spacing and 200kHz raster) (http://www.umtsworld.com).

1.4 RF applications.

RF radiation is widely used in a variety of applications. After outlining some of these applications, the relevance to the communications industry and the supposed adverse health effects of non-thermal levels of exposure that have been suggested in the literature will be discussed.

Mobile telephone base stations.

Base stations are low power radio relay stations. Antennas are typically mounted on towers or on the roofs of high buildings. The output power of the antenna is dependent upon the type of communications system used by the mobile phones. Global Standard for Mobile communications antennas output less than 40W whilst analogue, Total Access Communication System antennas produce 20W maximum. In the opinion of Gajsek, (2000), the general public should not be exposed to base station main beams nearer than 60 metres radial distance from the antenna. At this distance and in 'worst case conditions' the total E-field strength is 3 $V.m^{-1}$.

Citizens Band (CB) Radio.

CB radio devices operate at the frequencies of 27 and 446 MHz and at typical RF power of 4W. Strong electric fields may occur near to short antennas, E-field of up to 1 kV have been measured 2 centimetres from such a source, in excess of current guidelines. Antennas are mounted several meters above ground, electric field strength has been estimated to be less than 10 $V.m^{-1}$ at a distance of 3 metres from the source.

Television transmitters.

Television reception is achieved with a small number of high power transmitters mounted on very high towers. Because of the height of the tower and the radiation pattern of the antenna, exposure to the main beam only occurs at distances of around 1000m from the tower. At this distance, the E-field strength has been reported to be 5 $V.m^{-1}$ for a 400 kW transmitter (Gajsek, 2000).

RAdio Detecting And Ranging (RADAR).

Radar devices operate over a frequency range from 500 MHz to 15 GHz. Radar produces a narrow beam a few degrees in width, signals are pulsed having very short duty cycles and low average power; however, peak powers may be several orders of magnitude higher than average values. Modification of the signal is produced by rotation or elevation of the antenna and results in a reduction in the likelihood of excessive exposure. The peak power output emitted by a radar antenna is dependant on its use, and distance from the source. For example, measurements made near to a military radar operating at 3 GHz, peak output power 3 MW, found the peak power density of the rotating antenna to be 60 $W.m^{-2}$ at 250 metres distance from the source.

By comparison, air traffic control radar operating at 288 GHz with a peak power output of 70 kW gave the peak power density of a rotating antenna to be 2 $W.m^{-2}$ at 15 metres distance and only 0.03 $W.m^{-2}$ at a distance of 1000 metres (the nearest to which the public have access) (Gajsek, 2000).

Dielectric heating.

Dielectric heaters increase the temperature of electrically non-conducting materials by subjecting the material to high-frequency electromagnetic fields. The method is widely used in industry, for example, heating thermosetting glues, drying foam rubber and pre-heating plastics before moulding. These devices operate in the frequency range 11 to 50 MHz at maximum powers of between 0.5 and 100 kW.

Short wave and microwave diathermy units.

Diathermy is a form of physical therapy in which deep heating of tissues is accomplished by the use of high-frequency electrical current. Depending on the amount of heat generated, diathermy can be used to warm tissue in cancer treatment (short-wave diathermy), for the relief of muscle soreness and sprains or it can be used to prevent excessive bleeding and seal off damaged tissues (microwave diathermy).

Short-wave units operate at 27.12 MHz at powers of up to 400 W. The high intensity exposure is sufficient to cause a sustained increase in tissue temperature in the part of the body exposed to the radiation, hence exposure duration is limited to 20 minutes. Operators standing in front of their diathermy console may encounter 60 $V.m^{-1}$ and/or 0.16 $A.m^{-1}$ fields for some treatment routines. In 'worst case' conditions, exposure limits may be exceeded when the distance between the device and the operator is less than 1.5m. (Gajsek, 2000). Microwave diathermy units operate at the frequencies of 915 Hz, 433 MHz and 2450 MHz. Operators may exceed maximum permitted exposures within 2 metres of the patient (Gajsek, 2000).

Visual display units (VDU).

VDUs emit very low levels of ultraviolet light together with non-ionising radiation in the visible light range. The low levels of RF radiation and extremely low E & H fields emitted by the devices are far below current exposure limits (Gajsek, 2000).

1.5 Thermal and Non-thermal Effects.

While the thermal or heating effects of certain electromagnetic energy levels are accepted as having adverse health effects, the notion that RF fields may produce subtle, non-thermal effects is becoming an increasingly prevalent issue. But what does the term 'non-thermal effect' mean in the context of RFR research? The Royal Society of Canada published a review of the potential health risks of radiofrequency fields (RSC, 1999). They defined thermal and non-thermal effects as follows:

Thermal effect

Thermal effects occur when sufficient RF energy is deposited to cause a measurable increase in the temperature of the sample in question (e.g. more than 0.1°C).

Athermal effect

Those effects occurring when sufficient energy is deposited to nominally cause an increase in the temperature of the sample, but no change in temperature is observed due to endogenous (internal) temperature regulation or exogenous (external) temperature control.

Non-thermal effect

Non-thermal effects occur when the energy deposited in the sample is less than that associated with normal temperature fluctuations of the biological system being studied.

Since exposure to an RF field transfers energy to the exposed object at a rate that is proportional to the exposure level, it is important to know the absolute temperature value and its distribution in the exposed sample. Detailed dosimetry data concerning the exposure conditions (SAR, intensity and orientation of the incident electromagnetic field) should be rigorously measured in electromagnetic field studies. If a biological effect of RFR is detected, dosimetry will confirm whether the effects are thermal in nature. Additionally, RFR effects in animals can be extrapolated to include human beings.

1.6 Effects on the nervous system.

Effects on cell membranes.

Eukaryotic cells are surrounded by a lipid bilayer, embedded with specialised proteins in the form of receptors, ion channels and pumps. Receptors detect extracellular molecules such as hormones or neurotransmitters and trigger changes in the conductivity of associated ion channels. Protein pumps actively transport ions across the membrane, against their concentration gradient using energy derived from adenosine tri-phosphate (ATP). Others proteins act as channels, through which ions can move across the membrane and cause changes in the cells membrane potential and alter excitability in neurones and other electrically excitable cells.

Very little research has been carried out on the effect of RF electromagnetic fields on the cell membrane. Reports indicate that RF fields can affect membrane proteins and the movement of ions across membranes; however, some effects have only been observed at low temperatures or at intensities sufficient to cause thermal heating of tissues. For example, Phillipova *et al.*, (1994) found that the binding of odorant molecules to receptor proteins in rat olfactory receptor neurones was affected by 900 MHz RF radiation at SAR's of 1 and 100 $W.kg^{-1}$. The authors suggested that shedding of the protein from the membrane had occurred because of increased peroxidation of membrane lipids.

Cleary (1990a, b; 1995) reported that the flux of sodium and potassium ions across the cell membrane can be affected by RF exposure in the 27 MHz to 10 GHz frequency range. (see IEGMP, 2000 for review). Although most of these experiments were carried out at very high SAR's (up to 200 $W.kg^{-1}$), the author suggests that Na^+ and K^+ efflux is affected at much lower intensities in the temperature range 17.7 to 25°C, although these effects are unlikely to occur *in vivo*, in humans, since normal body temperature is much higher.

D'Inzeo *et al.*, (1988) used a horn antenna at a carrier frequency of 10.75 GHz CW ($50\mu W.cm^{-2}$ power density) to determine the effect of radiofrequency fields on cultured chick myotubes. Patch clamp recordings of whole-cell and single channel currents activated by acetylcholine (ACh) revealed a decrease in the frequency of channel openings during the microwave exposure. Whole-cell currents recorded in the

presence of acetylcholine decayed faster in RF exposed cells than in control, indicating an increased rate of receptor desensitisation.

In contrast, a study by Tattersall *et al.*, (1999) used a horn antenna at a carrier frequency of 10 GHz, (50 $\mu W.cm^{-2}$ field strength) to attempt to replicate the findings of D'Inzeo *et al.*, (1988) on cultured chick myotubes and also on dissociated mouse muscle fibres. Later experiments used a parallel plate waveguide exposure system (Tattersall *et al.*, 1999) to produce a more even field distribution than the horn antenna. Tattersall *et al.*, (1999) found no significant effect on the opening frequency of ACh-activated channels in cultured chick myotubes in either exposure set-up. Similarly, the opening frequency of acetylcholine-activated channels in dissociated mouse muscle fibres in response to RF exposure was not significantly altered.

Effects on calcium efflux.

Calcium has a vital role in the function of neurones and other cells, being involved in the regulation of many intracellular processes including glial cell function, membrane excitability and synaptic plasticity. Increased $[Ca^{2+}]_i$ has been implicated in a number of toxic processes (Berridge *et al.*, 1998), so unregulated increases in the calcium ion concentration could have deleterious consequences for the cell. Changes in intracellular calcium ion concentration resulting from the firing of neurones can lead to long-term changes (either potentiation or depression) in the strength of synaptic inputs onto the neurons.

Reports of increased calcium efflux in response to RFR exposure have been contradictory. For example, several groups have reported that RFR can induce changes in the efflux of calcium ions from brain tissue. For example, Bawin *et al.*, (1975) measured the efflux of calcium from explants of chick brain. Exposure to 147 MHz fields at low intensity (1-2 $W.m^{-2}$), amplitude modulated at 16 Hz increased the efflux of calcium from the brain. No effects were observed in response to unmodulated RFR. Two studies by Blackman *et al.*, (1979; 1980) exposed chick cerebral hemispheres to 147 MHz RFR amplitude modulated between 3 and 30 Hz. In line with the Bawin *et al.*, (1975) study, they found increases in calcium efflux at a modulation frequency of 16 Hz. However, the increases in efflux were dependant upon a power-density

'window' since calcium efflux was observed at a field intensity of 0.75 $W.m^{-2}$ but not at higher (1, 1.5 or 2 $W.m^{-2}$) or lower (0.5 $W.m^{-2}$) intensities.

In contrast, (Shelton and Merrit, 1981; Meritt *et al.*, 1982) failed to detect any increase in calcium efflux in response to 1 or 2.45 GHz RFR, pulse modulated at either16 or 32 Hz. The authors suggest that direct comparisons could not be made between their results and previous studies because of differences in exposure parameters. A study by Albert *et al.*, (1987) exposed chick cerebral hemispheres to 147 MHz, 16 Hz amplitude modulated RFR at an SAR of 7.5 $W.m^{-2}$, as before, these authors did not find any evidence of increased calcium efflux.

Effects on neuronal excitability.

Neurones communicate with each other using neurotransmitters that are released from vesicles on the presynaptic membrane. The neurotransmitters diffuse across the synaptic cleft between the pre and postsynaptic neurone and bind to specialised receptor proteins on the postsynaptic cell. Since the release of neurotransmitters from the presynaptic neurone is dependant upon the intracellular calcium ion concentration, several groups have examined whether chemical transmission is affected by RFR.

Modak *et al.*, (1981) examined the whole brain content of the neurotransmitter acetylcholine in mice exposed to a single 15 or 25 ms pulse of 2.45 GHz RFR. The RF pulse resulted in a 2-4°C increase in brain temperature and a significant decrease in the ACh content. The authors suggest that the decrease in ACh content may be accounted for by increases in membrane permeability. A series of experiments by Lai *et al.*, (1987; 1989a; 1989b; 1990; 1991, 1994) examined the uptake of choline by nerve cells in rats exposed to pulsed, low intensity 2.45 GHz, 0.3-0.65 $W.kg^{-1}$ SAR RF fields. The authors found an increase in choline uptake and a reduction in the concentration of ACh receptors after 20 minutes exposure, whereas 45 minutes exposure had the opposite effect. These effects were blocked by pre-treatment with the opioid receptor antagonist naltrexone or with corticotrophin-releasing hormone. A later study by Lai *et al.*, (1994) reported that deficits in radial arm maze performance induced by microwave exposure could be prevented by pre-treatment with the anticholinesterase (AChE) inhibitor physostigmine or with naltrexone but not with naloxone methiodide (which cannot cross the blood brain barrier).

Gavin *et al.*, (1981) and Millar *et al.*, (1984) examined the effect of CW and pulsed (16.7 ms pulses at rate of 10-90 Hz) 2.45 GHz, RF fields on purified solutions of AChE. No effects were found. In contrast, Baranski *et al.*, (1972) reported a decrease in AChE activity in guinea pigs exposed to pulsed 3 GHz RF fields however they suggest that this may be due to thermal effects.

Learning and Memory.

Several studies have suggested that RF may interact with brain activity and cognitive processes. Behavioural experiments on animals have been used to investigate the biological basis of memory. For example, Mickley *et al.*, (1994) examined cognitive behaviour in rats exposed for 20 minutes to 600 MHz RF fields at SAR rates of up to 10 $W.kg^{-1}$. Comparison of the time taken in exploration of a new object before and after RF exposure revealed significant deficits in memory in microwave-exposed rats. These changes were correlated with increased expression of the c-*fos* gene in the cortex, but not in the hippocampus, when brain temperature had increased by $\geq 1°C$ above baseline.

Lai *et al.*, (1989a) examined the effect of 20 minutes of low level, pulsed 2.45 GHz RF fields at an average whole body SAR of 0.6 $W.kg^{-1}$ on the learning rate of rats searching for food pellets in a radial-arm maze. The study found that animals exposed immediately before the maze test showed improved learning rates for the first two days of the study than that of the control group although final performance or overall accuracy of the task was not affected. A subsequent study by Lai *et al.*, (1994), exposed rats to pulsed, 2.45 GHz fields (0.6 $W.kg^{-1}$ whole body SAR) for 45 minutes per day. Rats exposed immediately before testing in a 12-arm radial maze made more errors than the control animals. Further work by Wang and Lai (2000) suggested that rats exposed for 60 minutes to pulsed 2.45 GHz RF fields took longer to find a submerged platform in a circular water maze than did the control group. The authors concluded that RF exposure (1.2 $W.kg^{-1}$, SAR) had disrupted spatial reference memory since the exposed animals spent less time swimming in the area of the platform and more time trying to climb up the sidewalls of the maze.

It is possible that stress caused by 'microwave hearing' (an audible popping and hissing sound caused by thermoelastic expansion effects within the soft tissues of the head) may have been responsible for some of the Lai *et al* findings.

Recently, Sienkiewicz *et al.,* (2000) used an eight-arm radial maze to examine the behaviour of mice exposed to 45 minutes per day for 10 days to 900 MHz RF radiation pulsed at 217 Hz at a whole body SAR of 0.05 $W.kg^{-1}$. No significant effect on performance was observed in either choice accuracy or task completion time when compared with non-exposed animals. However, animals tested immediately following exposure took longer to complete the task and were more variable in performance than other groups.

Effects on human brain function and cognition.

A study by Preece *et al.,* (1999) found that radiation emitted by a simulated GSM digital mobile phone (915 MHz, either CW or pulsed at 217 Hz, 12.5% duty cycle) positioned at the left temple resulted in a significant decrease (increase in speed) in choice reaction time in human subjects. The increase in responsiveness was observed in both analogue and digital simulations. The finding was endorsed by Koivisto *et al.,* (2000a,b) who reported the effects of radiation emitted by a 902 MHz, 217 Hz pulse modulated mobile telephone on cognitive function in humans; they found a reduction in simple reaction time and the time needed for mental arithmetic tasks under mobile phone conditions.

More recently, Haarala *et al.*, (2003) performed a replication and extension study of the effect of a 902MHz, 217 pulse modulated mobile telephone (0.25W mean power, 577μs pulse width) in an attempt to replicate their earlier findings (Koivisto *et al.*, 2000a). On this occasion, although the telephone and cognitive tests were similar to their earlier study, the methodology was improved to include a larger sample size, additional tests were performed and the study was of a double blind design. The authors failed to replicate their earlier findings on reaction time (Koivisto *et al.*, 2000a) and concluded that the results from this study showed that GSM telephones do not have an effect on cognitive function. The authors contribute their negative findings on this occasion to better experiment design, particularly the fact that the study was carried out blind, since on the previous occasion the experimenter was aware of the EMF condition. Haarala *et al.*, (2003) report that only 5 studies on cognitive function and mobile telephone EMF are cited in the literature; of these, 4 studies (Koivisto *et al.*, 2000a,b;

Lee *et al.*, 2001; Edelstyn and Oldershaw, 2001) would have been less statistically significant, if authors had used a Bonferroni correction for multiple comparisons in their statistical analysis. The conclusion from this replication study is that the EMF effect is so small that it can be detected on a behavioural level only occasionally.

Effects on the hippocampal slice preparation.

That low frequency electromagnetic fields can affect the excitability of nervous tissue was first shown by Jefferys (1981). DC electric fields of the order of $4V.m^{-1}$ applied to guinea pig hippocampal slices via large current passing electrodes positioned parallel to the somatic-dendritic axis of the pyramidal cells of the dentate gyrus was able to modify the excitability of these neurons. Changes in population spike amplitude were dependant on the polarity of the applied field with respect to neurone orientation. A later series of *in vitro* studies by Bawin *et al.*, (1984; 1986a,b; 1996) looked at the effects of 1-60Hz sinusoidal electric and magnetic fields on excitability in rat hippocampal slices. The studies showed that these fields could produce increases or decreases in the amplitude of evoked population spikes in the CA1 region. Additionally, rhythmic slow activity induced by carbachol was disrupted and potentiation or depression of penicillin-induced epileptiform activity was observed.

To date, the only study to have assessed the effects of radiofrequency electromagnetic fields on neuronal activity in slices of brain tissue was carried out by Tattersall *et al.*, (2001). This study indicates that exposure to 700 MHz, 125mW power CW, RFR could affect the amplitude of the evoked population spike in the CA1 region of the rat hippocampal slice. Transient changes in evoked and spontaneous activity occurred in response to short-term exposure to RF fields in the absence of any detectable increase in temperature.

The aim of the work reported in this thesis was to determine the effects of radiofrequency electromagnetic fields on nervous tissue. The hippocampus, a part of the limbic system in the brain, has been implicated in spatial learning in animals and in the laying down of episodic memories in people (Morris and Frey, 1997). According to the Independent Experts Group on Mobile Phones, "the hippocampal slice preparation shows great potential for the study of RF field affects" (IEGMP, 2000). Consequently, the rat hippocampal slice preparation was used as a model to examine the effects of RF

radiation on neuronal brain activity *in vitro* in the current study. The hippocampus is a particularly suitable preparation for studies of neuronal activity as it is an accepted tool for investigations into the cellular mechanisms underlying learning and memory.

1.7 Anatomy of the hippocampus.

The hippocampus is a C-shaped structure situated within the limbic system of the temporal lobe of the mammalian brain; its name is derived from the Greek root *hippo* meaning 'horse' and *kampos* meaning 'sea monster' in reference to its sea horse shape when cut into transverse slices.

1.7.1 Structure of the hippocampus.

The hippocampus is composed of four regions; these are the dentate gyrus, the hippocampus proper, the subicular complex and the entorhinal cortex. With the exception of the dentate gyrus, each of the regions can be divided into sub-fields; for the hippocampus proper these are Cornu Ammonis (CA) areas 1, 2 and 3, usually abbreviated to CA1, CA2 and CA3 (Lorenté de Nó, 1934). The sub-fields of the subicular cortex are known as the subiculum, presubiculum and parasubiculum. The last region, the entorhinal cortex is usually divided into lateral and medial subdivisions. The subicular and entorhinal complexes are sometimes jointly referred to as the parahippocampal region.

The hippocampal cortex was divided into a series of layers or strata by Ramon y Cajal (1893) these layers are the alveus, stratum oriens, stratum pyramidale, stratum radiatum, stratum lucidum, stratum lacunosum, and stratum moleculare (Figure 1.4). In the rodent hippocampus, the stratum lacunosum and the stratum moleculare are not well defined; accordingly, this layer is known as the stratum lacunosum-moleculare. Ramon y Cajal (1911) suggested that the hippocampus is divided into two distinct regions called the *regio inferior* and the *regio superior*. The *regio inferior* corresponds to CA1 and CA2 and the *regio superior* to CA3 as outlined by Lorenté de Nó, (1934).

1.7.2 Principal neurones of the hippocampus and dentate gyrus.

The principal neurons in the hippocampus proper are called pyramidal neurons; these cell bodies (20 to 40μm in diameter at the base and 40 to 60 μm in height) are

arranged in an organized layer 3-6 cells deep called the pyramidal cell layer (Johnston and Amaral, 1998).

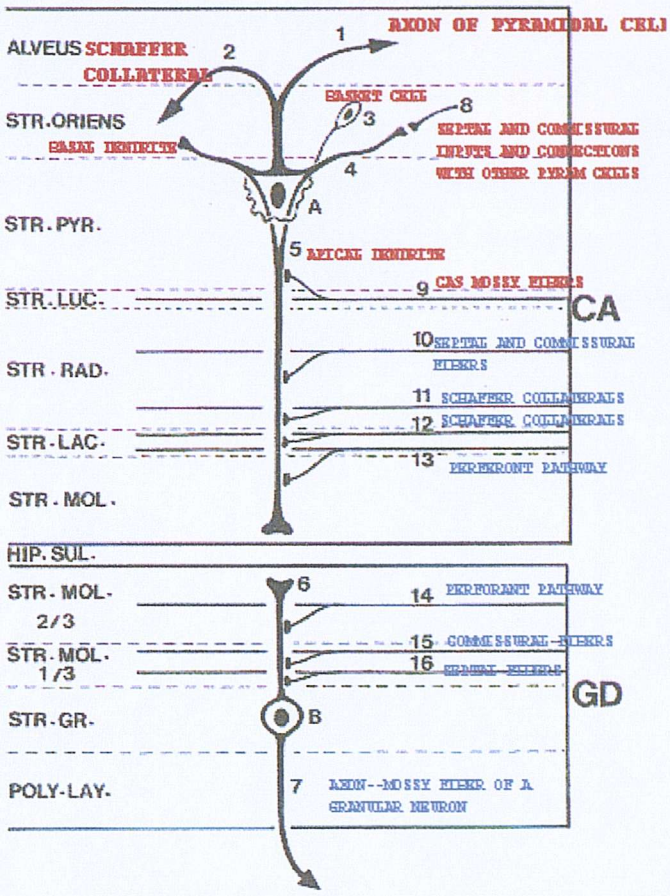

Figure 1.4 *Hippocampal cell layers.*

(From: http://muskingum.edu/~biology/hippocp/anatomy/cagd.htm)

Pyramidal cells are triangular in appearance and are positioned with the apex of the cell body orientated towards the centre of the hippocampus (Labelled 'A' in Figure 1.4). Long dendrites extend from the apex of the cell body towards the dentate gyrus perpendicular to the pyramidal cell layer; shorter basal dendrites extend from the base of the cell body to the stratum oriens. In the dentate gyrus, the principal neurons are called granule cells. These cells have small spherically shaped cell bodies about 10μm in diameter arranged in a layer 4 to 6 cells thick called the granule cell layer (Johnston and Amaral, 1998). Granule cells are monopolar; dendrites extend from the apical part of the cell body towards the molecular layer.

1.7.3 The trisynaptic pathway

The basic connections of the hippocampus were determined in the classic Golgi studies of Ramon y Cajal (1893) and Lorenté de Nó (1934) and the degeneration studies

of Blackstad (1956; 1958), Raisman *et al.,* (1965) and Blackstad *et al.,* (1970). However, the term 'trisynaptic pathway', was not defined until Andersen *et al.*, (1971) described the general basis of hippocampal connectivity from their study of the rabbit hippocampus. Andersen *et al.*, (1971) observed that there was a unique unidirectional progression of excitatory pathways orientated transversely to the longitudinal axis, with each of the four hippocampal regions being activated in turn in response to a stimulus delivered to the entorhinal cortex. An impulse evoked in the perforant path of the entorhinal cortex first activates the granule cells of the dentate gyrus. Mossy fibres projecting from the granule cells synapse with pyramidal cells in the CA3 region of the hippocampus proper.

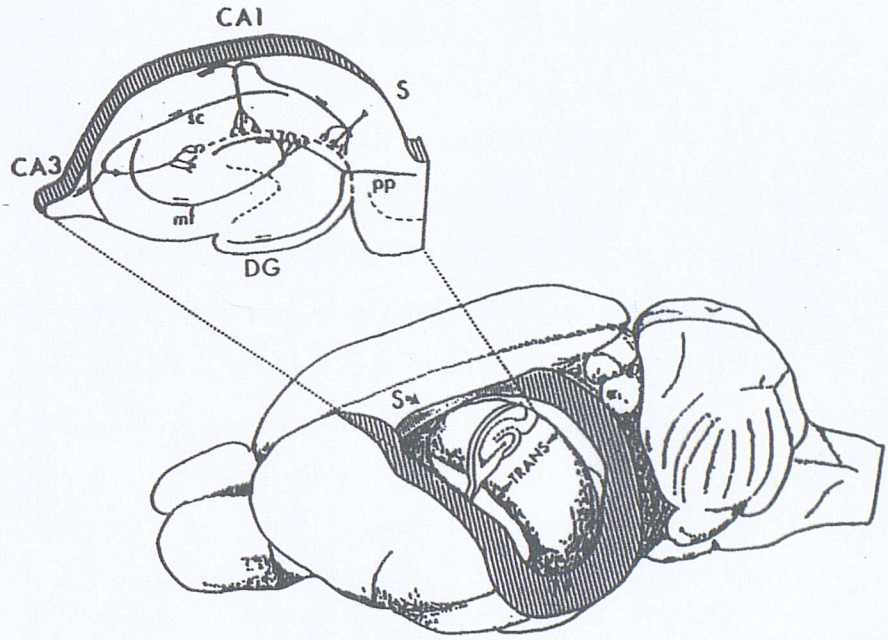

Figure 1.5 *Three-dimensional position of the hippocampus.*

Line drawing of the rat brain showing the position and orientation of the hippocampus. The expanded transverse cross section shows the hippocampal formation and the dentate gyrus. The long axis of the hippocampus is referred to as the septotemporal axis; the short axis is called the transverse axis. Abbreviations; pp, perforant path; mf, mossy fibres; sc; Schaffer collateral; DG, dentate gyrus; S; septal; T; temporal. From Amaral and Witter, (1989).

The CA3 field gives rise to axons that travel out to the fimbria and form commissural projections that synapse onto CA1 pyramidal cells on the contralateral hippocampus (Andersen, 1959; Raisman *et al,* 1965). Schaffer collaterals from the CA3 region are sent via the stratum radiatum to synapse with alvear fibres of the CA1 region. Finally, CA1 pyramidal cell axons run from the alveus and join the fimbria, which in turn projects via the subiculum to the entorhinal cortex. Each of the pathways is

orientated in the same direction, roughly transverse to the longitudinal axis of the hippocampus (Andersen *et al.*, 1971). Thus information leaving the entorhinal cortex passes through the entire hippocampal circuit via the excitatory trisynaptic pathway and is returned to the originating area.

1.7.4 Entorhinal cortex

As described earlier, the entorhinal cortex is divided into medial and lateral areas. These areas consist of six divisions labelled I to VI derived from differences in afferent and efferent projections (Lorenté de Nó., 1934; Ramon y Cajal., 1955). The major source of afferent input to the hippocampus is from the entorhinal cortex (Andersen *et al.*, 1971; Lothman *et al.*, 1991). Neurons originating in layer II of the entorhinal cortex give rise to the perforant path. This pathway is so called because it perforates the subiculum and terminates in both the dentate gyrus and the CA3 field of the hippocampus (Johnston and Amaral, 1998). Neurons from layer III of the entorhinal cortex give rise to axons that bifurcate and terminate in the CA1 field of the hippocampus and the subiculum. Fibres from the medial entorhinal cortex give rise to axons that travel along the perforant path and terminate in the middle third of the molecular layer of the dentate gyrus and in the stratum lacunosum-moleculare of CA1 near to the border of CA3 and in the molecular layer of the subiculum (Johnston and Amaral, 1998).

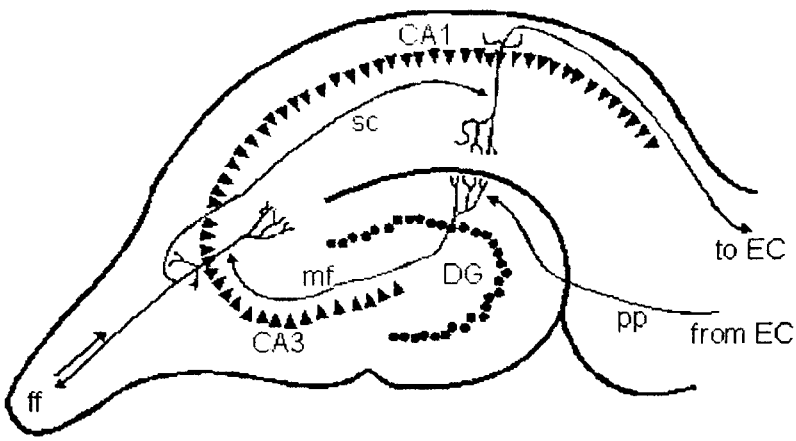

Figure 1.6 *The Trisynaptic Circuit.*

Triangles indicate the pyramidal cell layer (CA1 and CA3) and circles, the granular cell layer of the dentate gyrus. Abbreviations: EC, entorhinal cortex; DG, dentate gyrus; pp, perforant path; mf, mossy fibres; sc, Schaffer collaterals; ff, fimbria fornix. From Burwell *et al.*, (1995).

In contrast, the axons of cells originating in the lateral entorhinal cortex terminate in the outer third of the molecular layer and in that part of the stratum

lacunosum-moleculare that borders CA1 and the subiculum (Johnston and Amaral, 1998). The granule cells of the dentate gyrus are the next step in the trisynaptic pathway. Granule cells give rise to unmyelinated axons called mossy fibres. Each mossy fibre branches into thin collaterals in the polymorphic layer before entering the CA3 region of the hippocampus (Claiborne *et al.*, 1986).

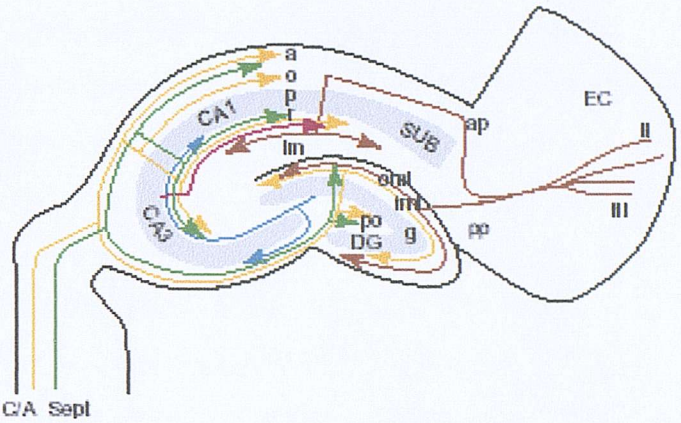

Figure 1.7 *Main axonal pathways of the dentate gyrus and hippocampus.*

Excitatory commissural/associational pathway (C/A) is shown in yellow. Septal projections are shown in green and the mossy fibre system (Mf) is shown in blue. From Skutella and Nitsch (2001).

1.7.5 Dentate gyrus.

The dentate gyrus is composed of three layers. The first of these, the molecular layer, receives its major input from the perforant path. As described previously, the principal cells of the dentate gyrus are called granule cells. These cells give rise to distinctive unmyelinated axons, called mossy fibres that in turn collateralise in the third layer, (the polymorphic layer) before entering the CA3 field (Amaral and Witter, 1989) and forming en passant synapses on pyramidal cell dendrites.

1.7.6 Additional connections.

Apart from the intrinsic connections of the trisynaptic pathway, dentate gyrus and entorhinal cortex, a number of other connections have been described. CA1 pyramidal cells project in a columnar fashion to the subiculum and do not appear to give rise to an extensive projection to other areas of CA1 unlike those CA3 pyramidal cells. Swanson *et al.*, (1978) describe a relatively weak projection from the CA1 region to the deep layers of the entorhinal cortex (EC). The subiculum projects fibres to both the pre and parasubiculum, fibres from these two areas give rise to a major projection that terminates in layers III and II of the entorhinal cortex respectively. Lastly, there are

intrinsic projections in the entorhinal cortex that appear to link the deep layers of the EC with the more superficial layers (Amaral and Witter, 1989).

1.7.7 Interneurones of the hippocampus.

Intrinsic neurones of the hippocampus were previously thought of as neurons with a locally restricted axon plexus, do not have dendritic spines and release γ-amino butyric acid (GABA) (Johnston and Amaral, 1998). Recent advances in cell labelling and staining methods have described a diverse range of interneurones in the dentate gyrus and hippocampus (Freund and Buzsaki, 1996).

Hippocampal GABAergic interneurones, with cell bodies near to the pyramidal cell layer have been classified into 3 groups, based on their synaptic targets; these are axo-axonic cells, basket cells and bistratified cells (Freund and Buzsaki, 1996). The first group, the axo-axonic cells synapse onto the initial segment of pyramidal neurons, these cells have a strong influence over action potential firing. The second group, basket cells surround the somata of pyramidal cell neurones and can make multiple contacts onto the pyramidal cell. The final group, bistratified cells synapse with the apical and basolateral dendrites of pyramidal neurones. The dendrites of each of the groups of interneurones project into the stratum radiatum (SR) and stratum oriens (SO) and may receive excitatory inputs from Schaffer collaterals and commissural-associational fibres (Buhl *et al.*, 1996). Furthermore, mutual inhibitory connections among interneurones are thought to synchronise interneurones that produce theta (5Hz) and gamma (40 Hz) oscillations (Jefferys *et al.*, 1996). In the dentate gyrus, the prominent class of interneurones is the basket cell. The cell bodies of these neurones are located at the border of the granule cell and polymorphic layers. There are at least five types of basket cells (Ribak and Seress, 1983), and axons from these cells innervate granule cell bodies. Another group of interneurones are located in the polymorphic layer; some have axons that remain in the polymorphic layer whilst others innervate the granule and molecular layers of the dentate gyrus (Freund and Buzsaki, 1996).

1.8 Excitatory neurotransmitters and their receptors.

The major excitatory neurotransmitter in the hippocampus is glutamate (Roberts *et al.*, 1981). Glutamate is released from the perforant path, mossy fibres, commissural-associational fibres and Schaffer collaterals as well as from excitatory interneurones.

Glutamate binds to two main types of receptor, ionotropic receptors and metabotropic receptors.

Ionotropic glutamate receptors are composed of three main groups; N-methyl-D-aspartate (NMDA), α-amino-3-hydroxy-5-methyl-isoxazole (AMPA) and Kainate named for the particular ligand used to characterize them. These receptors are all directly coupled to cation channels in the postsynaptic membrane (Table 1.3). Ionotropic glutamate receptors are non selective for the monovalent cations Na^+ and K^+ (Mayer and Westbrook, 1987) and, in addition, all of the NMDA receptors, and some of the AMPA and Kainate receptors are permeable Ca^{2+} (MacDermot *et al.*, 1986).

NMDA receptors are voltage dependant; Mg^{2+} blocks the channel from the extracellular side when the membrane potential is near to resting membrane potential (E_m). The block is not removed until the neurone becomes depolarised (Mayer *et al.*, 1984). These receptors are highly permeable to calcium but require the presence of glycine as a co-agonist to open the channel. NMDA receptors mediate excitatory postsynaptic potentials (EPSPs) that have a slow rising and decaying phase, this is in contrast to AMPA and Kainate receptors, which mediate fast EPSPs.

Metabotropic receptors mediate their actions through G-proteins that either gate ion channels or activate second messenger molecules. They are found on both the pre and postsynaptic sides of the membrane; they coexist on the postsynaptic membrane with ionotropic receptors and modulate neurotransmitter release presynaptically (Schoepp and Conn, 1993).

Table 1.3 *Properties of excitatory amino acid receptors.* (From Rang *et al.*, 1999).

	NMDA			AMPA		Kainate	Metabotropic
	Receptor site	Modulatory site (glycine)	Modulatory site (polyamine)	Receptor site	Modulatory site		
Endogenous agonists	Glutamate Aspartate	Glycine	Spermine Spermidine	Glutamate	Not known	Glutamate	Glutamate
Other Agonists	NMDA	D-serine		AMPA Quisqualate	Cyclothiazide Aniracetam	Kainate Quisqualate	D-AP4 ACPD
Antagonists	AP5, AP7 CGS 19755 CPP SDZ EAA 494	Kynurenate Chloro-kynurenate HA-466	Ifenprodil	NBQX CNQX		___	MCPG
Channel blockers	MK801, Mg^{2+} Phencyclidine Ketamine Dextromethorphan			___		___	Not applicable
Effector mechanisms	Ligand-gated cation channel slow kinetics, high Ca^{2+} permeability.			Ligand-gated cation channel fast kinetics, high Ca^{2+} permeability.		Ligand-gated cation channel fast kinetics, high Ca^{2+} permeability	G-protein coupled IP_3 formation Ca^{2+} released
Location	Postsynaptic (+ glial) Wide distribution			Postsynaptic		Presynaptic & postsynaptic	Presynaptic & postsynaptic
Function	Slow EPSP, Synaptic plasticity (LTP & LTD) Excitotoxicity			Fast EPSP Wide distribution		Fast EPSP Presynaptic inhibition. Limited distribution	Synaptic modulation Excititoxicity

Acetylcholine is another important excitatory neurotransmitter in the hippocampus. ACh acts on both ionotropic (nicotinic) and metabotropic (muscarinic) receptors. Nicotinic receptors modulate glutamate release from excitatory synapses and have been found both presynaptically and on inhibitory interneurones (Gray *et al.*, 1996). Muscarinic ACh receptors are found at both pre and postsynaptic sites in the hippocampus. Presynaptically, the action of ACh at muscarinic receptors is to reduce the amount of glutamate release. Postsynaptically, these receptors mediate a decrease in potassium conductance (gK^+) leading to depolarisation of the neurone and increased likelihood of action potential firing.

1.9 Inhibitory neurotransmitters and their receptors.

The major inhibitory neurotransmitter in the hippocampus is GABA (Roberts *et al.*, 1981). GABA is formed from glutamate by the enzyme glutamic acid decarboxylase (GAD) and can be broken down in a transaminase reaction in which the amino group is transferred to α-oxoglutaric acid in the presence of the enzyme GABA-transaminase (GABA-T). Inhibitory receptors are divided into 3 main groups; the ionotropic $GABA_A$ receptor, metabotropic $GABA_B$ receptor and the ionotropic glycine receptor. The $GABA_A$ and $GABA_B$ receptors differ in their selectivity to the agonists baclofen and muscimol (Table 1.4).

$GABA_A$ receptors are directly coupled to ligand-gated chloride channels and are blocked by picrotoxin and bicuculline. When ionotropic receptors open channels permeable to chloride, increases in $[Cl^-]_i$ causes hyperpolarisation of the postsynaptic neurone and decreases the probability of action potential firing. These receptors moderate postsynaptic inhibition through fast inhibitory postsynaptic potentials (IPSPs).

$GABA_B$ receptors moderate both pre- and postsynaptic inhibition. Presynaptically, inhibition is moderated through a combination of decreased Ca^{2+} entry and increased permeability to K^+. Postsynaptically, activation of G-proteins leads to increased potassium permeability. The increase in $[K^+]_i$ leads to hyperpolarisation which has a slower onset and decay phase than that of the $GABA_A$ response.

Table 1.4 *Properties of inhibitory amino acid receptors.* (From Rang *et al.*, 1999).

	$GABA_A$			$GABA_B$	Glycine
	Receptor site	Modulatory site (benzodiazapine)	Modulatory site (others)		
Endogenous agonists	GABA	Diazepam binding inhibitor ?	Progesterone metabolites	GABA	Glycine, β-alanine, taurine
Other agonists	Muscimol	Anxiolytic benzodiazapines	Steroid anaesthetics	Baclofen	
Antagonists	Bicuculline	Flumazenil		Phaclophen CGP 35348	Strychnine
Channel blockers	Picrotoxin			Not applicable	
Effector mechanisms	Ligand-gated chloride channel			G-protein-coupled receptor; inhibition of adenylate cyclase	Ligand-gated chloride channel
Location	Widespread Mainly GABA-ergic interneurones			Presynaptic & postsynaptic. Widespread	Postsynaptic. Mainly in brainstem and spinal cord
Function	Postsynaptic inhibition (fast IPSP)			Presynaptic inhibition (↓ Ca^{2+} entry) Postsynaptic inhibition (↑ K^+ permeability)	Postsynaptic inhibition (fast IPSP)

The third receptor type, the glycine receptor is a ligand-gated chloride channel found mainly in the brainstem and spinal cord; it is involved in postsynaptic inhibition of fast IPSPs (Rang *et al.*, 1999) but has little involvement in hippocampal inhibition.

Apart from GABA, the neurotransmitter serotonin may be considered inhibitory. Serotonin acts through 5-HT_3 receptors to directly gate non-selective cation channels and produce depolarisation. Although this would normally be considered excitatory, 5-HT_3 receptors often occur on inhibitory neurones and as such, their overall effect is mostly inhibitory.

2 MATERIALS AND METHODS.

2.1 Preparation of Acute Hippocampal Slices.

Adult male Wistar rats (150-300g. Biomedical Research Facility, Southampton, U.K.) were used for these experiments. Brain slices were prepared according to the method of Tattersall *et al.*, (2001). Animals were anaesthetised with halothane prior to decapitation with a small animal guillotine (model DCAP, World Precision Instruments, U.K.). The brain was quickly removed and placed into cold (4°C) (low calcium, high magnesium), cutting solution (artificial cerebrospinal fluid) containing in mM: 189 Sucrose, 26 $NaHCO_3$, 2.5 KCl, 5 $MgCl_2$, 0.1 $CaCl_2$, 10 D-Glucose and 1.2 NaH_2PO_4 pH 7.4, gassed with 95% O_2 and 5% CO_2. Mean osmolarity of the cutting solution was 275 mosmoles/litre.

After hemisection of the brain, a block of tissue containing the hippocampus was mounted on a Vibratome, (Leica, U.K.) immersed in cutting solution and parasagittal slices, 400μm thick were prepared. Slices were stored at room temperature in a holding chamber (Medical Systems Corp, U.K.) in artificial cerebrospinal fluid (ACSF) containing in mM: 120 NaCl, 2.5 KCl, 1.3 $MgCl_2$, 1.25 NaH_2PO_4, 26 $NaHCO_3$, 2.4 $CaCl_2$ and 10 D-Glucose, pH 7.4, gassed with 95% O_2 and 5% CO_2. The mean osmolarity of the ACSF was 282 mosmoles/litre. Slices were allowed to recover for a minimum of 30 minutes prior to transfer to the recording chamber.

2.2 Electrophysiological Recording System.

2.2.1. *Interface Chamber*

Electrophysiological recordings were carried out in a Haas type interface chamber, (Medical Systems Corp, U.K.) which was adapted to allow the BSC-HT top unit to be placed in the exposure area of the calibrated stripline waveguide exposure system (Wood *et al.*, 1997; Tattersall *et al.*, 2001) (Figure 2.1). Slices were transferred to the tissue holder within the recording chamber and allowed to equilibrate for 30 minutes prior to recording. The slice was maintained on thin nylon mesh within the holder at the interface between ACSF and warmed, humidified gas. The lower surface of each slice was perfused with warmed ACSF at a flow rate of 1 ml min^{-1} maintained at 33 ± 0.1°C and monitored with a bead thermistor (Digitimer Ltd, U.K.) placed under the nylon mesh, near the ACSF inlet ports, before coming into contact with the slice.

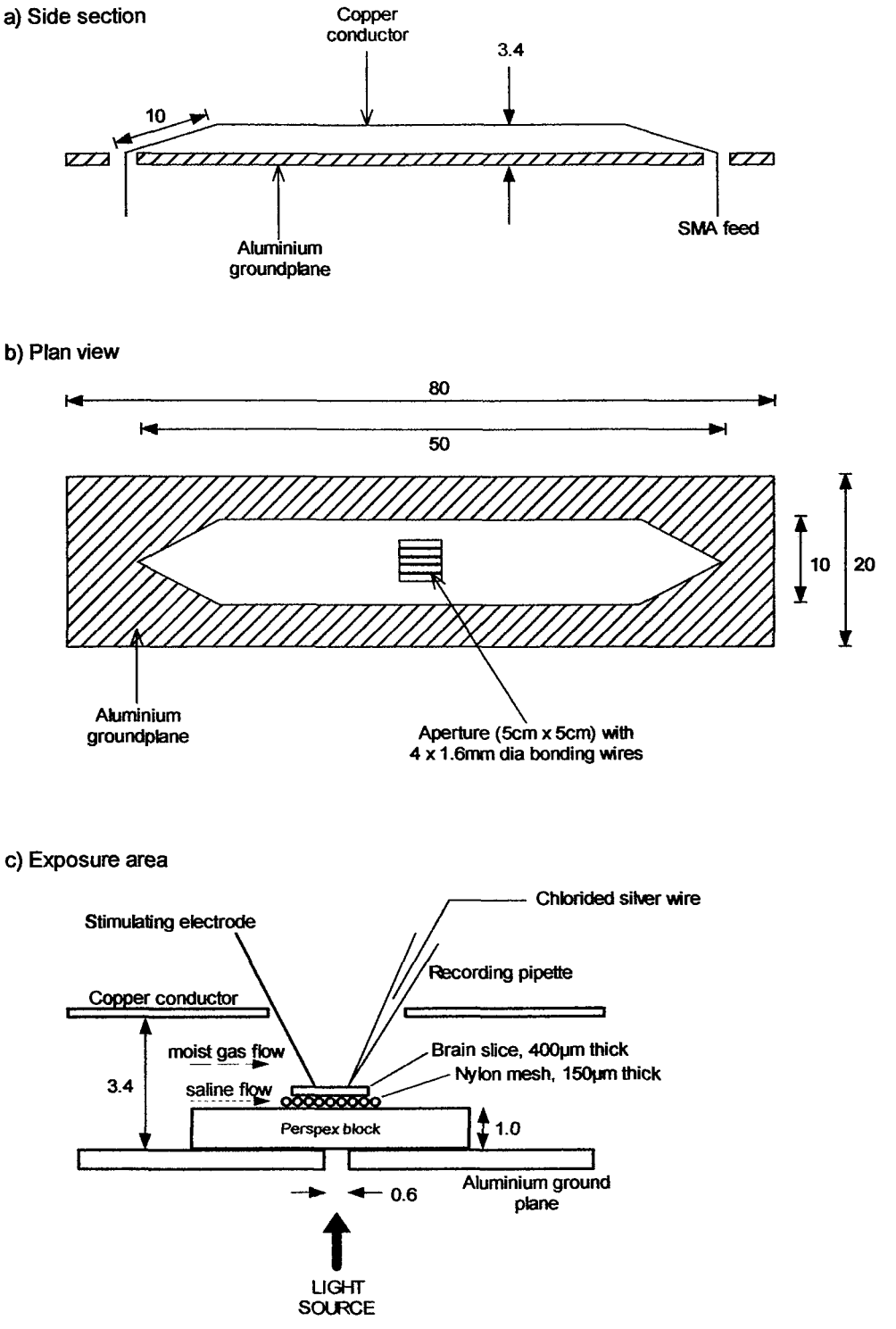

Figure 2.1 *Schematic representation of the electrophysiological recording and exposure system.* From Tattersall *et al.*, (2001).

Note that all dimensions are given in cms unless stated otherwise. **A:** Diagram of the waveguide as viewed from the front (see figure 2.2). **B:** View of the waveguide looking down from the top surface. **C:** Enlarged schematic highlighting the recording chamber and its perspective to the waveguide.

Warmed and humidified gas (95% O_2 -5% CO_2) was passed over the top of the slice. Slices were allowed to equilibrate for at least 30 min in the recording chamber before exposure to RF fields.

2.2.2. Extracellular Recordings.

Extracellular field potentials were recorded in CA1 stratum pyramidale using glass microelectrodes made from 1.5mm outside diameter borosilicate glass with an inner filament. (Clark Electromedical Instruments, U.K.). Electrodes were pulled with a PP-830 microelectrode puller (Narishige, Japan) and had d.c.tip resistances of 5-10 MΩ when filled with 2M sodium chloride. The microelectrode was connected to the recording circuit by a chlorided silver wire with a silver / silver chloride reference electrode placed in the bath near the ACSF inlet ports under the nylon mesh supporting the slice. Manipulation of the microelectrode onto the tissue was achieved by a stepping motor drive (Burleigh Ltd, U.K.) that allowed the microelectrode to be gently lowered onto the tissue in micrometre steps.

2.2.3. *Stimulation Protocol.*

Responses were evoked by a concentric bipolar stainless steel stimulating electrode (Harvard Apparatus IMS Ltd, U.K.) placed in stratum radiatum. Pairs of stimuli, 25ms inter-pulse interval (IPI) were evoked by constant. Stimuli were delivered every 30 seconds to avoid the development of long-term potentiation or depression (Stevens, 1998). In paired-pulse experiments, the current amplitude was chosen to evoke a half-maximal population spike (PS) as determined from the stimulus response curve for that slice. Evoked responses were displayed on a dual beam oscilloscope (Gould Ltd, U.K.). Digitized data were sampled at 10kHz with a Pico-42 computer interface (Pico Technology Ltd, U.K.) and stored on a PC (Novatech 550MHz, Novatech Ltd, U.K.) for analysis using the program LTP (Anderson and Collingridge, 2001).

During pharmacological experiments, the stimulation protocol was the same as for the paired-pulse recording except that single stimuli were delivered every 30 seconds. As before, stimuli were evoked by constant current (150 to 250μA amplitude, 70μs pulse width) generated by an isolated DS3 stimulator. D-APV (2-Amino-5-phosphonovaleric acid), MK801 (5R,10S)-(+)-5-Methyl-10,11-dihydro-5H-dibenzo[a,d]cyclohepten-5,10-imine hydrogen maleate) and Carbenoxolone (3β-Hydroxy-11-oxoolean-12-en-30-oic acid 3-hemisuccinate) were purchased from Sigma (U.K.). Stock solutions of D-APV and

Carbenoxolone were dissolved in distilled water, transferred to individual aliquots and frozen until required. MK 801 was dissolved in DMSO (Dimethyl Sulfoxide) and stored as for D-APV until needed.

2.2.4. Data Analysis and statistics.

Due to inhibitory circuits activated during the first (conditioning) pulse, the second (test) pulse evoked a smaller population spike than the first pulse. The ratio of the test PS2 to the conditioning PS1 was used as a measure of the degree of paired-pulse inhibition. In addition, the ratio between the slope of the field excitatory postsynaptic potential (fEPSP) and the PS amplitude was measured for the first response. This E-S ratio gives an indication of the excitability of the pyramidal cells in the slice. Data were normalised to 100% by averaging the last 10 values recorded in the 5 minutes before RF exposure.

A change in response was classified as a persistent change (either increase or decrease) in the amplitude of the response that was greater than twice the standard deviation of the response during the normalised pre-exposure period. Statistical analyses were performed using GraphPad Prism version 2.0 (GraphPad Software, San Diego, CA, USA). Data are expressed as mean ± S.D (number of observations), unless stated otherwise; data are considered statistically significant when $P = < 0.05$. Non-parametric tests were applied to test for significance; these were the Mann Whitney, (unpaired, two-tailed) test or the Wilcoxon matched pairs (two-tailed) test where appropriate.

One data set; baseline exposure in slices exposed to 700MHz RF (results section 4.2.2, figure 4.7), was subsequently re-analysed using time-series analysis. The results are presented in Appendix 2. The aim of the re-analysis was to determine whether the non-parametric statistics described earlier was the most suitable test for these results. Statistical analysis was performed using the CUSUM function in Minitab version 13 (Minitab Ltd, Birmingham, U.K.).

2.3 Exposure to Radiofrequency (RF) Electromagnetic Fields.

The recording system was surrounded by a Faraday cage, lined with radiation-absorbent material (RAM), (RFLS single layer lossy foam, R. and F. Products, CA., USA) to reduce the internal reflection of RF and to prevent radiation outside the cage interfering with induced electromagnetic (EM) fields (Figure 2.2). Slices were positioned with the electric field (E-field) perpendicular to the slice (E-field intensity $71 V.m^{-1}$). This orientation

produced the minimum induced electric field and specific absorption rate (SAR) in the slice (Tattersall *et al.*, 2001). Continuous wave (CW) RF signals were produced by an HP8648C signal generator (Hewlett Packard, U.K.), which supplied 125.9mW power at 700MHz. Stimulating and recording electrodes were placed in the brain slice at angle of approximately 45° to the E field. Baseline field potential recordings were made for 30 minutes prior to 5 minutes RF exposure. At the end of the exposure a further baseline period of 10 minutes was recorded.

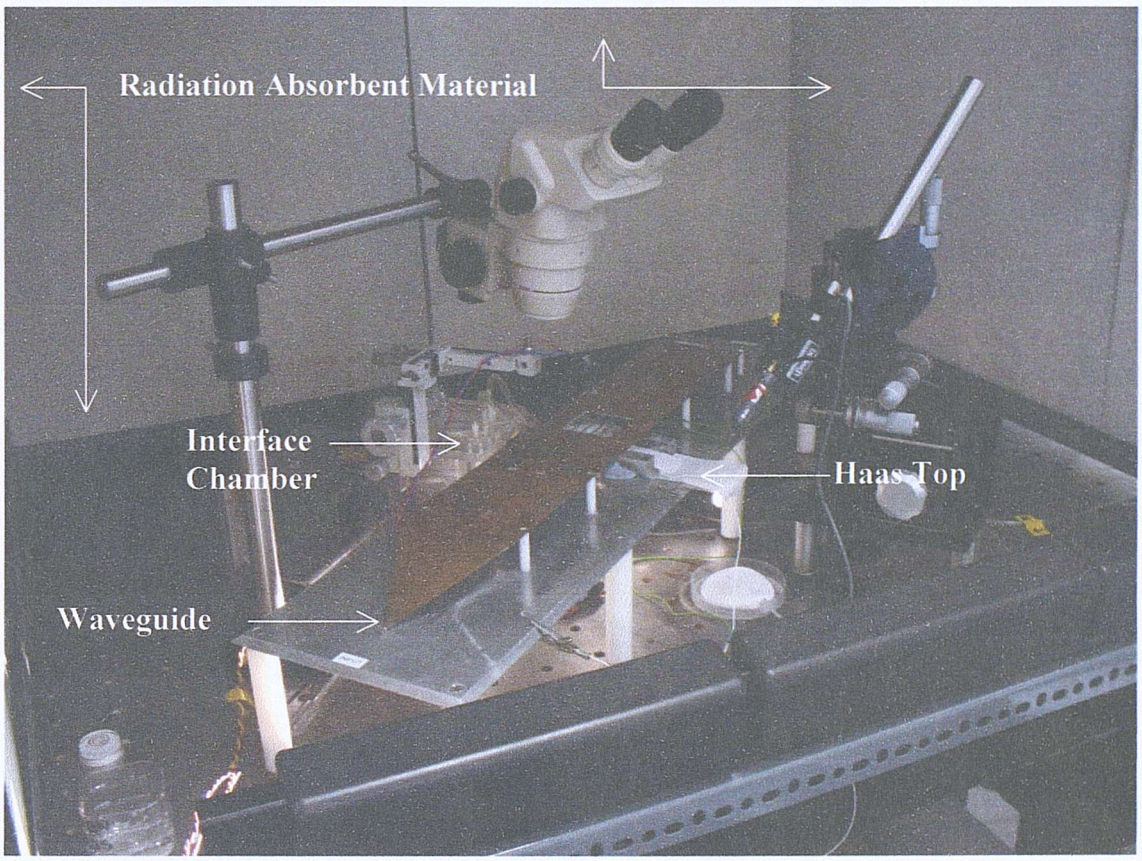

Figure 2.2 *Photograph of the electrophysiological recording system.*

In control experiments, the output of the RF generator was connected to a dummy load instead of the waveguide to produce a sham exposure. Bath temperature was monitored by bead thermistor (0.1°C resolution) throughout the experiment and did not increase during the period of RF exposure.

2.4 Preparation of Acute Slices for Dosimetry.

Parasagittal slices were prepared and stored as described in section 2.1 except that the slices were 1mm thick instead of 400μm as noted previously.

2.4.1 *Micro-thermocouple Recording System*

Micro-thermocouples (MTC) were prepared according to the method of Pakhomov *et al.*, (2000). Briefly, bare wire MTC's made of 25μm diameter copper and constantan wire were purchased from Omega Engineering, U.K. The wires were inserted and fixed into a custom-made glass capillary holder and the exposed tip coated in lacquer for electrical insulation. The holder containing the MTC was connected to the micromanipulator and recording circuit as described previously (Figure 2.2). MTC readings were amplified (Amplifier Research model 25S1G4, EMV Ltd, U.K.) low pass filtered at 50 Hz and digitised at 10 kHz. Digitised data were captured and stored on a PC (Novatech, 550Hz, Novatech Ltd, U.K.) for later analysis using the program Clampfit (Axon Instruments, USA). Incident and reflected powers in the waveguide were measured. (Amplifier Research model DC7146 directional coupler, EMV Ltd, U.K.) connected to a Hewlett Packard (model 437B) power meter and model 8481A power sensor (Hewlett Packard, U.K.).

2.4.2 *Exposure Protocol.*

Slices were exposed to continuous wave 700MHz for varying time periods ranging from 1 second to 5 minutes. During the exposure, it was not possible to measure any change in temperature due to contamination with recording artefacts produced by field distortion and induced currents within the micro-thermocouple. However, readings taken immediately after the RF artefact may offer a reliable estimate of temperature (Pakhomov *et al.*, 2000a, b; 2003).

In the first set of experiments, slices were mounted on a small plastic block ($1cm^2$) positioned vertically (parallel to the E-field) on the nylon mesh of the Haas top within the waveguide. In this configuration, and with the slice un-perfused the maximum possible E-field and SAR will be induced (Bevir, 1999) in response to exposure at powers of up to 25W. In a second series of experiments the slices were positioned horizontally, directly on the mesh (perpendicular to the E-field). As before, the slices were not perfused to maximise the possibility of a temperature increase being recorded in response to RF.

2.4.3. *Calibration of MTC.*

The micro-thermocouple does not measure temperature *per se*; only changes in the electrical potential between the thermocouple wires can be recorded. The MTC was calibrated at known temperatures from 20-30°C using a conventional thermometer accurate to 0.1°C. The tip of the MTC was immersed in water and the potential change noted enabling a calibration curve of MTC characteristics to be constructed.

2.4.4. *Luxtron fluoroptic thermometry system.*

Since the use of a microthermocouple to measure temperature change in RF exposed tissue is controversial (Pakhomov *et al.*, 2000a,b) a Luxtron fluoroptic thermometry system fibre-optic probe (Luxtron Model 790, Durham Instruments, U.K.) was used to determine temperature change in response to RF or sham exposure during electrophysiological recording. This particular temperature probe is sensitive to temperature with an accuracy of $\pm 0.1^{\circ}C$ and is reputed to be artefact free. The tip of the probe (1mm in diameter) was inserted into the slice during recording. For temperature measurement during exposure of organotypic hippocampal slice cultures to RF or sham fields (see methods, *2.5.1*), the tip of the probe was inserted through a small screw hole opening on the TEM cell and into the culture plate. The probe was positioned such that it was in contact with the culture medium below the semi-porous membrane on one of the wells of the culture plate. During temperature measurement, the Luxtron display unit was located outside the incubator; access between the probe and the display unit was via a small access port on the side of the incubator.

2.4.5. *Infrared Radiometric Imaging.*

As an alternative approach and to confirm or repudiate microthermocouple measurements of temperature change, some slices were monitored by a thermal imaging camera before and during exposure to RF or sham fields. The IRRIS-256ST infrared radiometric imager (CMC electronics, Cincinnati, USA) is reported to be sensitive to temperature fluctuations of $0.025^{\circ}C$ at $30^{\circ}C$. The camera was mounted above the waveguide with the iris pointed at the slice preparation whilst recordings were made. Data from these recordings was not used in either the baseline electrophysiology or pharmacology chapters in case interference between the camera and the RF signal should cause artefacts in the data. However, both the glass-recording pipette and the metal stimulating electrode were in place in the slice preparation, during the imaging to replicate the conditions used during RF or sham exposure in these chapters.

2.5 Organotypic Hippocampal Slice Cultures.

Organotypic hippocampal slice cultures were prepared according to the method of Stoppini *et al.*, (1991) modified by Pringle *et al.*, (1997). Eight to ten day old Wistar rat pups were killed by decapitation and the hippocampi dissected out. Transverse sections of hippocampus, 400μm thick were cut on a McIlwain tissue chopper (Mickle Laboratory Engineering Ltd, Surrey, U.K.) and placed into Gey's balanced salt solution supplemented with 28mM glucose. Slices were plated onto Millicell-CM semi-porous membranes (four per insert, Millipore) and maintained *in vitro* for 14 days at 37°C, in 5% CO_2 / 95% O_2 (4 slices per well) (Figure 2.3). Cultures were incubated in medium comprised of minimum essential medium, MEM (50%); Hank's balanced salt solution, HBSS (25%); and heat-inactivated horse serum (25%), supplemented with glutamine (1mM), D-glucose (4.5mg/mL) and fungizone (1.5%) (Pringle *et al.*, 2000). Medium was changed every 3-4 days.

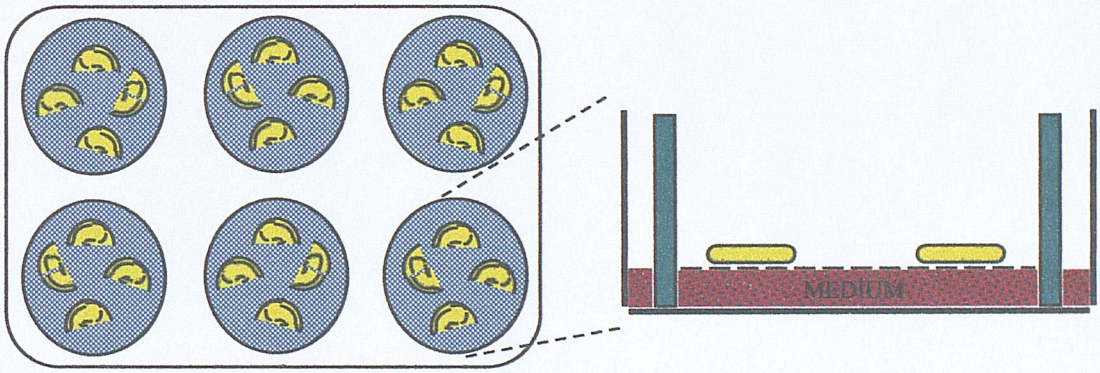

Figure 2.3 *Plating of organotypic cultures.* From Wilde, (1999).

2.5.1. Radiofrequency Radiation Exposure System.

Cultures were exposed to radiofrequency (RF) electromagnetic fields in a fully enclosed, calibrated transverse electromagnetic (TEM) cell mounted inside the incubator (Figure 2.5). RF signals were produced by an HP8648C signal generator (Hewlett Packard, U.K.), which supplied powers of up to 125.9mW at 700MHz.

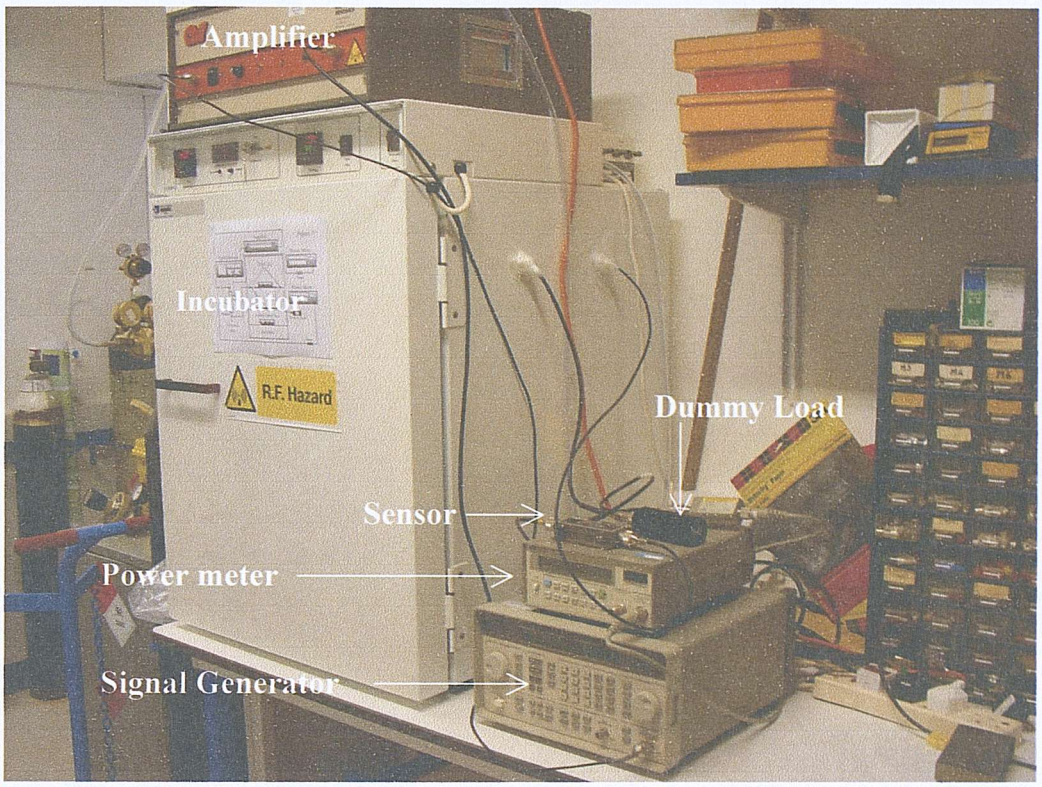

Figure 2.4 *Photograph of the exposure set-up for organotypic slice cultures.*

Signals were amplified (Amplifier Research model 25S1G4, EMV Ltd, U.K.) to supply a power of 1W at 700MHz. Incident and reflected power to the TEM cell was monitored by an HP8481A sensor connected to an HP437B power meter (Hewlett Packard, U.K.) via an Amplifier Research DC7146, 40dB differential coupler (EMV Ltd, U.K.). A reflected power of 10mW (1% of incident power) was monitored by a second sensor and power meter arrangement connected to the output terminal of the TEM cell. Slices were exposed for 4 hours to a 700MHz RF field with the E-field normal to the surface of the slice; E-field amplitude $42V.m^{-1}$ (de Pomerai *et al.*, 2000a.) Sham exposures were obtained by placing foil-shielded cultures on an alternative shelf in the same incubator whilst exposure continued simultaneously in the TEM cell.

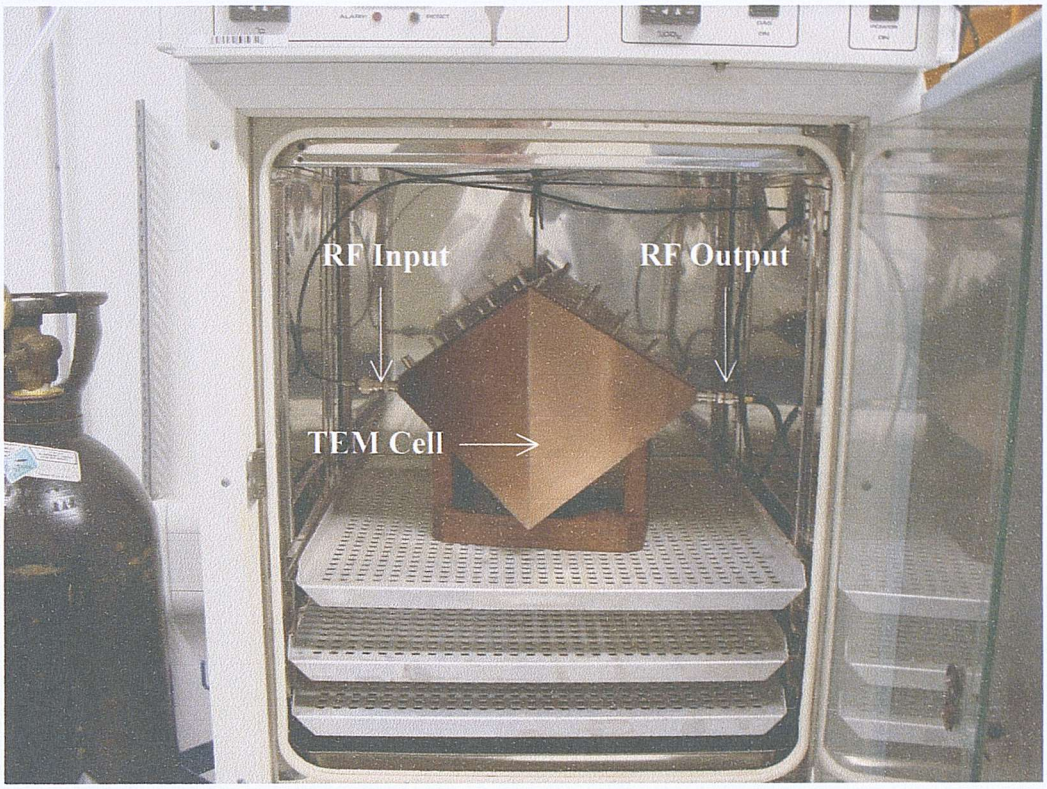

Figure 2.5 *Photograph of the incubator containing the TEM cell.*

3 DOSIMETRY

Dosimetry is the determination of the amount of electromagnetic energy absorbed by a system. The transfer of energy from electromagnetic fields to molecules in an absorber is described in terms of the specific absorption rate (Durney *et al.*, 1986). SAR measurements provide details of the energy absorbed and internal EM fields in the experimental animal or system. Safety standards quoted by ICNIRP (1998) are based in part on experimental data and the replication of these data, such that accurate dosimetry is essential to understanding the biological effects of RF exposure. Since biological effects are likely to be caused by internal fields, not incident fields, determination of SAR for given exposure conditions is essential.

3.1 Dosimetry methods.

There are several practical measurement methods used to determine specific absorption rate; a short description of each technique along with the major limitations for each method is discussed below (Chou *et al.*, 1996). SAR measurements are relatively difficult to make and require specialized equipment and conditions.

3.1.1 Implantable E-field probes.

E-field probes are of two types; the simplest, anisotropic probes consist of a single dipole, which measures the properties of the E-field in one direction only. Isotropic probes are more commonly used as they measure the E-field in each of the three orthogonal orientations of the field. A typical isotropic probe consists of three orthagonally-arranged dipoles directly loaded with metal-barrier diodes (Tay *et al.*, 1998). The RF signal is converted to a DC voltage by the diodes and this DC signal is transmitted to a data conversion unit by high resistance RF transparent lines. A typical isotropic probe requires a 5mm spherical or cubic volume to house the three dipoles of the probe. Field strength data may be obtained with spatial resolution of better than several millimetres at frequencies ranging from 300 MHz to 12 GHz enabling accurate measurement of the local SAR (Tay *et al.*, 1998).

This system is generally used for animal cadavers or phantom models; however, miniature E-field probes have been developed recently that allow measurement in anaesthetised animals. When the characteristics of the E-field and conductivity of the tissue are known, the specific absorption rate can be calculated from the relationship

SAR = $\sigma|E_i^2|/\rho$, where σ is the conductivity of the tissue (S/m), ρ, the mass density of the tissue (kg/m^3) and E_i is the total internal root mean square (RMS) E-field strength.

The advantages of this technique include accurate measurement in low-level fields and instant readout of results (Durney *et al.*, 1986). The latter advantage allows for SAR distribution throughout the tissue to be determined.

Although implantable probes measure local SAR, there are several sources of error associated with their use. Firstly, they require calibration in terms of the absolute field strength in high water content biological tissue. Secondly, large gradients in the internal E-field coupled with imprecise data on the conductivity or density of the biological material may lead to additional errors in calculation. In consequence, SAR measurement uncertainties of at least ± 2 decibels (dB) are to be expected (IEEE, 1998). Moreover, measurement of the E-field at more than one point is often not practical (Durney *et al.*, (1986).

3.1.2 Differential power method.

In this method, the absorbed power is calculated as the difference between the incident and scattered power in a closed exposure system. Several calculations must be made. Firstly the power absorbed by the empty exposure device (P_E) is calculated from the formula $P_E = P_I - P_O - P_R$ where P_I is incident, P_O output and P_R reflected powers respectively. The process is repeated with the tissue sample in the exposure device to obtain P_S (sample power) using the equation $P_S = P_I - P_O - P_R$. Finally, SAR is calculated by dividing the total absorbed power (P_S-P_E) by the mass of the sample. The limitation of this method is that it only enables calculation of the average SAR in a tissue sample and not the more important local SAR. Furthermore, this is an expensive system to establish as it requires the use of differential couplers and power meters on all input and output ports of the exposure system. Using an analogue to digital converter linked to a computer can increase the accuracy of differential power measurements. Further stability in the precision of measurements can be achieved by tightly controlling the temperature of the differential couplers and power meter leads (Durney *et al.*, 1986).

The possibility of using the differential power method to calculate the average SAR in slices exposed to 700MHz RF was discounted for several reasons;

a) The stripline waveguide exposure system used in these experiments is an open system; the differential power method of measuring SAR is best suited to an enclosed system. Consequently, sources of error would be introduced into the calculation of SAR through loss of power along the length of the waveguide (a known variable) and radiated power through the sides of the waveguide (an unknown variable).

b) The tissue samples used in these experiments are very small (less than 5mg in weight) and would absorb a relatively small amount of power. Errors associated with radiated power from other parts of the system would be much larger than the power absorbed by the tissue, leading to greater complexity of the results.

3.1.3 Calorific techniques.

This technique is most useful for measuring whole-body SAR in animal phantoms and cadavers (Durney *et al.,* 1986). Two methods are currently in use:

a) Twin-well calorimetry is, the simpler of the two methods. The main disadvantage of this technique is that it demands very expensive equipment, is difficult to detect failure in any of several thermocouples and measurements are very time consuming, taking a full day for a rat cadaver (Durney *et al.,* 1986).

b) Dewer calorimetry, is inexpensive in comparison with the twin-well method, simple to use and relatively fast, taking 1-2 hours to complete (Durney *et al.,* 1986). To check for heat loss during the exposure, it is necessary to compare the SAR measurement taken immediately after the exposure has ended with a second measurement, taken after a time delay equal to the exposure time of the original experiment.

3.1.4 Local temperature change.

High resolution systems using thermistor detectors on high resistance wires can measure temperature changes with a maximum 0.01° C resolution (Durney *et al.,* 1986). Measurement of the local temperature change is the simplest of the methods described and results compare favourably with those calculated mathematically for a given tissue sample (Pakhomov *et al.,* 2000a). If the rate of temperature rise is rapid and can be assumed to be linear, a reasonable estimate of the SAR is given by:

$SAR = C\frac{dT}{dt}$ (Figure 3.1), where C is the tissue specific heat (J/kg/°C), dT is the change in temperature (°C) and dt the exposure time (sec) (Pakhomov *et al.*, 2000a).

An alternative calculation of SAR is described by Durney *et al.*, 1986. Using this method, assuming the tissue conductivity to be 0.84 $S.m^{-1}$, SAR is calculated by multiplying the temperature rise (per 1°C/minute) by a fixed value of 58.6 $W.kg^{-1}$.

To minimise errors associated with this type of measurement exposure time must be kept to a minimum (Durney *et al.*, 1986). Using this approach, the change in temperature due to an RF pulse is detected by a probe inserted into the tissue. The main drawbacks of this system are that artefacts may occur due to the interaction of the RF field with the electrical leads attached to the probe, or, the probe itself may perturb the internal E-field and produce artefacts in the measurement (Durney *et al.*, 1986; IEEE, 1998; Pakhomov *et al.*, 2000a; 2003).

Figure 3.1 *Temperature measurement in response to an RF pulse.*

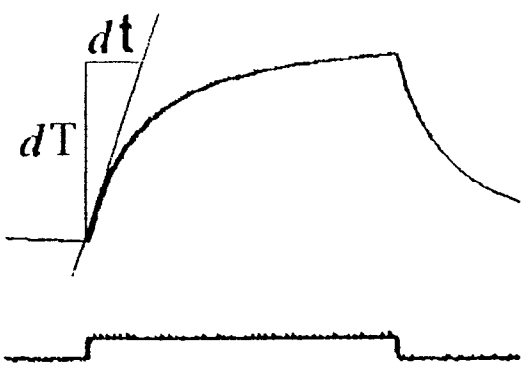

The lower of the two traces shows the RF pulse duration and the upper trace is the recorded heating curve. SAR is calculated from the initial slope of the heating curve, *dt*/*d*T. From Pakhomov *et al.*, (2000a).

3.1.5 Thermographic techniques.

Scanning thermographic cameras can be used to provide detailed SAR distributions in animal phantoms and cadavers (Durney et al., 1986); however, readout of the temperature at the end of the exposure period must be done quickly to avoid underestimation of SAR. The main drawback of this system is in very high cost of the equipment; additionally, the temperature resolution may be less than that achieved with

probes used to monitor local temperature change, it is, however, non-invasive and non-perturbing.

3.2 Computer Modelling.

Computer models are increasingly being used to predict local and whole-body specific absorption rates; predicted values from such models may be useful in the establishment of new safety guidelines or the revision of existing ones.

Finite Difference Time Domain (FDTD) modelling is a numerical method used to solve electromagnetic field interaction problems (IEEE, 1998). FDTD programs are based on a code described by Kunz and Leubbers (1993) (see Gajsek *et al.*, 2001 for review). The code predicts the E-field distribution in a body or tissue by providing a solution to Maxwell's equations (Taylor *et al.*, 1997). FDTD modelling has distinct advantages over experimentally determined SAR in that it can be used to predict SAR in any lossy object regardless of size. That FDTD can be used to predict SAR in very small lossy materials (such as a 400μM thick brain slice) is a distinct improvement over physical methods where the tip diameter of the temperature probe used to directly measure temperature change may be as large as the object itself.

The main disadvantage of FDTD is that it is limited by the speed and memory of the computer used to solve the differential equations (Gajsek *et al.*, (2001). Additionally, FDTD makes assumptions about tissue properties that may prejudice the calculated SAR. The FDTD method (www.fdtd.org) uses a geometric mesh of rectangular box shaped cells (voxels) developed from MRI or CT scans of humans (or animals), so irregular shapes may be difficult to resolve. Indeed, the FDTD Dosimetry described later in this chapter may be prejudiced by the lack of voxel resolution used to derive the results.

In particular, the tissue sample was not well meshed, the thickness being represented by only two voxels. A more accurate result would be achieved by using smaller voxels, which would in turn require more computer memory.

That said, FDTD modelling is considered an attractive alternative to laborious experimental methods (Walters *et al.*, 2000). Comparisons of E-field distributions

obtained from finite difference time domain modelling have been shown to demonstrate good agreement with values obtained via thermal methods that use calibrated, minimally perturbing E-field probes (Taylor *et al.*, 1997; Pakhomov *et al.*, 2000a, b; Walters *et al.*, 2000; Pakhomov *et al.*, 2003), the differences between theoretical and experimentally derived data are routinely quoted to be between 1-3dB (Taylor *et al.*, 1997; Pakhomov *et al.*, 2000a). FDTD is widely accepted as the dominant modelling technique in radiofrequency dosimetry for bioelectromagnetics applications in the frequency range from a few MHz to several GHz (Tay *et al.*, 1998; Samaras *et al.*, 2000; Wang *et al.*, 2000).

Finite difference time domain code has recently been used by two groups to predict the temperature rise in the head resulting from simulated exposure to 900 and 1800 MHz radiofrequency fields. Van Leeuwen *et al.*, (1999) used a finite difference time domain model coupled with a new thermal model to investigate the temperature rise in the head in response to a 915 MHz, time-averaged 0.25 W power output signal. This study used the bioheat equation determined for the heat sink model (Pennes, 1948) and corrected for the convective effects of discrete blood vessels in an anatomically correct model of the head. Van Leeuwen *et al* calculated the maximum head SAR to be 1.6 $W.kg^{-1}$ in this model and predicted the maximum rise in brain temperature to be 0.11°C in the steady state.

Wainwright (2000) applied the Pennes thermal model (Pennes, 1948) to SAR patterns predicted by Dimbylow and Mann (1994). Additionally, this model took account of metabolic heat production and the power absorbed from the electromagnetic field in its estimate of temperature rise.

In agreement with the findings of Van Leeuwen *et al.*, (1999), Wainwright calculated the steady state temperature rise in the head to be a maximum of 0.1°C in response to a 0.25 W antenna operating at either 900 or 1800 MHz frequencies.

Temperature changes in human subjects in response to RF exposure.

Direct measurements of temperature changes were carried out by Adair *et al.*, (1998; 1999). Forty-five minute, whole body dorsal exposures to 450 MHz (1998; 1999) and 2450 MHz (1999) continuous wave RF fields resulted in increased deep body (oesophageal) temperatures of 0.1°C above baseline levels that were counteracted efficiently by normal homeostatic heat loss mechanisms.

3.3 *Calibrated stripline waveguide exposure system.*

In the past, many RF investigators failed to provide adequate dosimetry or description of experimental design to enable replication of results gained from those studies (Durney *et al.*, 1986). In order to avoid this shortcoming, the waveguide exposure system used here has been subjected to several investigations by independent researchers (outlined below) to determine EM field distribution and estimate SAR in rat brain slices exposed to the device.

The waveguide (Figure 3.2) is a custom made rectangular, open-sided parallel plate transmission line exposure system consisting of an aluminium ground-plane with a copper conductive top plate, tapered at both ends to maintain constant impedance. The apparatus is designed to operate at input frequencies of between 300 kHz to 3 GHz and has been tested at normalised powers of up to 1W (Baldwin, 1996; Tattersall *et al.*, 1996). The electric field strength (E) of the apparatus was found experimentally to follow a simple formula: $E = 200\sqrt{P}(V.m^{-1})$, where P is the input power (in watts) to the TEM cell.

3.3.1 Waveguide Modelling.

Extensive modelling of the exposure system was carried out by Wang *et al.*, (2000, 2001a,b). They used a Finite Difference Time Domain package called XFDTD (REMCON Inc, USA) to assess the effects on the field distribution caused by various objects placed inside the TEM cell and to determine the specific absorption rate of a rat brain slice exposed to the RF field. Using this method, (Wang *et al.*, 2000; 2001a,b) modelled the structures of the TEM cell by meshing the whole area in 2mm*2mm*2mm grid giving a total of 972024 voxels.

Figure 3.2 *Photograph of waveguide exposure system.*

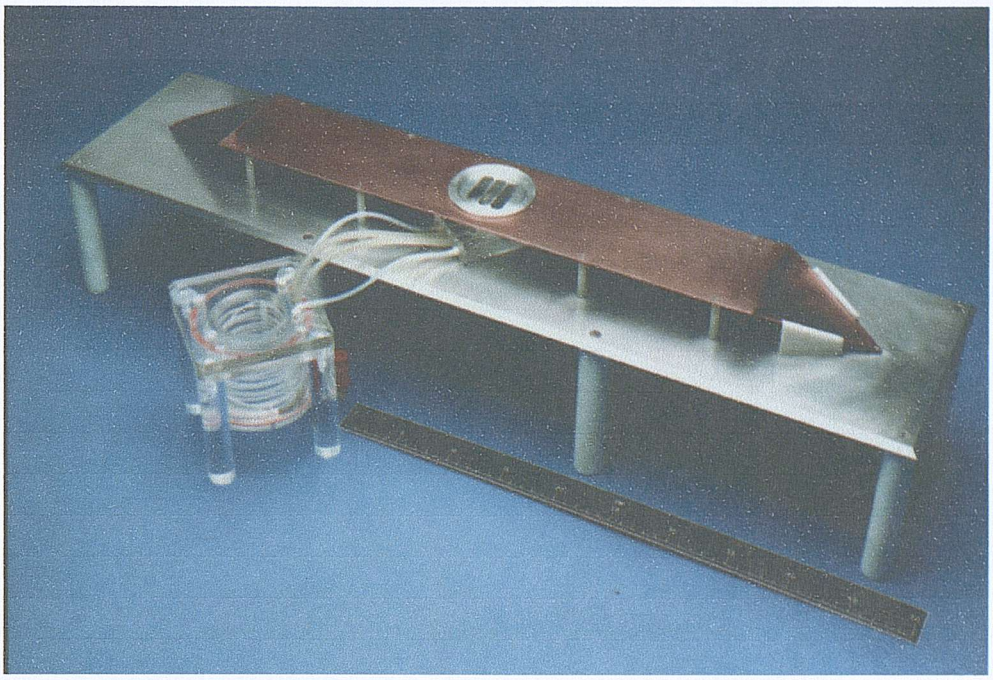

Photograph of the calibrated stripline waveguide showing the aluminium base plate and copper top plate. The Haas type interface chamber (Perspex structure in the foreground) is also shown. The slice chamber, which supports the brain slice, is positioned between the two plates of the waveguide. Note that the copper plate obscures the view of the slice chamber but its position within the waveguide is depicted more clearly in the schematic Figure 2.1

Validation of the modelling was carried out by comparing the Voltage Standing Wave Ratio (VSWR) and electric field strength data obtained experimentally with that of the XFDTD program. In both cases, the values determined by FDTD modelling compared well with those obtained experimentally: specifically, the VSWR value was 1.90 experimentally (Baldwin, 1996) compared to 1.84 modelled and the E-field value was 200V.m^{-1} experimentally (Baldwin, 1996) compared with 205.9V.m^{-1} for the modelled value.

More recently, Alfadhl *et al.,* (2002) used the finite integral method (which is equivalent to FDTD in time domain) to model the waveguide. The results of the analysis obtained from stimulating the empty waveguide showed good agreement with those measured on the physical structure. At 700MHz, the hippocampal slice has a permittivity of 53.898, conductivity (σ) of 0.8595 S.m^{-1} (c.f. 0.84, Durney *et al.,* 1986 & 0.86, Gabriel *at al.*, 1996) and density (ρ) of 1000 kg.m^{3}. The peak SAR value at 1W rms input power using the finite integral method was 0.033 W.kg^{-1}, this compares favourably with the value of 0.035 W.kg^{-1} from XFDTD modelling used by Wang *et al.,* 2000.

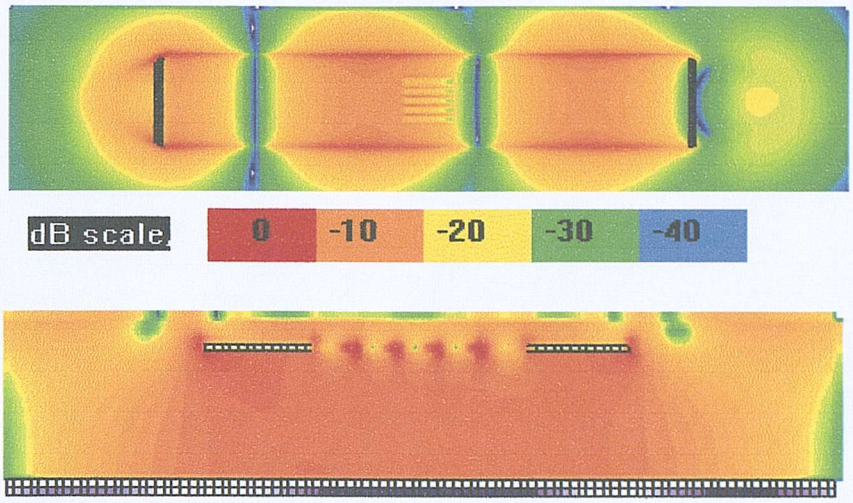

Figure 3.3 *FDTD snapshot of the field pattern in the TEM cell.*

Note that the physical scale size used differs between views. The bottom panel highlights the field pattern in the area immediately below the grid on the copper plate of the waveguide wheareas the top panel shows the fiels pattern along the complete length of the structure. Note that the RF signal enters the TEM cell through an SMA feed on the left of the picture (top panel). **Top panel:** Axial view showing the wavelength and standing wave as viewed from the top of the waveguide. **Bottom panel:** Enlarged view showing a cross section through the sample area. The transverse view shows that the field distribution is very even in the area in which the slice chamber is positioned.

Figure 3.4 *The E-field patterns with and without the mount.*

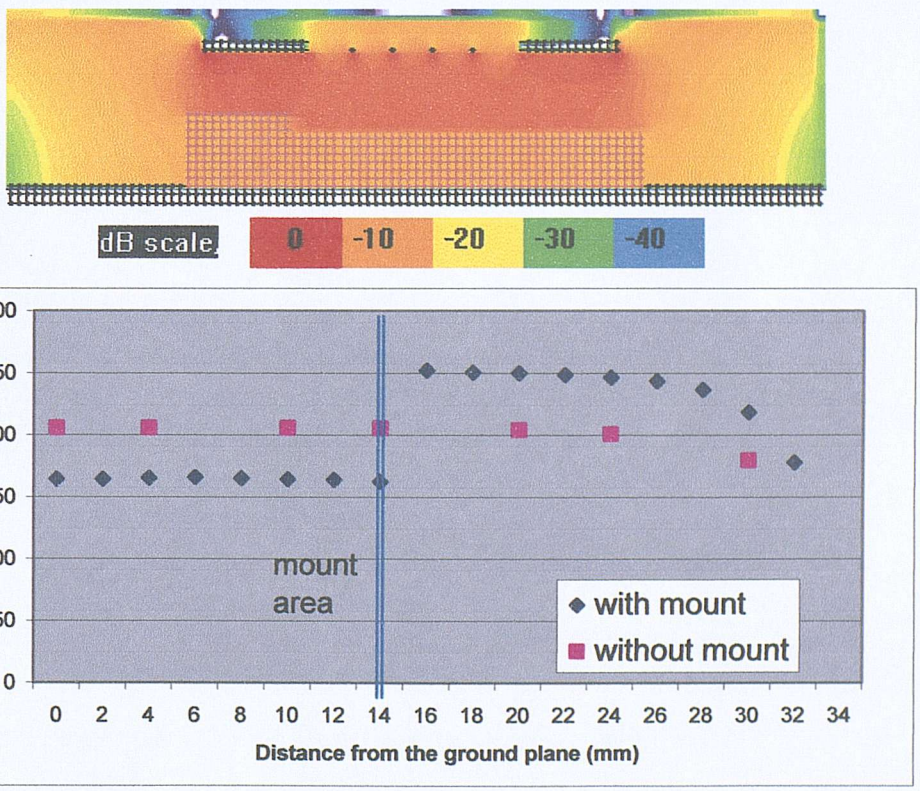

The field pattern with the slice chamber (mount) in place is shown in the top panel. As before, (c.f. Figure 3.3) the field distribution in the area where the slice chamber is positioned is very even. The bottom panel shows a graph of the field distribution with and without mount. Note that the E-field strength is substantially enhanced in the region above the mount.

Using XFDTD, Wang *et al.*, 2000 examined the effect of the Perspex tissue mount in which the brain slice is maintained was determined, and additional modelling examined the effect of the metal stimulating and glass recording electrodes in the EM field (see Figure 3.4).

3.3.2 Calculation of SAR.

Due to the small size of the hippocampal tissue slice used in these experiments, it was not possible to calculate the average SAR per 1g or 10g of tissue (the volumes used to average SAR in NRPB and ICNIRP guidelines respectively) (Wang *et al.*, 2000). However, the program was able to determine the SAR distribution and peak SAR values in the tissue sample (see Table 3.1). The tissue properties used in the calculation of the specific absorption rate were: ε_r=41.5, σ=0.86, ρ=1000 kg.m^{-3} (Gabriel *et al.*, (1996), Sphere Benchmark Phantom: Protocol, Microwave Consultants Limited).

Table 3.1 *Peak SAR values (W.kg^{-1}) determined for an incident power of 1W.*

Parameter measured	*Simulated Peak SAR (W.kg^{-1})*	*SAR Values (W.kg^{-1})*	*SAR Values (mW.kg^{-1})*
Surface of the brain slice	**0.035**	(0.0044)	(4.4)
Tip of the stimulating electrode	**0.92**	(0.1158)	(115.8)
Tip of recording electrode	**0.12**	(0.0151)	(15.1)

Note that the TEM cell is normally operated at 125.9mW input power (E field intensity, 71V.m^{-1}). At 1W input power, the peak SAR values are as noted in bold type. Extrapolated values (in brackets) are obtained by dividing the 1W values by 7.94 to take account of the difference in intensity used in electrophysiological experiments. From Wang *et al.*, (2000).

3.4 Mathematical modelling.

Mathematical modelling of the system was carried out by Bevir (1999). SAR was determined by calculating the relationship between the external electric field (E_0) and the electric field induced in the slice (E_i). Since the slice is small compared to the wavelength (at 700MHz, the wavelength is 42 cms), little perturbation is caused to the electromagnetic field (Durney *et al.*, 1986).

When the brain slice is considered to be a thin disk aligned with the E field perpendicular to the slice, E_i is approximately uniform and independent of the disc thickness. $E_i/E_0 = \sigma_0/\sigma_c$, where $\sigma_0 = -i\omega\varepsilon$ and $\sigma_c = \sigma - i\omega\varepsilon_0$

where σ is the conductivity of the tissue, i is the complex number $\sqrt{-1}$, ω is the frequency in radians ($=2\pi f$), ε_0 is the permittivity of free space. $\varepsilon = \varepsilon_r\varepsilon_0$, and ε_r is the permittivity of the tissue relative to that of free space.

The tissue properties used in these calculations were the same as those in the FDTD modelling. Assuming the brain slice to be a disk of radius 0.5cm and thickness 400μm, the induced field factors are $|E_i/E_0| = 0.019$ for the electric field contribution and $|E_i/E_0| = 0.0022$ for the magnetic field. The SAR was calculated using the formula $\sigma|E_i^2|/\rho$, giving a SAR of 1.9mW.kg^{-1} when E_0 is equal to 71V.m^{-1}. This result agrees well with the value of 4.4mW.kg^{-1} obtained from FDTD modelling. In his calculation of SAR, Bevir (1999) used the values for E-field and distance from the ground plane that were obtained from FDTD modelling (Figure 3.4, 'without the mount'). The agreement between calculated SAR values would have been even closer had the 'with mount' (Wang *et al.*, 2000) values in Figure 3.4 been used.

3.5 Micro-thermocouple measurement of local temperature change.

As described earlier, the accuracy of measurements made using the local temperature change method is limited by the possibility that the E-field is distorted by electric currents induced in the probe and wires. Other factors influencing the precision of the technique include the size of the probe, its heat capacity and response time (Pakhomov *et al.*, 2000a).

Since metal temperature probes induce perturbation of the EM field, one solution would be to use a non-perturbing fibre-optic probe to measure temperature change in RF exposed tissue, an approach that was adopted by Tattersall *et al.*, (2001). However, these probes, though invisible to the EM field, also have disadvantages; they have a slow response time and tend to be noisy (Pakhomov *et al.*, 2000a). Additionally, non-perturbing probes cannot detect temperature fluctuations over small 1-2 mm

distances since they are comparable with the diameter of the probe itself (Pakhomov *et al.*, 2000a).

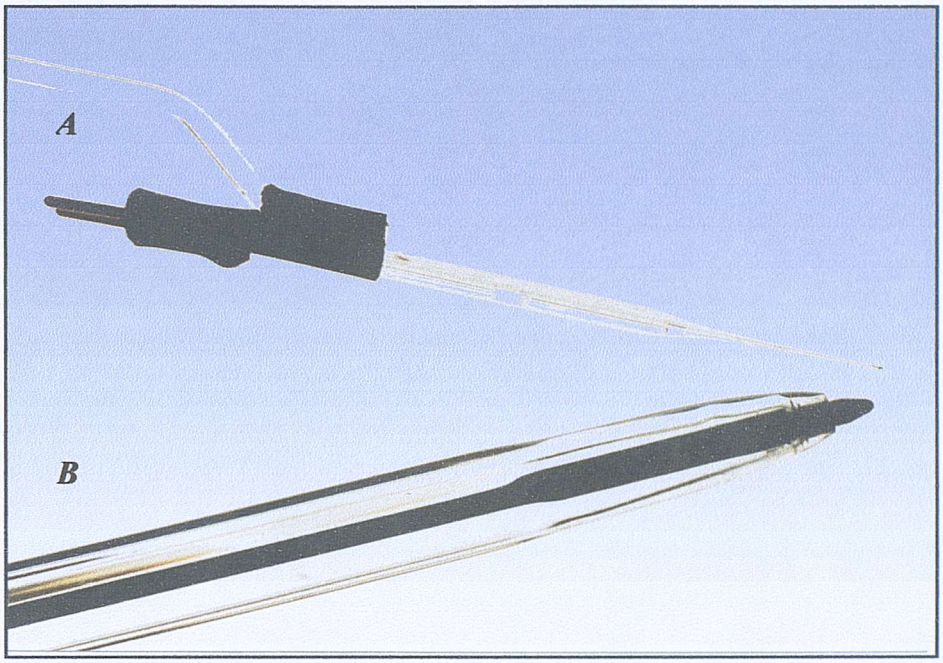

Figure 3.5 *Photograph of the micro-thermocouple probe used in these experiments.*

A: Microthermocouple temperature probe. Note that the tip diameter of the MTC probe is 25μM, this compares with the tip diameter of approximately 1mm for the pen (typical commercially available non perturbing fibre-optic probes have a tip diameter of 1mm).
B: 'BIC' ballpoint pen photographed for size comparison.

A recent study by Pakhomov *et al.*, (2000a) suggested that miniaturization of temperature probes may reduce erroneous readings associated with heating of the probe and wires and provide better spatial and temporal resolution as well as a reduction in the heat capacity of the device. The authors compared the heating dynamics of a Luxtron fluoroptic thermometer with those of a 25 μm diameter, copper and constantan micro-thermocouple (MTC). Simultaneous temperature recordings of both probes in response to 9.5 GHz, 1μs wide, 100-115 kW peak power microwave pulses enabled calculation of the local SAR.

3.5.1 Exposure system comparison.

The exposure system used in the Pakhomov *et al.*, (2000a,b) studies comprises of a vertical section at the end of the waveguide, separated by a quarter-wave matching plate, filled with 6ml of physiological salt solution (Figure 3.6). Extremely high peak power pulses (9.5 GHz, 1μs width, 75-115kW) are produced by this system, providing

specific absorption rates of 610, 304, 145 and 69 $kW.g^{-1}$ at distances of 0, 1, 2 and 3 mm above the matching plate respectively (at 9.5 GHz and 25°C). Pakhomov *et al.*, (2000a,b) found the presence of the MTC in the physiological salt solution did not produce a measurable field distortion nor did it affect the heating of the medium. Heating curves recorded by the micro-thermocouple in this system differ from the conventional heating curves recorded from larger probes (see Figure 3.8). The main difference between the conventional and MTC recorded heating curves is an extended temperature plateau that occurs after short microwave pulses or brief trains of pulses in MTC recordings. This plateau is not present in the recordings made by conventional probes (Figure 3.8). The presence of the plateau occurs because the brief intensive microwave exposure creates a significant SAR and vertical temperature gradient (non-uniform E-field) in the exposed medium.

When the exposure ends, heat dissipates from warmer to cooler areas of the medium and into the environment. The MTC, submerged in the medium, is simultaneously warmed up by heat flow from the warmer areas and cooled down by heat flow to the cooler areas.

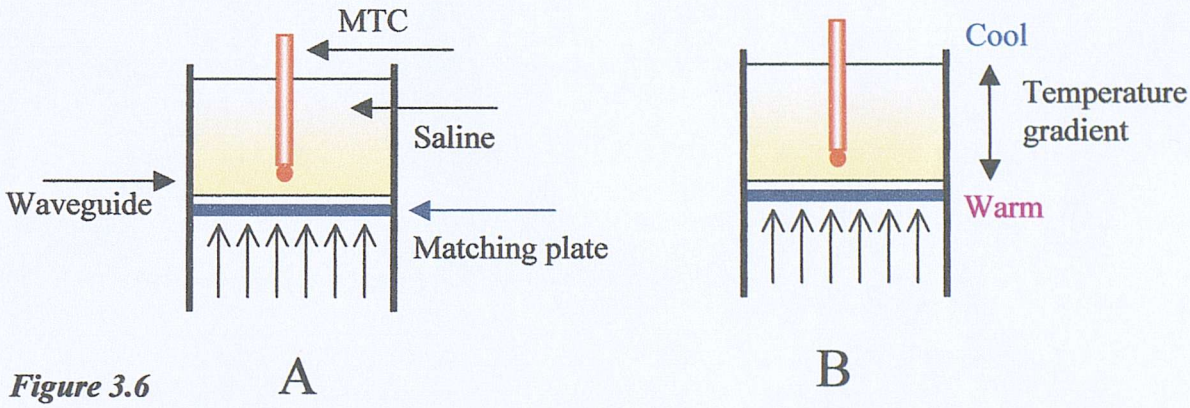

Figure 3.6

Diagram of the exposure set-up used by Pakhomov et al., (2000a).

A: Extremely high peak power pulses of microwave energy are applied to the saline solution from the direction of the open arrows. **B:** Intensive microwave exposure in the small (6ml) volume of saline creates a significant SAR and temperature gradient in the exposed medium.

With time, the heat flow to cooler areas will prevail and the temperature of the medium cools down to ambient room temperature. However, for a very brief period of time after the exposure has ended and within a small volume of medium, the warming and cooling flows will be virtually equal. As a result, the micro-thermocouple will

record a temperature plateau as if no heat dissipation had taken place. Pakhomov *et al.*, (2000a) observed that the difference between the temperature before the exposure, and the plateau is linearly proportional to the delivered energy. Hence, SAR can be calculated from the 'alternative method' (Figure 3.8) using values from the product of the plateau level and the specific heat capacity of the medium.

The waveguide exposure system used in these experiments differs from that of the Pakhomov *et al.*, studies in several important respects. Firstly, the exposure systems operate at very different frequencies. The parallel plate waveguide system has been designed to operate at input frequencies of between 300 kHz to 3 GHz, very much lower than the 9.5 GHz in the other system. Secondly, the input powers differ by 6 orders of magnitude, 129mW waveguide c.f. 75-115 kW powers used by Pakhomov *et al.* Thirdly, and most importantly, the parallel plate transmission exposure system does not induce a vertical temperature gradient in the hippocampal brain slice. This system produces a very uniform E-field (see Figure 3.3) and since there is no vertical temperature gradient in this system, the plateau is not observed (Deans *et al.*, 2000).

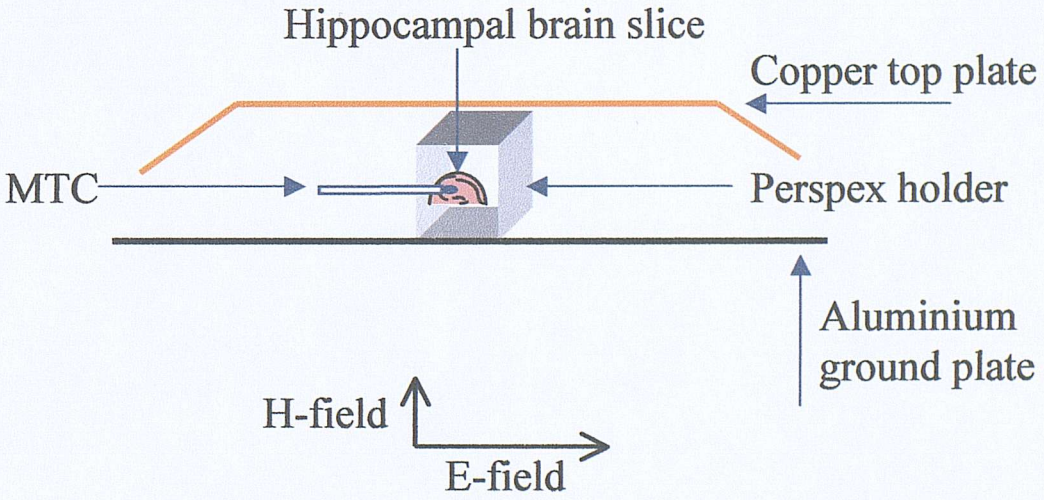

Figure 3.7 *Diagram of the exposure set-up used in the current experiments.*

Schematic showing the arrangement for vertically exposed slices. The MTC was positioned to enter the slice from between the two plates of the waveguide. Slices exposed to RF electro-magnetic fields in this configuration will be subject to maximal increases in temperature and hence SAR (Bevir, 1999). In an alternative configuration (not shown), slices are placed horizontally on a Perspex chamber, positioned above the aluminium ground plane. Slices positioned horizontally will be subject to a smaller temperature increase and SAR than those of vertically positioned slices (Bevir, 1999; Furse and Gandhi 1998).

The experimental protocols also differ in exposure durations; long (ranging from 1 second to 5-minutes) low power, square wave pulses were used in Deans *et al.*, (2000) experiments c.f. 1μs duration square wave pulses used in the Pakhomov *et al.*, (2000a) study.

3.5.2 Validation of MTC model.

The Pakhomov *et al.*, studies demonstrated that it was not possible to calculate SAR from the initial slope of the heating curve of MTC data because of contamination by recording artefacts occurring during the microwave pulse, a finding which was confirmed by Deans *et al.*, (2000). Pakhomov *et al.*, (2000a) showed that the micro-thermocouple was able to detect a temperature plateau immediately after the microwave pulse ended (bottom panel, Figure 3.8).

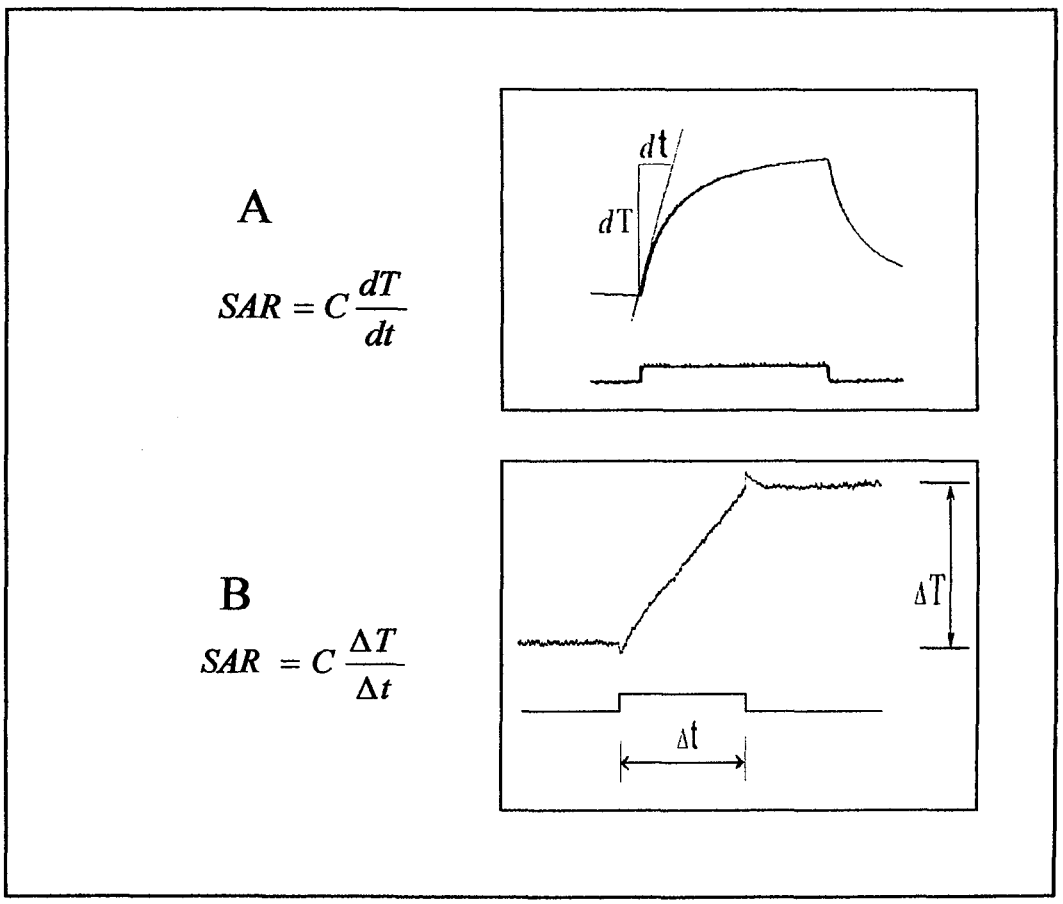

Figure 3.8 *Deriving SAR from heating dynamics.* From Pakhomov *et al.*, (2000a).

In each panel, the lower trace shows the RF pulse duration and the upper trace is the recorded heating curve. The standard method (**A**) uses the initial slope of the heating curve to calculate SAR. The alternative method (**B**) calculates SAR from the change in temperature between the pre-pulse baseline and the equilibrium value at the after-pulse plateau. In both panels, C is the specific heat capacity of the tissue in kJ/kg/°C. The alternative method of SAR calculation correlates well with the standard method when the plateau is present and no artefacts are recorded.

Local SAR calculated according to the alternative method (Pakhomov *et al.*, 2000a) (bottom panel, figure 3.8) provided a good correlation with the standard method of SAR calculation in exposure system used by Pakhomov *et al.*

3.6 Results

3.6.1 MTC measurements in the calibrated stripline waveguide.

Micro-thermocouples do not measure temperature *per se* but record the change in voltage that occurs at the junction of two dissimilar metals. The change in voltage is a fixed value for a given pair of metals (45μV per °C at the junction of copper and constantan) and can be used to estimate temperature after calibration of the micro-thermocouple. To calibrate the micro-thermocouple, measurements of temperature were made in warm water by calibrated thermometer at alternate high and low temperatures between 19.3 and 26.6°C. At the same time as temperature was recorded, the voltage change between the MTC wires was monitored and recorded. This enabled construction of a calibration curve and demonstrated that there was a linear relationship between temperature and voltage in both directions.

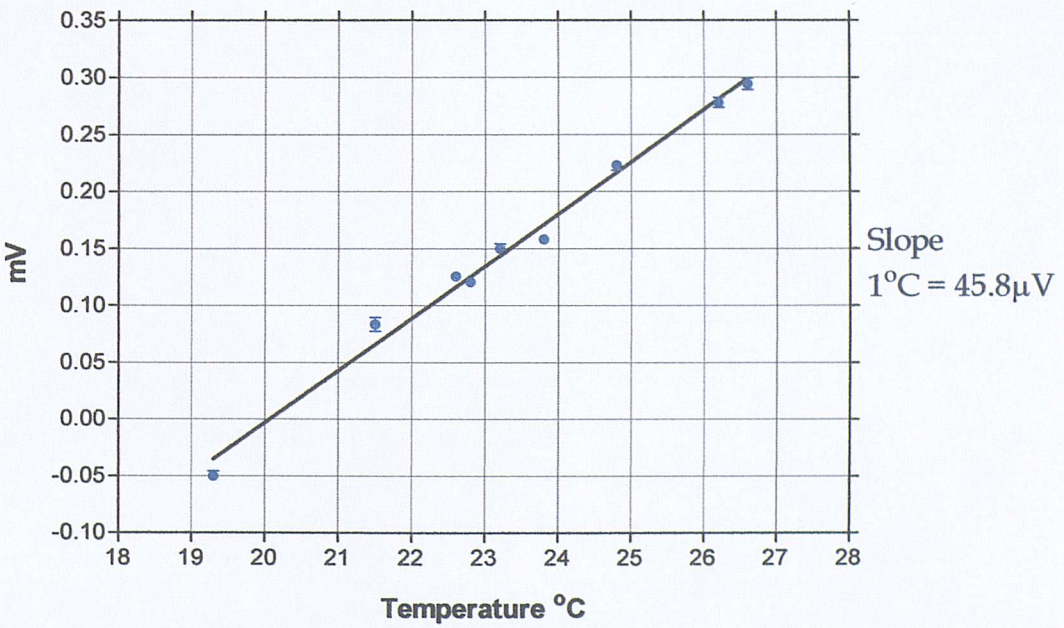

Figure 3.9 *MTC calibration curve.*

The change in voltage recorded by the micro-thermocouple in response to each of eight temperature points was measured by calibrated mercury thermometer. Slope of the line was calculated to be 45.8μV for each 1°C change in temperature. Error bars indicate the mean ± S.D. of five measurements at each temperature point.

For copper-constantan thermocouples, the voltage potential at temperatures ranging from –150 to +350°C is 45μV/°C (http://www.seas.smu.edu). This value is almost identical to that obtained from the micro-thermocouple calibration curve (Figure 3.9). Having demonstrated that the micro-thermocouple could be accurately used to record changes in temperature, a second series of experiments looked at baseline (125.9mW incident power) MTC responses and the effect of increasing the power to 25W.

The MTC response to a single RF pulse consisted of three phases: a downward deflection which lasted for the duration of the RF pulse, labelled (0); an artefact peak lasting for <1 second which always ended above the initial level, labelled (1) and a slow decline to the initial level labelled (2) (see Figure 3.10). No temperature plateau was recorded in any of the individual traces even at high input powers.

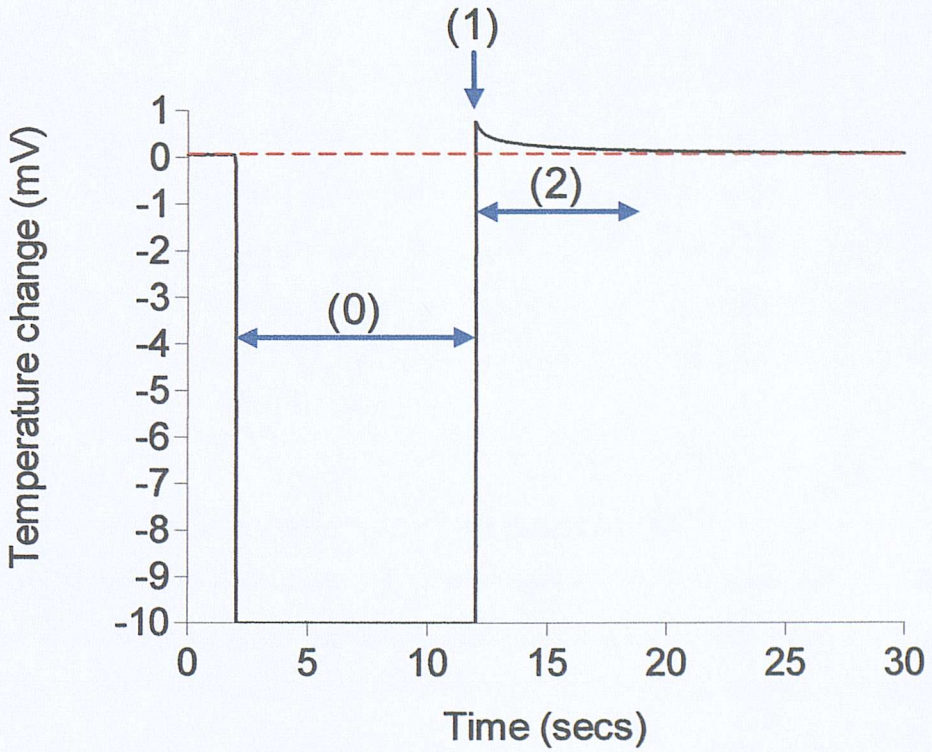

Figure 3.10 *Representative MTC recording in brain slice exposed to a 10 second 25W pulse of 700MHz RF.*

The large downward deflection across phase (0) between 2 and 12 seconds shows that the voltage change recorded by the micro-thermocouple had saturated the Neurolog during the RF pulse causing an unusual stimulus artefact. Arrows shown below each phase indicate the duration of that phase. The red dashed line is inserted to give an indication of the time required for phase (2) to decay to baseline levels.

A number of groups suggested that the micro-thermocouple might prove useful in measuring the local SAR in brain tissue exposed to 700 MHz RF. However, as expected, the presence of the metal MTC wires in the RF field produced excessive interference during exposure. Additionally, the voltage change detected at the end of the exposure period was shown to be an artefact produced by heating of the wires whilst the field was on (Deans *et al.*, 2000). As a result, calculations of SAR derived from micro-thermocouple measurements in this exposure system should not be used.

In a very recent study, Pakhomov *et al.*, (2003) investigated temperature and determined SAR from readings obtained by 3 different sensor types in their waveguide system. The preliminary results from this abstract showed that the microthermocouple and another sensor, FOT-HERO fibre optic sensor (a new type of miniature fibre optic sensor) readings were of a similar amplitude and dynamics upon exposure to RF, whereas the third sensor (TP-21), a 'typical' fibre optic probe read significantly higher when placed next to the other sensors. The authors noted that this 'typical' fibre optic probe did not detect the plateau phase they reported in their earlier papers and was subject to local heating. Furthermore, despite being classed as immune to EMF interference, it could produce markedly erroneous readings because of local field distortion. The inference is drawn that other 'artefact free' probes including the Luxtron probe used to examine the temperature rise in organotypic hippocampal slice culture experiments should be used with caution since errors caused by field distortion can be significant.

3.6.2 Infrared radiometric imaging of temperature change.

The IRRIS-256ST infrared radiometric imager (CMC electronics, Cincinnati, USA) used in these experiments is reported to be sensitive to temperature fluctuations of 0.025°C at 30°C. Estimation of local SAR was made with the thermal imaging camera mounted above the waveguide exposure system. The camera monitored the temperature in a brain slice before and during exposure to RF or sham fields.

Temperature measurements were made at room temperature with the slice unperfused, using high input power RF to maximise the probability of observing an induced temperature rise. The reasoning for this step was that any temperature rise

induced by the electromagnetic field would be more readily masked by perfusion with warmed ACSF.

The amplifier used to deliver the signal was set to a nominal power of 25W. Measurement of the input power delivered through the waveguide was initially made with an HP437B power meter and DC7140 coupler; this gave a reading of 10.5W. A second set of input power readings made with an Agilent E4417A meter and DC7140 directional coupler provided an input power of 1.9W.

Figure 3.11 *Temperature measurement in response to 700MHz or sham RFR.*

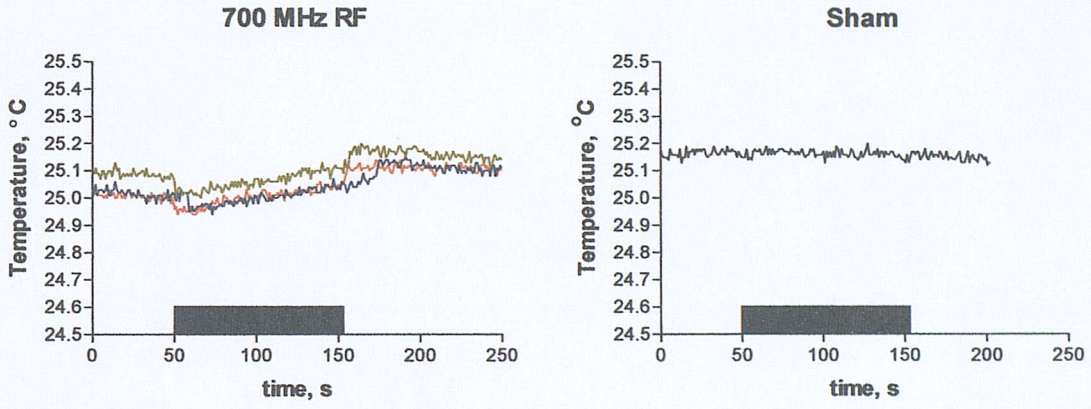

Left panel: Temperature recording in acute hippocampal slice exposed to 700MHz RFR at room temperature (n = 3 observations). Each observation is shown in a different colour; the field was applied for a period of 100 seconds commencing at 50 seconds. Note the dip in temperature when RF is switched on and a corresponding rise when exposure ends.

Right panel: Sham exposed slice maintained at room temperature. Exposure occurred at the same time point as in the RF exposed slice, however, temperature remains constant throughout the exposure. The black bar in each graph shows the period when RF or sham exposure occurred.

In Figure 3.11, (left panel) exposure to RF caused an initial downward temperature deflection at the time the exposure commenced; this was followed by a slow rise in temperature for the duration of the exposure period. At the termination of the exposure, a further sharp increase in 'temperature' was detected. These deflections at the start and end of the exposure were not observed in the sham-exposed control slice. Deflections seen during RF in the exposed slice look similar (though of a much smaller amplitude) to those recorded by the MTC at the start and end of the RF period (Figure 3.10), this seems to indicate that the temperature rise seen here is also an artefact caused by interaction between the camera and the electromagnetic field.

SAR was calculated by taking the average slope value from the three RF exposed readings (0.00095°C/sec) (Figure 3.11) multiplied by the brain specific heat capacity (3700J/kg/°C) to give a specific absorption rate of **3.517 ± 0.16 W.kg^{-1}** at 10.5W input power (using the method of Pakhomov *et al.*, (2000a). Extrapolation of this value to 125.9mW (the input power used during the electrophysiological experiments) gives a value of **0.0419W.kg^{-1}.** Using the method of Durney *et al.*, (1986) SAR = ((0.00095 (°C.$^{-1}$) x 60 seconds) x 58.6 (W.kg^{-1})) = **3.34 W.kg^{-1}** at 10.5W input power and **0.04 W.kg^{-1}** for the extrapolated value.

If the value of 1.9 W obtained from the Agilent meter was correct, SAR would be **0.232 W.kg^{-1}**, with the Pakhomov *et al.*, (2000a) method and **0.209 W.kg^{-1}** with the Durney *et al.*, (1986) method when both values were extrapolated to 125.9mW input power.

3.7 Discussion, calibrated stripline waveguide exposure system.

The most likely source of experimental error in the present study is the susceptibility of thermocouples and other temperature sensing devices to interference caused by the RF electromagnetic field (Pakhomov *et al.*, 2003).

3.7.1 Comparison of SAR from FDTD, theoretical & thermal camera methods.

FDTD modelling of a hippocampal slice exposed to 125.9 mW input power set a local SAR of **4.4 mW.kg^{-1}** at the surface of the brain slice (Wang *et al.*, 2000, 2001a,b). Theoretical modelling using similar tissue properties predicts a value of **1.9 mW.kg^{-1}** (Bevir, 1999).

The specific absorption rate calculated from infrared camera measurement of temperature (**41.9 or 231 mW.kg^{-1}** (using the Pakhomov *et al.*, (2000a) method), **40.0 or 209 mW.kg^{-1}** (using the Durney *et al.*, (1986) method) respectively for 10.5W or 1.9W input powers differs considerably (by a factor of x 10 or x 50 respectively) from FDTD or mathematical modelling.

In particular, it is disappointing that the two types of power meter used here reported dramatically different input powers (10.5 W HP437B power meter c.f. 1.9 W Agilent E4417A power meter). Ideally, the two meters should be returned to their

respective manufacturers for servicing and the experiments repeated. Consequently it is not clear which power meter, if either, displayed the correct value of input power.

Ideally, the thermal camera experiment should be repeated with properly calibrated power meters so that input and output powers to the waveguide are known with certainty. Part of the problem may be that the waveguide exposure system has been tested at input powers of up to 1W. Since the nominal power was set to 25W, it is possible that radiated power from the sides of the open waveguide affected the readout from the power meters. As such, one solution would be to reduce the input power to 1W since the FDTD dosimetry (Wang *et al.,* 2000) suggests the RF field to be very uniform at that power.

Thermographic techniques have been successfully used to determine SAR distribution in animal phantoms and cadavers in the past (Durney *et al.,* 1986) and should be a suitable method of determining SAR distribution in a tissue slice preparation. Although it is unlikely that the artefact observed in Figure 3.11 is a result of the camera itself being affected by the RF field (since it is being mounted above the waveguide), it is possible that the leads from the camera to the computer were exposed to radiated power from the waveguide. In repeating the experiment, extra care should be taken to shield these wires and prevent artefact contamination of the results. Until these experiments have been repeated, it will be difficult to draw firm conclusions from the SAR values obtained from the different methods.

3.8 Transverse electromagnetic (TEM) cell dosimetry.

3.8.1 FDTD modelling.

Experiments in Chapter 6 describe exposure of organotypic hippocampal slice cultures to radiofrequency or sham fields in a custom made transverse electromagnetic (TEM) cell placed inside an incubator.

Motorola Florida Research Laboratories (U.S.A.) (M. Swicord, personal communication) carried out FDTD modelling of the TEM cell exposure system. The modelling predicts SAR distribution in the TEM cell exposed to 0.5W input power, 750MHz RF fields. A culture dish, containing 1, 10 or 20mm deep lossy media is included in the simulations.

Figure 3.12 ***FDTD modelling of TEM cell, 10mm thick lossy layer.***

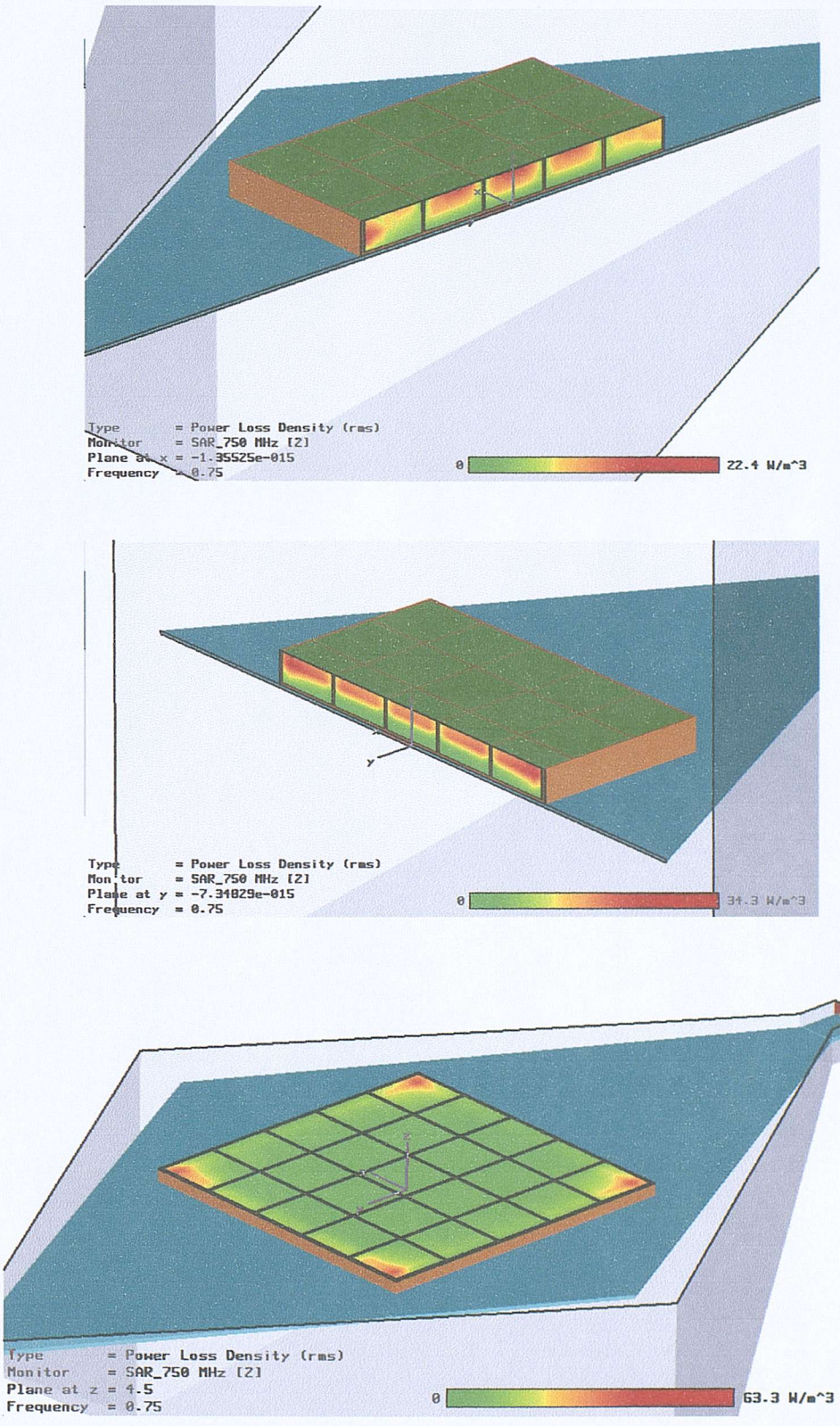

Parameters used in the modelling were frequency, 750 MHz, input power 0.5 W and lossy dielectric layer, 10 mm. Top panel: vertical section through the long axis of the TEM cell. Middle panel: transverse section. Bottom panel: vertical section across the short axis of the tem cell. In all diagrams, the coloured scale bar at the bottom of the plate indicates the field pattern; red areas are subject to the largest SAR values. In all experiments, the culture plate was positioned as in panel B, in line with the x axis. Note that when the lossy material is modelled to be 10mm deep, the maximum SAR values are to be found at the edges of the culture plate.

Figure 3.12 shows the SAR distribution in the culture plate placed on the metal septum of the TEM cell. In this and the latter simulations, the plastic culture dish is modelled to be 1mm thick with a dielectric constant of 2.5; the lossy media has a dielectric constant of 45.

Figure 3.13 FDTD modelling of TEM cell, 20mm thick lossy layer.

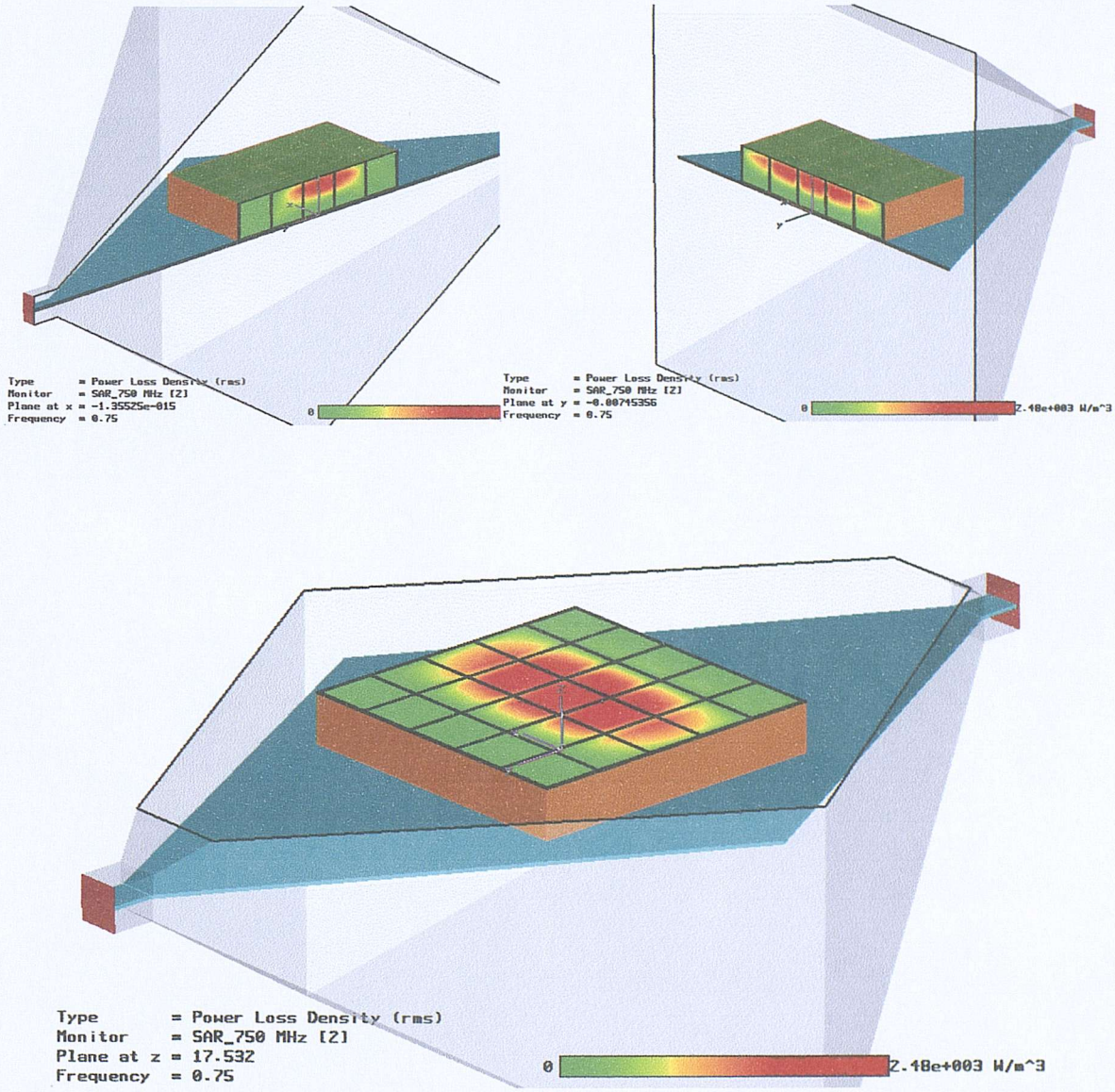

Parameters used in the modelling were frequency, 750 MHz, input power 0.5 W and lossy dielectric layer, 20 mm. Top left and right panels: transverse section through the short axis of the TEM cell. Bottom panel: vertical section across the long axis of the tem cell. In all diagrams, the coloured scale bar at the bottom of the plate indicates the field pattern; red areas are subject to the largest SAR values. Note that as the depth of the lossy media is increased, the larger SAR areas shift from the edges of the culture plate towards the centre (c.f. figure 3.12 for 10mm depth of lossy media).

Figure 3.14 FDTD modelling of TEM cell, 2mm thick lossy layer.

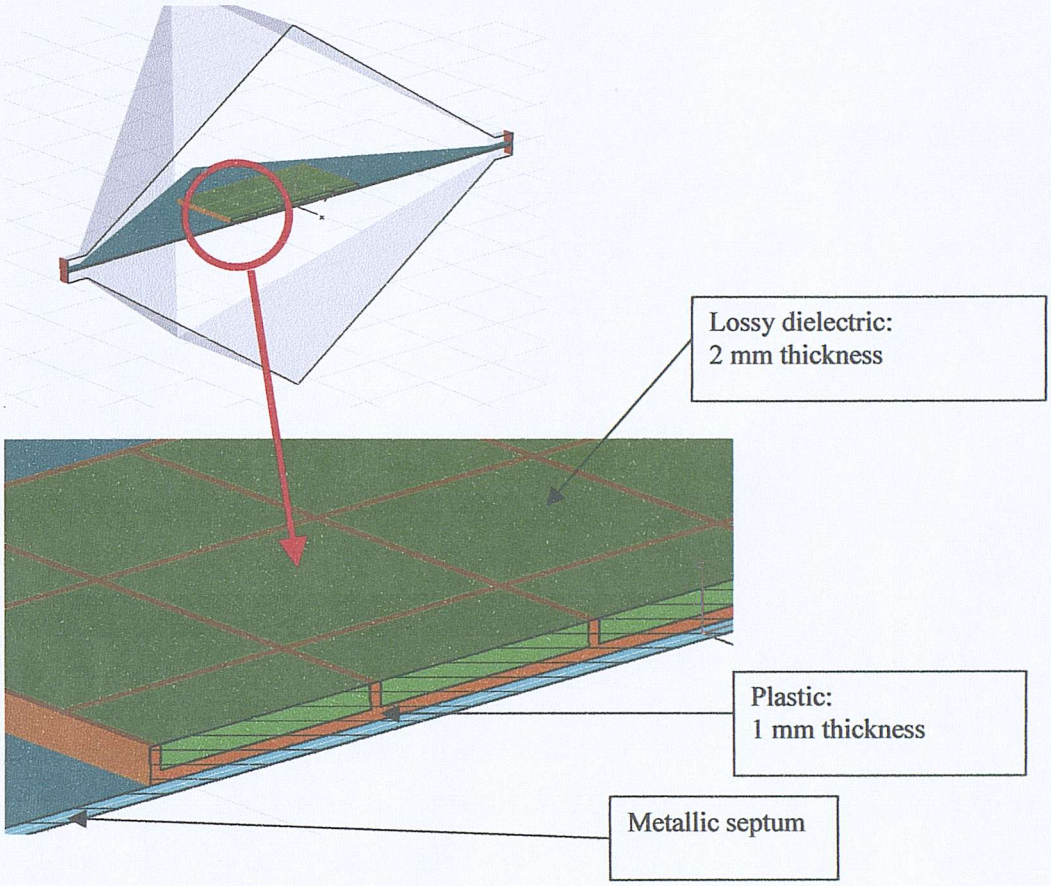

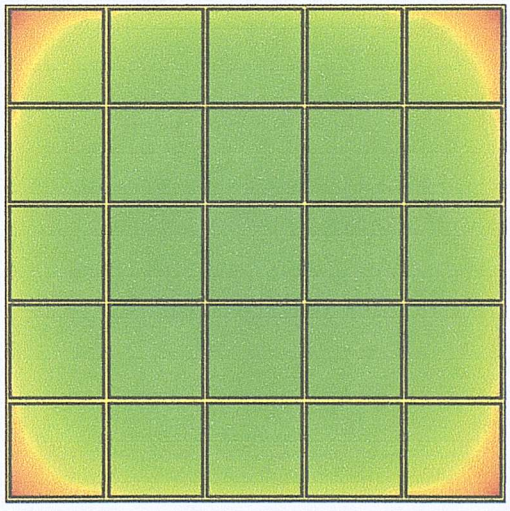

Max. SAR: 90 mW/kg
Max. 1g Avg. SAR: 10

Normalized to 0.5 W

The Motorola modelling predicts that the absorbed power is minimal nearest the septum of the TEM cell. As the culture dish is raised from the septum, the absorbed power increases and the maximum SAR distribution shifts from the edges of the culture plate (Figure 3.12) towards the centre (Figure 3.13). When the depth of lossy media is 10mm, Motorola predict that the maximum SAR will be 0.2 $W.kg^{-1}$ normalised to 0.5W

input power. At 2mm deep, the peak SAR (0.045 $W.kg^{-1}$) is located at the corners of the culture plate. Motorola calculate that the average SAR distribution in 1g of lossy material is 0.005 $W.kg^{-1}$ at the edge of the plate and much smaller in the central portion.

3.8.2 Luxtron temperature measurement in organotypic hippocampal slice cultures.

Temperature measurements were made by my supervisor, Dr. J.E.H. Tattersall using a Luxtron model 790 biomedical fibreoptic thermometer (0.1°C temperature resolution, 1 Hz sample rate). Measurements were made inside the TEM cell during exposure to RF fields by inserting the tip of the fibreoptic thermometer through a small screw hole opening on the TEM cell and into the culture plate.

The probe was positioned so that it was in contact with the culture medium below the semi-porous membrane that supports the slice cultures. During temperature measurement, the Luxtron display unit was located outside the incubator and access between the probe and display unit was via an access port on the side of the incubator (Figure 2.5). Slice cultures exposed to the RF field during the dosimetry experiments were not used in subsequent analysis of heat shock protein expression. During exposure, cultures were placed inside the TEM cell located within an incubator, maintained at 37°C throughout the experiment. Luxtron measurements were sampled at a rate of 1Hz before, during and after exposure.

Figure 3.15 *Luxtron temperature measurement in cultures exposed to 700MHz RF.*

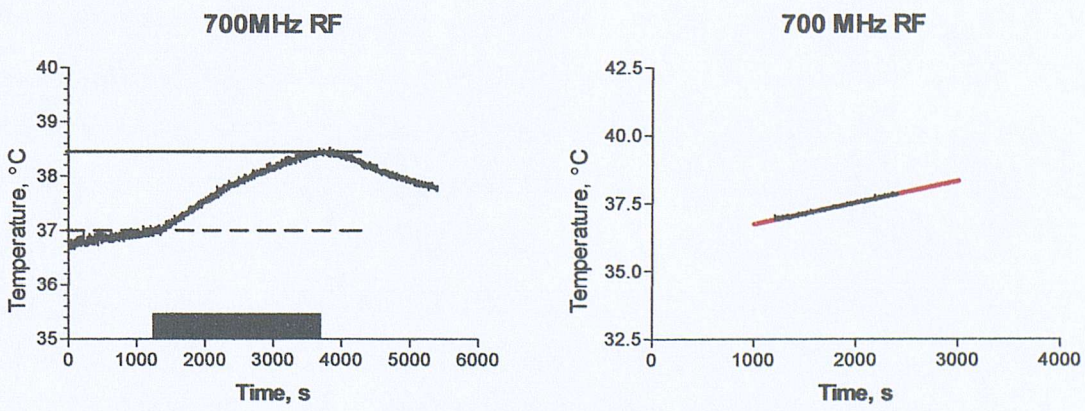

Left panel: RF (1W input power) was applied for 40 minutes, commencing after 20 minutes. Black bar shows the period of RF exposure. Luxtron readings were taken every second during the experiment. **Right panel:** Regression line for the data on the left panel, black line is a selected portion of the data during RF exposure starting at T = 20 minutes; red line is the calculated regression line. Slope = 0.0007840°C.$^{-1}$ Calculated SAR = 2.9 ± 0.011W.kg^{-1}.

Exposure to RF caused a gradual increase in temperature that did not abate during the exposure period. Upon termination of the field, the temperature slowly decreased towards the control value but remained elevated above control values for the duration of the recording period. The regression slope for the RF imposed temperature rise was 0.0007840°C.$^{-1}$. Using the regression slope value and the specific heat capacity of brain tissue (3.7kJ/kg/°C, Walters *et al.*, 2000) SAR was calculated to be **2.9 W.kg^{-1}** for 1W input power, (Pakhomov *et al.*, 2000a). Extrapolation of this value to 125.9mW gives a specific absorption rate of **0.365W.kg^{-1}.**

Using the value of slope detected by the Luxtron probe and the method of Durney *et al.*, (1986) SAR = ((0.0007840 (°C.$^{-1}$) x 60 seconds) x 58.6 (W.kg^{-1})) = **2.76 W.kg^{-1}** for 1W input power and **0.347 W.kg^{-1}** for the extrapolated value.

3.8.3 Discussion – TEM cell dosimetry.

The Finite Difference Time Domain dosimetry completed by Motorola assumes the depth of the lossy material to be between 2 and 20mm (Figures 3.12, 3.13 & 3.14). Clearly, as the depth of the lossy media is increased, the maximum SAR increases and its distribution changes from the edges of the culture plate to the central portion. This finding is counter-intuitive, as one would expect that peak SAR would decrease with distance above the septum.

It is unclear from the simulations however, if the x30 increase in maximum SAR is brought about by a greater volume of lossy media or the height of the media above the septum. In the organotypic hippocampal slice culture experiments described in Chapter 6, the cultures sit on a semi-porus membrane resting in a six-well culture plate. The culture media bathing the slices occupies a depth of 2 to 3mm and the plastic culture plate is approximately 1mm thick. Slice cultures are prepared at a thickness of 400μm and during the two weeks incubation period, thin down to around 150μm (A. Pringle, personal communication). If the depth of lossy media is the only factor in SAR distribution, the estimation of SAR in figure 3.14 should be the most accurate. Evidently this is not the case in the hippocampal slice culture experiments as the calculated SAR of 1.45 W.kg^{-1} (extrapolated to 0.5W) is far higher than the Motorola estimate of 0.045W.kg^{-1} peak SAR.

In the design of future experiments, it would be helpful to have the six-well culture plate modelled to include the smaller depth of lossy material (the dosimetry modelled previously was for a culture plate containing nematode worms (De Pomerai *et al.*, 2000a) exposed in an identical TEM cell. If additional dosimetry showed that the height above the septum was a significant factor in determining SAR, then alternative experiments should be designed in which the slice cultures were position closer to the septum to reduce the maximum SAR the slices are exposed to.

3.84 Discussion – Luxtron temperature probe.

The results of the Luxtron dosimetry presented here strongly suggest that slice cultures were exposed to RF induced heating during the experiment. As such, the increased heat shock protein expression reported in Chapter 6 may be partly due a thermal mechanism of interaction with the tissue and caution should be taken in interpreting the results. The large temperature rise observed after RF exposure may be related to the fact that the culture plate is fully enclosed in the TEM cell so any rise in temperature is unable to dissipate to the surrounding airspace.

3.9 Conclusions.

These experiments have established that it has not been possible to record accurate temperature measurements in the transmission line system using a micro-thermocouple probe or thermal imaging camera during the period of exposure because of the presence of field distortions and recording artefacts whilst the RF field is on. Consequently, it is not possible to use MTC or thermal imaging camera-derived data to calculate local SAR in this preparation.

Measurements from the Luxtron probe do not seem to have suffered from the same artefacts as the MTC and thermal imaging camera. Cultures exposed to 1W input power, 700MHz RF in the TEM cell were subjected to an additional temperature stress as a result of the exposure that may have been due in part, to the design of the transverse electromagnetic cell. Although there were no obvious artefacts attributed to the use of the Luxtron probe during exposure it seems clear from the work of Pakhomov *et al.*, (2003) that probes of this type may report much higher heating than other temperature sensors and results should be viewed with caution.

Overall, the results from this section are disappointing; none of the temperature sensors used here are entirely suitable for accurate determination of the local SAR. For the moment, the question of whether minute thermal changes are involved remains unsure, and this needs to be addressed by further experiment. Thus it would appear that FDTD modelling, which should be artefact free, gives the best estimate that the exposure is essentially athermal at the power levels used. Future experiments should address the use of smaller tip diameter fibreoptic sensors such as the FOT-HERO (FISO Technologies, Canada) as this would allow insertion of the probe directly into the brain slice preparation during exposure.

4 EXTRACELLULAR FIELD POTENTIALS

Electrical stimulation of the perforant path, mossy fibres or Schaffer collaterals result in a characteristic sequence of excitation followed by inhibition in target neurones. Inhibition from feed-forward and recurrent connections has two phases, a fast phase mediated by $GABA_A$ and a slow phase mediated by $GABA_B$. Paired-pulse recordings from stimulation of Schaffer collaterals reveal changes in the excitatory and inhibitory output to pyramidal cells in the CA1 region.

Field potential events were recorded in the stratum pyramidale of field CA1 in response to afferent stimulation of the stratum radiatum. The field potential response obtained in CA1 stratum pyramidale cells is a tri-phasic response consisting of positive going field excitatory postsynaptic potential (*f*EPSP) and a negative going population spike (PS) (Figure 4.1). The *f*EPSP can be used as an index of the number of excitatory synapses activated by a given afferent impulse volley. The negative going population spike grows in size as the *f*EPSP increases and can be used as an index of the number of cells discharging in response to the stimulus (Moser, 1995).

4.1 Control responses and baseline stimulus response curve.

Paired-pulses of equal amplitude and duration were delivered every thirty seconds at an inter-pulse interval (IPI) of twenty-five milliseconds to avoid the induction of long-term potentiation (LTP) or long-term depression (LTD) (Stevens, 1998). Extracellular field potential responses were recorded in slices subjected to 5-minutes exposure to 700 MHz, 125.9 mW input power radiofrequency or sham fields positioned with the E-field normal to the surface of the slice. The E-field intensity was 71.0 $V.m^{-1}$. Responses were normalised by averaging the responses of the five minutes preceding the RF exposure such that baseline was 100%. A change in response was defined as a sustained (> 1 minute) increase or decrease of greater than twice the standard deviation of the response during the 5 minutes preceding the exposure in the same slice (Tattersall *et al.*, 2001).

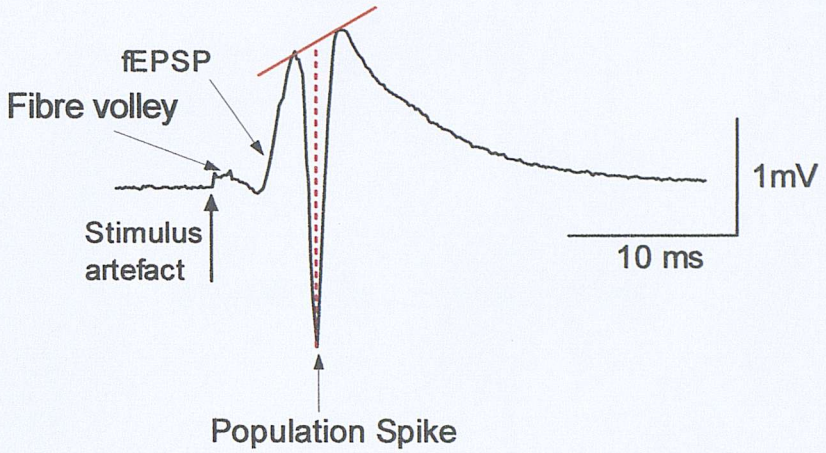

Figure 4.1 *Representative field potential recording.*
A typical control field potential recorded in the CA1 pyramidal layer evoked by stimulation (70μs pulse width) of the Schaffer collaterals in stratum radiatum. The stimulus artefact, presynaptic fibre volley, field excitatory postsynaptic potential (fEPSP) and population spike (PS) are labelled on the diagram. The dashed red line indicates the method used to calculate the population spike amplitude. The LTP program (www.LTP.com) measures the PS amplitude by drawing a straight line between the two peaks of the fEPSP (indicated as a solid red line) and then drops a vertical line (dashed red line) from the midpoint between the two peaks to the apex of the population spike.

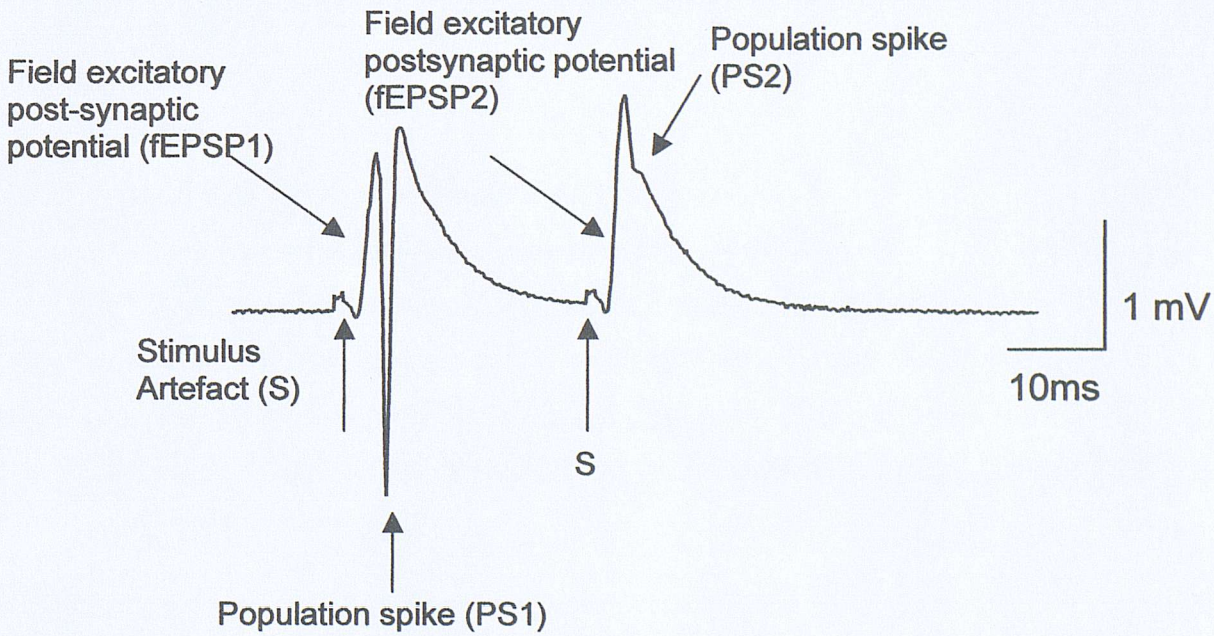

Figure 4.2 *Representative paired-pulse field potential recording.*
A typical control field potential recorded in the CA1 pyramidal layer evoked by stimulation of the Schaffer collaterals in stratum radiatum, pulse duration 70μs as before. Due to inhibitory circuits activated following the first (conditioning) pulse, the second (test) pulse evoked a smaller population spike than the first pulse. Note that labelling of the fibre volley has been omitted on both population spikes for clarity, however its position is as indicated in Figure 4.1, immediately after the stimulus artefact.

A stimulus response curve was obtained by measuring the amplitude of the evoked population spike in response to incremental increases in stimulus intensity. The intensity required to evoke a half-maximal response in each slice was used in later paired-pulse experiments.

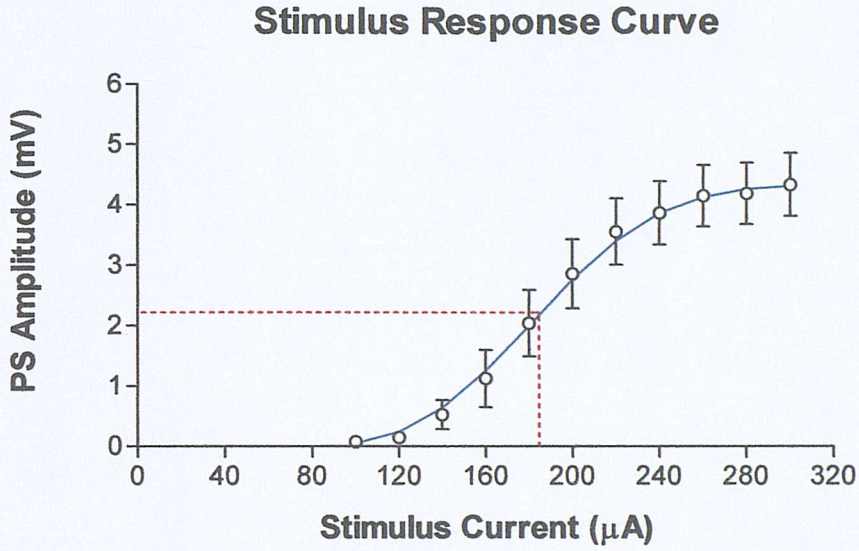

Figure 4.3 *Stimulus response curve.*

Control PS1 stimulus response curve showing the mean ± S.E. for 12 slices. Red dotted line indicates the mean half-maximal stimulus intensity (185μA).

4.2 Results.

4.2.1 Effect of RF fields on population spike amplitude.

During the exposure period, 7 out of 8 slices exposed to the RF fields showed a biphasic response consisting of an initial decrease in the CA1 population spike (PS1) amplitude followed by an increase in PS1 amplitude above baseline levels that continued after the exposure period had ended (Figure 4.7). In the eighth slice, the amplitude of PS1 decreased during exposure to the RF field, a change that persisted after the exposure was terminated.

4.2.2 Population Spike Amplitude.

In RF exposed tissue, 7 out of 8 slices displayed a maximal increase in PS1 amplitude of between 37 and 139%; the eighth slice showed a maximal decrease in amplitude of 20%. Increases in PS2 amplitude were observed in all 8 slices, these increases were generally larger than those of PS1, being between 9 and 230%.

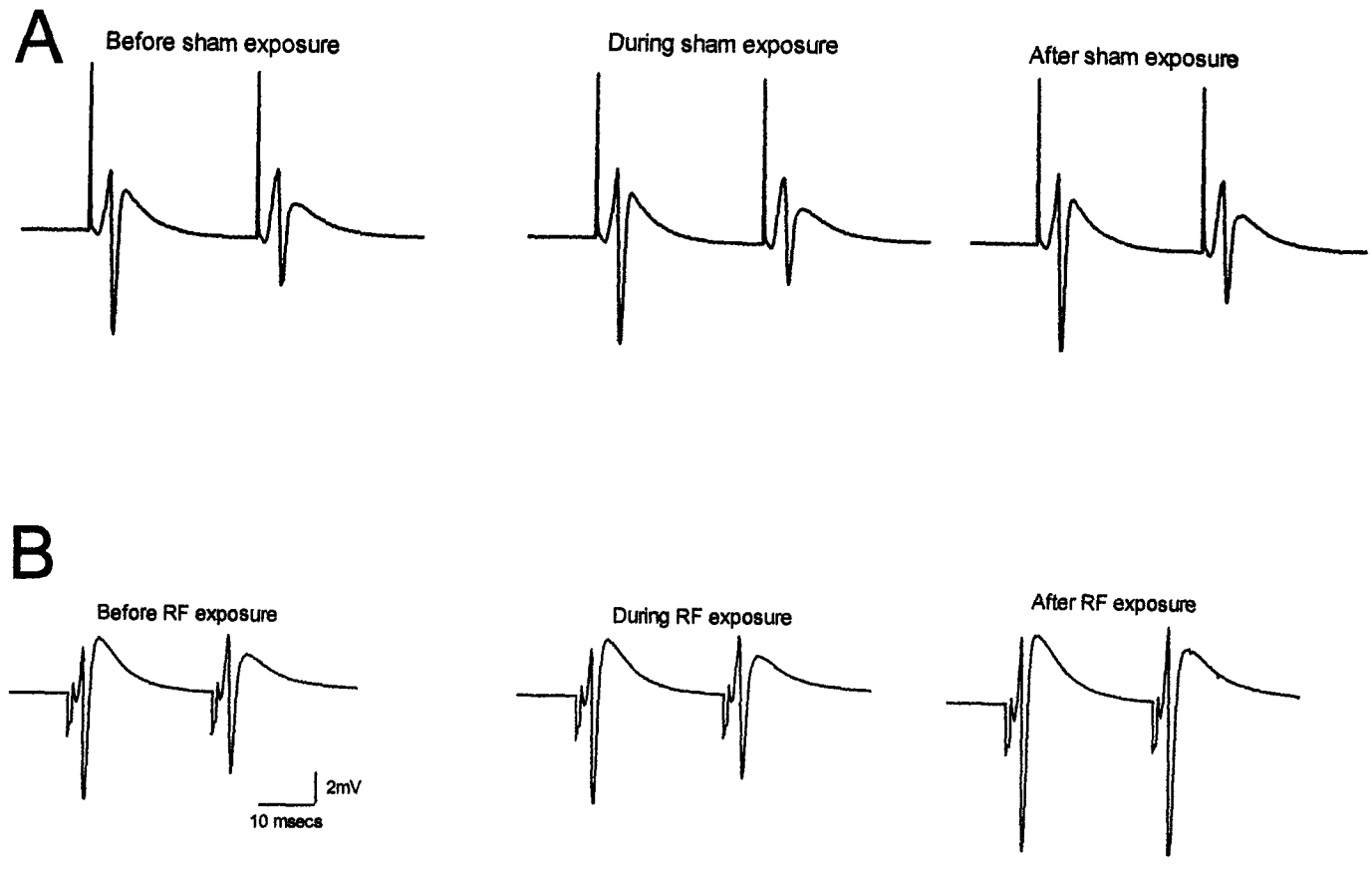

Figure 4.4 *Representative field potentials recorded before, during & after exposure to 700 MHz RF fields or sham RF fields.*
A: Sham-exposed control slices. Note the inhibition of PS2 relative to PS1. Additionally, the amplitude of both spikes is constant throughout.
B: RF exposed slices. In the before and during RF exposure traces, the amplitude of PS2 is less than PS1. After exposure, inhibition has been lost and the amplitude of both spikes has increased. Scale applies to all traces.

Figure 4.5 *Individual graphs of PS1 and 2 in slices exposed to 700MHz RF.*

Each of the 8 graphs is devoted to a single slice. In all traces, PS1 is shown as a solid blue line and PS2 as a dashed red coloured line. For comparison of data, the same Y-axis scale is applied to all eight graphs in this section and to the eight graphs of Figure 4.6 (individual graphs of PS1 and 2 in sham-exposed control slices).

Six of the eight slices showed a similar pattern of PS1amplitude in response to RF exposure, this consisted of an initial dip in PS1A at the start of the exposure period, followed by an increase PS1A towards the end of exposure and which usually remained elevated until the end of the recording period. The biphasic response of PS1A was not observed in slices 7 and 8. In contrast, five of the eight slices showed an increase in PS2A following RF exposure, the exceptions being slices 2 and 4 which showed no effect after exposure and slice 7 which displayed an increasing PS2 amplitude throughout the recording period. In general, the increase in PS2 amplitude was larger than the increase seen in PS1 amplitude.

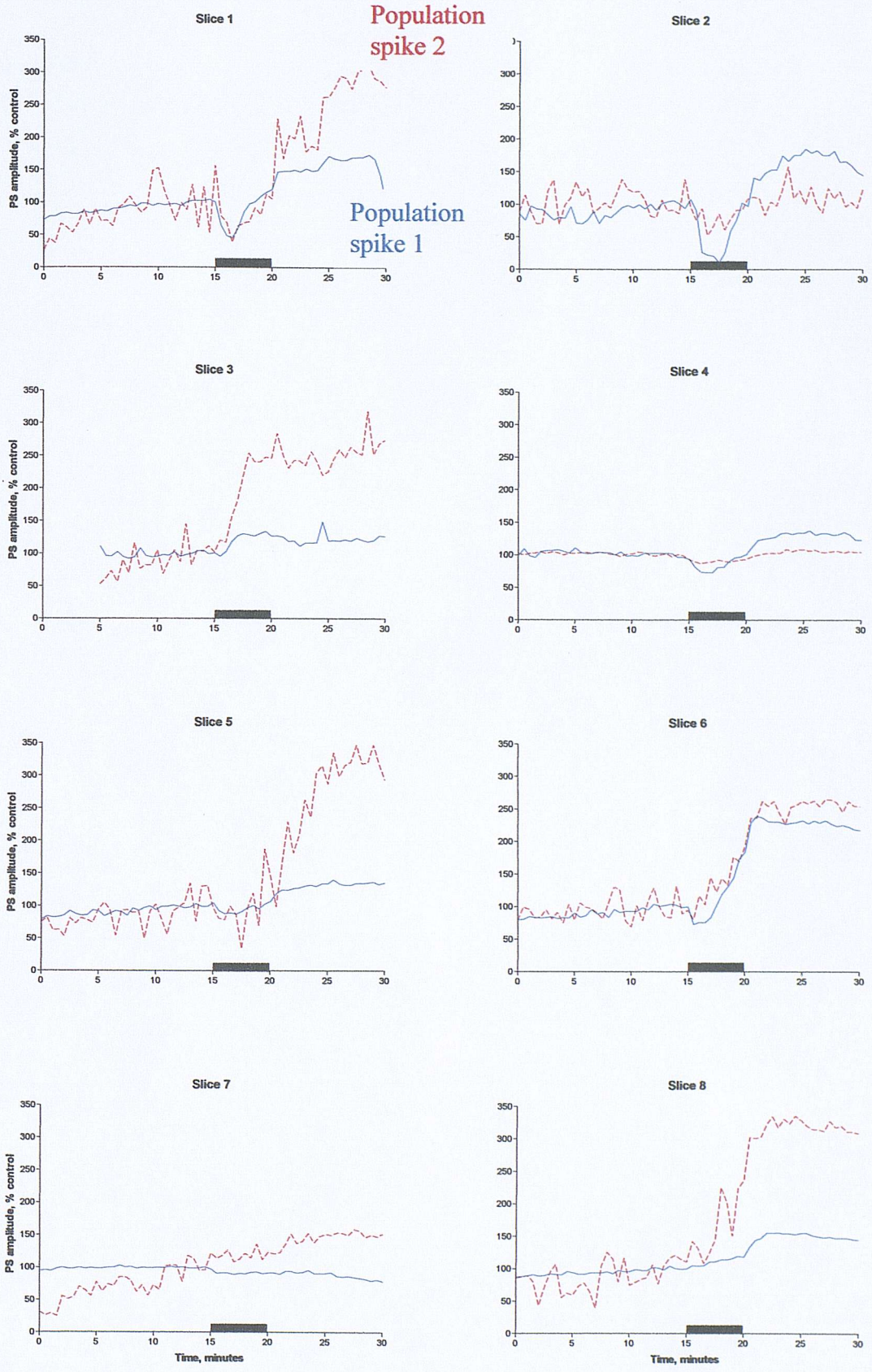

Figure 4.5 *PS1 & PS2 amplitude in slices exposed to 5-minutes 700MHz RF.*

Figure 4.6 *Individual graphs of PS1 and 2 in sham-exposed control slices.*

Each of the 8 graphs is devoted to a single slice (see figure 4.? for legend). In all traces, PS1 is shown as a solid blue line and PS2 as a dashed red coloured line. For comparison of data, the same Y-axis scale is applied to all eight graphs in this section and to the eight graphs of Figure 4.5 (individual graphs of PS1 and 2 in slices exposed to 700MHz RF fields).

In six of the eight slices, the amplitude of PS2 closely followed that of PS1. In a further 2 slices (slice 4 & 5) the amplitude of PS2 varied considerably from PS1, however, both these slices showed very good inhibition of the test response compared to the conditioning response and were therefore included in the data set.

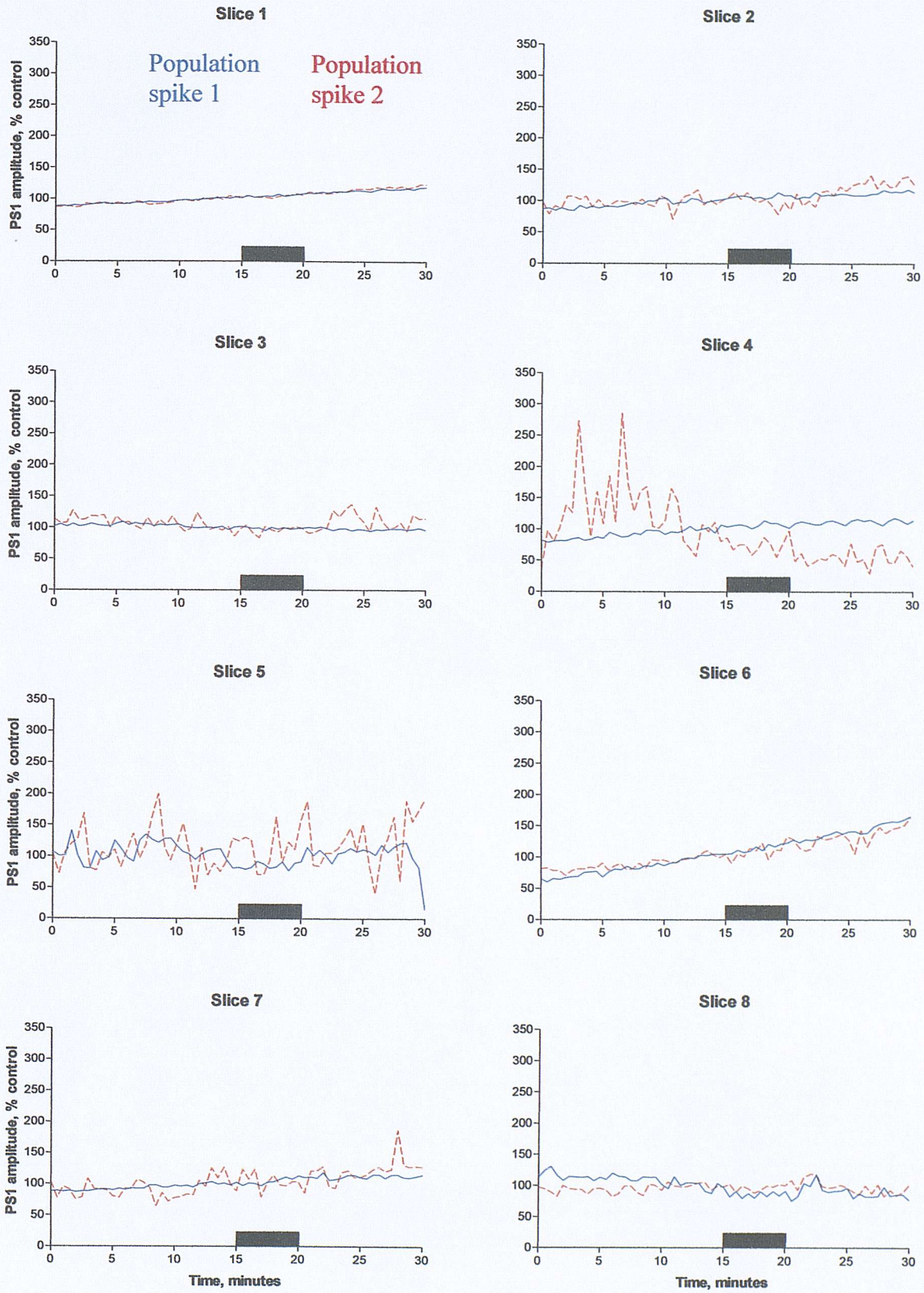

Figure 4.6 *PS1 & PS2 amplitude in slices sham-exposed to 5-minutes 700MHz RF.*

The mean change (mean ± S.D.) for all 8 slices was + 41.6 ± 15.4% for PS1 and + 81.7 ± 26.1% for PS2. The mean change in PS1 amplitude (post exposure) was significantly different from sham exposed control slices (5.8 ± 4.3%, $n = 8$) (Figure 4.8 and Table 4.3); however, the RF exposed slices showed a significant increase in the variance of the data, compared with pre-exposure levels (F-test, $P < 0.0001$) and with sham exposed controls ($P = 0.0016$) (Table 4.3). Additionally, the PS1 amplitude in sham-exposed control slices was not significantly different (either Wilcoxon matched pairs test or variance) from that of the pre-exposure baseline (Table 4.2). In common with the results for PS1, the mean change in RF exposed PS2 amplitude (+ 81.7 ± 26.1%, $n = 8$) was significantly different ($P = 0.0047$) from that of the sham exposed control slices (- 3.5 ± 6.8%, $n = 8$) (Table 4.2). As before, the RF exposed slices produced a significant increase in the variance of the data compared with both pre-exposure levels (F-test, $P < 0.0001$, PS1 and $P = 0.0115$ PS2) and with sham exposed controls (F-test, $P = 0.0016$, PS1 and $P = 0.0010$, PS2).

Table 4.1 *RF exposed slices, comparison of field potential amplitude and E-S ratio before exposure (T = 9 minutes) with after exposure (T = 21 minutes).*

	Exposure Conditions	***% Change after RF c.f. baseline***	***Statistical significance***	***Variance (F-test)***
PS1	700 MHz RF	+ 41.6 ± 15.4 (8)	P = 0.0104	P < 0.0001
PS2	700 MHz RF	+ 81.7 ± 26.1 (8)	P = 0.0047	P = 0.0115
fEPSP1	700 MHz RF	+ 28.5 ± 9.6 (8)	P = 0.0070	P = 0.0003
fEPSP2	700 MHz RF	+ 24.7 ± 9.9 (8)	P = 0.0030	P < 0.0001
E-S ratio	700 MHz RF	- 6.5 ± 6.1 (8)	N.S.	P = 0.0035

All values are given as mean ± 1 S.D. (n). Significance was assessed by unpaired, two-tailed Wilcoxon matched pairs test of values before and after RF. N.S. is not significant. P-values compare data in RF exposed slices with normalised pre-exposed levels in the same slice.

Figure 4.7 *Effect of 5-minutes exposure to 700MHz RF fields on the amplitude of PS1 and PS2.*

A: Individual slice data of the effect of RF on the amplitude of PS1.
B: Averaged data (mean ± S.D., n = 8 slices) from slices shown in figure 4.7A.
C: Individual slice data of the effect of RF on the amplitude of PS2.
D: Averaged data (mean ± S.D., n = 8 slices) from slices shown in figure 4.7C.
Note that the same colour has been used in both graphs for an individual slice, for example, slice 1, shown in red on figure 4.7A is also shown in red on figure 4.7C.
The black bar in all graphs indicates the period of RF exposure.

Figure 4.7 *Effect of 5-minutes exposure to 700MHz RF fields on the amplitude of PS1 and PS2.*

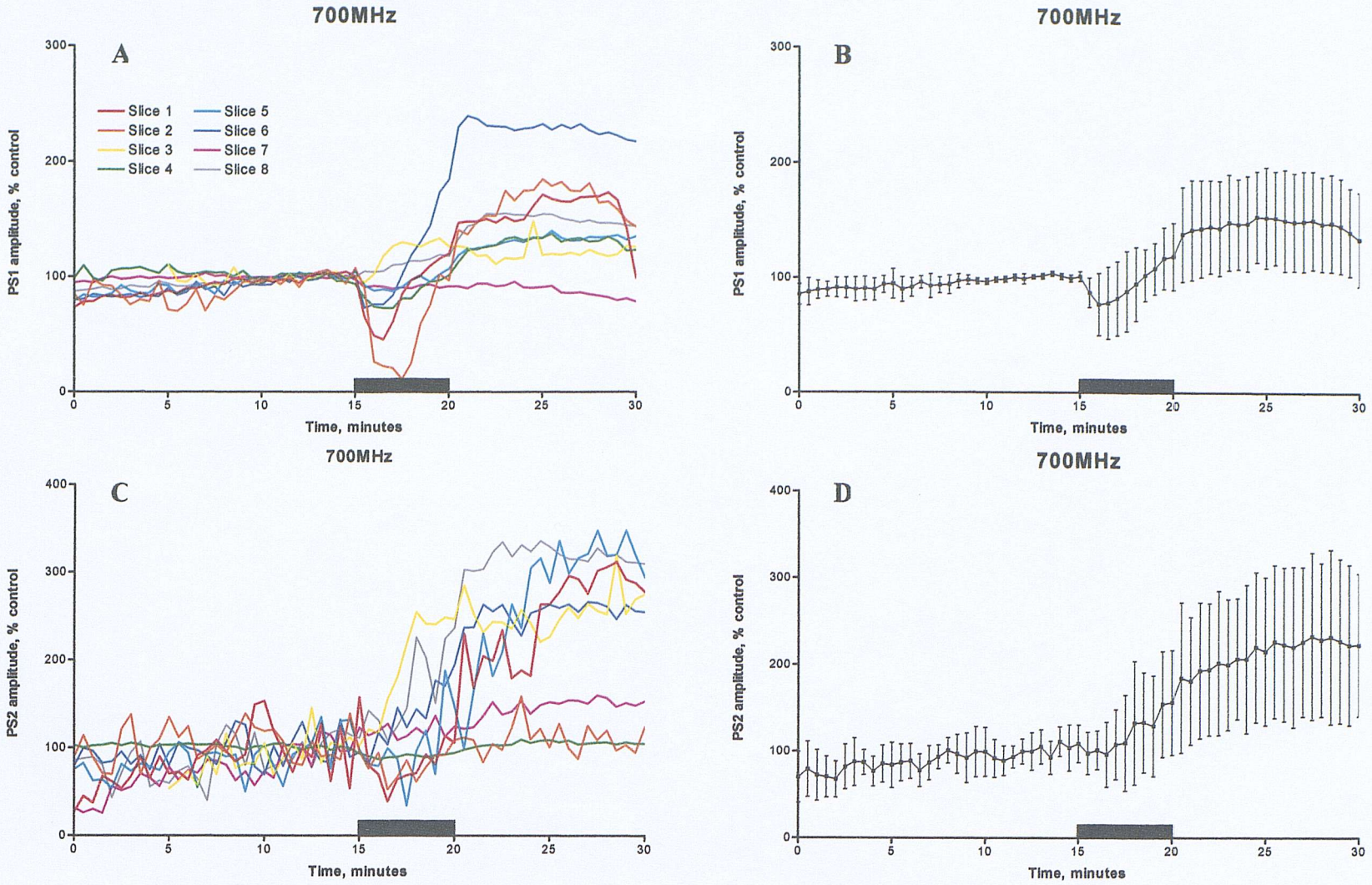

Figure 4.8 *Changes in individual population spike amplitude in sham-exposed control slices.*

Top left: Individual slice data of the effect of sham-exposure to RF on the amplitude of PS1. **Top right:** Averaged data (mean ± S.D., n = 8 slices) from slices shown in the top left panel. **Bottom left:** Individual slice data of the effect of sham-exposure to RF on the amplitude of PS2. **Bottom right:** Averaged data (mean ± S.D., n = 8 slices) from slices shown in the bottom left panel. Note that the same colour has been used in both graphs for an individual slice, for example, slice 1, shown in red on the top left figure is also shown in red on the bottom left figure. The black bar in all graphs indicates the period of sham exposure; the dashed blue line on the right hand figures indicates the baseline level of 100%.

Figure 4.8 *Changes in individual population spike amplitudes in sham-exposed control slices.*

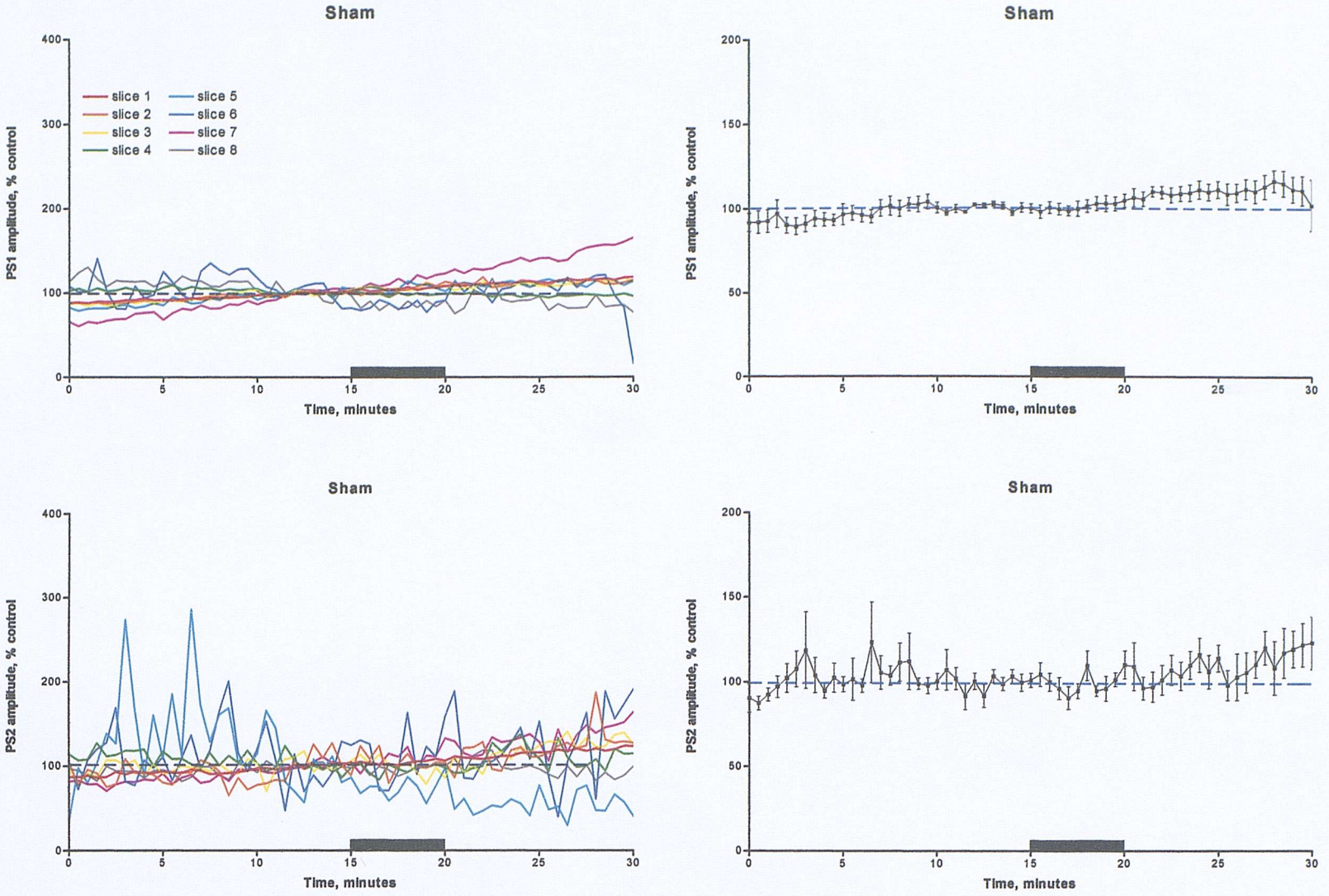

Table 4.2 Sham exposed slices, comparison of field potential amplitude and E-S ratio before exposure (T = 9 minutes) with after exposure (T = 21 minutes).

	Exposure conditions	*% Change after sham c.f. baseline*	*Statistical significance*	*Variance (F-test)*
PS1	Sham	+ 5.8 ± 4.3 (8)	N.S.	N.S.
PS2	Sham	- 3.5 ± 6.8 (8)	N.S.	P = 0.0409
fEPSP1	Sham	+12.8 ± 4.6 (8)	P = 0.0047	P = 0.0028
fEPSP2	Sham	+ 6.4 ± 3.6 (8)	P = 0.0499	P = 0.0104
E-S ratio	Sham	- 5.82 ± 3.6 (8)	P = 0.0379	N.S.

All values are given as mean ± 1 S.D. (*n*). Significance was assessed by unpaired, two-tailed Wilcoxon matched paire test of values before and after sham exposure. N.S. is not significant. P-values compare data from sham-exposed control slices with normalised pre-exposed levels in the same slice.

Table 4.3 *Comparison of field potential amplitudes and E-S ratio between RF and sham-exposed control slices (1 minute after exposure ended).*

	Exposure conditions	*% Change after RF or sham exposure c.f. baseline*	*Statistical significance*	*Variance (F-test)*
PS1	700 MHz RF	+ 41.6 ± 15.4 (8)		
	Sham	+ 5.8 ± 4.3 (8)	P = 0.0104	P = 0.0016
PS2	700 MHz RF	+ 81.7 ± 26.1 (8)		
	Sham	- 3.5 ± 6.8 (8)	P = 0.0047	P = 0.0010
fEPSP1	700 MHz RF	+ 28.5 ± 9.6 (8)		
	Sham	+12.8 ± 4.6 (8)	N.S.	P = 0.0339
fEPSP2	700 MHz RF	+ 24.7 ± 9.9 (8)		
	Sham	+ 6.4 ± 3.6 (8)	N.S.	P = 0.0078
E-S ratio	700 MHz RF	- 6.5 ± 6.1 (8)		
	Sham	- 5.82 ± 3.6 (8)	N.S.	N.S.

All values are given as mean ± 1 S.D. (*n*). Significance was assessed at 1-minute post exposure by unpaired, two-tailed Mann Whitney test. N.S. is not significant. P-values compare data between RF and sham exposed groups.

4.2.3 Effect of RF fields on field excitatory postsynaptic potential amplitude.

The effects of RF exposure on the field excitatory postsynaptic potential (*f*EPSP) were of similar direction, although of smaller amplitude than those of population spike amplitude. In line with the results for PS amplitude, 7 out of 8 slices exposed to the RF fields showed an initial decrease in the amplitude of the CA1 *f*EPSP during the first minute of RF exposure but increased in amplitude by the end of the exposure (Figure 4.9). At the end of the exposure period, all 8 slices displayed a maximal increase in *f*EPSP1 amplitude of between 8 and 93%.

In common with the *f*EPSP1 results, the amplitude of *f*EPSP2 increased during RF exposure in all 8 slices. Increases in *f*EPSP2 amplitude occurred towards the end of the exposure period (8 out of 8 slices). Increases ranged from 4 to 119% and were larger than those of *f*EPSP1; the mean change for all 8 slices was + 57.1 ± 28.6%, *f*EPSP1 and + 57.5 ± 43.2% *f*EPSP2. The mean change in *f*EPSP1 amplitude (+ 57.1 ± 28.6%, $n = 8$) was not significantly different from sham exposed control slices (+12.8 ± 4.6 %, $n = 8$) (Table 4.2) although the variance of the data was significantly different (*F*-test, P = 0.0330). The *f*EPSP1 amplitude in RF exposed slices was significantly different from pre-exposure baseline levels (P = 0.0070) (Table 4.1). *f*EPSP1 amplitude in sham-exposed slices was significant at P = 0.0047 compared to pre-exposure levels in the same slices. As before, the variance of the data was significantly different (*F*- test, P = 0.0028) (Table 4.2).

Similar results to *f*EPSP1 were obtained for *f*EPSP2 in slices exposed to RF. As before, the mean change in amplitude (+24.7 ± 9.9%, $n = 8$) was not significantly different from sham-exposed control slices (+6.4 ± 3.6%, $n = 5$) post exposure (Table 4.3) but the variance was significant (*F*-test, P = 0.0078). Comparison of the *f*EPSP2 amplitude in RF exposed slices revealed a significant difference (P = 0.0030) when compared with pre-exposure baseline levels (Table 4.1). As was the case for *f*EPSP1 in sham-exposed slices, significant differences were observed when compared to pre-exposure level in the same slices (P= 0.0499) additionally, the variance of the data was significant at P = 0.0104, ($n = 8$, *F*-test) (Table 4.2).

Figure 4.9 Effect of 5-minutes exposure to 700MHz RF fields on *f*EPSP1 *and fEPSP2 slope.*

Top left: Individual slice data of the effect of exposure to 700MHz RF on *f*EPSP1 slope. **Top right:** Averaged data (mean ± S.D., n = 8 slices) from slices shown in the top left panel. **Bottom left:** Individual slice data of the effect of exposure to 700MHz RF on *f*EPSP2 slope. **Bottom right:** Averaged data (mean ± S.D., n = 8 slices) from slices shown in the bottom left panel. Note that the same colour has been used in both graphs for an individual slice, for example, slice 1, shown in red on the top left figure is also shown in red on the bottom left figure. The black bar in all graphs indicates the period of RF exposure; the dashed blue line on the right hand figures indicates the baseline level of 100%.

Figure 4.9 *Effect of 5-minutes exposure to 700MHz RF fields on fEPSP1 and fEPSP2 slope.*

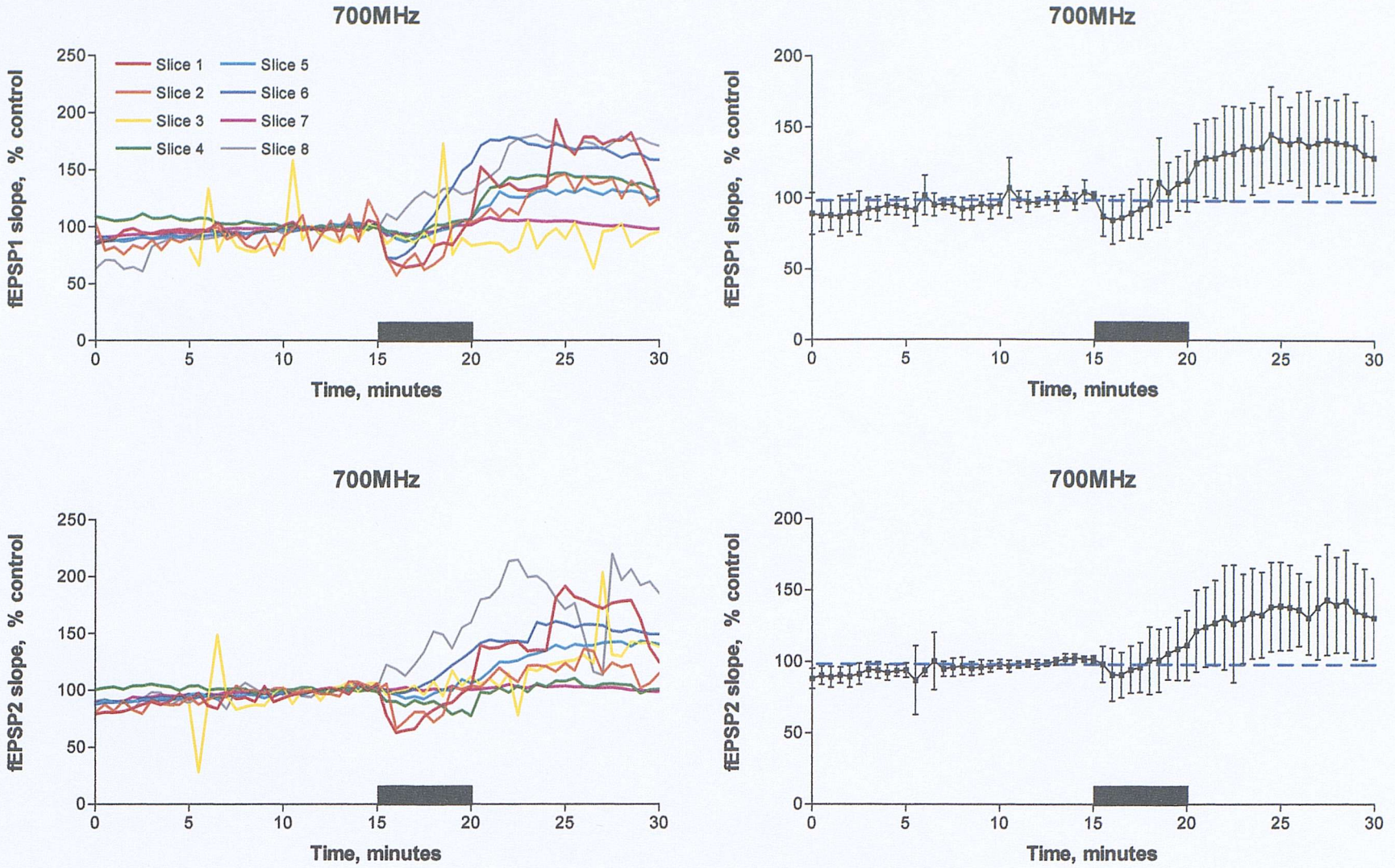

Figure 4.10 *Effect of 5-minutes sham exposure to 700MHz RF fields on fEPSP1 and fEPSP2 slope.*

Top left: Individual slice data of the effect of sham- exposure to 700MHz RF on *f*EPSP1 slope. **Top right:** Averaged data (mean ± S.D., $n = 8$ slices) from slices shown in the top left panel. **Bottom left:** Individual slice data of the effect of sham-exposure to 700MHz RF on *f*EPSP2 slope. **Bottom right:** Averaged data (mean ± S.D., $n = 8$ slices) from slices shown in the bottom left panel. Note that the same colour has been used in both graphs for an individual slice, for example, slice 1, shown in red on the top left figure is also shown in red on the bottom left figure. The black bar in all graphs indicates the period of sham exposure; the dashed blue line on the right hand figures indicates the baseline level of 100%.

Figure 4.10 *Effect of 5-minutes sham-exposure to 700MHz RF fields on fEPSP1 and fEPSP2 slope.*

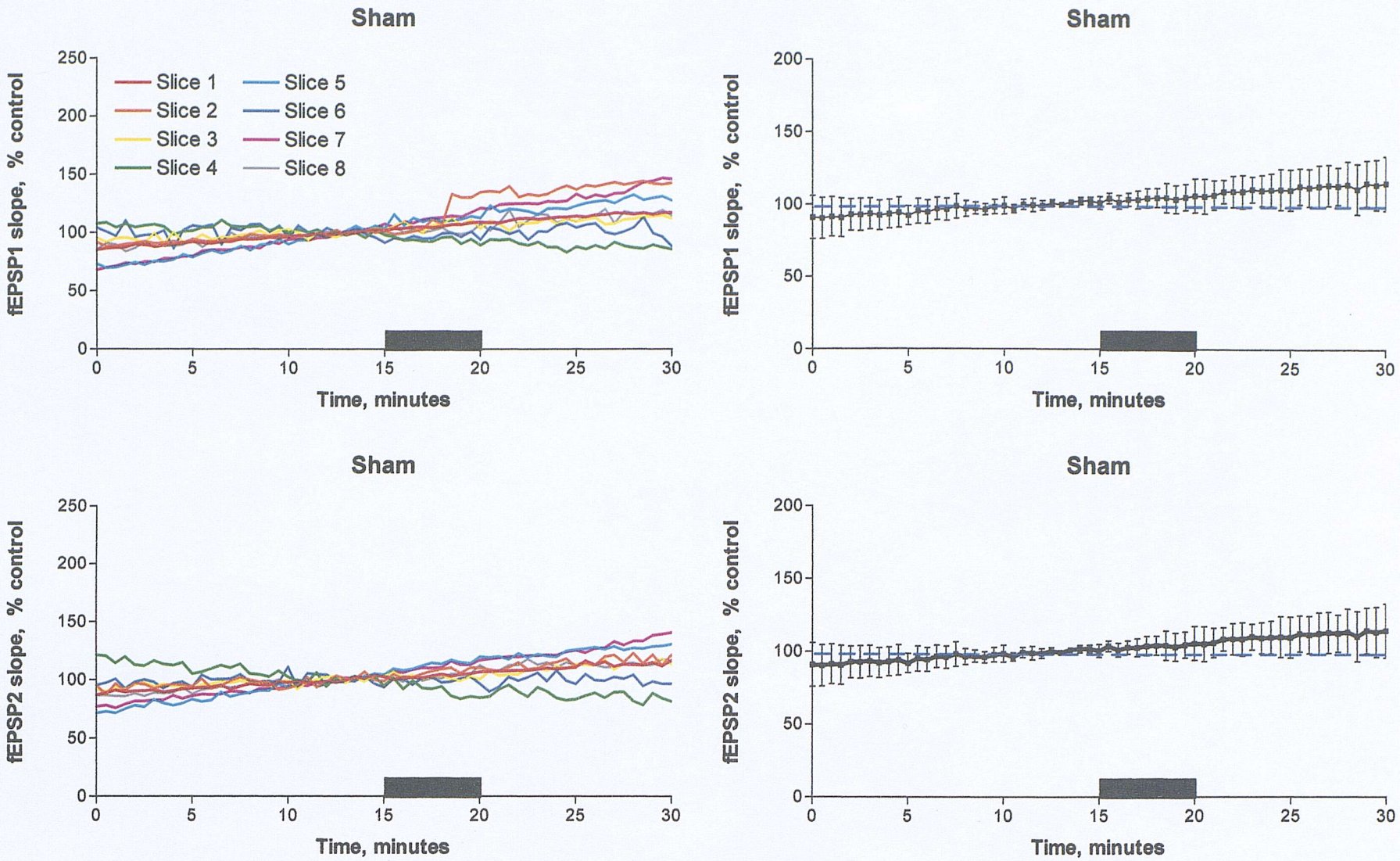

4.2.4 Effect of RF fields on the fEPSP-PS (E-S) ratio.

The effect of RF fields on the ratio of *f*EPSP slope and the PS amplitude were determined for the first response (PS1 and *f*EPSP1) of the paired-pulse paradigm. The E-S ratio gives an indication of the excitability of the pyramidal cells in the slice; an increase in E-S ratio above 100% indicates an increase or potentiation of pyramidal cell excitability and a decrease below baseline levels indicates a reduction or depression of excitability. During RF exposure ($n = 8$ slices), a transient increase in the E-S ratio was observed that returned to baseline levels by the end of the exposure period. On further examination of the data it was found that the transient peak was brought about by one of the eight sets of data (orange line on top right panel of figure 4.11), removal of this data set from the averaged traces removed this transient peak. No transient was seen in any of the sham-exposed control slices ($n = 8$) or in any of the other seven RF exposed slices. The mean peak of the transient in RF exposed slices was + 55.0 ± 60.7% above baseline levels but was not significantly different from the baseline response.

4.2.5 Effect of RF fields on inhibition.

Paired-pulse inhibition is seen as a reduction in the size of the test (T) field potential response resulting from a previously evoked conditioning (C) spike. For each pair of conditioning and test field potential events, the inhibition or facilitation of the response was determined from the ratio (test response (PS2) / conditioning response (PS1)). A T/C of zero indicates total inhibition of the test population spike whilst a T/C of >1 indicates facilitation of the test population response.

Slices exposed for 5-minutes to 700MHz radiofrequency fields clearly displayed paired-pulse inhibition (mean ratio = 0.67 ± 0.2, $n = 8$ slices) prior to the RF insult (figure 4.4 and 4.12). At 1-minute post RF, the mean ratio had decreased to 0.81 ± 0.1, ($n = 8$ slices) however comparison of RF fields before and after insult was not significantly different. During the exposure period, the first population spike (PS1) amplitude transiently decreased (7 out of 8 slices) before subsequently increasing in amplitude beyond the pre-exposed level. The increases in PS1 amplitude persisted after the exposure was terminated.

Figure 4.11 *Effect of 700MHz or sham fields on E-S ratio.*

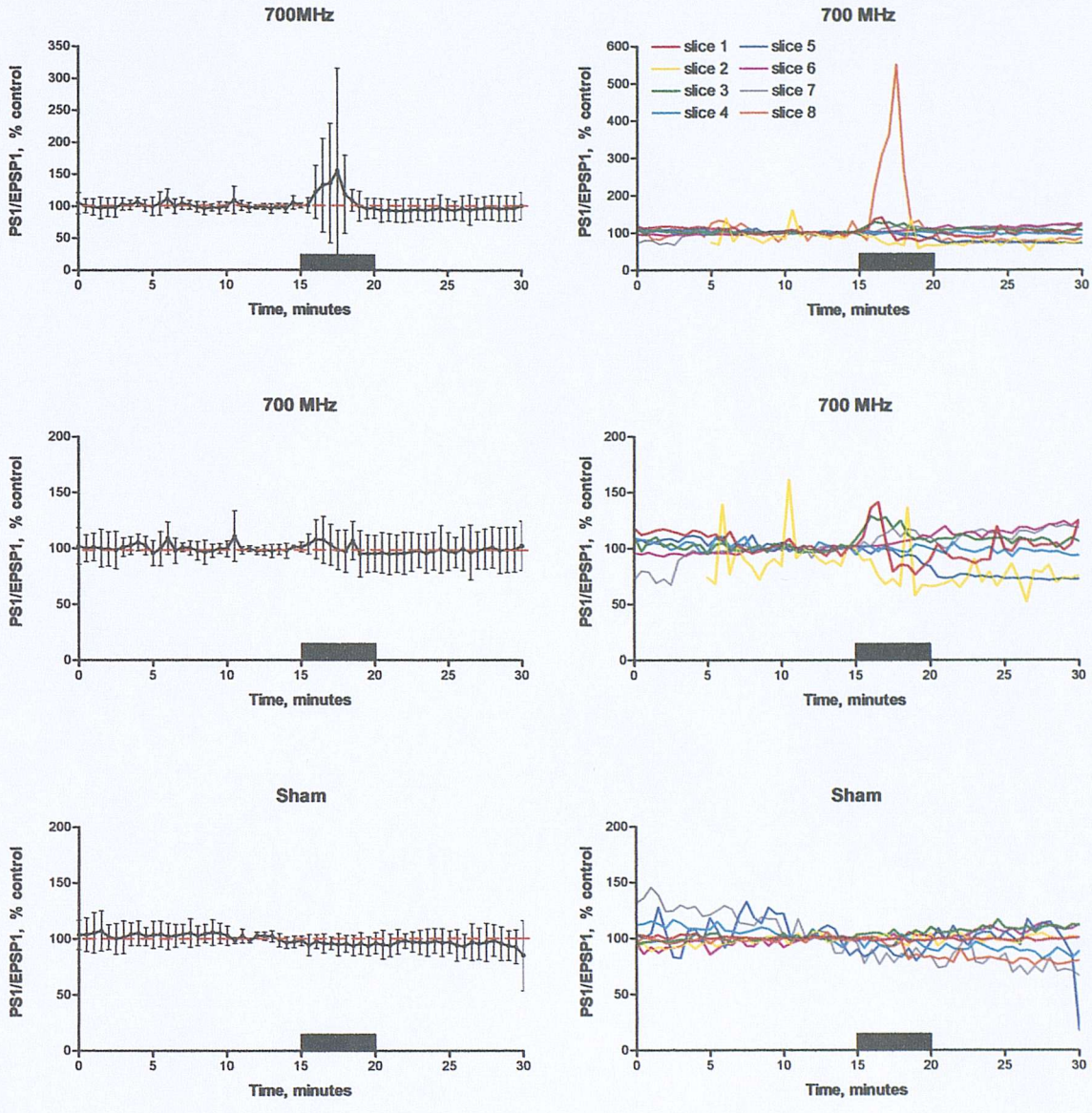

Legend: The three graphs printed on the left of the figure show averaged data (mean ± S.D) of the effect of RF or sham exposure on the E-S ratio. The dashed red line indicates the baseline value of 100% and the solid black bar is the period of RF or sham exposure. The coloured graphs to the right of the figure show individual slice data. Graphs are arranged in pairs such that individual slice data and its corresponding averaged data graph appear side by side.

Top left: Averaged data of E-S ratio for all eight slices exposed to RF. **Top right:** Individual slice data corresponding to top left graph. The transient peak in E-S ratio observed during RF exposure has been caused by one data set (slice 8). Note that the maximum value on the Y-axis differs between top left and right graphs to display the transient peak to best advantage. **Middle left:** similar data to top left except that slice 8 (orange line) data has been removed. Removal of this data abolishes the transient peak during RF exposure. **Middle right:** Individual traces of remaining seven RF exposed slices. **Bottom left:** Averaged data of E-S ratio for all eight slices sham-exposed to RF. **Bottom right:** Individual slice data corresponding to bottom left graph.

Figure 4.12 *Effect of 700MHz RF or sham fields on inhibition.*

Top left: Graph shows eight individual recordings of the ratio of PS2/PS1 in eight slices exposed to 700MHz RF. Each slice is represented by a different colour. **Bottom left:** Averaged data (mean ± 95% confidence limit) of the eight slices in the top left graph. **Top right:** Effect of sham-exposure to 700MHz RF fields on the ratio of PS2/PS1 (n = 8 slices). **Bottom right:** Averaged data (mean ± 95% confidence limit) of the eight slices in the top right graph. Note that in all graphs, the black bar indicates the period of sham or RF exposure. Additionally, the dashed blue line commencing at 1.0 on the Y-axis of the bottom two graphs indicates the point where the amplitude of PS2 is equal to PS1. Data points with a value of <1 indicate inhibition and data points with a value >1 indicate facilitation of the response.

Figure 4.12 *Effect of 700MHz RF or sham fields on inhibition.*

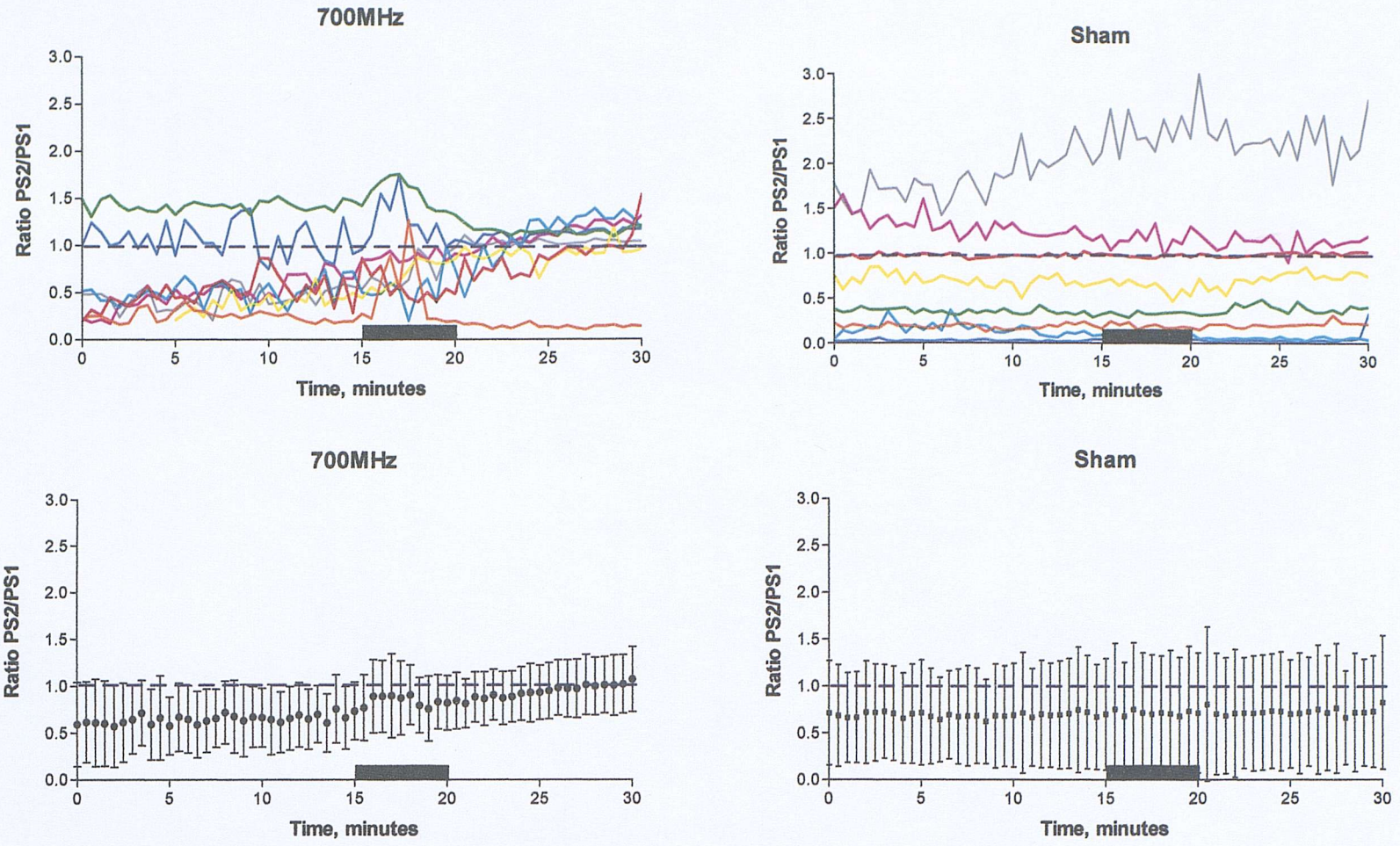

In the RF exposed slices, there was reduced inhibition and facilitation of the second population spike response by the end of the recording period. By comparison, sham-exposed control slices displayed paired-pulse inhibition before, during and after the RF insult (Figure 4.4 and 4.12). The mean paired-pulse inhibition ratio in sham-exposed control slices was 0.68 ± 0.66, (n = 8 slices) prior to the insult, decreasing to 0.70 ± 0.78 (n = 8 slices) at 1-minute post exposure. As before, these ratios were not significantly different from the pre-exposure baseline or from post exposure RF values.

4.3 Discussion.

The results of the extracellular field potential experiments indicate that acute exposure to 700 MHz electromagnetic fields produced significant changes in the inhibitory response of hippocampal pyramidal cells.

At the low field intensity (71.0 $V.m^{-1}$, ~ 4.4$mW.kg^{-1}$, SAR) used in these experiments, the predominant effect was a potentiation of the amplitude of the evoked population spike of both PS1 and PS2 with the increase being greater for PS2 (+ 41.6 ± 15.4% for PS1 and + 81.7 ± 26.1%, PS2) in RF exposed slices. These results are in agreement with Tattersall *et al* (2001), who reported similar effects on PS1 amplitude; however, no comparison can be made for the PS2 results, as the authors did not examine that parameter.

The mean change in PS1 amplitude in RF exposed slices was significantly different from baseline data obtained in the same slices and from sham-exposed control slices compared at a time after the exposure had ended. Similarly, the mean change in PS2 amplitude was different from baseline data obtained in the same slices and from sham-exposed control slices compared 1-minute post exposure. As was expected, neither PS1 nor PS2 in sham-exposed control slices were significantly different from baseline data in the same slices (Table 4.2) although the variance of PS2 sham-exposed data was significantly different from the pre-exposure baseline. Changes in the *f*EPSP amplitude (both *f*EPSP1 and 2) were smaller than those of the population spike amplitude (PSA1 and 2). However, the change in amplitude was of a similar magnitude in both *f*EPSP's in a given group (Table 4.1 and 4.2).

It is possible that the changes in excitability will have been due in part to the presence of the metal stimulating electrode in the RF field. One method of determining

whether the increases in excitability were due to artefacts induced by the metal stimulating electrode would be to remove the electrode from the preparation. This approach was adopted by Tattersall *et al.*, (2001); who used the potassium channel blocker 4-aminopyridine (4-AP) to induce spontaneous epileptiform activity in the tissue, thereby removing the requirement for a stimulating electrode. The authors demonstrated that changes in the spontaneous activity occurred in approximately one third of the slices exposed to RF electromagnetic fields, a similar proportion to that seen in the evoked slice experiments. These experiments indicate that the presence of the stimulating electrode did not have an effect on the evoked response at the low field intensity used here.

A second possible source of artefact could be the presence of the glass-recording electrode in the electromagnetic field. Several studies have shown that the glass-recording pipette does not measurably distort EM fields in biological tissue (for example, Johnson and Guy, 1972; Field *et al.*, 1992). Furthermore, a study by Seaman and Wachtel (1978) found that less than 10pA of current was generated in glass microelectrodes filled with 2.5M KCl during exposure to 1.5 or 2.5 GHz EM fields in a stripline waveguide exposure system. Since the current required to evoke electrical activity in a brain slice is several orders of magnitude larger than the current that may be induced by the recording electrode, it is doubtful that an interaction between the recording electrode and the RF field could be responsible for the observed effects on evoked field potentials.

Normally, potentiation or depression of the postsynaptic response is assessed from stimulus response curves (SRC's) obtained before, during and after the experimental treatment (Chavez-Noriega and Bliss, 1991; Bernard and Wheal, 1995a, b; Wheal *et al.*, 1998). The extracellular field generated by the post-synaptic current (E, amplitude of the fEPSP slope) and action potential generation in the population of post-synaptic neurones (S, amplitude of the population spike) are recorded at a range of stimulus intensities. Plotting the population spike amplitude as a function of the EPSP amplitude provides an input/output (I/O) relationship or EPSP/spike curve (E/S curve) (Wheal *et al.*, 1998). Comparison of the E/S curves obtained before and after conditioning stimuli provides an indication of altered pyramidal cell excitability. A shift of the E/S curve to the left indicates a potentiation of the response; cells are closer to firing threshold (Wheal *et al.*, 1998). A leftward shift occurs after the induction of

long-term potentiation (LTP) (Teyler and DiScenna, 1987; Bernard and Wheal, 1995a, b; Wheal *et al.*, 1998) & after application of the $GABA_A$ antagonist picrotoxin or the muscarinic agonist carbachol (see Chavez-Noriega and Bliss (1991) for review). A shift to the right indicates a depression of the response. These shifts are associated with long-term depression (LTD) (Wheal *et al.*, 1998;) or by application of the NMDA receptor antagonist APV (Chavez-Noriega and Bliss (1991).

In the current experiments, although SRC data was recorded before baseline recording of field potentials, it was not possible to obtain a stimulus response curve during the exposure period because the amplitude of the response changed repeatedly during RF exposure even when stimulus intensity was constant; this factor would make for difficult interpretation of SRC data. For this reason, and although not the normal method of assessing potentiation as described above, the ratio of the field excitatory postsynaptic potential divided by the population spike at half-maximal stimulus intensity was used as a surrogate measure to examine excitability. An increase in E-S ratio above 100% indicates an increase in pyramidal cell excitability (similar to a leftward shift is the E-S curve) whereas a reduction in E-S ratio below 100% indicates reduced excitability.

In the present study, increases in population spike amplitude seen after exposure to RF electromagnetic fields (Figure 4.4 and 4.7) appeared similar to those obtained from LTP induced by high-frequency or theta stimulation (Bliss & Lomo, 1973; Jefferys, 1985; Buzsaki *et al.*, 1987; Bliss & Collingridge, 1993). Furthermore, the E-S ratio in RF exposed slices showed an increase in excitability that was similar to the leftward shift seen in LTP. However, the E-S ratio increase was only transient, (having occurred in only one slice) is contrary to the long-lasting potentiation that occurs during LTP.

Tattersall *et al.*, (unpublished observations) examined the induction of LTP after 5-minutes exposure to 700 MHz RF fields. The authors found that LTP could still be induced by theta stimulation of afferent pathways after RF exposure. That LTP can still be induced after RF exposure does not rule out the possibility that the increases in excitability observed in this and the Tattersall *et al.*, (2001) study were due to LTP. A study by Barnes *et al.*, (1994) examined the induction of LTP in the fascia dentate of rats subjected to high frequency stimulation (ten 25-millisecond bursts of 400 Hz,

delivered at 0.1 Hz). The authors found that standard protocols used to induce LTP do not saturate the process at any dorsoventral level.

Pharmacological experiments in the next chapter will attempt to ascertain whether the effects on field potential amplitude seen in response to RF fields are a form of long-term potentiation. Application of the NMDA receptor antagonists APV or MK801 to the preparation would be expected to block the induction of LTP and help to define a potential mechanism of the observed effects.

5 PHARMACOLOGY

Because the effects of RF exposure on slice electrophysiology (Chapter 4) showed some similarity to LTP and LTD a series of experiments were conducted to investigate the contribution of the N-methyl-D-aspartate (NMDA) receptor to the amplitude of the population spike and *f*EPSP. Two selective NMDA receptor antagonists were used to block these receptors during exposure to RF electromagnetic fields. The first of these, D-APV is a competitive antagonist, which competes with glutamate and NMDA for the same ligand-binding site (Magnusson, 1998). The second, MK801 is a non-competitive antagonist, which binds within the ion channel and blocks the flow of ions (Magnusson, 1998).

A subsequent set of experiments explored the possibility that gap junctions may be involved in the RF induced effects. Gap junctions are specialised connections between cells that consist of many pores that allow the passage of molecules up to about 900 Daltons (described later). Gap junctions are required for some emergent properties of neuronal networks in the hippocampus such as gamma frequency (30-100Hz) oscillations (Jefferys *et al.*, 1996; Traub, *et al.*, 1998; 1999) and have been implicated in the spread of epileptic activity. Several compounds have been reported to block gap junctions, one of the most selective being carbenoxolone, which was used in the present study.

5.1 Glutamate and the NMDA receptor.

As reported in Chapter 1, glutamate is the major neurotransmitter in the hippocampus (Johnston and Amaral 1998). Glutamate is released from several sites in the hippocampus including the perforant path, mossy fibres, commissural-associational fibres and Schaffer collaterals and is also released from certain types of excitatory interneuron (see Johnston and Amaral 1998 for review).

Glutamate acts on two main types of receptor, the metabotropic glutamate receptor (mGluR) and ionotropic glutamate receptors. Metabotropic glutamate receptors are found on both the pre and postsynaptic side of the synapse (Johnston and Amaral 1998) and coexist with different combinations of ionotropic receptors postsynaptically. These receptors modulate transmitter release presynaptically (Johnston and Amaral, 1998) and mediate their actions through G-proteins, which either gate ion channels or

activate second messenger molecules. The second type of glutamate receptor, the ionotropic receptors, are a family of receptors that include AMPA, kainate (KA) and NMDA receptors, all named for the ligand used to characterize them. These receptors directly gate ion channels that are part of the receptor-molecule complex (Johnston and Amaral, 1998), and all open channels that are nonselective for Na^+ and K^+ ions, additionally, some AMPA / KA receptors and all NMDA receptors are permeable to Ca^{2+}.

The NMDA receptor is voltage dependant (Mayer *et al.*, 1984; Ben Ari *et al.*, 1997; Winder and Schramm., 2001). At membrane potentials near to the resting membrane potential (E_m) the channel pore is blocked by magnesium from the extracellular side. Removal of the magnesium block is achieved by repetitive synaptic activation, leading to depolarisation and allowing calcium to enter the neuron (Greenamyre, 1994; Magnusson, 1998). NMDA receptors have been implicated in the initiation of LTP, a cellular phenomenon that is believed to underlie some types of memory (Bliss & Lomo., 1973; Bliss & Collingridge., 1993; Collingridge & Watkins, 1994; Teyler *et al.*, 1995; Morris & Frey., 1997).

5.1.1 Structure of the NMDA receptor.

The NMDA receptor complex is a large protein formed from multimeric heteromers (Greenamyre, 1994). Two families of NMDA-receptor subunits have been identified in rats and humans, they have been termed NMDAR1 and NMDAR2 (Greenamyre, 1994; Magnusson, 1998).

The NMDAR1 subunit is found extensively, throughout the cortex and hippocampus (Greenamyre, 1994; Magnusson, 1998). Functional homomeric receptors formed from NMDAR1 subunits have been shown to respond to glutamate, glycine and MK801 (see Magnusson, 1998 for review) suggesting that the binding sites for these ligands are present on this subunit. The NMDAR2 subunit shows a more restricted distribution in the central nervous system (Greenamyre, 1994). This family contains at least four members (Magnusson, 1998) and shows a high degree of homology between species. Each of the four subunits can combine with the NMDAR1 subunit to form heteromeric NMDA receptors. In the human and rat, the NMDAR2-D subunit has been demonstrated to enhance the activity of the NMDA receptor when coupled with the NMDAR1 subunit.

The NMDA receptor has multiple binding sites for different ligands including glutamate, NMDA, glycine, magnesium, and zinc and also includes a site within the channel pore which binds certain non-competitive antagonists (Meldrum., 1994; Magnusson., 1998).

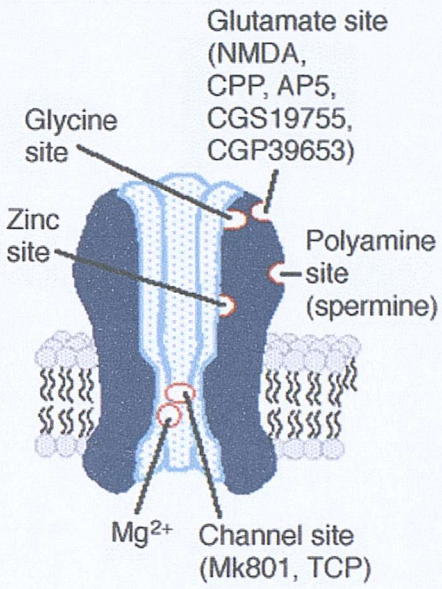

Figure 5.1 *Binding sites associated with the NMDA receptor complex*
Diagram adapted from Magnusson. (1998).

Table 5.1 *Agonists and antagonists at the NMDA receptor complex.*
Adapted from Greenamyre (1994)

Receptor binding site	***Agonist***	***Antagonist***
Transmitter site	Glutamate NMDA Ibotenate Quinolinate	D-AP5 D-AP7 CPP CGS 19755
Glycine site	Glycine D-serine	5,7-Dichlorokynurenate HA 966
Ion channel site		MK 801 TCP PCP Remacemide
Polyamine site	Spermine	Ifenprodil

D-AP5 2-amino-5-phosphovaleate D-AP7 2-amino-7-phosphovaleate
MK 801 Dizocilpine maleate PCP Phenyclidine
CPP 3-((±)-2-carboxypiperazin-4-yl) propyl-1-phosphonic acid
HA 966 3-amino-1-hydroxy-2-pyrrolidone
TCP (1-(2-thienyl) cyclohexyl) piperadine)/N-(1-thienyl)-cy-clohexyl-3, 4-piperadine
CGS 19755 1-(cis-2-carboxypiperadine-4-yl) methyl-1-phosphonic acid

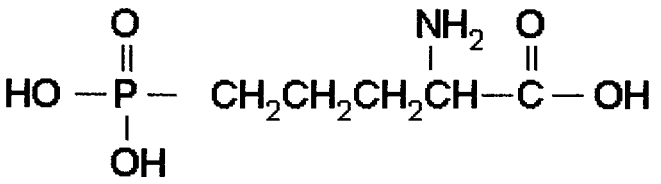

Figure 5.2 *Chemical structure of D-APV*

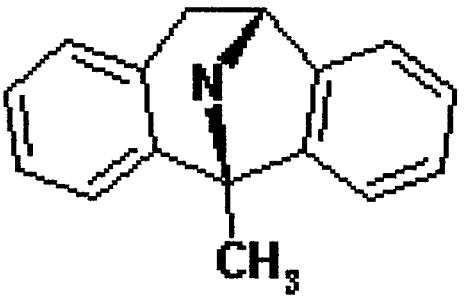

Figure 5.3 *Chemical structure of MK801*

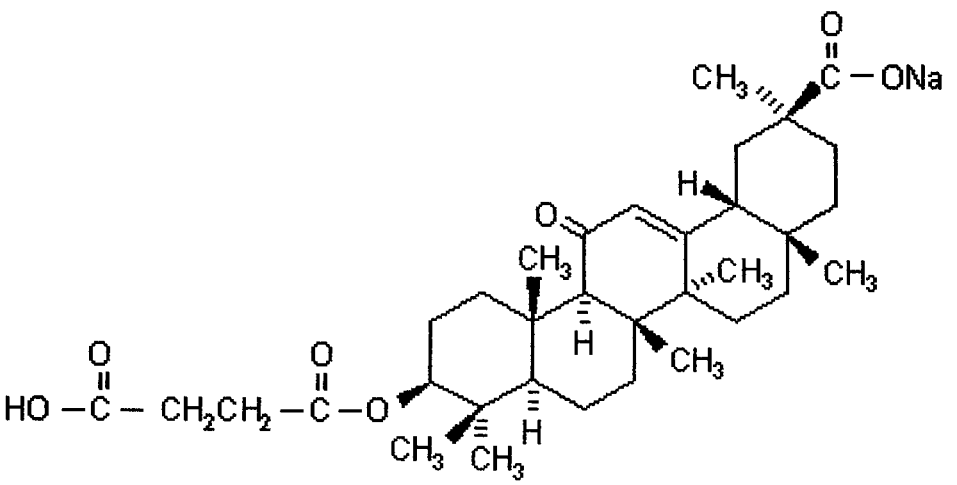

Figure 5.4 Chemical *structure of Carbenoxolone.*

In addition to a binding site for glutamate, NMDA receptors also have a binding site for glycine. Both the glutamate and glycine sites must be occupied for channel activation to occur (Greenamyre, 1994; Johnston and Amaral, 1998; Magnusson, 1998). Although the presence of both co-agonists is required for activation this is insufficient to open the channel because of the voltage-dependent blockade of the channel pore by Mg^{2+} at hyperpolarized potentials (Greenamyre, 1994; Magnusson, 1998). As the

neuron becomes more depolarised through synaptic activation, the magnesium block is reduced, allowing calcium ions to enter the channel.

5.2 Gap Junctions

Gap junctions are specialised structures located in the plasma membranes of virtually all cell types in mammals (Rozental *et al.*, 2000). Each gap junction (GJ) is composed of a pair of connexons aggregated together to form a hemichannel in the cell membrane (Carlen et al., 2000; Rozental *et al.*, 2000). Each connexon is assembled from six homologous proteins subunits called connexins (Cxs). To date, more than 15 connexins have been cloned in mammals (Ross *et al.*, 2000; Carlen *et al.*, 2000; Rozental *et al.*, 2000) of which Cxs 26, 30, 32, 36, 37, 40, 43 and 45 are expressed in the central nervous system (Carlen et al., 2000). Cxs 26, 32, 36 and 43 are known to be expressed by neurons, the most widespread of which is Cx 43, found in glia and in CA1 pyramidal cells (Carlen *et al.*, 2000).

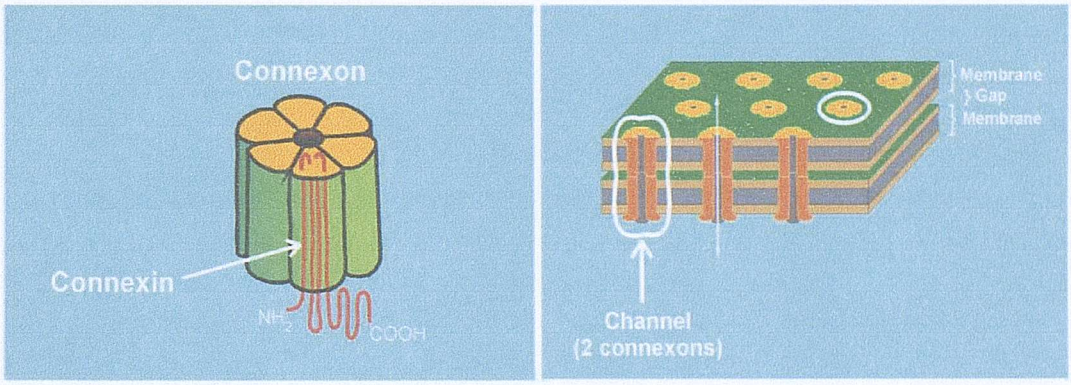

Figure 5.5 *Schematic of gap junction.* Adapted from http://www.med.ic.ac.uk

Evidence of direct communication between neurons in the hippocampus was first provided by MacVicar and Dudek (1981; 1982), who used dye-coupling between neurons recorded with an electrode containing Lucifer Yellow to demonstrate communication between cells. In a further study, MacVicar and Dudek (1982) used paired-intracellular recordings between two neurons in CA3 to show that there was direct intercellular passage of current between pairs of cells.

5.2.1 Carbenoxolone

Carbenoxolone, (18β-glycyrrhetinic acid 3β-*O*-hemisuccinate) is a synthesized derivative of glycyrrhetinic acid, an aglycone sapomin extracted from liquorice root and known to be a potent blocker of gap junctions (Ross *et al.*, 2000). It has been proposed that glycyrrhetinic acid derivatives bind directly to gap junctions inducing a

conformational change that leads to channel closure (See Ross *et al.*, 2000 for review). Evidence for the conformational change was provided by Goldberg *et al*, (1996) who used freeze-fracture analysis on glioma cells exposed to 18α-carbenoxolone.

Carbenoxolone is one of a range of non-specific chemicals that have been reported to block gap junctions (Jefferys *et al.*, Ross *et al.*, 2000; Kohling *et al.*, 2001). Other putative gap junction blockers are the anaesthetic halothane, octanol (Ross *et al.*, 2000; Kohling *et al.*, 2001; Margineanu & Klitgaard., 2001) and acidification of the intracellular pH (Ross *et al.*, 2000). Carbenoxolone is considered to be the best GJ antagonist with the least effect on other systems and so was chosen for these experiments (J.G.R. Jefferys, personal communication). However, carbenoxolone is known to require a significant period of perfusion, with a lag time of 40 minutes being reported previously (Leslie *et al.*, 1998; Ross *et al.*, 2000) so perfusion of the antagonist was carried out for 60 minutes prior to application of the RF or sham fields.

5.3 Preparation of solutions.

Stock solutions of D-APV and carbenoxolone were made by dissolving in distilled water to the required concentration. MK801 was dissolved in DMSO. Compounds were stored in aliquots maintained at –20°C until required. At the start of each experiment, an aliquot of the appropriate compound was dissolved in warmed ACSF to give a final concentration of 100μM D-APV, 10μM MK801 or 100μM carbenoxolone.

5.4 Electrophysiological recording protocol.

Slices were prepared as discussed earlier (Chapter 2) and placed in the recording chamber for 30 minutes prior to recording. Recordings were made of evoked field potentials in the CA1 stratum pyramidale whilst being perfused with ACSF gassed with carbogen (95% O_2/5% CO_2).

At the end of a 15-minute, baseline-recording period, slices were perfused with ACSF containing D-APV, MK801 or carbenoxolone. Perfusion with the antagonist continued for fifteen minutes prior to exposure to 700MHz RF fields, in the case of D-APV or MK 801, or for sixty minutes in the case of carbenoxolone. Perfusion with antagonist was continued during RF exposure and for 15-minutes post exposure, prior to

wash in ACSF for the final 15 minutes of recording. Sham-exposed control slices were treated in exactly the same way except that they were sham-exposed in place of the RF.

As reported earlier (chapter 4) a change in response was defined as a sustained (> 2 min) increase or decrease of greater than twice the standard deviation of the response during the 5 minutes preceding the exposure (Tattersall *et al.*, 2001). Statistical analyses were performed using GraphPad Prism version 2.0 (GraphPad Software, San Diego, CA, USA). Data are expressed as mean ± S.D., unless stated otherwise; data are considered statistically significant when $P = < 0.05$. Because the data sets did not follow a normal Gaussian distribution, non-parametric statistical tests were applied to test for significance, these were the Mann Whitney, (unpaired, two-tailed) test or the Wilcoxon matched pairs (two-tailed) test where appropriate.

5.5 Results

5.5.1 Population spike amplitude, D-APV.

In the presence of D-APV, exposure to the RF field produced an initial decrease in population spike amplitude that lasted for up to 2 minutes. In common with the results for paired-pulse slices exposed to 700 MHz RF in the absence of any drug (paired-pulse, RF control slices), this initial decrease in PS amplitude was followed by an increase in population spike amplitude that persisted after the exposure was terminated (all four slices). In sham-exposed control slices, no effects on PSA were observed either during or immediately after the sham-exposure in the presence of D-APV.

The maximal increase in PS amplitude after RF exposure varied between 32 and 192%, the mean change (mean ± S.D.) for all four slices was +82.0 ± 74.1%. In sham-exposed control slices, the maximal increase in PS amplitude after exposure varied between 0.2 and 21.5%, the mean change (mean ± S.D.) for all four slices was +12.9 ± 9.81%. At 1-minute post exposure, the mean change in population spike amplitude was not significantly different from pre-exposure values in either RF or sham-exposed slices; +44.8 + 38.4% (RF, $n = 4$) and 3.3 ± 3.7% (sham, $n = 4$) but the variance of the data was significant for RF exposed slices (F-test, $P = 0.0019$). Between groups treated with D-APV, differences in PS amplitude at 1-minute post exposure were not significantly different but variance was (F-test, $P = 0.0015$).

Comparison of the population spike amplitude at 1-minute post RF exposure between D-APV treated slices and paired-pulse; RF control slices (+44.8 ± 38.4%, $n = 4$ and +41.6 ± 15.4%, $n = 8$ respectively) showed that neither the PS amplitude nor variance of the data was significantly different. Similarly, population spike amplitude at 1-minute post sham exposure between D-APV treated slices and paired-pulse; sham control slices (+3.3 ± 3.7%, $n = 4$ and +5.8 ± 4.3%, $n = 8$ respectively) showed that neither the PS amplitude nor variance of the data was significantly different. During the wash period, all 4 RF exposed slices showed further increases in PS amplitude compared to baseline values. Post D-APV increases in population spike amplitude were also observed in sham-exposed control slices.

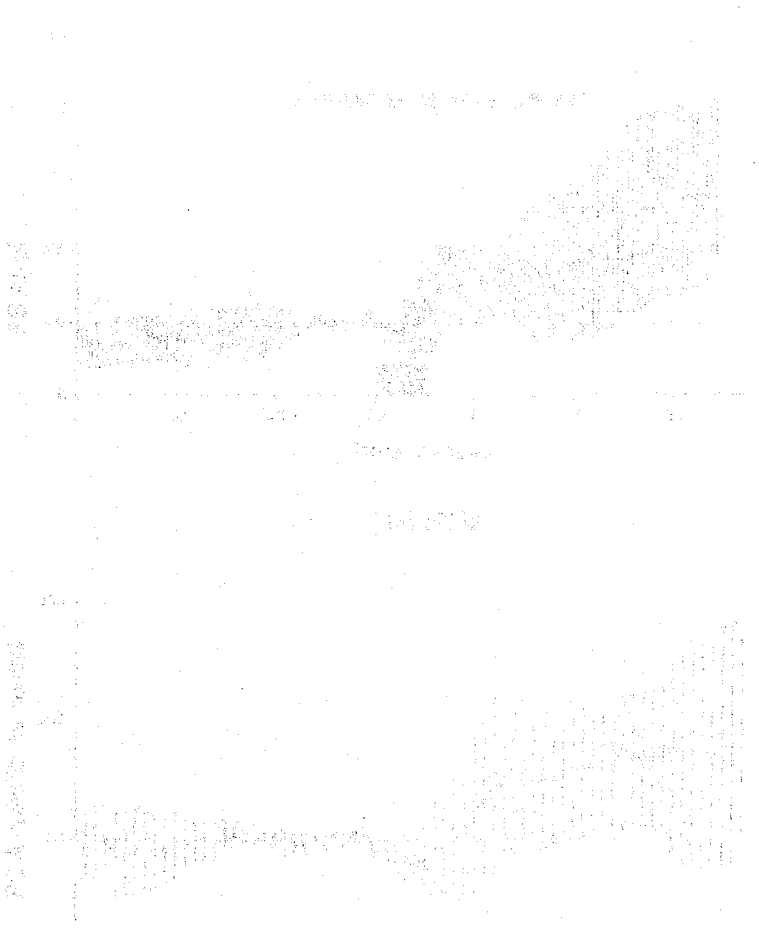

Figure 5.6 *Effect of 700MHz RF on population spike amplitude in slices treated with 100μM D-APV.*

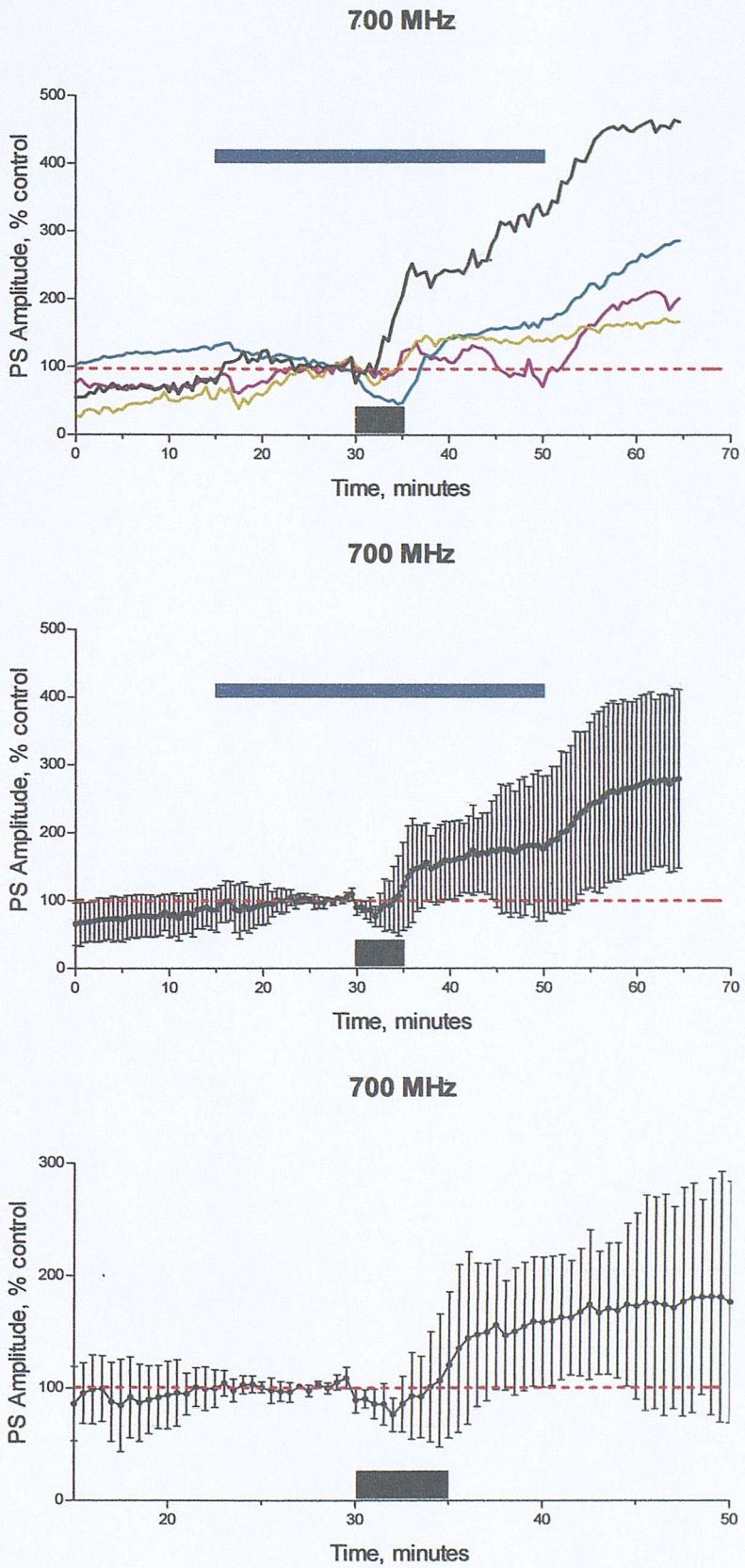

Top panel: Individual traces of PS amplitude in 4 slices exposed to 5-minutes, 700MHz RF in the presence of 100μM D-APV. In all graphs in this figure, the solid black bar indicates the period of exposure to the field; blue bar indicates the time of D-APV application and the dashed red line is the baseline level of 100%. **Middle panel:** Averaged data (mean ± S.D.) for the four slices shown in the top panel. **Bottom panel:** Expanded view of the period of drug application.

Figure 5.7 *Effect of sham-exposure to 700MHz RF fields on population spike amplitude in slices treated with 100μM D-APV.*

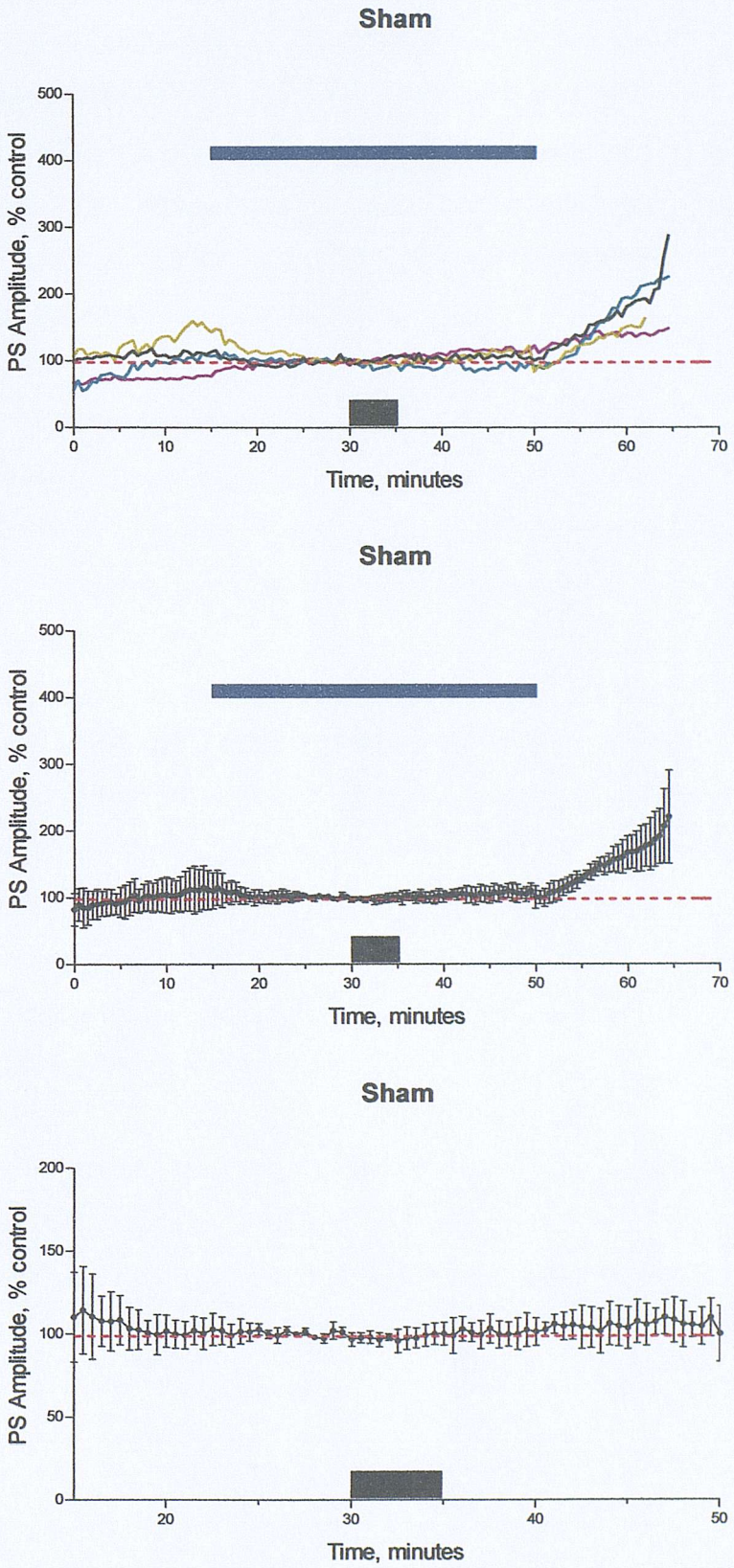

Top panel: Individual traces of PS amplitude in 4 slices exposed to 5-minutes, 700MHz sham fields in the presence of 100μM D-APV. In all graphs in this figure, the solid black bar indicates the period of exposure to the field; blue bar indicates the time of D-APV application and the dashed red line is the baseline level of 100%. **Middle panel:** Averaged data (mean ± S.D.) for the four slices shown in the top panel. **Bottom panel:** Expanded view of the period of drug application.

5.5.2 Field excitatory postsynaptic potential, D-APV.

The effects of RF fields on the amplitude of the *f*EPSP slope were smaller than on the population spike amplitude. The maximal increase in *f*EPSP slope within 15 minutes of exposure varied between +9 and +70%, the mean change (mean ± S.D.) for all four slices was +49.0 ± 27.7%. As was the case for PS amplitude, the *f*EPSP slope showed an initial transient decrease in amplitude that reversed within 2 minutes of RF application. The maximal *f*EPSP slope change in sham-exposed control slices ranged from +3 to +18%, (mean change = +9.5 ± 8.2%, $n = 4$).

At 1-minute post exposure, the mean change in *f*EPSP slope was not significantly different from pre-exposure values in either RF or sham-exposed slices; (+25.5 ± 10.4% (RF, $n = 4$) and –4.71 ± 3% (sham, $n = 4$). Between groups, differences in PS amplitude at 1-minute post exposure were not significantly different and neither was the variance.

Comparison of the *f*EPSP slope at 1-minute post exposure in RF exposed D-APV treated slices (+25.5 ± 10.4%, $n = 4$) with a similar time point in the RF paired-pulse control slices (+28.5 ± 9.6%, $n = 8$) showed no difference in either significance or variance of the data. In contrast, comparison of the *f*EPSP slope at 1-minute post exposure in sham-exposed, D-APV treated slices (–4.71 ± 3%, $n = 4$) with a similar time point in the sham-exposed paired-pulse control slices (+12.8 ± 4.6%, $n = 8$) revealed a significant difference ($P = 0.0283$) in the slope.

In common with the results for population spike amplitude, during the wash period, all 4 RF exposed slices showed further increases in *f*EPSP slope compared to baseline values. Post D-APV increases in *f*EPSP slope were also observed in sham-exposed control slices.

Figure 5.8 *Effect of 700MHz RF on fEPSP slope in slices treated with 100μM D-APV.*

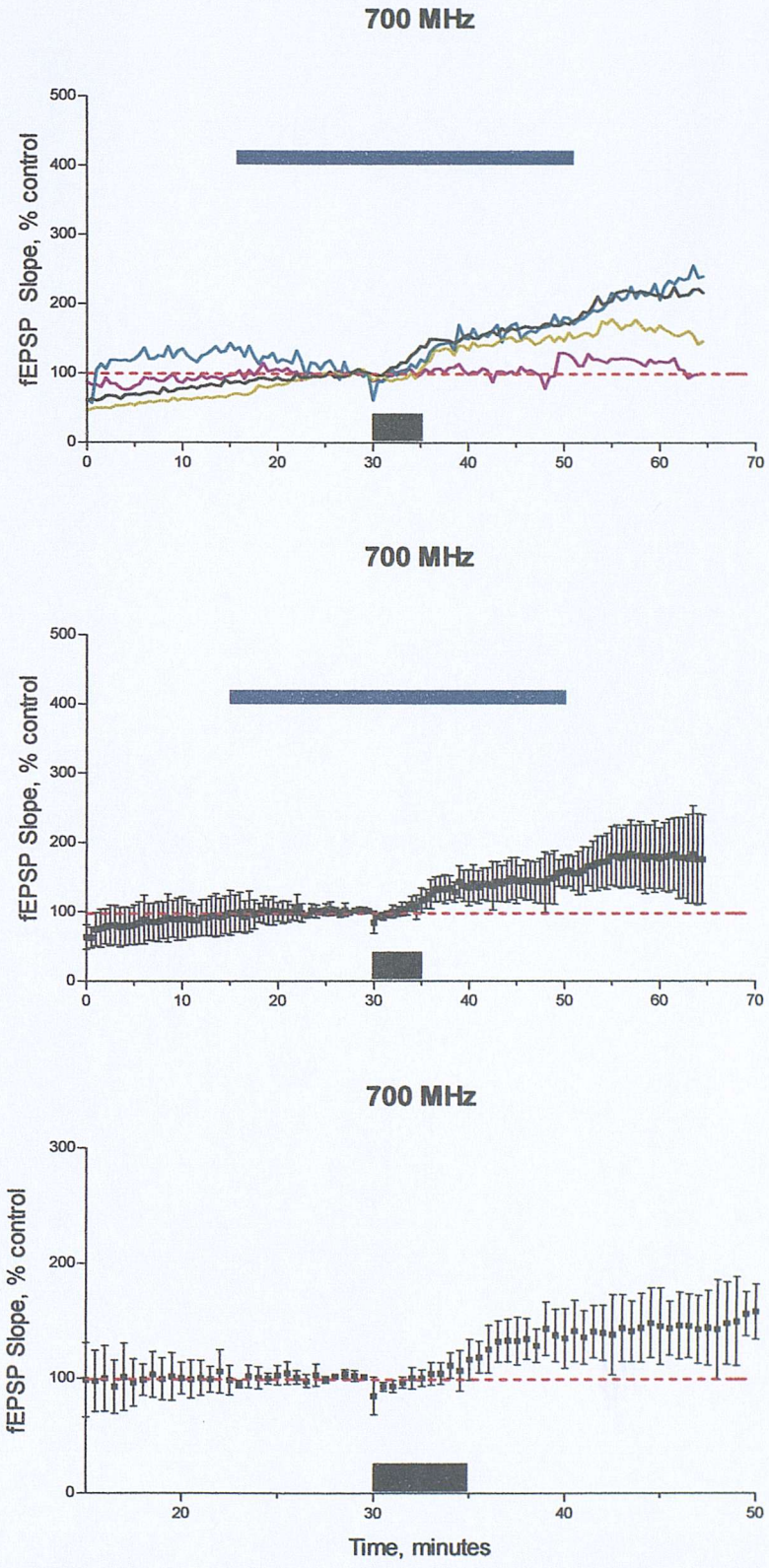

Top panel: Individual traces of *f*EPSP slope in 4 slices exposed to 5-minutes, 700MHz RF in the presence of 100μM D-APV. In all graphs in this figure, the solid black bar indicates the period of exposure to the field; blue bar indicates the time of D-APV application and the dashed red line is the baseline level of 100%. **Middle panel:** Averaged data (mean ± S.D.) for the four slices shown in the top panel. **Bottom panel:** Expanded view of the period of drug application.

Figure 5.9 *Effect of sham-exposure to 700MHz RF fields on fEPSP slope in slices treated with 100μM D-APV.*

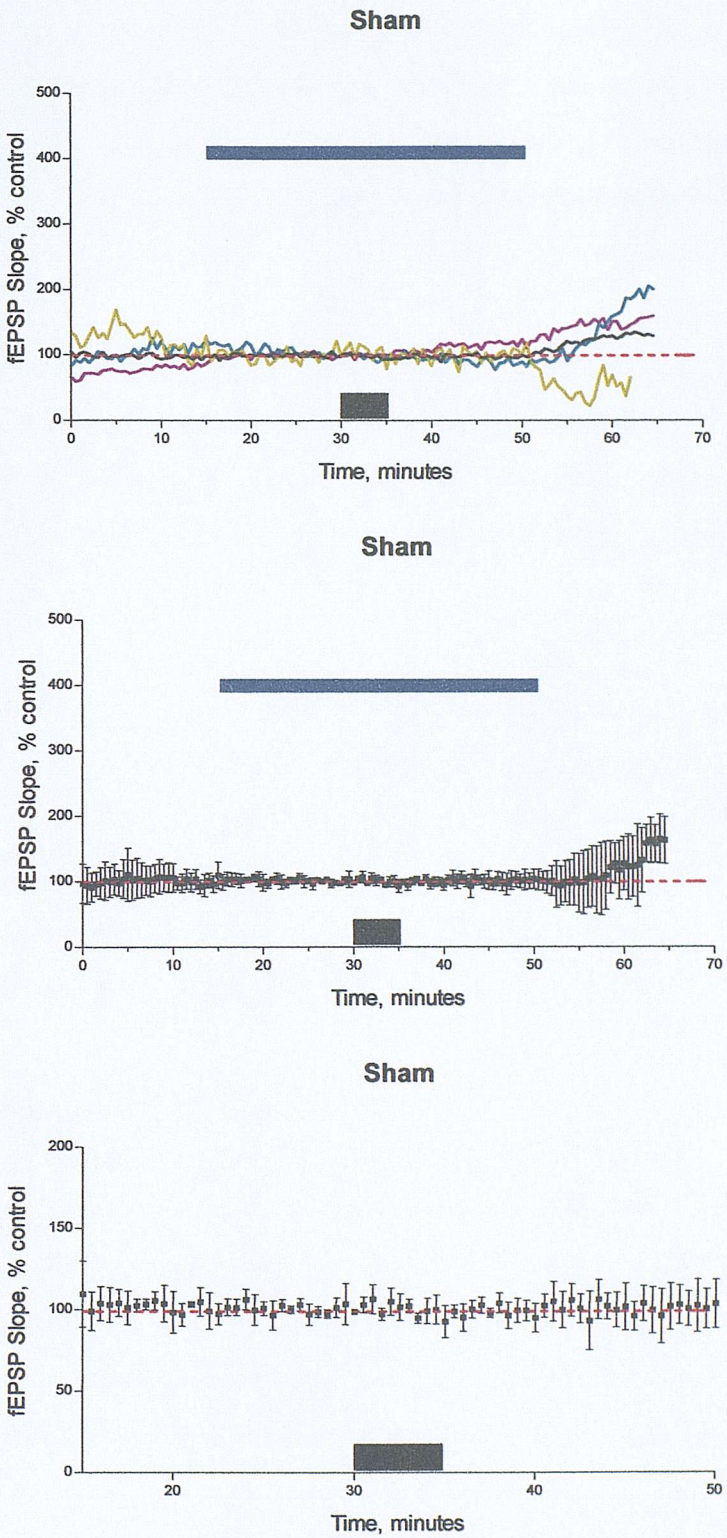

Top panel: Individual traces of *f*EPSP slope in 4 slices sham-exposed to 5-minutes, 700MHz RF in the presence of 100μM D-APV. In all graphs in this figure, the solid black bar indicates the period of exposure to the field; blue bar indicates the time of D-APV application and the dashed red line is the baseline level of 100%. **Middle panel:** Averaged data (mean ± S.D.) for the four slices shown in the top panel. **Bottom panel:** Expanded view of the period of drug application.

5.5.3 Population spike amplitude – MK801.

In the presence of MK801 exposure to the RF field produced an initial decrease in population spike amplitude (all four slices) that lasted for up to 2 minutes; this initial decrease in PS amplitude was followed by an increase in population spike amplitude that persisted after the exposure was terminated. In sham-exposed control slices, no effects on PSA were observed either during or immediately after sham-exposure in the presence of MK801.

The maximal increase in PS amplitude after RF exposure varied between +31 and +71%, the mean change (mean ± S.D.) for all four slices was +62.3 ± 25.3%. In sham-exposed control slices, the maximal increase in PS amplitude after exposure varied between +49 and +63%, the mean change (mean ± S.D.) for all four slices was +56.8 ± 6.1%.

At 1-minute post exposure, the mean change in population spike amplitude was not significantly different from pre-exposure values in either RF or sham-exposed slices; +16.0 ± 2.6% (RF, $n = 4$) and +15.7 ± 4.7% (sham, $n = 4$) and neither was the variance in either group. Between groups of slices treated with MK801, there were no significant differences in PS amplitude at 1-minute post exposure. Additionally, the variance of the data did not differ between groups.

Comparison of the population spike amplitude at 1-minute post RF exposure between MK801 treated slices and paired-pulse; RF control slices (+16.0 ± 2.6%, $n = 4$ and + 41.6 ± 15.4%, $n = 8$ respectively) showed that the PS amplitude was significantly different between groups ($P = 0.0485$). Comparison of population spike amplitude at 1-minute post sham exposure between MK801 treated slices and paired-pulse; sham control slices (+15.7 ± 4.7%, $n = 4$ and +5.8 ± 4.3%, $n = 8$ respectively) showed that neither the PS amplitude nor variance of the data was significantly different.

During the wash period, all 4 RF exposed slices showed further increases in PS amplitude compared to baseline values. Post MK801 increases in population spike amplitude were also observed in three of the four sham-exposed control slices.

Figure 5.10 *Effect of 700MHz RF fields on population spike amplitude in slices treated with 10μM MK801.*

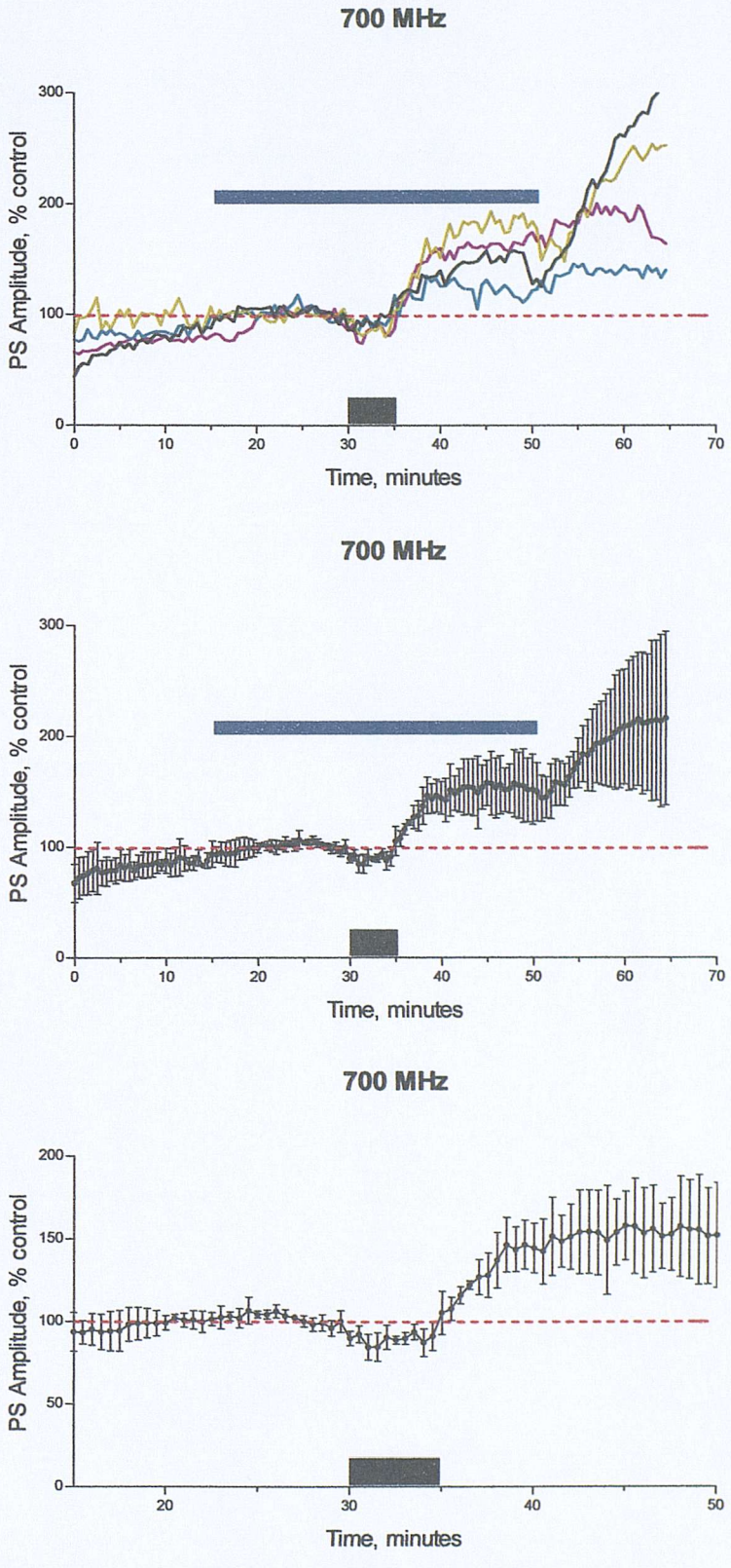

Top panel: Individual traces of PS amplitude in 4 slices exposed to 5-minutes, 700MHz RF in the presence of 10μM MK801. In all graphs in this figure, the solid black bar indicates the period of exposure to the field; blue presence of bar indicates the time of MK 801 application and the dashed red line is the baseline level of 100%. **Middle panel:** Averaged data (mean ± S.D.) for the four slices shown in the top panel. **Bottom panel:** Expanded view of the period of drug application.

Figure 5.11 *Effect of sham-exposure to 700MHz RF fields on population spike amplitude in slices treated with 10μM MK801.*

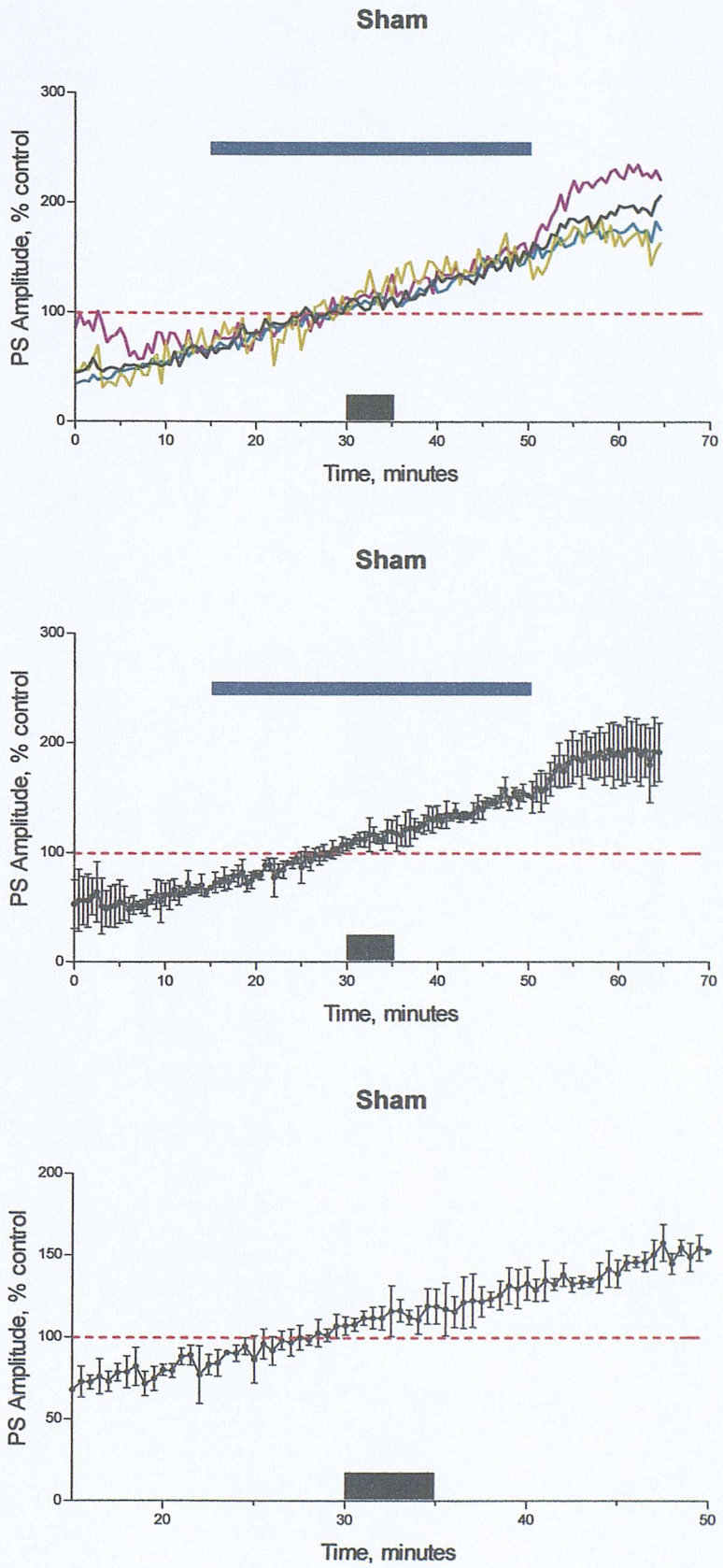

Top panel: Individual traces of PS amplitude in 4 slices sham-exposed to 5-minutes, 700MHz RF in the presence of 10μM MK801. In all graphs in this figure, the solid black bar indicates the period of exposure to the field; blue presence of bar indicates the time of MK 801 application and the dashed red line is the baseline level of 100%. **Middle panel:** Averaged data (mean ± S.D.) for the four slices shown in the top panel. **Bottom panel:** Expanded view of the period of drug application.

5.5.4 *Field excitatory postsynaptic potential, MK801.*

The effects of RF fields on the amplitude of the *f*EPSP slope of MK801 treated slices were smaller than on the population spike amplitude. The maximal increase in *f*EPSP slope after exposure varied between +18 and +75%, the mean change (mean ± S.D.) for all four slices was +50.8 ± 27.5%. As was the case for PS amplitude, the *f*EPSP slope showed a decrease in amplitude but this decrease did not reverse until the end of the RF application. The maximal *f*EPSP slope change in sham-exposed control slices ranged from +20 to +59%, (mean change = +39.3 ± 21.7%, $n = 4$).

At 1-minute post exposure, the mean change in *f*EPSP slope was not significantly different from pre-exposure values in either RF or sham-exposed slices; (+20.6 ± 8.2% (RF, $n = 4$) and +15.8 ± 4.3 (sham, $n = 4$). Between groups, differences in PS amplitude at 1-minute post exposure were not significantly different. In RF exposed, but not sham-exposed slices, there was a significant difference in the variance of the data (*F*-test, P= 0.0065).

Comparison of the *f*EPSP slope at 1-minute post exposure in RF exposed, MK801 treated slices (+20.6 ± 8.2%, $n = 4$), with a similar time point in the RF paired-pulse control slices (+28.5 ± 9.6%, $n = 8$) showed no difference in either significance or variance of the data. In agreement with these results, comparison of the *f*EPSP slope at 1-minute post exposure in sham-exposed, MK801 treated slices (+15.8 ± 4.3%, $n = 4$) with a similar time point in the sham-exposed paired-pulse control slices (+12.8 ± 4.6%, $n = 8$) revealed no significant differences in the data.

During the wash period, three of the four slices tested showed further increases in *f*EPSP slope compared to baseline values, the fEPSP slope in the fourth slice was unaffected by the wash process. Post D-APV increases in *f*EPSP slope were also observed in two of the four sham-exposed control slices.

Figure 5.12 *Effect of 700MHz RF fields on fEPSP slope in slices treated with 10μM MK801.*

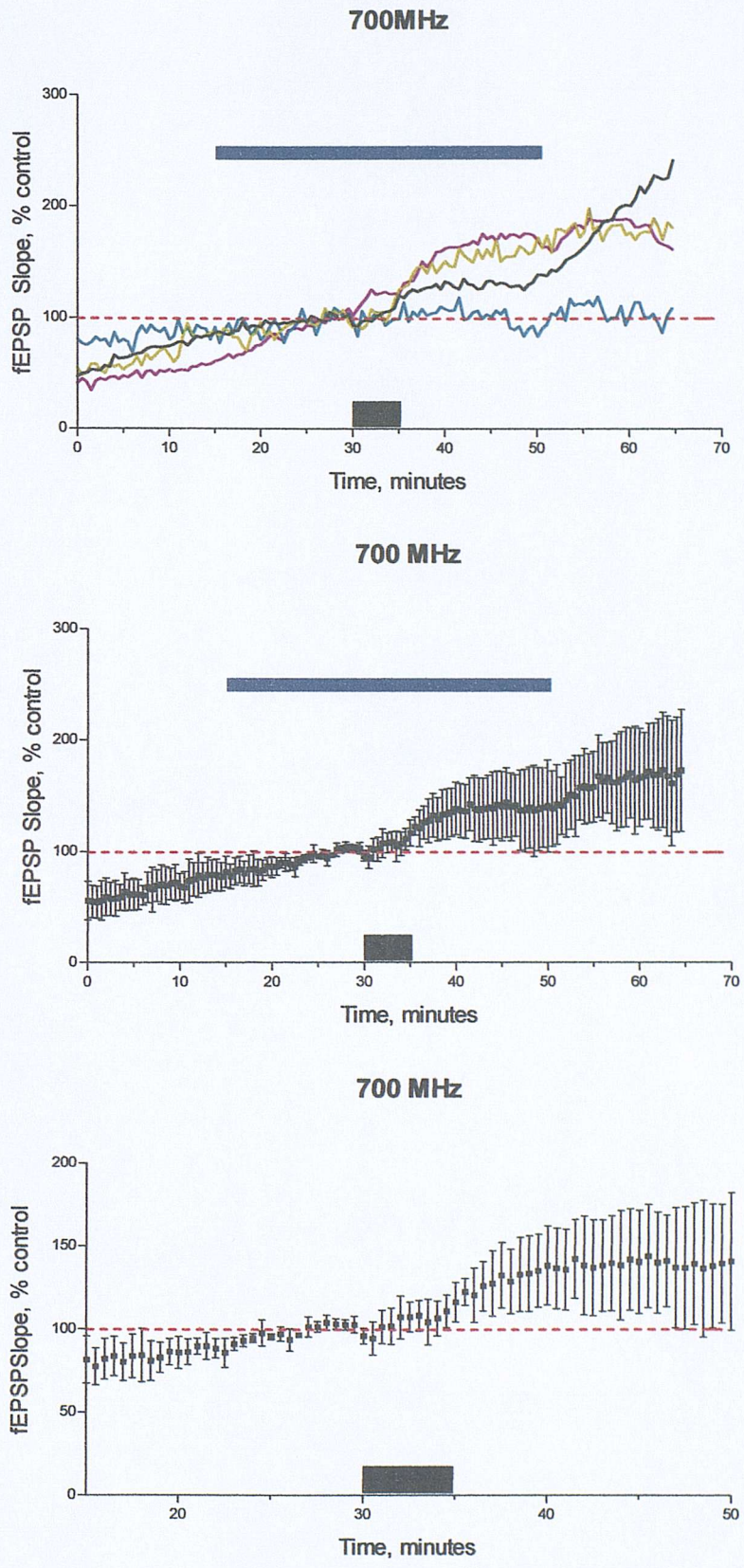

Top panel: Individual traces of *f*EPSP slope in 4 slices exposed to 5-minutes, 700MHz RF in the presence of 10μM MK801. In all graphs in this figure, the solid black bar indicates the period of exposure to the field; blue presence of bar indicates the time of MK 801 application and the dashed red line is the baseline level of 100%. **Middle panel:** Averaged data (mean ± S.D.) for the four slices shown in the top panel. **Bottom panel:** Expanded view of the period of drug application.

Figure 5.13 *Effect of sham-exposure to 700MHz RF fields on fEPSP slope in slices treated with 10μM MK801.*

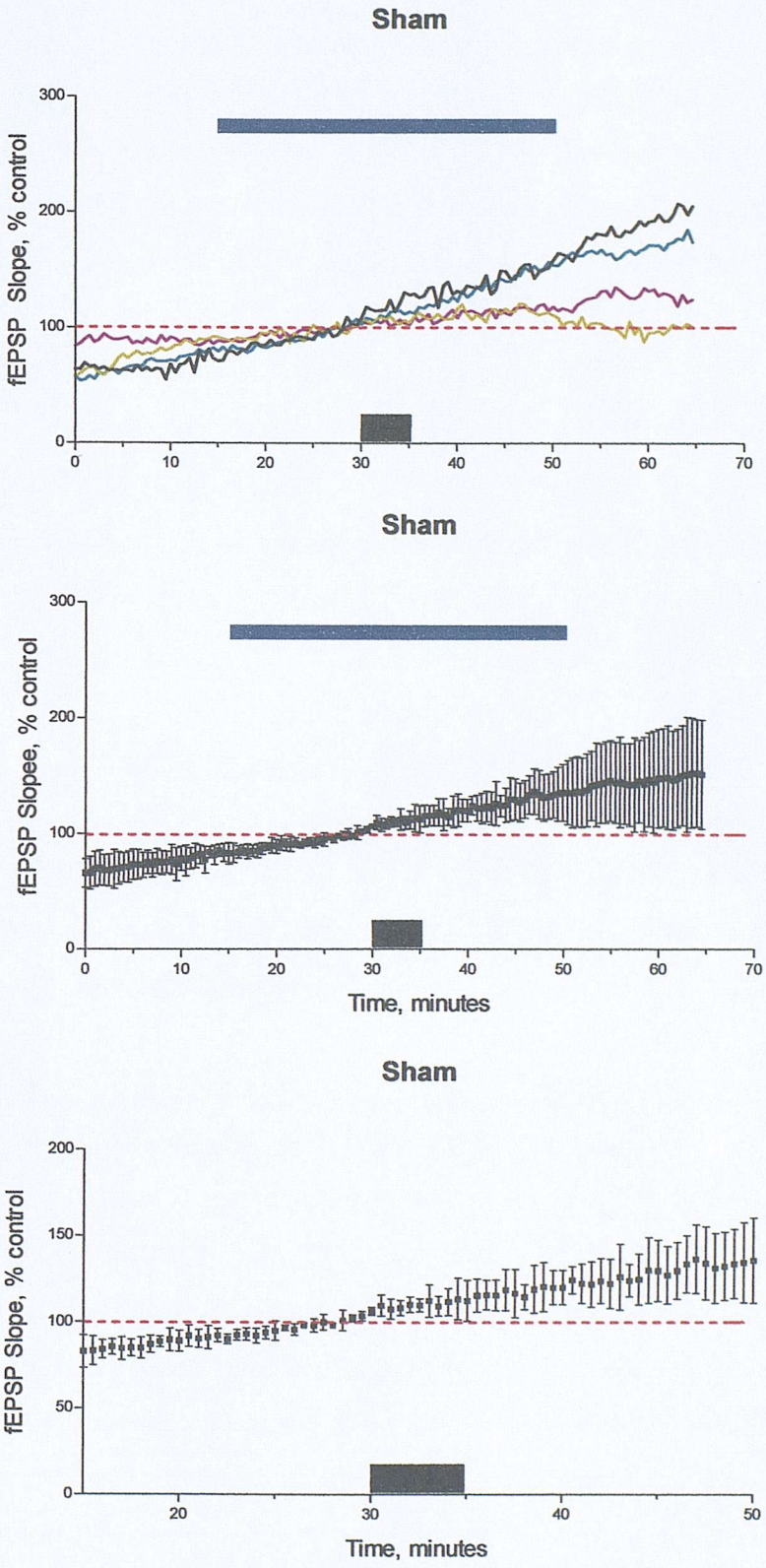

Top panel: Individual traces of *f*EPSP slope in 4 slices sham-exposed to 5-minutes, 700MHz RF in the presence of 10μM MK801. In all graphs in this figure, the solid black bar indicates the period of exposure to the field; blue presence of bar indicates the time of MK 801 application and the dashed red line is the baseline level of 100%. **Middle panel:** Averaged data (mean ± S.D.) for the four slices shown in the top panel. **Bottom panel:** Expanded view of the period of drug application.

5.5.5 Population spike amplitude - carbenoxolone

In the presence of carbenoxolone, exposure to the RF field produced variable changes in amplitude in the five slices studied. In two slices, application of the field had no apparent effect. Of the three remaining slices, application of the field caused failure of the population spike immediately (in one slice) and had a biphasic response, similar to that observed in control RF exposed slices in a further two slices. In sham-exposed control slices, the amplitude of the population spike decreased during the field in two slices and was unaffected in the remaining three slices.

The maximal change in PS amplitude after RF exposure varied between -99 and +37%; the mean change (mean ± S.D.) for all five slices was –44.2 ± 69.3%. In sham-exposed control slices, the maximal change in PS amplitude after exposure varied between -30 and +17%, the mean change (mean ± S.D.) for all five slices was –2.8 ± 19.5%.

At 1-minute post exposure, the mean change in population spike amplitude was not significantly different from pre-exposure values in either RF or sham-exposed slices, -0.07 ± 5.2% (RF, $n = 5$) and +1.5 ± 1.6% (sham, $n = 5$) however, the variance was significantly different in both cases F-test, P = 0.0074 and P = 0.0180 for RF and sham slices respectively.

Comparison of the population spike amplitude at 1-minute post RF exposure between carbenoxolone treated slices and paired-pulse; RF control slices (-0.07 ± 5.2%, $n = 5$, and + 41.6 ± 15.4%, $n = 8$ respectively) showed that the PS amplitude was significantly different between groups (P = 0.0127). Comparison of population spike amplitude at 1-minute post sham exposure between carbenoxolone treated slices and paired-pulse; sham control slices (1.5 ± 1.6%, $n = 5$ and +5.8 ± 4.3%, $n = 8$ respectively) showed that neither the PS amplitude nor variance of the data was significantly different. During the wash period, three RF exposed slices showed further increases in PS amplitude compared to baseline values. In the remaining slices, the population spike amplitude was zero during the wash period. Post carbenoxolone increases in population spike amplitude were not observed in any the five sham-exposed control slices.

Figure 5.14 *Effect of 700MHz RF on population spike amplitude in slices treated with 100μM carbenoxolone.*

Top panel: Individual traces of PS amplitude in 5 slices exposed to 5-minutes, 700MHz RF in the presence of 100μM carbenoxolone. In all graphs in this figure, the solid black bar indicates the period of exposure to the field; blue bar indicates the time of carbenoxolone application and the dashed red line is the baseline level of 100%.
Middle panel: Averaged data (mean ± S.D.) for the five slices shown in the top panel.
Bottom panel: Expanded view of the period of drug application.

Figure 5.14 *Effect of 700MHz RF fields on PS amplitude in slices treated with 100μM Carbenoxolone.*

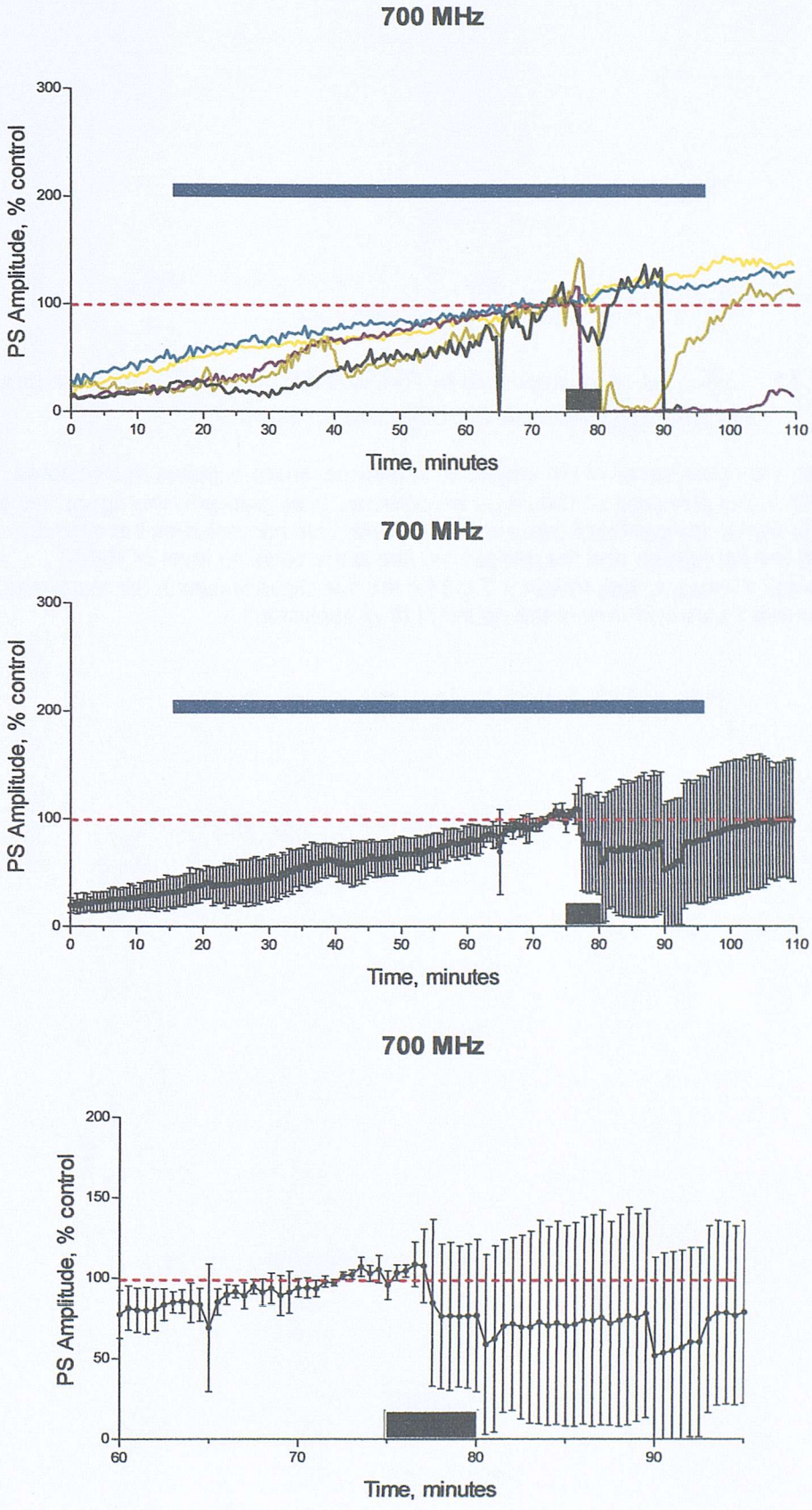

Figure 5.15 *Effect of sham-exposure to 700MHz RF on population spike amplitude in slices treated with 100μM carbenoxolone.*

Top panel: Individual traces of PS amplitude in 5 slices, sham-exposed to 5-minutes, 700MHz RF in the presence of 100μM carbenoxolone. In all graphs in this figure, the solid black bar indicates the period of exposure to the field; blue bar indicates the time of carbenoxolone application and the dashed red line is the baseline level of 100%.
Middle panel: Averaged data (mean ± S.D.) for the five slices shown in the top panel.
Bottom panel: Expanded view of the period of drug application.

Figure 5.15 *Effect of sham-exposure to 700MHz on RF fields on PS amplitude in slices treated with 100μM Carbenoxolone.*

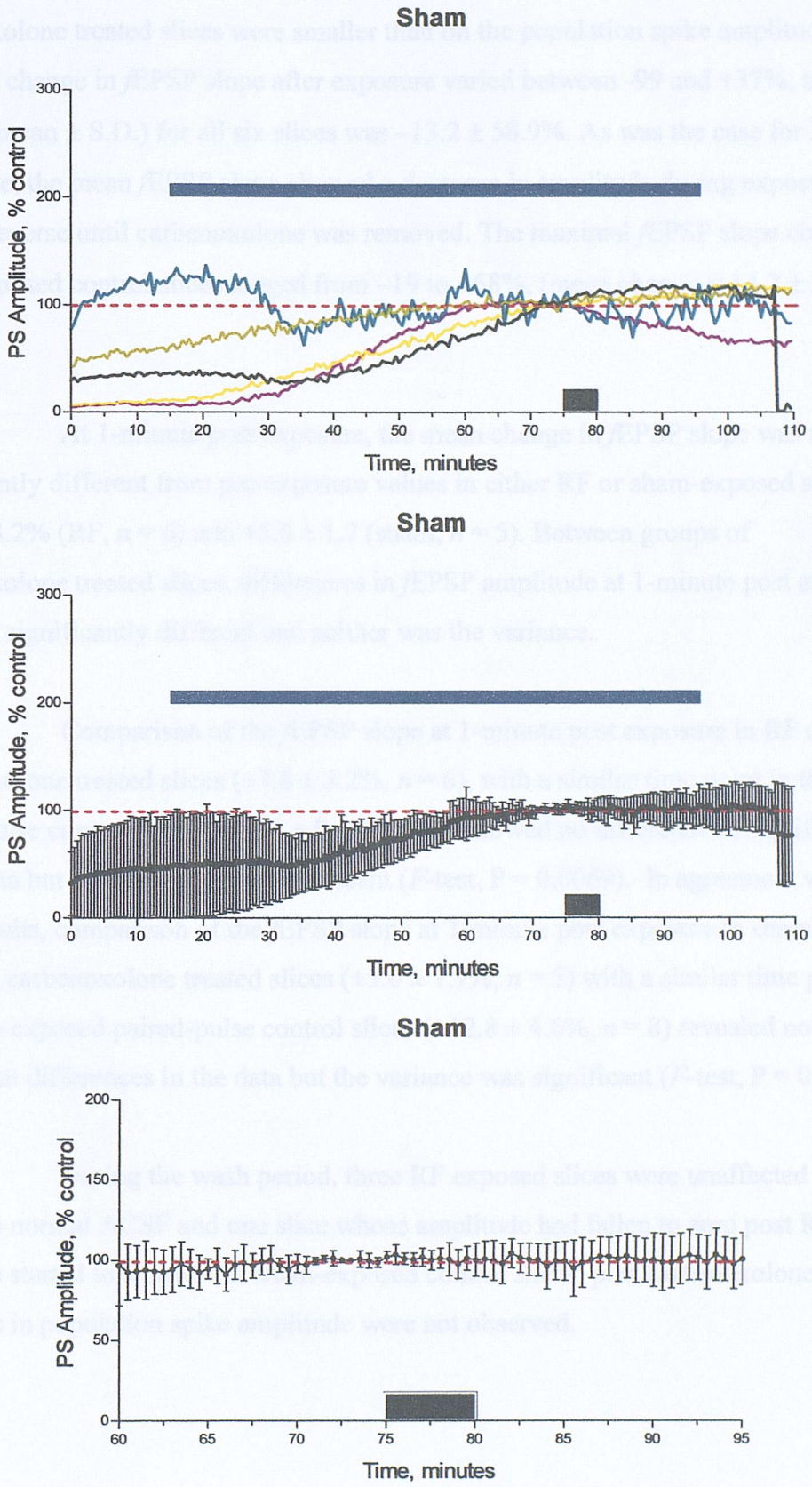

5.5.6 *Field excitatory synaptic potential slope, carbenoxolone.*

The effects of RF fields on the amplitude of the *f*EPSP slope of carbenoxolone treated slices were smaller than on the population spike amplitude. The maximal change in *f*EPSP slope after exposure varied between -99 and +37%, the mean change (mean ± S.D.) for all six slices was –13.2 ± 58.9%. As was the case for PS amplitude, the mean *f*EPSP slope showed a decrease in amplitude during exposure that did not reverse until carbenoxolone was removed. The maximal *f*EPSP slope change in sham-exposed control slices ranged from –19 to +58%, (mean change = 14.2 ± 27.7%, $n = 5$).

At 1-minute post exposure, the mean change in *f*EPSP slope was not significantly different from pre-exposure values in either RF or sham-exposed slices; (+7.8 ± 3.2% (RF, $n = 6$) and +5.0 ± 1.7 (sham, $n = 5$). Between groups of carbenoxolone treated slices, differences in *f*EPSP amplitude at 1-minute post exposure were not significantly different and neither was the variance.

Comparison of the *f*EPSP slope at 1-minute post exposure in RF exposed, carbenoxolone treated slices (+7.8 ± 3.2%, $n = 6$), with a similar time point in the RF paired-pulse control slices (+28.5 ± 9.6%, $n = 8$) showed no difference in significance of the data but the variance was significant (*F*-test, P = 0.0069). In agreement with these results, comparison of the *f*EPSP slope at 1-minute post exposure in sham-exposed, carbenoxolone treated slices (+5.0 ± 1.7%, $n = 5$) with a similar time point in the sham-exposed paired-pulse control slices (+12.8 ± 4.6%, $n = 8$) revealed no significant differences in the data but the variance was significant (*F*-test, P = 0.0171).

During the wash period, three RF exposed slices were unaffected by the switch to normal ACSF and one slice whose amplitude had fallen to zero post RF exposure started to recover. In sham-exposed control slices, post carbenoxolone increases in population spike amplitude were not observed.

Figure 5.16 *Effect of 700MHz RF on fEPSP slope in slices treated with 100μM carbenoxolone.*

Top panel: Individual traces of *f*EPSP slope in 5 slices exposed to 5-minutes, 700MHz RF in the presence of 100μM carbenoxolone. In all graphs in this figure, the solid black bar indicates the period of exposure to the field; blue bar indicates the time of carbenoxolone application and the dashed red line is the baseline level of 100%.
Middle panel: Averaged data (mean ± S.D.) for the five slices shown in the top panel.
Bottom panel: Expanded view of the period of drug application.

Figure 5.16 *Effect of 700MHz RF fields on fEPSP slope in slices treated with 100μM carbenoxolone.*

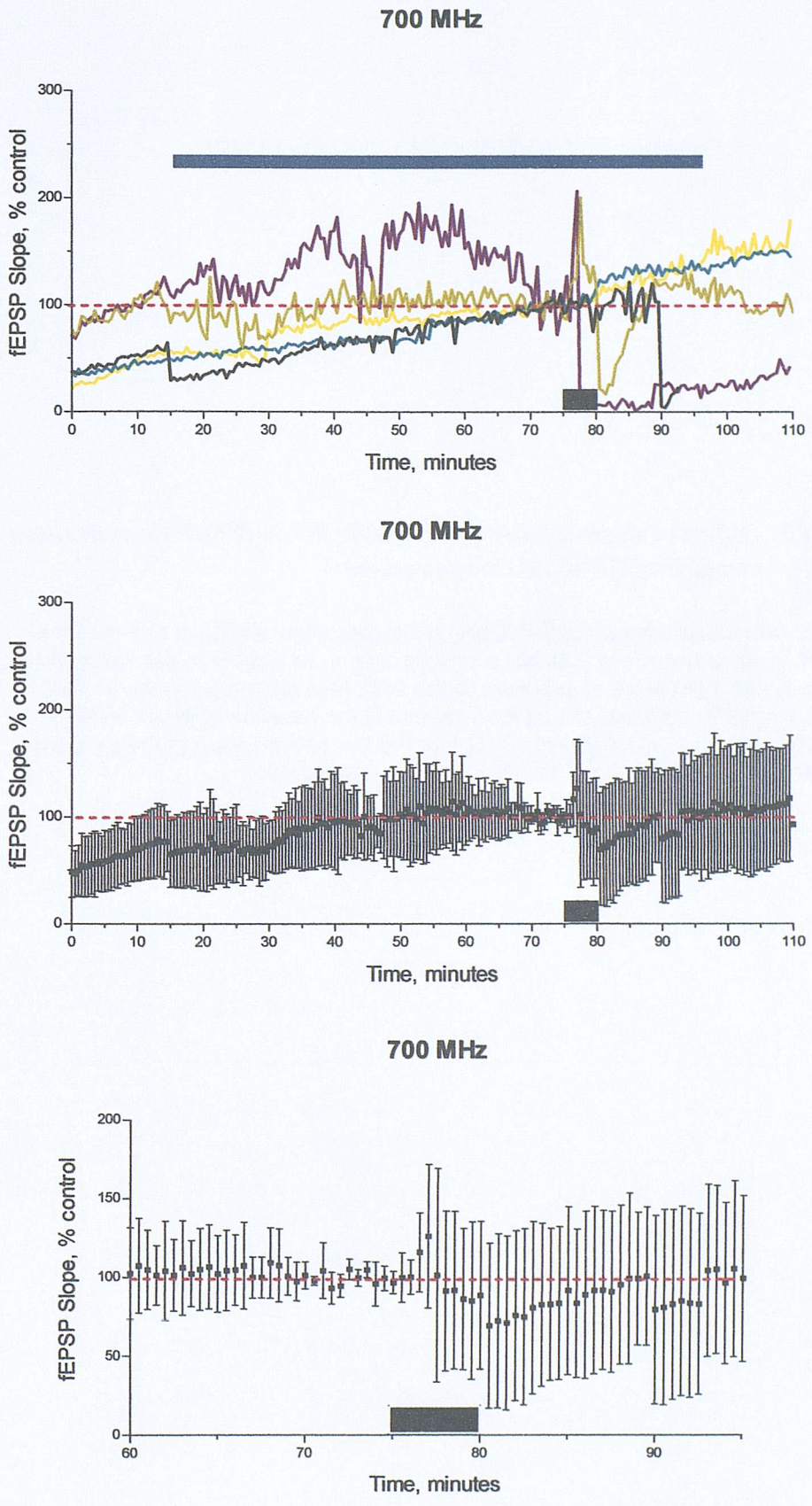

Figure 5.17 *Effect of sham-exposure to 700MHz RF on fEPSP slope in slices treated with 100μM carbenoxolone.*

Top panel: Individual traces of *f*EPSP slope in 5 slices, sham-exposed to 5-minutes, 700MHz RF in the presence of 100μM carbenoxolone. In all graphs in this figure, the solid black bar indicates the period of exposure to the field; blue bar indicates the time of carbenoxolone application and the dashed red line is the baseline level of 100%.
Middle panel: Averaged data (mean ± S.D.) for the five slices shown in the top panel.
Bottom panel: Expanded view of the period of drug application.

Figure 5.17 *Effect of sham-exposure to 700MHz on RF fields on fEPSP slope in slices treated with 100μM Carbenoxolone.*

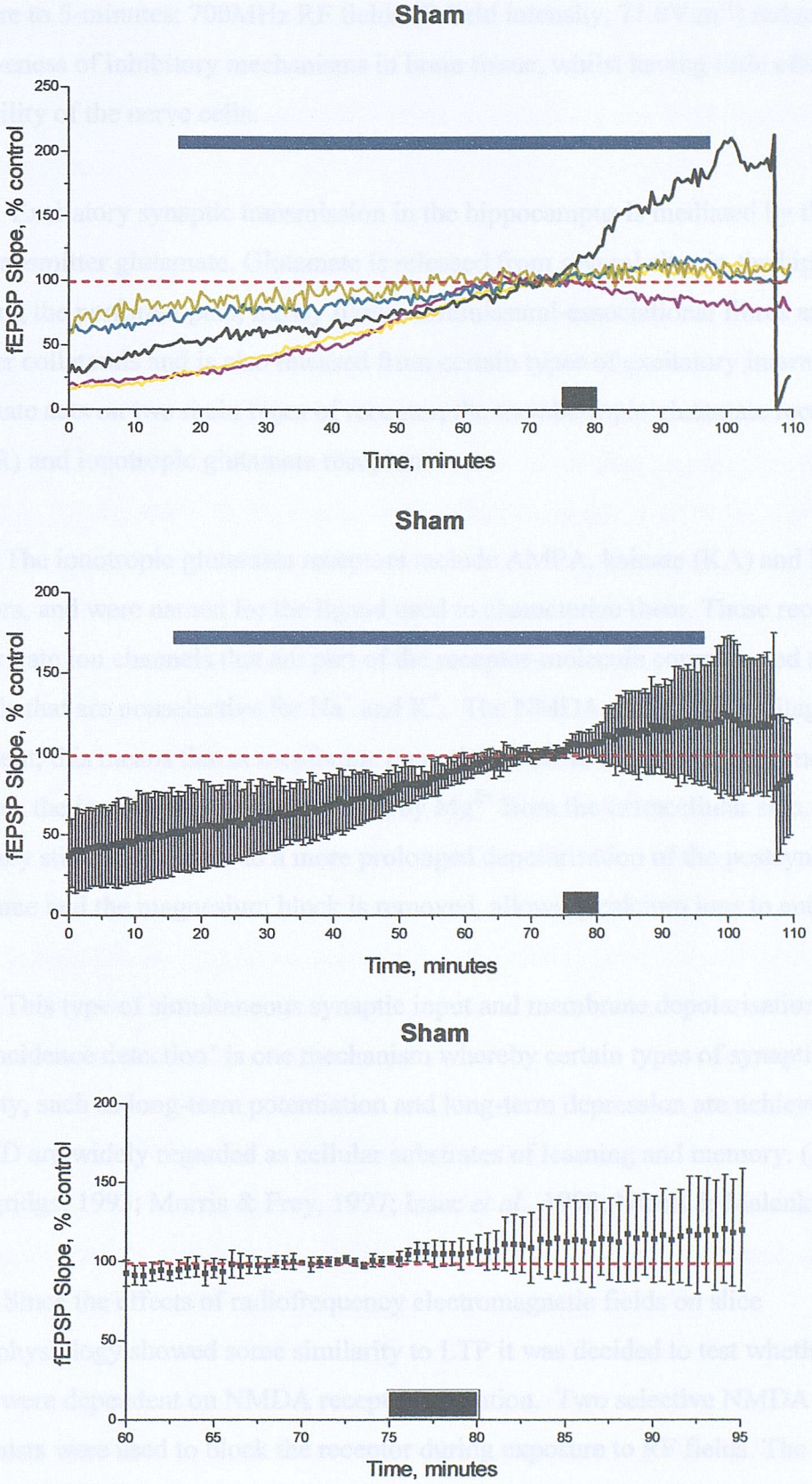

5.6 Discussion

In chapter 4, the results from the extracellular field experiments indicated that exposure to 5-minutes; 700MHz RF fields (E field intensity, 71.0V.m^{-1}) reduced the effectiveness of inhibitory mechanisms in brain tissue, whilst having little effect on the excitability of the nerve cells.

Excitatory synaptic transmission in the hippocampus is mediated by the neurotransmitter glutamate. Glutamate is released from several sites in the hippocampus including the perforant path, mossy fibres, commissural-associational fibres and Schaffer collaterals and is also released from certain types of excitatory interneuron. Glutamate acts on two main types of receptor, the metabotropic glutamate receptor (mGluR) and ionotropic glutamate receptors.

The ionotropic glutamate receptors include AMPA, kainate (KA) and NMDA receptors, and were named for the ligand used to characterize them. These receptors directly gate ion channels that are part of the receptor-molecule complex and all open channels that are nonselective for Na^+ and K^+. The NMDA receptors is voltage dependent, this means that at membrane potentials close to the cells resting membrane potential, the ion channel pore is blocked by Mg^{2+} from the extracellular side. Higher frequency stimulation leads to a more prolonged depolarisation of the postsynaptic membrane and the magnesium block is removed, allowing calcium ions to enter the cell.

This type of simultaneous synaptic input and membrane depolarisation, known as 'coincidence detection' is one mechanism whereby certain types of synaptic plasticity, such as long-term potentiation and long-term depression are achieved. LTP and LTD are widely regarded as cellular substrates of learning and memory. (Bliss & Collingridge, 1993; Morris & Frey, 1997; Isaac *et al.*, 1998; Nicoll & Malenka, 1999).

Since the effects of radiofrequency electromagnetic fields on slice electrophysiology showed some similarity to LTP it was decided to test whether the effects were dependent on NMDA receptor activation. Two selective NMDA receptor antagonists were used to block the receptor during exposure to RF fields. The first of these, D-APV is a competitive antagonist, which competes with glutamate and NMDA for the same ligand-binding site.

5.6.1 Effect of D-APV treatment on evoked CA1 responses.

In the presence of 100μM D-APV, exposure to the RF field produced increases in both population spike amplitude and *f*EPSP slope. These changes were not significantly different from the changes observed in slices exposed to RF in the absence of any drug; this finding indicates that NMDA receptors are not involved in the RF induced effects.

The finding that the population spike amplitude variance in RF exposed of the data (P= 0.0019), was significantly different from slices exposed to RF in the absence of any drug was not expected. This may be due to either the small sample size ($n = 4$ slices) or may indicate that the antagonist (which competes for the same binding site as glutamate and NMDA) did not provide sufficient block on the receptor. It is possible that during RF exposure the binding efficacy of the antagonist is compromised and endogenous glutamate or NMDA can preferentially occupy the receptor. A further possibility is that the antagonist was applied for an insufficient time, however, close scrutiny of the population spike amplitude reveals a dip in amplitude of approximately 5% of baseline values in two of the four RF exposed slices. This tends to indicate that antagonist binding to the receptor had occurred soon after application of the drug. Additionally, the drop in PS amplitude was also seen in 3 of the 4 sham exposed slices at a similar time point.

There were no significant changes in population spike amplitude in the sham-exposed control slices compared to the paired-pulse sham slices; there was however a significant difference in *f*EPSP slope in the sham-exposed slices compared to the sham-exposed control slices (P = 0.0283). As before these differences may have been observed because of the small sample size ($n = 4$ slices) since there was no indication in the individual D-APV sham group of variability in *f*EPSP slope post exposure. Additionally, the tight distribution of sham slice data ($n = 8$ slices) in the control group may mean that differences between groups were emphasised.

5.6.2 Effect of MK801 treatment on evoked CA1 responses.

The second compound used in this study, MK801 (10μM) is a non-competitive antagonist of the NMDA receptor. Changes in population spike amplitude and *f*EPSP slope were smaller than those of the D-APV treated slices exposed to RF but were of similar amplitude and slope to changes in slices exposed to RF in the absence of any

drug. At one-minute post RF exposure, changes in PS amplitude were significantly different between the MK801 and non-drug group (P = 0.0485). This finding is contrary to that of the D-APV group and indicates the involvement of NMDA receptors in the RF effects on evoked synaptic potentials. In contrast, significantly different differences in the *f*EPSP slope were not observed in RF exposed slices. A plausible explanation for this difference may be that the *f*EPSP (which indicates synaptic excitation) is mediated, at least in part by non-NMDA receptors (AMPA and KA); which were not blocked by the MK801 application. No significant differences in PS amplitude or *f*EPSP slope were observed in sham-exposed slices treated with MK801.

In view of the contradictory results from D-APV and MK801 treated slices, it would be interesting to use another pharmacological model, for example the low Ca^{2+}, model of epilepsy (a non-synaptic model of epilepsy) to examine the effects of RF on evoked field potentials. This model was recently used by Ghai *et al.*, (2000), to examine the effect of low amplitude DC electric fields (1-5 $V.m^{-1}$) on low calcium induced bursting. Exogenously applied fields were capable of suppression or modulation of the epileptic activity in this model. This approach could be used to investigate whether the effects of RF electromagnetic fields were dependent upon polarisation of the CA1 pyramidal cells.

A second possibility would be to examine the contribution of non-NMDA (AMPA and KA) receptors to the RF induced effects. This could be achieved by studying emergent network oscillations (gamma oscillations, 30-90Hz). Gamma frequency oscillations have been implicated in higher mental activity, including perception and consciousness (Jefferys *et al.*, 1996; 1999) and may be especially sensitive to applied electromagnetic fields. Application of RF fields to slices treated with kainic acid (to induce 40Hz network oscillations) could provide valuable insight into the potential mechanism of the RF effect in evoked slices.

5.6.3 Effect of Carbenoxolone treatment on evoked CA1 responses.

Gap junctions are necessary for some emergent network properties in the hippocampus and have also been implicated in the spread of epileptic activity (Traub *et al.*, 1999). Several compounds have been shown to block gap junctions, the most selective of which is carbenoxolone (JGR Jefferys, personal communication). Slices treated with 100μM carbenoxolone and exposed to RF displayed an inconclusive variety

of response to the applied EM field. The mean change in PS amplitude decreased during exposure and this reduction was significant (P = 0.0127) at 1-minute post exposure. Comparison of the fEPSP slope in RF treated slices revealed a significant variance of the data at one-minute post exposure (F-test, P = 0.0069).

These results indicate that gap junction communication between cells may, in part, be responsible for some of the changes observed in evoked field potential responses. Carbenoxolone caused a reduction in PS amplitude during RF exposure compared to the increase in PS amplitude observed in slices exposed to RF in the absence of any drug. One reason for these differences may be due to the fact that maintenance of the slices for 75 minutes prior to the RF insult proved to be difficult. PS amplitude increased steadily in all five RF exposed slices and in four of the five sham-exposed slices during the period before RF or sham-exposure, this may indicate that the slices were not maintained in an optimum condition during carbenoxolone treatment.

Possible reasons for the 'poor' condition of the slices prior to RF or sham exposure include inadequate gassing during perfusion, intracellular acidification of the cell interior due to application of the drug and toxic effects of carbenoxolone. The Haas chamber was adapted to sit between the plates of the waveguide during experiments, it may therefore follow that the flow of carbogen gas across the top surface of the slice may have been compromised. Additionally, intracellular changes in pH brought about by application of carbenoxolone may result in changes to the osmolarity of the cell. Ghai *et al.*, (2000) report that changes to the osmolarity of neurones has shown to modulate the efficacy of applied electric fields. Finally, Ross *et al.*, (2000) report that slices exposed to 100μM carbenoxolone did not recover after extensive washing, this they suggest shows that the drug had a deleterious effect on the hippocampal slice. The authors review evidence, which shows that carbenoxolone has a toxic concentration (TC_{50}) of 50μM in fibroblast cells, half the concentration used in this study.

Suggestions for future study include application of alternative gap junction blockers, for example octanol and halothane, as well as ammonium chloride, which is reported to open gap junctions by causing a transient alkalisation of the cell interior (Ross *et al.*, 2000).

6. ORGANOTYPIC HIPPOCAMPAL CULTURES.

6.1 Heat shock proteins.

Heat shock proteins (HSPs) are a group of polypeptides (containing both constitutive and inducible forms) whose molecular size ranges from 8-110 kDa. Inducible HSPs are produced by most organisms in response to stressful stimuli that would otherwise result in damage to cellular proteins (Table 6.1). Inducible HSPs can prevent protein unfolding and enhance cell survival in response to stressors including high temperature (Li *et al.*, 1992; Krueger *et al.*, 1999; Bechtold *et al.,* 2000), ischemia (Nowak *et al.*, 1990; Planas *et al.*, 1997) and excitotoxicity (Kochevar *et al.*, 1991; Best *et al.,* 1996; Krueger *et al.,* 1999).

The notion that heat shock proteins are induced in response to radiofrequency (RF) radiation or electromagnetic (EM) fields is controversial. Several authors have examined the induction of stress proteins by electro-magnetic fields without elevated temperature. For example, Pipkin *et al.*, (1999) studied the effect of sinusoidal 0.1 or 1mT (Tesla) magnetic field at 60Hz on the induction of heat shock proteins in HL-60 human leukaemia cells. They found that two-hours exposure to 1mT fields increased both inducible and constitutive forms of *HSP70* compared to control. Similarly, Lin *et al.*, (1997) found increased heat shock factor (HSF) to heat shock element binding (HSE) in HL-60 cells exposed to a 60Hz, 8μT (peak) magnetic field. In contrast, Morehouse & Owen, (2000) found no significant effect on either *HSP70* induction or HSF-HSE binding in HL-60 cells exposed to 6.3 or 8μT, 60Hz magnetic fields.

A study by Cleary *et al.*, (1997) observed that log-phase HeLa or CHO cells which were subjected to continuous wave 27MHz RF radiation, specific absorption rate (SAR) 25W.kg^{-1}, for 2 hours did not induce 70kDa stress proteins. More recently, de Pomerai *et al.*, (2000a,) showed that the heat shock response is activated in the soil nematode *Caenorhabditis elegans* after exposure to low intensity microwave fields. These studies examined the non-thermal expression of *HSP16* after overnight exposure to continuous-wave RF radiation

at 750MHz and 0.5W power in a transverse electromagnetic (TEM) cell identical to the one used in this series of experiments.

Table 6.1 *Eukaryotic heat shock proteins.* (From Kochevar *et al.*, 1991)

Family	***Proteins***	***Alternative names***	***Function***
hsp110	hsp110		May protect heat-sensitive ribosome production.
hsp90	hsp90		Polypeptide binding activity and transport of $pp60^{src}$ and other tyrosine kinases; stimulation of eIF-2α kinase. Binding of inactive steroid receptors and prevention of DNA binding. Primarily localised to the ER Golgi; may have polypeptide binding capabilities.
	α-form	hsp86	
	β-form	hsp84	
	grp94	grp100	
hsp70	hsc70	hsp73, hsc73, 73K, p72	Constitutive protein that interacts in an ATP-dependant fashion with exposed hydrophobic surfaces of polypeptides to promote or correct protein folding or assembly; in vitro uncoating ATPase activity; post-translational translocation of proteins into microsomes and mitochondria.
	hsp70	hsp72, hsx70, hsp68	Inducible protein with general function similar to hsc 70; associated with p53 and selected viral antigens; binds certain steroid receptors; cell-cycle regulated.
	grp78	BiP, grp80	Abundant ER protein with polypeptide binding capabilities; facilitates Ig assembly.
	grp75		*Constitutive protein localised to mitochondria.*
hsp60	hsp60	hsp58; GroEL homolog; RuBisCo subunit binding protein homolog	Eukaryotic protein important in the proper translocation and oligomeric assembly of proteins in mitochondria.
Small heat shock proteins	hsp28	hsp27	Forms highly polymeric heat shock granules; has homology to vertebrate α-crystallins; may be involved in the regulation of mRNA.
	hsp32		Induced by oxidative stress; related to heme oxygenase.
Ubiquitin	Ubiquitin		Conjugated to proteins destined for selective ATP-dependent degradation.

The *HSP70* family is the largest and best studied of the heat shock proteins in eukaryotes, comprising at least four and perhaps up to eight members (Kochevar *et al.*, 1991), (see Table 6.1). They are thought to be activated by the presence of denatured proteins (Ananthan *et al.*, 1986) and function as chaperones, interacting transiently with many proteins in an ATP-dependent manner. When denatured proteins are present, heat shock factors (HSFs) in the cytosol that are bound to other HSPs dissociate, leaving free HSFs that become phosphorylated, form trimers and bind to heat shock elements (HSEs) within the promoters of different heat shock genes. This activates transcription and synthesis of HSPs in stressed cells (Sharp *et al.*, 1999). *HSP70* and other chaperones then bind to the denatured protein to aid the restoration of structure and function. *HSP70* is not usually detectable under normal conditions and its synthesis is vigorous under stressful conditions, making it an excellent diagnostic marker for cellular injury (Nowak *et al.*, 1990; Best *et al*, 1996).

The present study has examined the expression *HSP72*, the inducible form of the *HSP70* family of stress proteins. Experiments were designed to test the hypothesis that induction of *HSP72* will be potentiated by exposure to RF electromagnetic fields. It was previously shown by de Pomerai *et al.*, (2000a,b) that the *HSP16* induction curve in the soil nematode *C. elegans* is subject to a leftward shift of approximately 3°C after RF exposure in that model system.

6.2 C-Fos.

The nervous system is dynamic in that neurons respond to changes in their environment brought about by pharmacological and or pathological stimuli. C-*fos* is one of a family of immediate early genes (IEG) that includes *fos*-B, c-*jun*, *jun*-B, *jun*-D, *krox*-20 and *krox*-24 (see Hughes and Dragunow, 1995 for review). C-*fos* can only regulate gene expression once it has been transcribed and translated; excessive build-up of c-*fos* is prevented by negative feedback with the cycle ending when the c-*fos* gene product (FOS) is present (Hughes and Dragunow, 1995).

This particular IEG is not usually expressed constitutively, however, noticeable expression of fos-like immuno-staining has been observed in the nuclei of adult nerve cells in the amygdala, striatum, piriform cortex and hippocampus (Morgan *et al.*, 1987; Dragunow and Robertson, 1988). Induction of c-*fos* is achieved by diverse range of external stimuli including ischemia (Zhou *et al.*, 1995; Sanz *et al.*, 1997), amygdaloid stimulation (Hsieh & Watanabe, 2000) and estradiol (Rudick & Wooley, 2000). Excitotoxicity (Kasof *et al.*, 1995; Sanz *et al.*, 1997), anticonvulsants (Morgan *et al.*, 1987; Dragunow and Robertson, 1987) and RF radiation (Mickley *et al.*, 1994; Mickley, 1995; Fritze *et al.*, 1997) are also known to elicit c-*fos* induction. In response to stressful stimuli cells respond with a combination of early and late responses (Hughes and Dragunow, 1995). These early responses are the result of interactions between first-messengers and cell-surface located receptors. Initiation of the second-messenger systems causes active phosphorylation of specific neuronal proteins and brings about a biological response that lasts for the duration of the protein phosphorylation event.

When a cell is exposed to a stressor, the previously translated c-*fos* re-enters the nucleus where it activates other late-response genes leading to the initiation of a cascade of compensatory physiological responses (Marx, 1987; Mickley, 1995). C-*fos* induction is rapid, transient and protein-synthesis independent (Hughes and Dragunow, 1995). Transcription occurs within 1 hour and falls away rapidly toward baseline levels within 4 hours (Hughes and Dragunow, 1995) with expression in neurons being more long lasting than cell culture systems (Dragunow and Robertson, 1989). Many investigators believe that c-*fos* and other IEGs are involved in neuronal plasticity. In particular, Hughes and Dragunow (1995) suggest that IEGs may be involved in learning and memory, and pathologically in epileptogenesis, by linking nerve cell membrane events to the neuronal genome, leading to changes in the neuronal phenotype.

Very few authors have examined the induction of c-*fos* in response to magnetic or electric fields insult; of those that have, results have been contradictory. For example, Mickley *et al.*, (1994) looked at the effects of RF

induced hyperthermia on a putative working memory task in rats. The authors used the expression of c-*fos* as a metabolic marker to trace areas of the brain activated or possibly damaged by exposure to the resonant 600 MHz, CW fields. Mickley *et al.*, (1994) found increased c-*fos* expression in the irradiated group compared to sham exposed controls in the periventricular strata, hypothalamic nuclei, amygdala and several areas of the cortex. However, c-*fos* expression was not observed in the hippocampus, even at high SAR (10 $W.kg^{-1}$) values. Mickley *et al.*, (1994) indicate that the c-*fos* expression pattern may be used to indicate candidate brain nuclei responsible for behavioural changes associated with working memory tasks.

More recently, Fritze *et al.*, (1997) examined the effect of exposure to GSM frequency EM fields on the expression of HSP*70*, *c-fos*, *c-jun* and glial fibrillary acidic protein (GFAP). The authors exposed rats for 4 hours to 1 or 5W maximum power, GSM signals (900 MHz) pulsed at 217 Hz or to 25W maximum power, 900 MHz CW RF fields; brain averaged SAR's were 0.3 and 1.5 $W.kg^{-1}$ for the GSM exposure and 7.5 $W.kg^{-1}$ for CW exposure. Both irradiated and sham-exposed control animals were restrained in a carousel irradiator during the 4-hour experimental period. Semi-quantitative *in-situ* hybridisation measurements revealed a slight induction of *HSP70* mRNA in the cerebellum and hippocampus after the 7.5 $W.kg^{-1}$ exposure but not at lower intensities. As with the *HSP70* results, a slight induction of c-*fos* mRNA was observed in the cerebellum, neocortex and piriform cortex of all groups of animals that had been restrained, including sham-exposed control animals, however, exposed animals did not express more c-*fos* mRNA than restrained animals. In contrast to the Mickley *et al.*, (1994) study, a slight but significant increase in c-*fos* mRNA was also observed in the hippocampus of the 0.3 $W.kg^{-1}$ GSM group compared to free moving controls.

A third study, (Snyder *et al.*, 2000) exposed rats for 30 minutes to a 9.4 T magnetic field, both exposed and control rats were restrained during the experimental period in a Plexiglas chamber. The authors observed significantly more *c-fos* positive cells in the visceral and vestibular nuclei than the sham-

exposed controls. Snyder *et al.*, (2000) suggest that magnetic field exposure may promote conditioned taste aversion (CTA) learning since it has previously been shown that rats exposed to a 9.4 T magnetic field developed a CTA response to glucose-saccharin solution (Nolte *et al.*, 1998, see Snyder *et al.*, 2000 for review).

In view of the contradictory nature of reports on c-*fos* induction in the hippocampus, the effects of acute exposure to 700 MHz, continuous wave RF fields will be examined in rat organotypic hippocampal slice culture model.

6.3 Materials and method

6.3.1 Preparation of slice cultures

Organotypic hippocampal slice cultures were prepared according to the method of Stoppini *et al.*, (1991) modified by Pringle *et al.*, (1997). Briefly, eight to ten day old Wistar rat pups were killed by decapitation and the hippocampi dissected out. Transverse sections of hippocampus, 400μm thick were cut on a McIlwain tissue chopper (Mickle Laboratory Engineering Ltd, Surrey, UK) and placed into Gey's balanced salt solution supplemented with 28mM glucose. Slices were plated onto Millicell-CM semi-porous membranes (four per insert, Millipore) and maintained *in vitro* for 14 days at 37°C, in 5% CO_2. Cultures were incubated in medium comprised of minimum essential medium, MEM (50%); Hank's balanced salt solution, HBSS (25%); and heat-inactivated horse serum (25%), supplemented with glutamine (1mM), D-glucose (4.5mg/mL) and fungizone (1.5%) (Pringle *et al.*, 2000). Medium was changed every 3-4 days.

Figure 6.1 *Plating of organotypic cultures.*

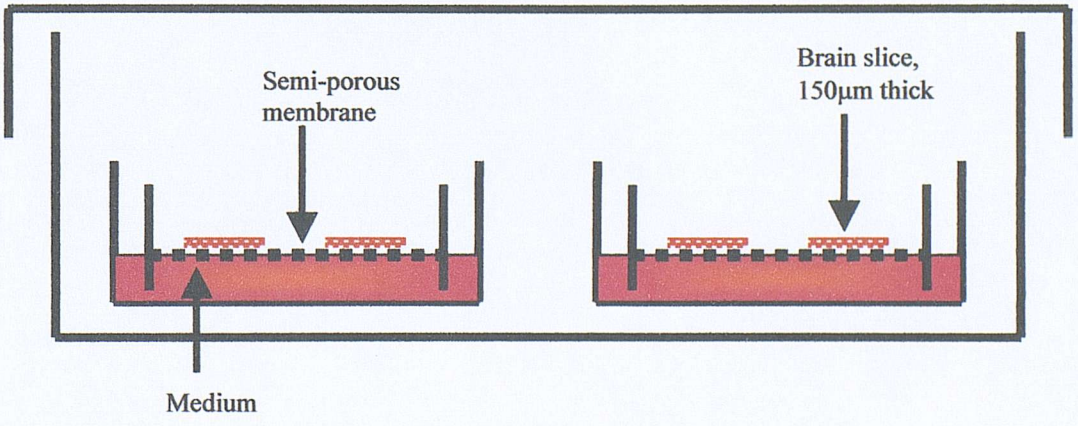

6.3.2 *Radiofrequency radiation exposure system.*

Cultures were exposed to radiofrequency (RF) electromagnetic fields in a fully enclosed, calibrated transverse electromagnetic (TEM) cell mounted inside the incubator. RF signals were produced by an HP8648C signal generator (Hewlett Packard, UK), which supplied powers of up to 1W. Slices were exposed for 4 hours to a 750MHz RF field with the E-field normal to the surface of the slice; E-field amplitude 42V.m^{-1} (de Pomerai *et al.*, 2000a). Incident and reflected powers in the waveguide were measured, (Amplifier Research model DC7146 directional coupler, EMV Ltd, UK) connected to a Hewlett Packard (model 437B) power meter and model 8481A power sensor (Hewlett Packard, UK) which were connected to the output terminal of the waveguide. Sham exposures were obtained by placing foil-shielded cultures on an alternative shelf in the same incubator whilst exposure continued simultaneously in the TEM cell.

6.3.3 *Thionin staining.*

Cultured tissue slices were placed onto Superfrost Plus (Menzel-Glaser, Germany) microscope slides and allowed to dry overnight. Slides were placed in thionin stain for 5-minutes followed by 70% alcohol for 90 seconds and differentiator for 90 seconds. Thionin stain consisted of 1% thionin, 1.36% sodium acetate and 0.6% glacial acetic acid in RO water. After differentiation, the intensity of stain was checked and adjustments made by replacing the slides in thionin and or differentiator as required. Once the required level of staining had been achieved the tissue was dehydrated in a series of graded alcohols and Xylene. Cover slips were 'glued' in place with DPX and allowed to dry.

6.3.4 *Immunocytochemistry.*

Slice cultures were carefully removed from the membranes and prepared for immunocytochemistry as free-floating sections. Control slices consisted of age matched, untreated slices, cultured in parallel with those slices used in thermal, RF or kainic acid protocols.

6.3.5 HSP72 immunoreactivity.

The HSP72 staining procedure was a modification of that used by Best *et al.*, (1996). Incubation times were as follows: mouse monoclonal IgG (1:200 dilution; Oncogene Science), 24 hours; biotinylated anti-mouse IgG from sheep (1:200 dilution; Amersham Life Science, UK), 1 hour; avidin-biotin-horseradish peroxidase complex, 1 hour and diaminobenzidine tetrachloride (DAB), 30 minutes. All incubations were in Tris-buffered saline (TBS, pH 7.4) to which Triton X-100 (0.3%) had been added. Sections received three washes of ten minutes duration in TBS before and after each incubation period.

6.3.6 C-Fos immunoreactivity.

The *c-fos* staining method was obtained from Cullinan *et al.*, (1995). Briefly, endogenous tissue peroxidase was blocked with a ten minute incubation using hydrogen peroxide (0.05%) in Phosphate buffered saline (PBS) + Triton X-100 (0.3%). Incubation times were as follows: sheep/goat IgG (1:500 dilution; Chemicon International), 24 hours; biotinylated anti-sheep/goat IgG from donkey (1:500 dilution; Amersham Life Science, UK), 1 hour; avidin-biotin-horseradish peroxidase complex, 1 hour and diaminobenzidine tetrachloride (DAB), 30 minutes. All incubations were in Phosphate-buffered saline (PBS, pH 7.4) to which Triton X-100 (0.3%) had been added. Slices received three washes of ten minutes duration in PBS before and after each incubation period.

6.3.7 Statistics.

Averaged values are presented as mean ± 1 S.E. (number of cultures). Where appropriate, statistical significance was assessed by Mann-Whitney test. In all cases, differences were taken to be significant if $P < 0.05$.

6.4 Experimental design.

The experimental protocol is illustrated in Figure 6.2

6.4.1 Kainic acid (KA) lesion.

As reported by Best *et al.*, (1996) the effect of kainic acid on organotypic cultures is to create a lesion of CA3 pyramidal neurones that is similar to that

obtained *in vivo* following an intracerebroventricular injection of kainic acid. The Best *et al.,* (1996) study established that the optimum concentration of kainic acid producing a similar lesion to that seen *in vivo* was 5μM. Consequently, organotypic slice cultures were incubated in full medium containing 5μM KA for 1 hour prior fixing in 4% paraformaldehyde (PFA). KA treated slices were used as positive controls for the *HSP72* and *c-fos* immunohistochemistry protocols.

6.4.2 Temperature dependence of HSP72 induction.

The next set of experiments was designed to determine the temperature dependence of HSP72 immunoreactivity in organotypic hippocampal cultures. Sadgrove (1999) indicated that HSP72 is expressed at temperatures of 39°C and above in the rat organotypic hippocampal slice culture model. Furthermore, it was shown by de Pomerai et al., (2000a,b) that the HSP16 induction curve in the soil nematode C. elegans is subject to a leftward shift of approximately 3°C after RF exposure in that model system.

In order to determine whether RF electromagnetic radiation induces a similar shift in *HSP72* induction in rat organotypic hippocampal cell cultures a range of temperatures (35 - 41°C) were examined. Slices were subjected to one of two treatments; (a) placed in the transverse electromagnetic cell during exposure (RF group) or (b) foil shielded and placed on a lower shelf in the incubator (sham-exposed control group) to prevent contamination from reflected RF electromagnetic energy that may have been emitted from the TEM cell.

Figure 6.2 *Schematic of the experimental protocol.*

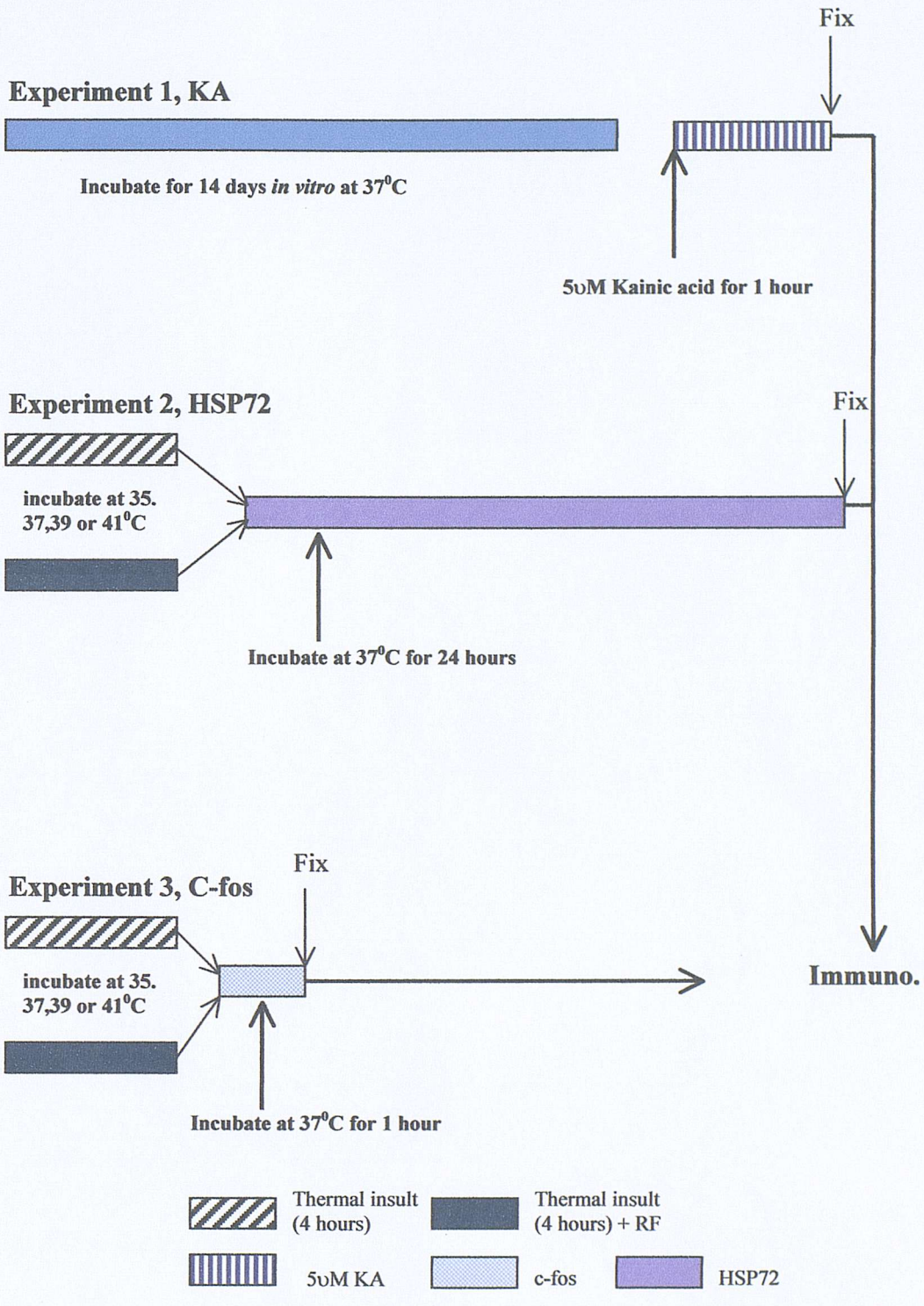

Note that the bars used to indicate time in this figure are not drawn to scale.

Figure 6.3 *Slice culture (TEM Cell)*

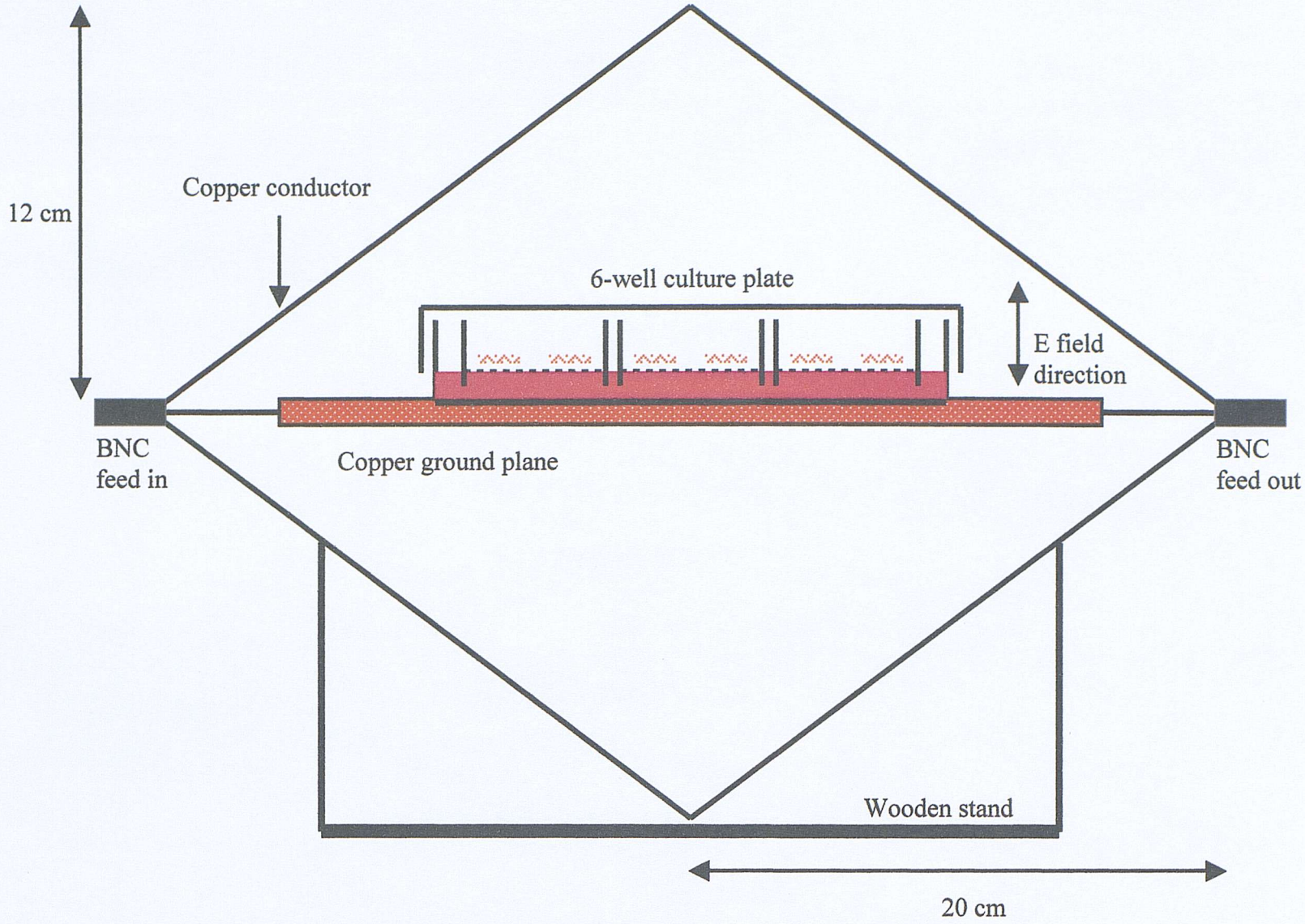

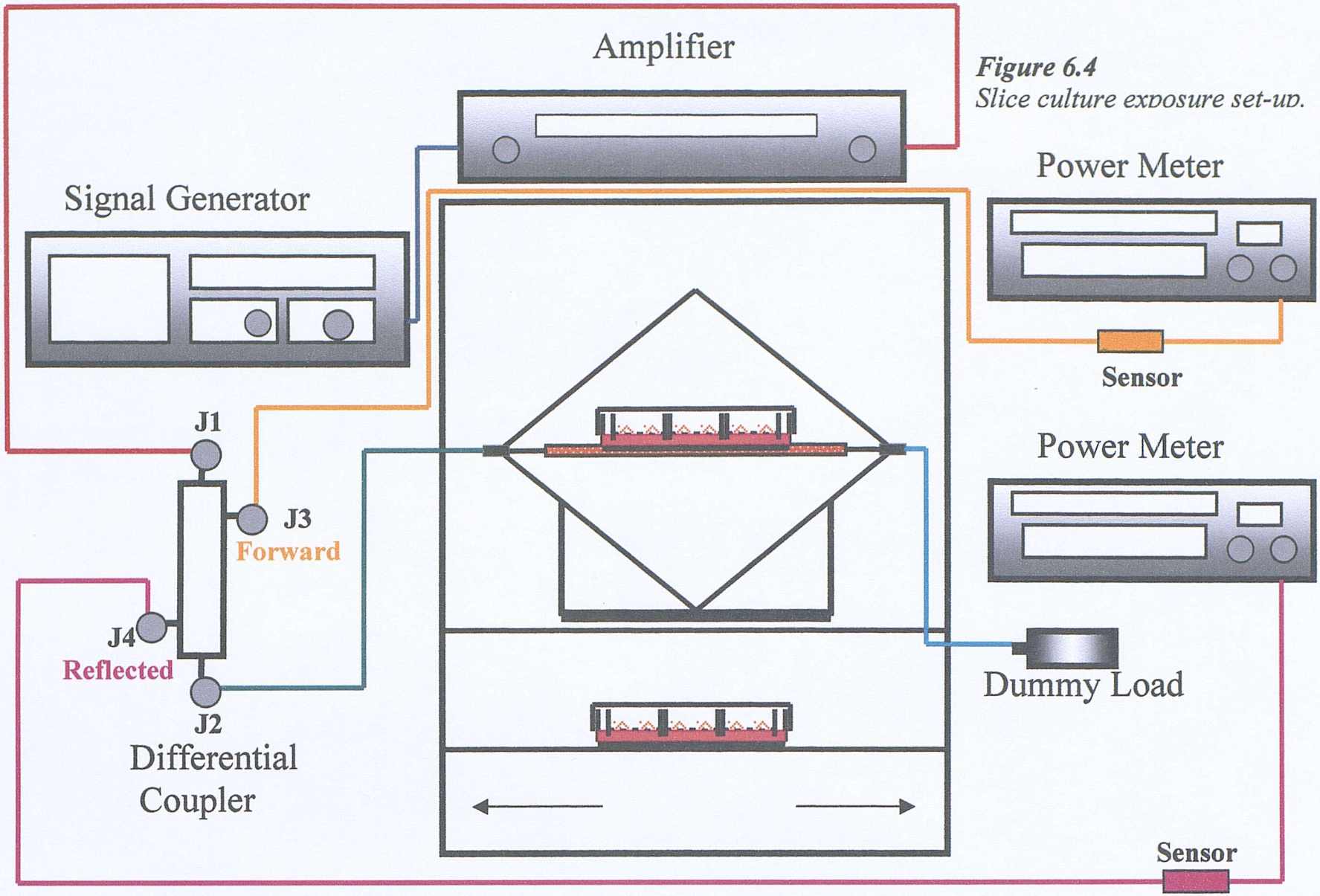

Figure 6.4
Slice culture exposure set-up.

In addition, slices were exposed to an alternative temperature (either 35, 39 or 41°C) or maintained at 37°C (controls) for 4 hours before returning to the 37°C incubator for twenty-four hours. Slices were fixed in 4% PFA at the end of the 24-hour post insult incubation period before later determination of HSP72 IR.

6.4.3 Temperature dependence of C-fos induction.

Several authors, for example Curran & Morgan, (1994) and Rudick & Woolley, (2000) report a phasic *c-fos* response in hippocampal tissue in response to stimuli such as ischemia (Zhou *et al.*, 1995; Sanz *et al.*, 1997), estradiol (Rudick & Woolley, 2000) and kainic acid (Kasof *et al.*, 1995; Sanz *et al.*, 1997). Between them, these studies indicate that c-*fos* levels increase within 0.5 hours of the insult, peak within 2 to 6 hours and return to baseline levels by 24 hours. Because c-*fos* was shown to increase after 30 minutes of insult, c-*fos* IR was examined 1-hour post insult.

In common with the protocol for *HSP72* IR, cultures were exposed to an alternative temperature (35, 39 or 41°C) for 4 hours or maintained at 37°C (controls) for 4 hours before being returned for 1 hour to the 37°C incubator. As before, slices were subjected to one of two treatments; (a) placed in the transverse electromagnetic cell during exposure (RF group) or (b) foil shielded and placed on a lower shelf in the incubator (sham-exposed control group) to prevent contamination from reflected RF electromagnetic energy. At the end of the exposure period, slices were fixed in 4% PFA before processing for *c-fos* IR.

6.5 Results

6.5.1 HSP72

Two methods were used to evaluate *HSP72* induction. Analysis was conducted in a blind manner by my supervisor, Dr J.E.H. Tattersall. The scorer was unaware of which experimental group or temperature each slide came from. Qualitative evaluation of *HSP72* IR staining was assessed on a scale of 0-6 (Table 6.2). In slices where there was staining of cell bodies (equivalent to scores of between 3 and 6 on qualitative scale), a subsequent quantitative analysis of the number of positively stained cells was obtained (Table.6.2 and Figure 6.11).

Score	*Score Key*
0	No staining
1	Slight staining (above background)
2	Diffuse staining (dendrites)
3	Some cell bodies apparent
4	Light cell body staining
5	Heavy cell body staining
6	Heavy staining throughout

Table 6.2 *Score key used in qualitative scoring of HSP72 stained slices.*

Qualitative scoring of *HSP72* positive slices revealed increased staining as slices were exposed to increasing temperature. The staining score increased in a temperature-dependant manner with slices exposed to radiofrequency electromagnetic fields showing a greater score than that of the temperature matched sham-exposed control slices (Figure 6.5 and 6.6). These changes were highly significant at 41°C in the CA1 and dentate gyrus areas ($P< 0.01$) and significant in the CA3 region ($P< 0.05$). At all other temperature points, the score number was larger for RF exposed slices than that of the sham-exposed control slices (Figure 6.5). Interestingly, the score number for *HSP72* staining rose consistently (RF exposed slices) in the CA1 and CA3 regions with each temperature increment, but remained at a similar level in the dentate gyrus until cultures were exposed to 41°C. At this temperature, the DG score number increased dramatically in RF exposed cultures (Figure 6.5). In sham-exposed control slices, the DG score number remained at baseline levels even at high (41°C) temperature (Figure 6.5), indicating that cells of the dentate gyrus are particularly susceptible to RF exposure when combined with high temperature insult.

The dose-response curve for sham-exposed control slices was more variable than that of RF exposed slices. In the CA1 region, score number increased with each temperature rise until 39°C; thereafter, the score number

dipped below that obtained at 39°C, contrary to the incremental rises seen with RF exposure (Figure 6.5 and 6.6).

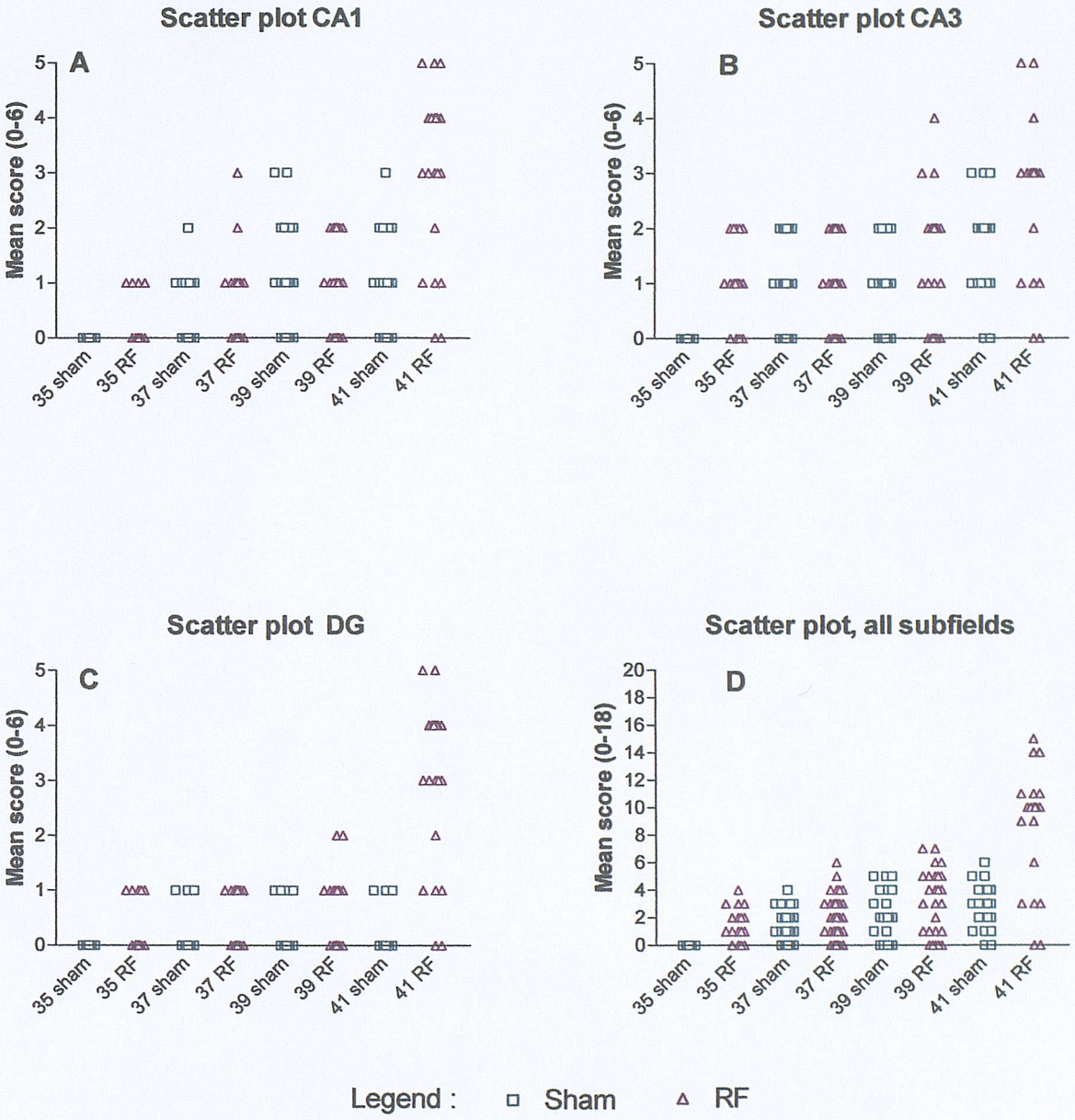

Figure 6.5 *Scatter plot of HSP72 scored data.*

Organotypic slice cultures exposed for 4-hours to temperature insult and 700 MHz RF (RF) or temperature insult and sham-exposure (sham). In both cases, the initial temperature insult was followed by 24 hours incubation at 37°C without RF or sham exposure. **A:** HSP72 induction in CA1 pyramidal cells. **B:** HSP72 induction in CA3 pyramidal cells. **C:** HSP72 induction in granule cells of the dentate gyrus. **D:** Pooled data of HSP70 induction from all subfields.

Figure 6.6 *Line graph of HSP72 induction from scored data.*

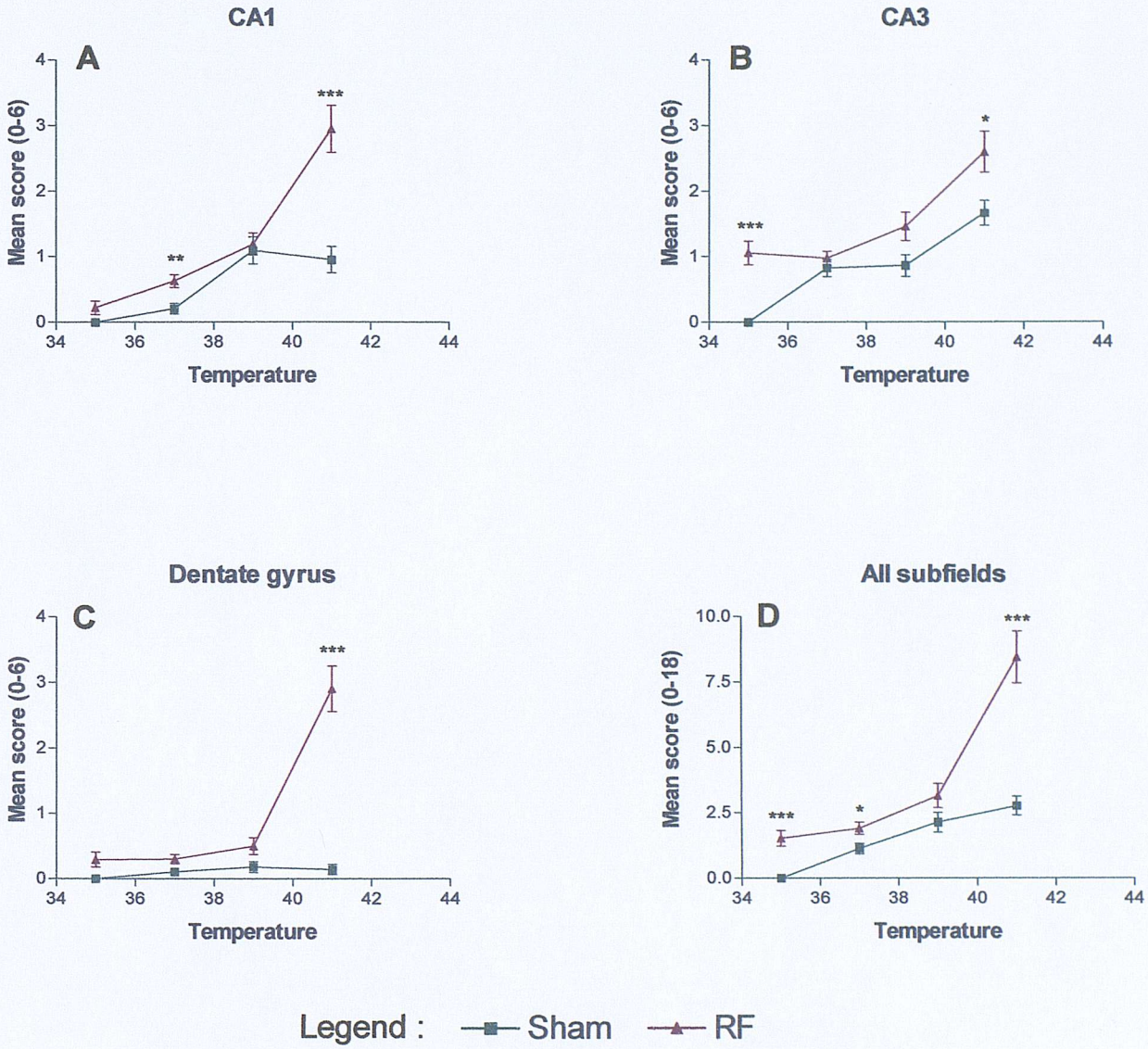

All figures in A-D show the mean ± S.E. Significance was assessed by Mann-Whitney test. Asterisks above data points depict significance as follows: * = $P < 0.05$, ** = $P < 0.01$ and *** = $P < 0.001$. Temperature is shown in °C.

The number of cultures (*n*) assigned to each group were as follows:
RF: 17, 43, 26 and 20 cultures for temperatures of 35, 37, 39 and 41°C respectively.
Sham: 15, 37, 22 and 21 cultures for temperatures of 35, 37, 39 and 41°C respectively.
A: Heat shock induction in CA1 pyramidal cells.
B: Heat shock induction in CA3 pyramidal cells.
C: Heat shock induction in granule cells of the dentate gyrus.
D: Pooled data of HSP70 induction from all subfields.

Figure 6.7
Photomicrographs of organotypic hippocampal slice cultures.

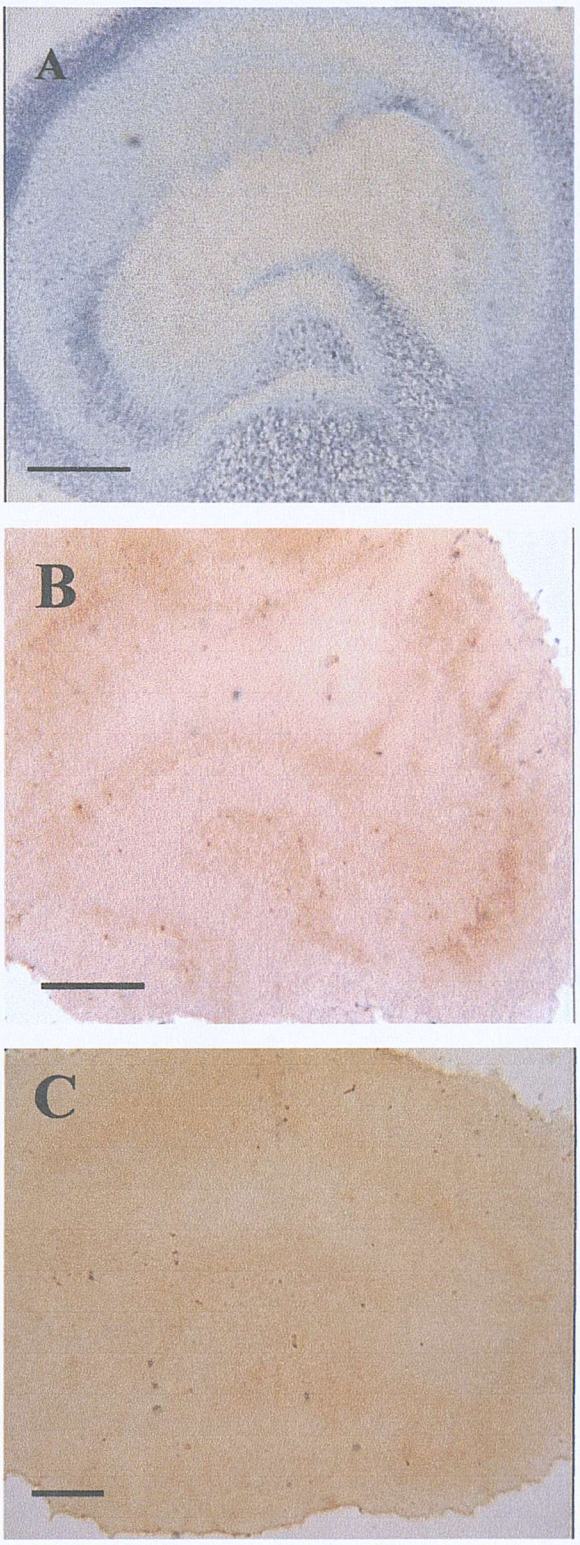

A: Thionin stained control culture maintained for 14 days in vitro at 37°C. **B:** *HSP72* stained culture that was exposed to 700 MHz RF for 4-hours at 37°C. **C:** HSP72 stained culture that was sham-exposed to 700 MHz RF at 37°C. Scale bar = 1mm in all photomicrographs.

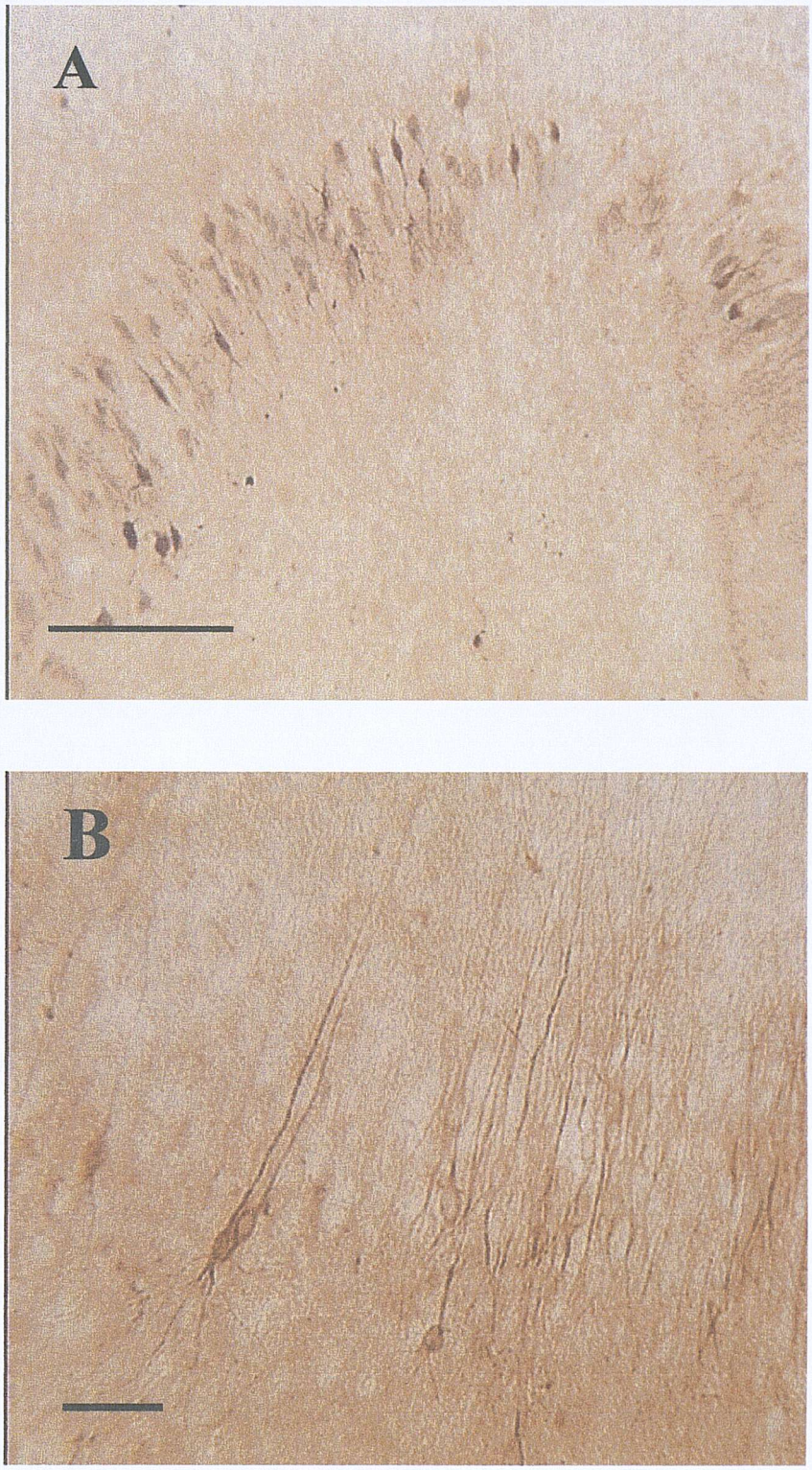

Figure 6.8 *Photomicrographs of HSP72 immunostaining.*

Slices exposed to 700 MHz RF, 1W input power for 4-hours, at 39°C. **A:** HSP72 induction in the CA3 regions. **B:** Individual neurones in the CA1 region stained for HSP72, the cell bodies, apical and basolateral dendrites can be clearly seen. Scale bars = 100μm.

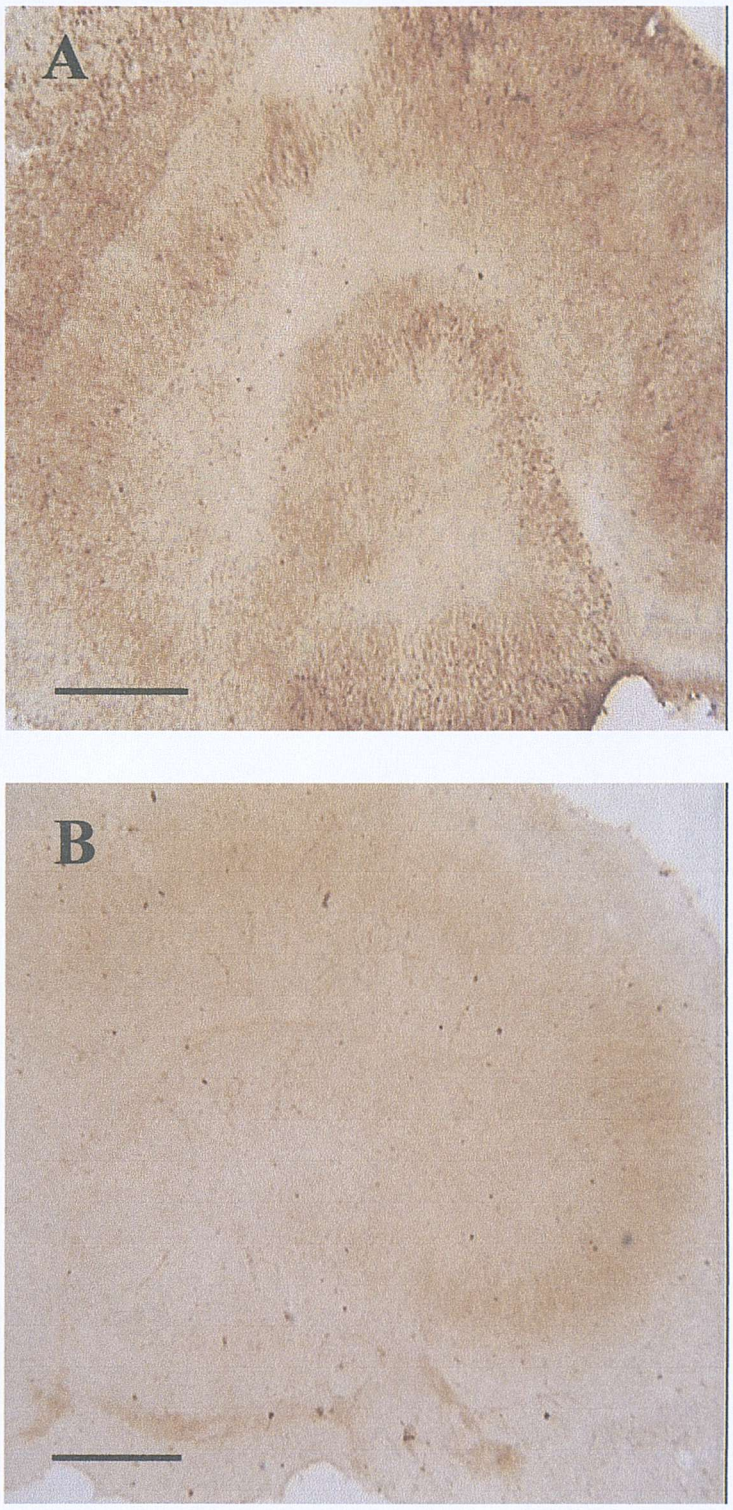

Figure 6.9 *HSP72 immunostaining of cultures exposed to 41 ℃.*

A: *HSP72* staining in slices exposed to 700 MHz RF, 1W input power for 4-hours, at a temperature of 41°C. **B:** *HSP72* staining in sham-exposed control slices exposed for 4 hours to 41°C temperature insult. Scale bar for both A and B = 1mm.

In the CA3 region, the score number for sham-exposed slices closely followed that of RF exposed slices throughout the temperature range studied; although the score was consistently less than that of the RF exposed group (Figure 6.6). In this instance, the number of *HSP72* positively stained cells per slice was plotted as a function of temperature (Figure 6.10 and 6.11) for RF or sham exposure. Results of the cell count in the CA1 region revealed very little positive staining in RF exposed slices until 41°C. In contrast, sham-exposed control slices displayed some positive staining at 39 and 41°C, although none of the changes was significantly different (Mann-Whitney test). In the CA3 and dentate gyrus regions, positive staining of cells only occurred at high temperatures (39 and 41°C for RF exposed slices and 41°C for sham-exposed control slices. Once again these changes were not significant (Mann-Whitney test) when compared with their temperature-matched controls (Figure 6.10 and 6.11).

6.5.2 C-Fos

Unfortunately, the *c-fos* results are not presented because of difficulties with the immunocytochemical staining. Cultures exposed to radiofrequency or sham-exposed RF fields were stained for *c-fos* at the same time as the positive control slices (5μM kainic acid (KA) applied for 1 hour). All organotypic slice cultures (RF, sham and KA) were positively stained for *c-fos* using the method of Minson *et al.*, (1994). Very high background levels of staining were observed even when extremely low concentrations of primary and secondary antibody had been used, making it difficult to discern nuclear staining from the background noise. Furthermore, the finding that the negative controls (which had no primary antibody applied) also had background staining indicates that the initial positive results were due to non-specific binding of the secondary antibody.

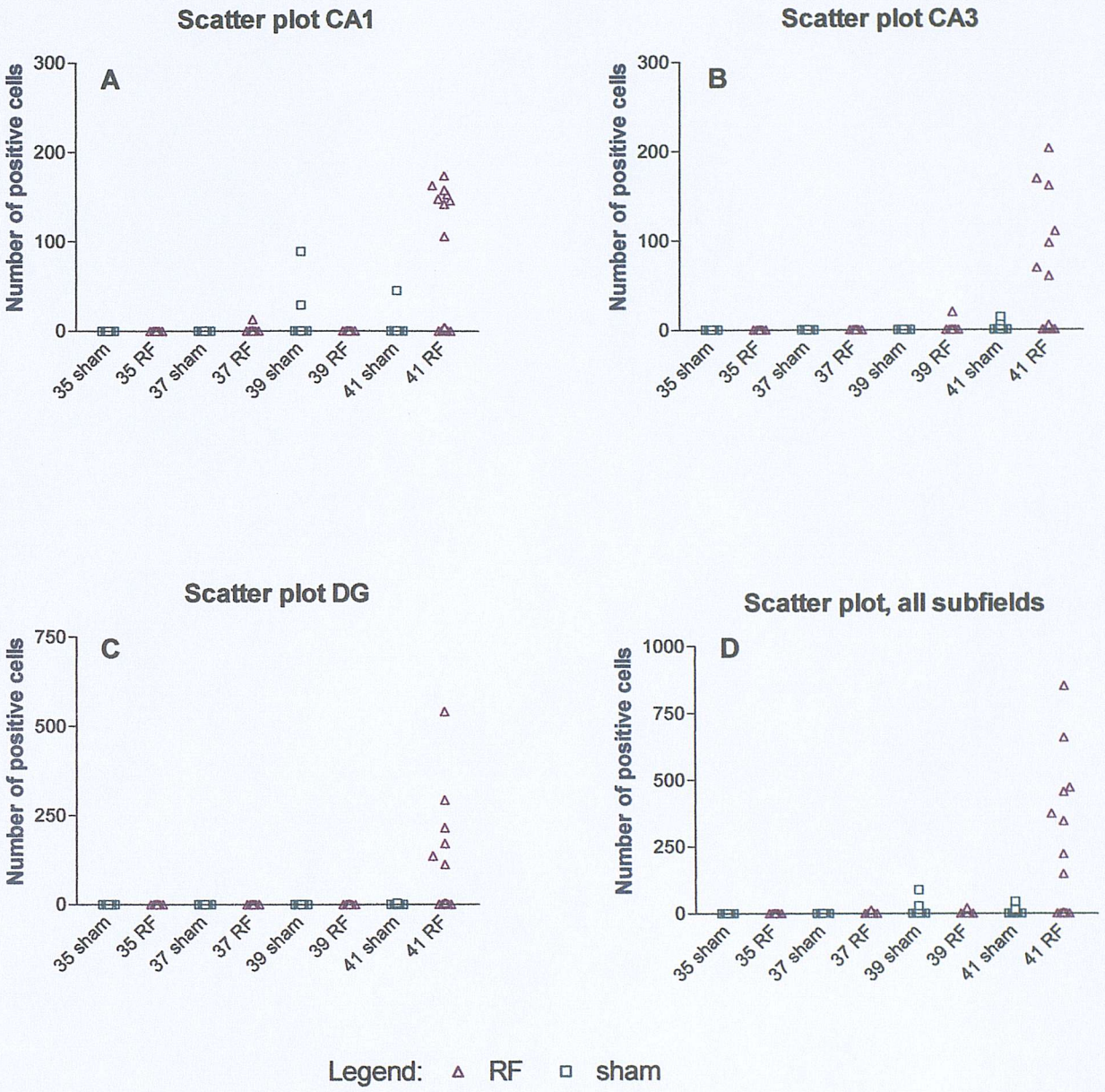

Figure 6.10 *Scatter plot of HSP72 cell count data.*

All figures in A-D show the number of positively stained cells in each slice. There were no significant differences between groups of counted cells (Mann-Whitney test). Temperature is shown in °C. The number of cultures (*n*) assigned to each group was:
RF: 17, 43, 26 and 20 cultures for temperatures of 35, 37, 39 and 41°C respectively.
Sham: 15, 37, 22 and 21 cultures for temperatures of 35, 37, 39 and 41°C respectively.

A: Number of HSP72 positive cells per slice in CA1 pyramidal cells.
B: Number of HSP72 positive cells per slice in CA3 pyramidal cells.
C: Number of HSP72 positive cells per slice in granule cells of the dentate gyrus.
D: Pooled data of HSP72 positive cells from all subfields.

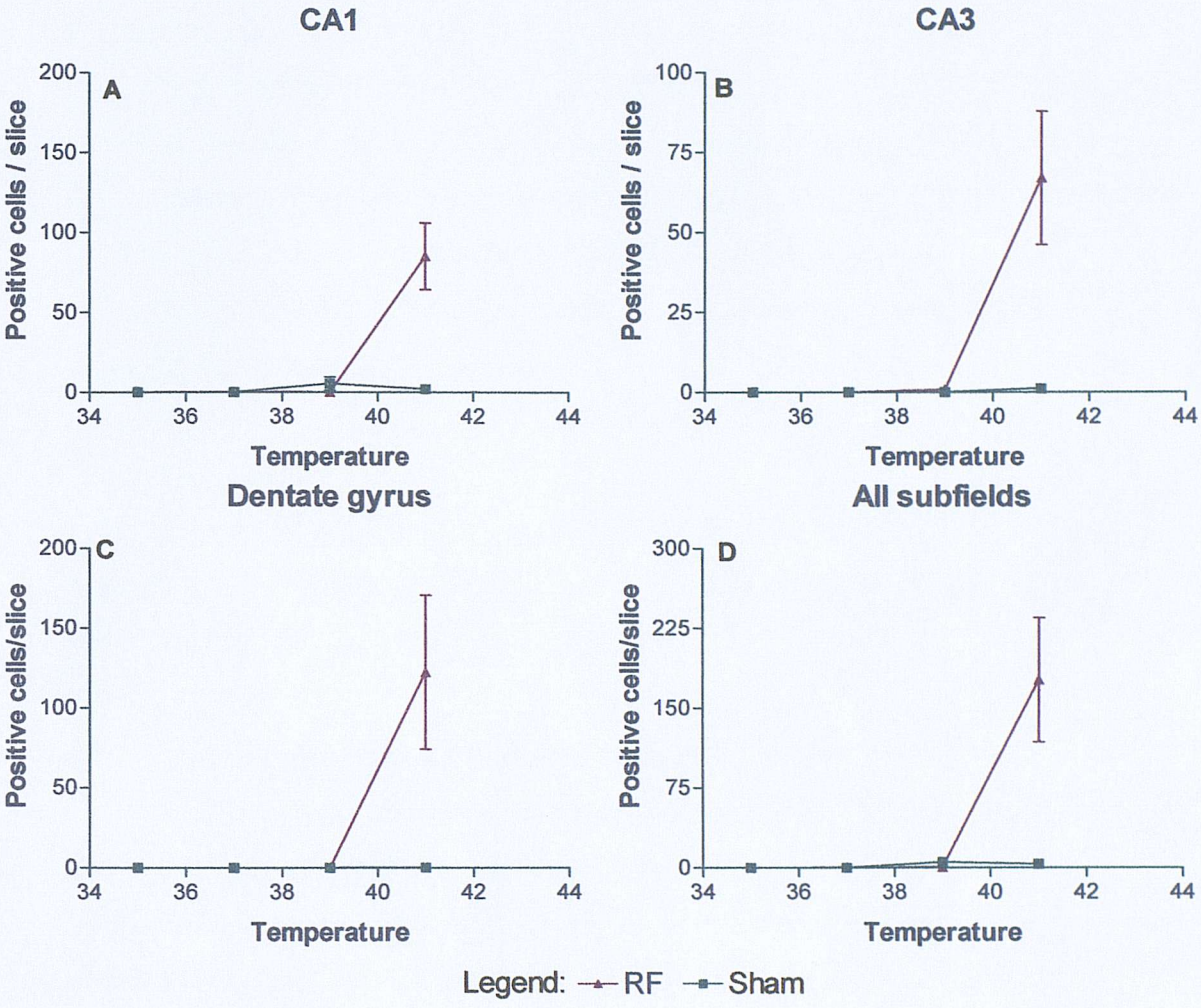

Figure 6.11 *Number of HSP72 positive cells per slice culture.*

All figures in A-D show the mean ± S.E. Temperature is shown in °C. There were no significant differences between groups of cells (Mann-Whitney test).
The number of cultures (*n*) assigned to each group were:
RF: 17, 43, 26 and 20 cultures for temperatures of 35, 37, 39 and 41°C respectively.
Sham: 15, 37, 22 and 21 cultures for temperatures of 35, 37, 39 and 41°C respectively.
A: Number of HSP72 positive cells per slice in CA1 pyramidal cells.
B: Number of HSP72 positive cells per slice in CA3 pyramidal cells.
C: Number of HSP72 positive cells per slice in granule cells of the dentate gyrus.
D: Pooled data of HSP72 positive cells from all subfields.

Moreover, since the Cullinan *et al.*, (1995) study used 15μm thick coronal brain slices in the staining protocol gives rise to the theory that the current technique may not be suitable for thick tissue slices. Given that 400μm thick organotypic hippocampal slices flatten considerably, but are still in the region of 175μm thick after 14 days *in vitro* (Buchs, *et al.*, 1993; Best *et al.*, 1996), it is possible that the antibodies did not penetrate the tissue adequately. Because of the problems encountered in finding suitable positive and negative controls for the immunohistochemistry, completion of this part of the study will have to wait until the necessary controls can be obtained.

6.6 Discussion.

Previous studies that have examined the induction of heat shock proteins and/or induction of the immediate early gene *c-fos* after exposure to RF radiation insult have reported contradictatory results.

6.6.1 HSP70 expression in mammalian cell lines.

There has been surprisingly little work done on the effect of RFR electromagnetic fields on heat shock protein induction. Two studies have investigated the effect of radiofrequency electromagnetic fields on mammalian cell lines. In the first of these, Cleary *et al.*, (1997) observed that log-phase HeLa or CHO cells which were subjected to 2 hours, continuous wave 27MHz, or 2450 MHz RF radiation, specific absorption rates of 25W.kg^{-1} or 100 W.kg^{-1} respectively did not induce 70kDa stress proteins. The second (Velizarov *et al.*, 1999), examined the effects of a 960 MHz, RF signal modulated at 217 Hz, 2.1μW.g^{-1} SAR on the cell proliferation rate of transformed human epithelial amnion cells.

The authors found that cell proliferation was significantly increased in RF exposed cells at both 35 and 39°C compared to control cells. They suggest that biological effects occurring in response to RF radiation cannot be attributed solely to a change in temperature. Velizarov *et al.*, (1999) found in one of their earlier studies, that exposure to low-frequency electromagnetic fields resulted in an increase in *HSP70* and *HSP90* which could not be obtained by a rise in temperature alone of up to 40°C (see Velizarov *et al.*, (1999) for review).

Although the authors did not look at the induction of *HSP70* directly, they propose that heat shock proteins involved in the cellular stress response to electromagnetic fields could be responsible for the changes in cell cycle rates.

6.6.2 HSP70 expression in invertebrate models.

A recent series of studies (Daniels *et al.*, 1998; de Pomerai et *al.*, (2000a,b) indicated that the heat shock response is activated in the soil nematode *Caenorhabditis elegans* after exposure to low intensity microwave fields. These studies examined the expression of *HSP16* after overnight exposure to continuous wave RF radiation at 750MHz, 0.5W power, 0.002 $W.kg^{-1}$ SAR in a transverse electromagnetic (TEM) cell. De Pomerai *et al.*, (2000a) demonstrated significant induction of the heat-shock response during prolonged exposure to the RF fields. De Pomerai *et al.*, suggests that since no measurable increases in ambient or worm culture temperatures during exposure was observed, these changes could involve non-thermal mechanisms. They postulated a number of potential mechanisms including disruption of the hydrophobic interactions that maintain the active folded forms of proteins, enhanced formation of reactive oxygen species or interference with cellular signalling systems involved in the phosphorylation of heat shock factors.

In the present study, the *HSP72* induction curve increased markedly with RF exposure (Figure 6.6), a similar finding to that of de Pomerai *et al.*, (2000a). In sham-exposed slices, the *HSP72* score number did not show the rapid phase of induction that occurs some 3°C above the normal 24°C maintenance temperature of cultured *C. elegans* nematodes. One possibility that must be addressed in future work is that the rapid induction phase may occur at higher temperatures than used here so additional experiments will need to be completed at higher temperatures to see if the current trend in RF exposed slices continues. Additionally, results from experiments carried out at higher temperatures would provide valuable insight into the marked differences between groups that occurred in the dentate gyrus.

6.6.3 HSP70 expression in rat brain.

The first study to have investigated *HSP70* induction in the rat brain in response to high power microwave exposure was carried out by Walters *et al.*, (1998). These authors investigated the induction of *HSP70* in each of 10 brain regions (not including the hippocampus) after short duration (< 30 second) exposure to 2.06 GHz microwaves at a power density of 1.7 W/cm^2 and time-averaged SAR of 983 $mW.g^{-1}$. These exposures were of sufficient intensity to briefly raise brain temperature to 44°C. Comparison of the results obtained from microwave-induced hyperthermia in animals exposed to exertional (aerobic) and/ or environmental heat stress revealed differences in the pattern of *HSP70* expression between groups. *HSP70* expression in sedentary animals exposed to high environmental temperatures was comparable to that of the exercising group, producing *HSP70* throughout the brain. In contrast, high power microwave induced *HSP70* expression was confined primarily to the ventral areas of the mid and hindbrain. Furthermore, the authors point out that exercise alone did not produce significant *HSP70* expression in the absence of hyperthermia.

A subsequent study by Walters *et al.*, (2001) compared the regional distribution of *HSP70* in the central nervous system of young adult and aged rats following hyperthermia. Briefly, 6 or 25 month old rats were exposed for short time periods to 2.06 GHz microwave radiation at a power density of 2.2 W/cm^2 and SAR of 1.231 $W.kg^{-1}$ which raised tympanic temperature to 42.2°C within 30 seconds. As before, *HSP70* induction was determined for each of the 10 brain areas that had been selected for their function in motor behaviour, balance, somatosensory or autonomic control. No significant changes were observed between the young adult and aged animals; however, it is important to note that only minor *HSP70* accumulation was found in sham-exposed animals, which were restrained during the sham-exposure. This finding suggests that restraint stress is not a confounding variable, unlike that which occurs with *c-fos* during restraint (Fritze *et al.*, 1997; Cullinan *et al.*, 1995).

6.6.4 C-fos.

Although the results for *c-fos* are not presented here, a short review of the published data reveals that evidence of IEG activation in response to microwave exposure can be explained by a combination of thermal or restraint stress. For example, Fritze *et al.*, (1997) exposed rats to CW, 900 MHz microwaves at a specific absorption rate of 7.5 $W.kg^{-1}$. This exposure protocol resulted in slightly elevated levels of heat shock protein mRNA in the cerebral cortex (assessed by in situ hybridisation techniques). In an alternative group of animals, exposure to pulsed microwaves at specific absorption rates of 0.3 – 1.5 $W.kg^{-1}$ found no effects in the rat cerebral cortex.

At high 1.5 and 7.5 $W.kg^{-1}$ exposures, slightly elevated but significant levels of *c-fos* mRNA were found. However, these changes were consistent with the immobilization stress that occurred during the exposure since similar alterations in *c-fos* mRNA levels were seen in the non-exposed immobilized group but not in the non-exposed, freely moving rats. Furthermore, Cullinan *et al.*, (1995), demonstrated that *c-fos* mRNA expression is activated in the brain after 30-minutes acute, swim restraint stress. This finding suggests that care must be taken in the interpretation of data from animals subjected to immobilization during exposure since the *c-fos* induction seen in restrained rats is similar to that observed in the Fritze *et al.*, (1997) study.

A study by Walters *et al.*, (1995) exposed rats to 2 minutes of pulsed (60Hz, 5-10 nsec) ultra-wide band (UWB) microwaves (bandwidth, 0.25 to 2.5 GHz). They determined that there were no significant differences in *c-fos* protein induction in immunohistologically-stained sections of the brain of rats in either the UWB or sham-exposed groups. In contrast to these studies, Mickley *et al.*, (1994) reported an increase in *c-fos* protein levels following microwave-induced hyperthermia after 20 minutes exposure to CW, 600 MHz RF, 9.3 $W.kg^{-1}$ SAR (which caused a 2°C increase in rectal temperature). Together, these studies indicate that acute exposure to CW or pulsed RF at non-thermal levels does not lead to any relevant activation of *c-fos* gene expression in the brain; increases in c-*fos* expression can be accounted for either by immobilization stress (Fritze *et al.*, (1997), or thermal stress (Mickley *et al.*, 1994).

7 DISCUSSION

Recently, the Royal Society of Canada, (1999), the Independent Experts Group on Mobile Phones (2000) and the Advisory Group on Non-ionising Radiation (AGNIR) (2003) highlighted a growing number of studies focussing on the safety of exposure to RF and the potential of RF exposure to cause biological effects. The presence of non-thermal biological interactions of RF would require extensive review of the current safety guidelines. The work presented in this thesis aimed to verify the findings of Tattersall *et al.*, (1999; 2001) who reported that low-intensity RF fields (700MHz, E field intensity 71.0 $V.m^{-1}$) could affect electrical activity in hippocampal slices in the absence of measurable heating. Characterisation of some of the mechanisms underlying the effects of RF would help to advise future safety standards.

Current safety guidelines covering exposure to radiofrequency electromagnetic fields (ICNIRP, 1998) are derived from the well-established thermal effects of RF (see for example Sienkiewicz, 1998). These guidelines are based on the gross thermal effects of heating and may not fully predict the hazards associated with exposure to short, high power pulses of low average power (Tattersall *et al.*, 2001). RF and other forms of electromagnetic energy are used in a variety of applications ranging from television transmission, wireless communications, radar and medical applications. RF is routinely used in day-to-day life and in particular, for communications purposes so it is therefore essential to have a thorough understanding of the conditions to which an object is exposed and a knowledge of the amount of energy absorbed (SAR) by an object within the field.

7.1 Dosimetry

The importance of accurate dosimetry has been emphasised by the World Health Organisation and the IEGMP. For this reason, the study of dosimetry associated with a particular exposure system must be systematically and adequately described so that the modelling of an animal or phantom can be extrapolated to relate to exposure conditions that would apply to a whole animal or person exposed to the electromagnetic field. Dosimetry is fundamental to this study; both in order to determine the likelihood of thermally mediated effects and to enable comparison of energy absorption in the *in vitro* experiments to exposure *in vivo*.

7.1.1 Calibrated stripline waveguide exposure system.

The present work has examined the components of the electromagnetic field in the waveguide exposure system and supplemented the theoretical assessment of SAR obtained from the FDTD and mathematical modelling methods. Theoretical and mathematical dosimetry confirmed that the RF field effects observed in these experiments could not be explained by thermal interaction.

7.1.2 Micro-thermocouple measurement of temperature.

Tattersall *et al.*, (2001) observed that direct measurement of the temperature rise within a small (400μM thick) slice of brain tissue had not been possible during electrophysiological recording by conventional artefact free, fibre optic probes because of limitations in the probes size (1mm diameter) and resolution (maximum sensitivity, 0.1°C). Accordingly, the use of micro-thermocouples to directly measure the RF induced temperature rise was an attractive proposition for the present study.

The use of microthermocouples to measure SAR in systems exposed to RF is controversial (Pakhomov *et al.*, 2000a,b). The main reason for controversy surrounding their use in RF projects stems from distortion of the electric field by electric currents induced in the probe and wires leading to erroneous temperature readings.

Extensive testing of MTC during the project showed that they were unsuitable for use under these conditions. The presence of the metal MTC wires in the RF field produced excessive interference during exposure (Deans *et al.*, 2000), additionally, the voltage change detected at the end of the exposure period was shown to be an artefact produced by heating of the MTC wires whilst the field was on. Accordingly, the use of micro-thermocouples to record local SAR in the stripline calibrated waveguide exposure system used here is not recommended unless adaptations to the system prevent or minimise recording artefacts during and immediately after exposure.

Future experiments should look at adaptation of the waveguide exposure system so that the slice is positioned parallel to the E-field. This could be achieved by rotating the waveguide through 90° (although it would also require adaptations to the recording chamber and perfusion system); in this configuration, with the MTC inserted from above the slice, minimal heating of the wires would occur and hence lessen the possibility of recording an artefact upon termination of the field.

Besides the adaptation to the stripline waveguide described above, additional experiments should be carried out with one of the new smaller diameter, miniature fibreoptic probes to measure temperature. The advantage of using this type of system is that the probe is 'invisible' to the RF signal and should not produce the artefacts associated with micro-thermocouples. Additionally, the tip diameter is small enough that it may be inserted directly into the slice during electrophysiological recording. The (FOT-HERO) temperature sensor, tested by (Pakhomov *et al.*, 2003) in their waveguide exposure system was found provide a good approximation of local SAR and agreed well with MTC recorded data; it may be an appropriate choice for future experiments.

7.1.3 Thermal imaging of temperature change.

Thermographic imaging techniques have been successfully used to determine the specific absorption rate in animal phantoms and cadavers (Durney *et al.*, 1986) and should be a suitable method of determining SAR distribution in a tissue slice. Temperature measurements were made in slices exposed to 700MHz RF in the waveguide exposure system with an IRRIS-256ST infrared radiometric imager (0.1°C temperature resolution). FDTD estimation of the temperature rise in the head predicted to occur from RF exposure at mobile telephone frequencies (Dimbylow, 1994) indicates a maximum temperature rise of 0.11°C. Since the thermal camera operates with a resolution at the upper end of this scale it will not register small (< 0.1°C) changes in temperature that may occur during exposure.

In common with the results of the micro-thermocouple experiments, temperature measurement in the presence of the thermal camera was unsuccessful. The main reason for failure to determine local SAR was the presence of a recording artefact during the period of exposure. This artefact presented as a downward deflection in the recording at the start of the RF application and an upward deflection upon termination of the signal, these deflections were not observed in the sham-exposed control slices, tending to indicate that they are artefacts caused by interaction with the wires from the thermal camera with the electromagnetic field.

In designing future experiments, extra care should be taken to minimise these artefacts by shielding the camera wires from the electromagnetic field. Until these

experiments have been repeated, it will be difficult to draw firm conclusions from SAR values obtained by these methods.

FDTD estimation of the temperature rise in the head predicted to occur from RF exposure at mobile telephone frequencies (Dimbylow, 1994) indicates a maximum temperature rise of 0.11°C. Since the thermal cameras operate with a resolution at the upper end of this scale they will not register small (< 0.1°C) changes in temperature that may occur during exposure.

7.1.4 Conclusions – waveguide dosimetry.

In conclusion, theoretical dosimetry (FDTD or mathematical modelling), which should be artefact free, gives the best estimate that the exposure is essentially athermal at the power levels used. Suggestions for improvements to the experimental dosimetry include rotating the waveguide through 90°, to increase coupling of the tissue to the E-field; exposing a larger pieces of tissue (10g, as in the ICNIRP, 1998 guidelines) to the field and scaling the value to that of a brain slice; measurement with a smaller fibreoptic probe, and investigation of fluorescent dyes which may be sensitive to temperature.

7.1.5 TEM cell dosimetry.

The results of the Luxtron dosimetry reported in Chapter 3 (section 3.8.4) strongly suggest that slice cultures were exposed to RF induced heating during the exposure period. The additional heating may account for some of the increased expression of heat shock protein described in Chapter 6. The large temperature rise recorded by the non-perturbing temperature probe may be due to the culture plate being fully enclosed in the TEM cell so that any temperature rise is unable to dissipate to the surrounding area. FDTD modelling carried out by Motorola for lossy media exposed to 0.5W input power, 750MHz RF indicates that the depth of the lossy media and height above the TEM cell septum are important parameters in determining local SAR.

Average SAR at the edge of the culture plate is estimated to be $0.005 W.kg^{-1}$ per gram of lossy media and much less in the central portion of the culture dish when a depth of 2mm lossy media is used in the simulations, so the predicted SAR should be much less in the organotypic slice cultures (which weigh less than 5mg weight and are less than 0.2mm in depth). Although it is likely that it is a combination of thermal and non-thermal effects which contributed to the increase in heat shock protein expression

reported in Chapter 6, the question of whether minute thermal changes caused by RF exposure alone are responsible for the reported effects remains unclear. Additional theoretical and experimental dosimetry should be completed for the TEM cell exposure system before a thermal mechanism of interaction can be excluded.

7.2 Extracellular field potential recordings.

These experiments have provided the first independent confirmation of results of the Tattersall *et al.*, (2001) study, that exposure to low-intensity RF fields can affect the evoked response of CA1 pyramidal cells. These effects were seen at specific absorption rates of up to 4.4mW.kg^{-1} and were therefore not associated with heating.

The experiments reported here are an extension of that study and include paired-pulse extracellular field potential recordings from CA1 pyramidal cells; this allowed examination of the additional parameters, E-S ratio and paired-pulse inhibition. The E-S ratio is an important factor as it provides an indication of the excitability of pyramidal cells in the slice; an increase in E-S ratio indicates an increase in excitability and a decrease indicates a reduction in excitability. During exposure to 700MHz RF fields, one slice (1 of 8) showed a transient increase in E-S ratio, which returned to baseline levels by the end of the exposure period. This transient increase in E-S ratio was not observed in any other slice exposed to RF or in any of the sham-exposed control slices.

Paired-pulse inhibition is calculated from the ratio of PS2/PS1, a ratio of <1 indicates an inhibition of the test response whereas a ratio of >1 is indicative of facilitation of the second response. In RF exposed slices, the paired pulse ratio increased from a mean value of 0.67± 0.2 (n = 8 slices) prior to exposure to 0.81 + 0.1 after exposure. In contrast, the paired-pulse ratio in sham-exposed slices remained at a similar value throughout. This change in paired-pulse ratio suggests that the changes in evoked field potentials in response to RF exposure may be the result of a specific effect on inhibitory pathways, reducing inhibition in the tissue and not a change in neuronal excitability as measured by the E-S ratio.

It has been suggested that the effects of RF on evoked field potentials may be due to the presence of the metal stimulating electrode in the slice during RF exposure. Although this remains a possibility, data from the Tattersall *et al.*, (2001) study, in

which the effects of RF exposure on spontaneous epileptiform activity induced in the CA3 region by the potassium channel blocker 4-AP was examined, suggests that this is not the case. In these experiments, suppression of epileptiform activity was observed in response to RF exposure in the absence of the metal stimulating electrode.

In conclusion, the experiments on evoked potentials reported here clearly demonstrate the reduced effectiveness of inhibitory mechanisms in the brain whilst having little effect on the excitability of nerve cells.

7.3 Pharmacology.

Chapter 4 reported that the effects of RF exposure on slice electrophysiology showed some similarity to long-term potentiation and long-term depression. In order to test whether the effect was dependent upon NMDA receptor activation, two selective NMDA antagonists were used to block these receptors during RF exposure.

7.3.1 D-APV

The first of these, D-APV, is a competitive antagonist that competes with glutamate and NMDA for the same binding site (Meldrum, 1994; Magnusson, 1998). In the presence of D-APV, exposure to the RF field produced increases in both the population spike and *f*EPSP, which were not significantly different from the changes observed in slices exposed to RF in the absence of any drug. These results indicates that blockade of the NMDA receptors with a competitive antagonist does not block the influence of RF exposure on the evoked field potential.

7.3.2 MK801

The second antagonist, MK801 is a non-competitive antagonist that binds within the ion channel to block the flow of ions (Meldrum, 1994; Magnusson, 1998). In the presence of MK801, exposure to the RF field produced also produced increases in population spike and *f*EPSP. On this occasion however, the population spike amplitude in slices treated with MK801, was significantly different from that in slices exposed to RF in the absence of either drug. There were no significant differences in *f*EPSP amplitude between groups. These changes suggest that blockade of NMDA receptors by selective non-competitive NMDA antagonists is partially effective in abolishing the RF-induced effects.

Since the experiments on D-APV and MK801 provided contradictory results, it would be beneficial to explore the whether the RF field produced increases in amplitude through another LTP mechanism. Teyler *et al.*, (1995) describes a second type of LTP in CA1 neurones; voltage-dependent calcium channel LTP, which is induced by afferent activation and leads to calcium ion influx through metabotropic glutamate receptors (mGluRs). A sufficiently strong stimulus will induce both NMDA receptor LTP and the voltage-dependent calcium channel LTP. Bath application of the calcium channel antagonist nifedipine with concomitant application of MK801 would indicate whether there was more than one process involved in the RF-induced effects.

7.3.3 Carbenoxolone.

Carbenoxolone is a synthesised derivative of glycyrrhetinic acid, and known to be a potent, non-specific blocker of gap junctions (Ross *et al.*, 2000). Experiments explored the possibility that gap junctions may be involved in the RF-induced effects on evoked field potentials. Slices treated with carbenoxolone and exposed to RF displayed a variety of response to field application. In some slices, the population spike amplitude decreased to zero, followed by a period of recovery whilst in others there appeared to be no effect. Population spike amplitude was significantly different in carbenoxolone treated slices compared to slices exposed to RF in the absence of any drug. Moreover, the variance of the *f*EPSP slope was significantly different between the two groups.

The results from the study of gap junction blockade are the most promising of the three compounds tested. It proved difficult to maintain stable recordings during the one-hour pre RF exposure period. One reason for this difficulty may be related to the concentration of drug applied to the slices. Ross *et al.*, 2000 report that the concentration of compound used in these experiments (100μM) may be toxic since carbenoxolone was observed to have a TC_{50} of 50μM in fibroblast cells. Future experiments may wish to address this problem by using another gap junction blocker such as octanol. Alternatively, perfusion of slices with ACSF in which calcium has been removed; coupled with high concentrations of potassium and magnesium, has been used successfully at GlaxoSmithKline, Harlow and may provide insight into the mechanism whereby the decrease in amplitude has been observed.

7.4 Organotypic slice cultures

Experiments were designed to test the hypothesis that temperature-dependent induction of HSP*72* would be potentiated by exposure to RF electromagnetic fields. Slices were exposed to 700MHz RF fields (84 $V.m^{-1}$, at a SAR of approximately 3$mW.kg^{-1}$) for four hours in a transverse electromagnetic cell in a temperature-controlled incubator. The TEM cell was identical to the one used in the *C. elegans* studies of DePomerai *et al.*, (2000a,b). At the end of the exposure period, cultures were returned to an incubator maintained at 37°C for a further 24 hours before determination of HSP*72* immunoreactivity. Sham-exposed slices were treated in the same way as RF exposed slices except that they were foil-shielded and placed on an alternative shelf of the incubator during exposure.

Analysis revealed that a more of the RF-exposed slices were HSP*72*-positive compared to sham-exposed slices at all temperatures except 35°C, with the largest increase in immunoreactivity at 41°C. Mann-Whitney test of these data revealed a significant effect of temperature on HSP expression but the effect of RF did not reach significance. Many RF exposed slices at 41°C were excluded from the statistical analysis because neuronal staining was obscured by staining of large numbers of other unidentified cells which were not observed in the sham-exposed slices subjected to 41°C. Subsequent measurement of temperature in the TEM cell exposure system was carried out with the Luxtron 790 fibreoptic probe. Exposure to 40-minutes, RF at 1W input power revealed an appreciable temperature rise in the medium surrounding the cultures (approximately 1°C). Accordingly, part of the increase in HSP*72* staining seen in the RF exposed slices must be attributable to a thermal interaction with the tissue.

It is difficult to quantify how much of the HSP*72* staining can be attributed to RF heating since there was very little neuronal staining in sham-exposed cultures even at 41°C. The 84 $V.m^{-1}$ RF field applied to these cultures was suprathreshold for thermal effects, future experiments should address this problem by looking at lower powers to see if any non-thermal effects can be observed.

A further approach would be to look at the genomic expression of proteins (proteomics) after exposure to RF or sham fields. This method was recently used by M Gatherer (departmental PhD student) in a preliminary examination of protein expression in RF or sham-exposed slices incubated at 41°C (data not presented in this thesis).

Although this work is at an early stage, indications are that a total of 66 proteins had either increased or decreased in abundance by a factor of x5 in RF slices compared to sham-exposed controls. While these proteins have yet to be identified, this technique should provide valuable insight into potential mechanisms of the RF-induced effect in the future.

7.5 Conclusions.

This work has confirmed previous observations that exposure to low intensity (71.0 $V.m^{-1}$) RF fields can affect evoked responses in brain tissue slices *in vitro* in the absence of measurable heating.

Extensive dosimetric evaluation of the stripline waveguide exposure system has shown that microthermocouple temperature sensors cannot be used to measure temperature and hence derive SAR under these conditions. The lack of suitable, artefact free temperature sensors prevents accurate measurement of temperature in slices of rat brain tissue, and as such; it would appear that FDTD modelling provides the best estimate that the exposure is essentially athermal at the intensities used in these experiments.

Studies of the physiological mechanisms of RF interaction suggest the effectiveness of inhibitory mechanisms in brain tissue are compromised during exposure, whilst having little effect on the excitability of neurones. Pharmacological experiments, although inconclusive, point to the potential involvement of NMDA receptors and gap junctions in the RF-induced effects. Further experiments designed to combat inadequacies in the present study would be worthwhile.

Finally, organotypic hippocampal slice cultures are an ideal model to study the expression of inducible heat shock protein after exposure to RF. Experiments indicate that exposure to RF, potentiated the expression of HSP*72*; changes in expression of the protein may be associated with a thermal interaction between RF. Although it has not been possible to exclude athermal interactions, it is difficult to quantify how much of the increased HSP*72* expression can be attributed to thermal changes in the tissue. The most appropriate conclusion at this time is that a combination of factors, including tissue heating contributed to increased HSP*72* expression.

Further experiments including genomic and proteomic techniques should be carried out to characterise whether the observed effects can be replicated with lower intensity radiofrequency fields.

APPENDIX 1 STOCK SOLUTIONS

Cutting ACSF solution

Contents	*Quantity*
Sucrose	64.695 g
KCl	0.186 g
$NaHCO_3$	2.184 g
$NaH_2PO_4.H_2O$	0.165 g
Glucose	1.801 g
$MgCl_2$	0.476 g
$CaCl_2$ (1M solution)	0.1 ml
RO water	1000 ml

ACSF stock solution [x5]

Contents	*Quantity*
NaCl	35.064 g
KCl	0.932 g
$NaHCO_3$	10.921 g
$NaH_2PO_4.H_2O$	0.863 g
Glucose	9.008 g
$MgCl_2$	0.619 g
$CaCl_2$ (1M solution)	2.4 ml
RO water	1000 ml

Normal (Full) medium

Contents	*Quantity*
Minimal essential medium with Earle's salts	100 ml
Hank's balanced salt solution	50 ml
Heat inactivated horse serum	50 ml
200mM Glutamine	1 ml
45% Glucose solution	2 ml

0.2M Phosphate Buffer, pH 7.2

Contents	*Quantity*
KH_2PO_4	11.2 g
Na_2HPO_4	28.4 g
RO water	1000 ml

4% Paraformaldehyde, pH 7.4

Contents	*Quantity*
Paraformaldehyde	40 g
0.2M Phosphate buffer	500 ml
RO water	500 ml
NaOH to adjust pH	

Tris buffered saline (TBS)

Contents	*Quantity*
NaCl	40 g
Tris hydroxymethyl methylamine	3.025 g
1N HCl	19 ml
RO water	5000 ml

Phosphate buffered saline (PBS)

Contents	*Quantity*
KCl	0.2 g
NaCl	8 g
Na_2HPO_4	1.15 g
KH_2PO_4	0.2 g
RO water	1000 ml

APPENDIX 2

A2.1 CUSUM Analysis.

CUSUM charts detect small shifts in the mean of a process. This type of plot is suitable for showing variation in a random pattern of data centred around a given value. If the process mean shifts, the charted cusum points will drift upwards or downwards from the mean value as appropriate (*http://www.itl.nist.gov/div898/handbook/pmc /section3/pmc323.htm).*

Statistical significance can be assessed i) by deviation outside of limits 4 x SD either side of the centre line (target value) in a plot of two one-sided CUSUMs or ii) by the use of a visual mask (V-mask) superimposed on a plot of one two-sided CUSUM. The V-mask is placed so that the origin point of the V (with the V positioned on its side) is placed on the last point of the cumulative sum graph. If any cumulative sum points fall above or below the side of the V, the process is deemed to be 'out of control' and may be statistically significant dependant upon the value of 'k', the rise in the arm corresponding to one sampling unit. When 'k' is set to 2 x S.D. a significance value of P $\approx$ 0.05 is achieved.

Sample V-Mask demonstrating an out of control process

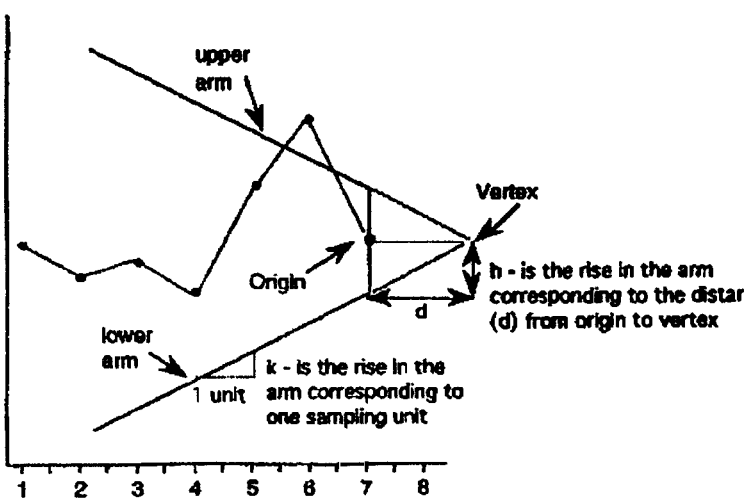

Figure A2.1 *Sample V-mask demonstrating an out of control process.*
From: http://www.itl.nist.gov/div898/handbook/pmc/section3/pmc323.htm

If any points of the cumulative sum graph lie out with the arms of the V-mask, the mask is subsequently moved backwards along the graph so that the origin point covers other cumulative sum data points. The first point at which the cumulative sum data falls out with the V-mask is deemed to signal an out of control situation.

Re-analysis of baseline control (700MHz RF) and sham data for paired pulse inhibition of the population spike 1 (PS1) was carried out using the CUSUM function in Minitab version 13.1 (Minitab Ltd, Birmingham, U.K.). Re-analysis was carried out to determine whether the non-parametric statistics described in Chapter 4 and 5 were a suitable statistical test for those results; additionally, the results of the CUSUM analysis would act as confirmation of the earlier statistics.

A2.2 Results

A2.2.1 700MHz RF

Data for this section were taken from Chapter 4; Table 4.1 & Figure 4.7(A) for slices exposed to 700MHz RF. Only slices that displayed paired-pulse inhibition of population spike 2 (PS2) prior to RF exposure were considered for this section, consequently data from six of the eight slices from the RF group were included.

Since Figure A2.2 appears to show an out of control process, (cumulative data fall out-with the upper CUSUM limits), the V-mask was superimposed on the data (Figure A2.3) to determine the time point at which the out of control occurred. To test for statistical significance, 'k' (the rise in the arm corresponding to one sampling unit) was set to =1 [equivalent to 2xSD] and H (the rise in the arm corresponding to the distance (d) from origin to vertex) was set to = 4. Target = 0.42.

Figure A2.2 CUSUM graph for slices exposed to 700MHz RF.

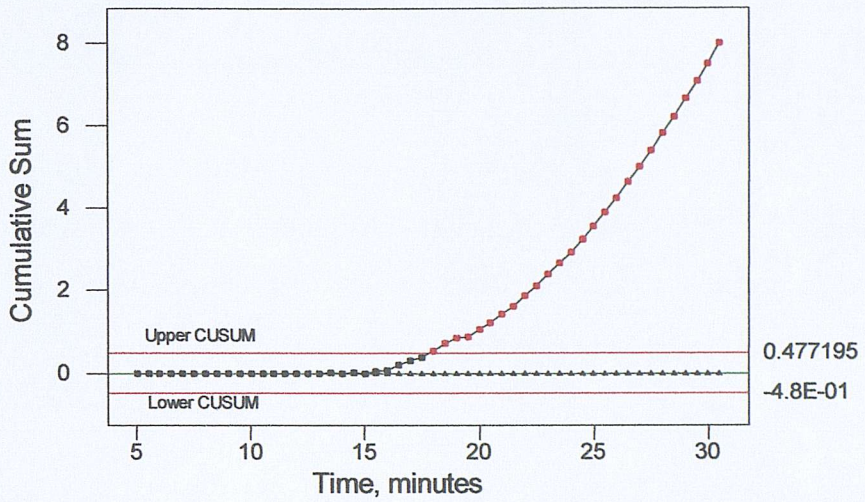

Figure A2.2 shows the cumulative sum plot of data points from 5 minutes after the experiment commenced. Note that RF exposure commenced at 15 minutes and ended at 20 minutes. The two parallel lines indicate the upper and lower CUSUM limits of the mean (Target) data prior to RF application. The graph shows a steep rise in cumulative sum immediately after the RF exposure commences. Target = 0.42, n = 6 slices.

Figure A2.3 *CUSUM graph with V-mask for slices exposed to 700MHz RF.*

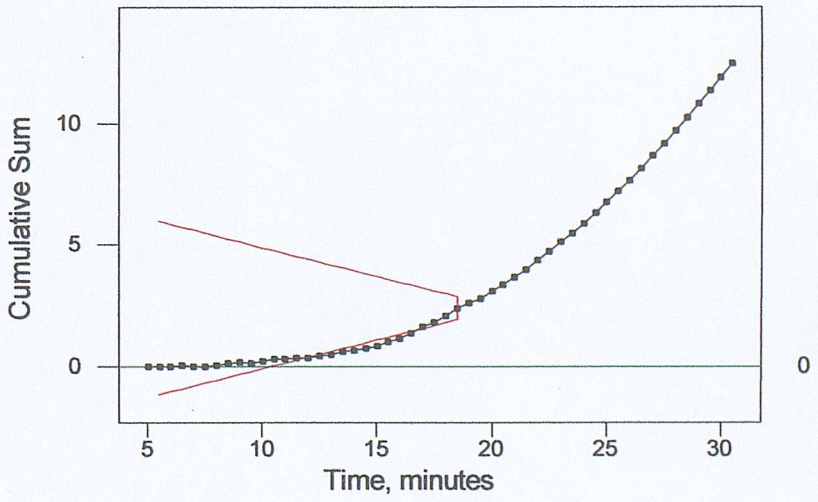

Figure A2.3 RF data with V-mask (red horizontal V on graph) using the parameters K = 1 [equivalent to 2xSD] and H =4. The target was 0.42. V-mask shows RF data fall out of "control process" at 19 minutes. As before, RF was applied from 15 to 20 minutes. RF data (n = 6).

This result compares favourably with the statistical analysis of PS1 examined in Chapter 4. The non-parametric tests described earlier compared population spike amplitude before exposure (T = 9 minutes) with after RF exposure (T = 21 minutes). In the previous case, exposure to RF was statistically significant (P = 0.0104) at 21 minutes (i.e. 1 minute post exposure), the point used for post RF analysis.

A2.2.2 Sham-exposed slices

Data for this section were taken from Chapter 4; Table 4.2 & Figure 4.8(A) for slices sham-exposed to 700MHz RF. As before, only slices that showed paired-pulse inhibition of PS2 were included in the re-analysis. Consequently, four of the eight sham-exposed control slices were tested in the CUSUM analysis.

Figure A2.4 *CUSUM graph for slices sham- exposed to 700MHz RF.*

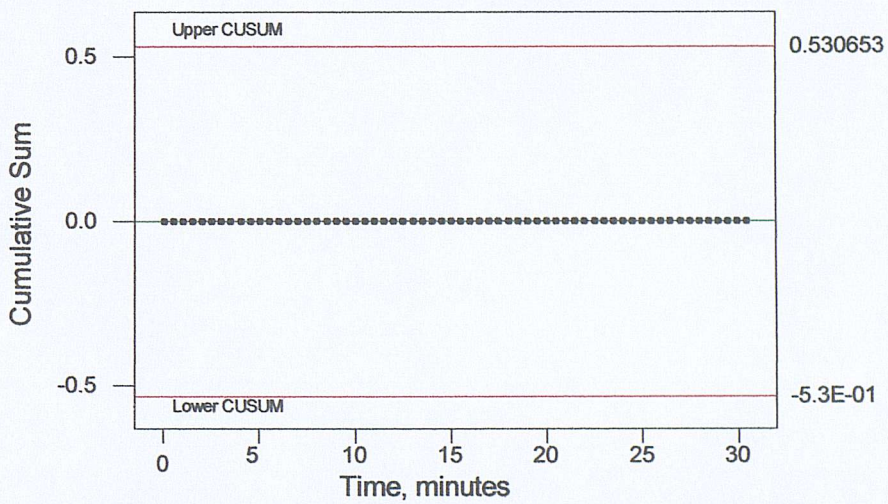

Figure A2.4 Cumulative sum plot of four, sham-exposed slices. Note that sham-exposure commenced at 15 minutes and ended at 20 minutes. The two parallel lines indicate the upper and lower CUSUM limits of the mean (Target) prior to sham exposure. The cumulative sum remained at target levels throughout sham-exposure and after exposure was terminated. Target value was = 0.35.

In figure A2.4, the 'out of control' process is not observed, the data does not deviate from the target value either during the sham-exposure period or after exposure ended. When a V-mask is applied to this data (figure A2.5) it is clear that the cumulative sum points do not exceed the arms of the mask at any time. This finding agrees with the non-parametric statistics for these data (Table 4.2, population spike 1) in that the amplitude of the population spike at 1 minutes post sham-exposure was not significantly different from the pre-exposure baseline.

Figure A2.5 *CUSUM graph with V-mask for sham-exposed control slices.*

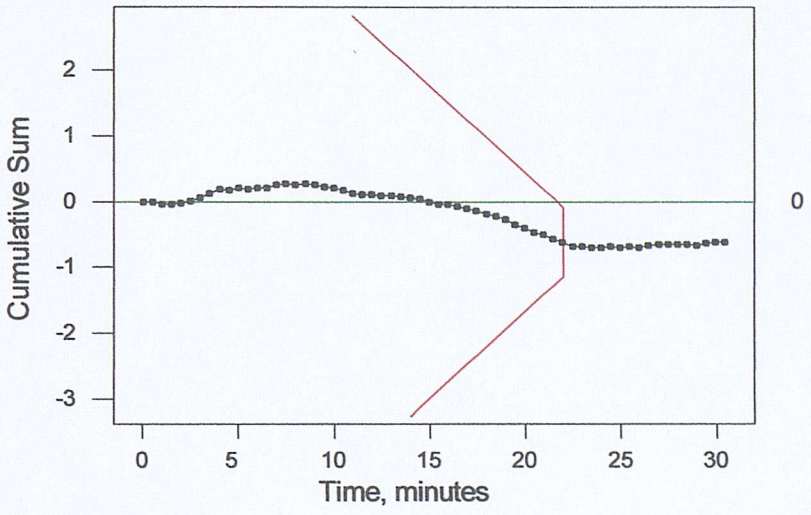

Figure A2.5 Sham-exposed slice data with V-mask (red horizontal V on graph) using the parameters K = 1 [equivalent to 2xSD], H =4 and target = 0.35. The V-mask shows that data from sham-exposed slices do not fall out of "control process" at any time (example shows mask at 22 minutes). Sham data (n = 4).

The benefit of CUSUM analysis is its ability to show the time point at which statistical significance is achieved, it does not depend upon examination of a single time point but upon the cumulative data as a whole. If used in conjunction with the non-parametric statistics, CUSUM provides a more accurate indication of when statistically significant changes occur.

GLOSSARY

Anechoic chamber.
A room or enclosure in which reflections of EM waves from the boundary surfaces have relatively small values.

Anisotropic.
Acting in different ways on the ray of polarized light. Possesses the power of right and left-handed polarization.

Antenna.
A device designed for radiating or receiving electromagnetic energy.

Athermal effect
Any effect of electromagnetic energy absorption not associated with or dependent upon the production of heat or a measurable rise in temperature.

Attenuation
A general term, expressed as a ratio, used to denote a decrease in magnitude of a field quantity in the transmission from one point to another.

Average power (P)
The time-averaged rate of energy transfer

Conductivity
The ratio of the electric field strength in a medium to the conduction current density.

CW
Continuous wave

Decibel (dB)
A measure of the increase or decrease in power at two points expressed in logarithmic form. Gain = 10 $\log_{10}(P2/P1)$.

Diode.
A semiconductor device having two terminals and exhibiting a non-linear voltage current characteristic; in more restricted usage, a semiconductor device that has the asymmetrical voltage-current characteristic exemplified by a single p-n junction.

Dipole.
A linear radiator, usually fed in the center, producing a maximum of radiation in the plane normal to its axis.

Duty cycle
The ratio of the pulse duration to the pulse period of a periodic pulse train.

Duty ratio.
The ratio of average to peak pulse power.

Electric field intensity
The force on a stationary positive charge per unit charge. Measured either in Newton's/coulomb or in volts/meter.

Electromagnetic fields
The electric and magnetic fields associated with electromagnetic radiation.

Electromagnetic radiation.
The propagation of energy in the form of EM waves through space.

ELF
Extremely low frequency.

Far-field
That region of the field of an antenna where the angular field distribution is essentially independent of the distance from the antenna.

Finite difference time domain (FDTD)
A numerical method used to solve electromagnetic field interaction problems.

Frequency
The number of complete cycles of an electromagnetic wave in a second. Measured in units of hertz (Hz).

GHz
Gigahertz, a frequency of 10^9 cycles per second.

GSM
Global System for Mobile Communication or *Groupe Spéciale Mobile.* The international, pan-European operating standard for the new generation of digital cellular mobile communications.

Horn antenna
An antenna consisting of a waveguide section whose cross-sectional area increases toward the open end that is the aperture through which electromagnetic energy is radiated or received.

Incident wave
A wave, travelling through a medium, in a specified direction, which impinges on a discontinuity or a medium of different propagation characteristics.

Ionizing radiation
Any electromagnetic or particulate radiation capable of producing ions directly or indirectly in its passage through matter.

Isotropic
Having the same properties in all directions.

Hertz (Hz)
Unit of frequency. One cycle per second.

Impedance
The overall opposition to an electric current, arising from the combined effect of resistance R and reactance X and measured by the ratio of the EMF to the resulting current.

Intensity
The power crossing unit area normal to the direction of wave propagation. Measured in units of watts per square metre (W/m^2).

Magnetic field intensity (H)
A vector field equal to the magnetic-flux density divided by the permeability. Measured in units of ampere per metre (A/m).

Maximum permissible exposure (MPE)
The RMS and peak electric and magnetic field strengths, their squares or the plane-wave equivalent power densities associated with these fields and the induced and contact currents to which a person may be exposed without harmful effect and with an acceptable safety factor.

Microwave
Electromagnetic radiation of ultra high frequencies between 1GHz and 300GHz.

MHz
Megahertz, a frequency of 10^6 cycles per second.

Modulation.
The process, or result of the process, whereby some characteristic of one wave is varied in accordance with another wave or signal.

Near-field
A region in the field of an antenna, located near the antenna, in which the electric and magnetic fields do not have a substantially plane-wave character, but vary considerably from point to point.

Nonionizing radiation
Any electromagnetic radiation incapable of producing ions directly or indirectly. Microwaves and RF energy are forms of nonionizing radiation.

Permittivity
The properties of a dielectric material or biological tissues, which are frequency dependent.

Phantom
A life-size model of part of the body made of material, which absorbs radiation in a similar way, used in investigations into the character and absorption of a beam of radiation.

Polarization
That property of a radiated electromagnetic wave describing the time-varying direction and amplitude of the electric field vector.

Power.
A physical quantity describing the rate of delivery or transmission of energy.

Power density
Power per unit area normal to the direction of propagation, usually expressed in watts per meter squared (W/m^2)

Planewave
A wave in which the wave fronts are planar. The E and H vectors are uniform in the planes of the wave fronts; and E, H and the direction of propagation (k) are all mutually perpendicular.

Polarisation
Orientation of the incident E- and H-field vectors with respect to the absorbing object.

RAdio Detecting And Ranging (RADAR)
A system that radiates pulsed or frequency-modulated electromagnetic waves and utilizes the reflection of such waves from distant objects to determine their existence or position.

Radiofrequency radiation
Electromagnetic radiation used for telecommunications and found in the electro-magnetic spectrum at wavelengths of 10kHz to 300GHz.

Root mean square (RMS)
A mean calculated as the square root of the arithmetic mean of the squares of a set of values.

Specific absorption rate (SAR)
Time rate of energy absorbed in an incremental mass, divided by that mass. Average SAR in a body is the time rate of the total energy absorbed divided by the total mass of the body. Measured in units of watts per kilogram ($W.kg^{-1}$).

Standing wave
A spatially periodic or repeating field pattern of amplitude maxima and minima that is generated by two equal-wavelength propagating waves traveling in different directions.

Standing wave ratio
The ratio of maximum field strength to minimum field strength along the direction of propagation of two waves traveling in opposite directions on a transmission line.

Thermocouple
A pair of dissimilar conductors so joined at two points that an electromotive force is developed by the thermoelectric effect when the junctions are at different temperatures.

UMTS
Universal Mobile Telecommunication Service.

Waveguide
An enclosed system capable of guiding electromagnetic waves from one place to another. Usually it consists of a hollow metallic tube or a solid dielectric material.

Wavelength.
The distance between two crests of the wave (or between two troughs or other corresponding points). Measured in metres (m).

LIST OF REFERENCE

ADAIR, E.R., KELLEHER, S.A., MACK, G.W. & MOROCCO, T.S. (1998) Thermo-physiological responses of human volunteers during controlled whole-body radio frequency exposure at 450 MHz. *Bioelectromagnetics.* **19:** 232-45

ADAIR, E.R., COBB, B.L., MYLACRAINE, K.S. & KELLEHER, S.A. (1999) Human exposure at two radio frequencies (450 and 2450 MHz): similarities and differences in physiological response. *Bioelectromagnetics.* **Suppl 4:** 12-20.

AFFADHL, Y., WANG, Z., CHEN, X., TATTERSALL, J.E.H. & HOLDEN, S.J. (2002) Numerical Dosimetry of a thin rat hippocampus in a controlled RF exposure system. *XXVIIth General Assembly of the International Union of Radio Science.* **K2.0.6:** p1175.

AGNIR (2003) Health effects from radiofrequency electromagnetic fields. *Documents of the NRPB.* 14(2).

AMARAL, D.G. & WITTER, M.P. (1989) The three-dimensional organization of the hippocampal formation: a review of anatomical data. *Neuroscience.* **31:** 571-591.

ANDERSEN, P., ECCLES, J.C. & LOYNING, Y. (1963) Recurrent inhibition in the hippocampus with the identification of the inhibitory cell and its synapses. *Nature.* **198:** 540-542.

ANDERSEN P., BLISS, V.P. & SKREDE, K.K. (1971) Lamellar organization of hippocampal excitatory pathways. *Experimental Brain Research.* **13:** 222-238.

ANDERSEN, P., SOLENG, A.F. & RAASTAD, M. (2000) The hippocampal lamella hypothesis revisited. *Brain Research Interactive.* BRES19180.

ANDERSON, W.W. & COLLINGRIDGE, G.L. (2001) The LTP program: a data acquisition program for on-line analysis of long-term potentiation and other synaptic events. *Journal of Neuroscience Methods.* **108:** 71-83.

ANANTHAN, J., GOLDBERG, A.L. & VOELLMY, R. (1986) Abnormal proteins serve as Eukaryotic stress signals and trigger the activation of heat shock genes. *Science.* **232:** 522-524.

BALDWIN, P.J. (1996) RF test feasibility study report. Serco Consultancy Division Report 2269/96.

BARNES, C.A., JUNG, M.W., MCNAUGHTON, B.L., KOROL, D.L., ANDREASSON, K. & WORLEY, P.F. (1994) LTP saturation and spatial learning disruption: effects of task variables and saturation levels. *Journal of Neuroscience.* **14:** 5793-5806.

BAWIN, S.M., SHEPPARD, A.R., MAHONEY, M.D. & ADEY, W.R. (1984) Influences of sinusoidal electric fields on excitability in the rat hippocampal slice. *Brain Research.* **323:** 227-237.

BAWIN, S.M., ABU-ASSAL, M.L., SHEPPARD, A.R., MAHONEY, M.D. & ADEY, W.R. (1986a) Long-term effects of sinusoidal extracellular electric fields in penicillin-treated rat hippocampal slices. *Brain Research.* **399:** 194-199.

BAWIN, S.M., SHEPPARD, A.R., MAHONEY, M.D., ABU-ASSAL, M.L. & ADEY, W.R. (1986b) Comparisons between the effects of extracellular direct and sinusoidal currents on excitability in hippocampal slices. *Brain Research.* **326:** 350-354.

BAWIN, S.M., SATMARY, W.M., JONES, R.A., ADEY, W.R. & ZIMMERMAN, G. (1996) Extremely-low-frequency magnetic fields disrupt rhythmic slow activity in rat hippocampal slices. *Bioelectromagnetics.* **17:** 388-395.

BECHTOLD, D.A., RUSH, S.J. & BROWN, I.R. (2000) Localization of the heat-shock protein Hsp70 to the synapse following hyperthermic stress in the brain. *Journal of Neurochemistry.* **74:** 641-646.

BEN ARI, Y., KHAZIPOV, R., LEINEKUGEL, X. CAILLARD, O. & GAIARSA, J.L. (1997) GABAA, NMDA and AMPA receptors; a developmentally regulated 'menage a trois'. *Trends in Neuroscience.* **20:** 523-529.

BERNARD, C. & WHEAL, H.V. (1995a) Expression of EPSP/spike potentiation following low frequency and tetanic stimulation in the CA1 area of the rat hippocampus. *Journal of Neuroscience.* **15:** 6542-6551.

BERNARD, C. & WHEAL, H.V. (1995b) Simultaneous expression of excitatory postsynaptic potential/spike potentiation and excitatory postsynaptic potential/spike depression in the hippocampus. *Neuroscience.* **67:** 73-82.

BEST, N., SUNDSTRÖM, L.E., MITCHELL, J. & WHEAL, H.V. (1996) Pre-exposure to subtoxic levels prevents kainic acid lesions in organotypic hippocampal slice cultures: effects of kainic acid on parvalbumin-immunoreactive neurons and expression of heat shock protein 72 following the induction of tolerance. *European Journal of Neuroscience.* **8:** 1209-1219.

BEVIR, M.K. (1999) Power deposition in tissue exposed to electromagnetic radiation. **PHV-R99-01:** 1-16. Poynting High Voltage Ltd.

BLACKSTAD, T.W. (1956) Commissural connections of the hippocampal region in the rat, with special reference to their mode of termination. *Journal of Comparative Neurology.* **105:** 417-537.

BLACKSTAD, T.W. (1958) On the termination of some afferents to the hippocampus and fascia dentate. An experimental study in the rat. *Acta. Anat.* **35:** 202-214.

BLACKSTAD, T.W., BRINK, K., HEM, J. & JEUNE, B. (1970) Distribution of hippocampal mossy fibres in the rat. An experimental study with silver impregnation methods. *Journal of Comparative Neurology.* **138:** 433-450.

BLISS, T.V.P. & LOMO, T. (1973) Long-lasting potentiation of synaptic transmission in the dentate area of the unanaesthetized rabbit following stimulation of the perforant path. *Journal of Physiology.* **232:** 331-356

BLISS, T.V. & COLLINGRIDGE, G.L. (1993) A synaptic model of memory: long-term potentiation in the hippocampus. *Nature.* **361:** 31-39.

BUHL, D.L., HARRIS, K.D., HORMUZDI, S.G., MOYNER, H. & BUZSAKI, G. (2003) Selective impairment of hippocampal gamma oscillations in connexin-36 knock-out mouse *in vivo*. *Journal of Neuroscience.* **23(3):** 1013-1018.

BURKHARDT, M. SPINELLI, Y. & KUSTER, N. (1997) Exposure setup to test effects of wireless communications systems on the CNS. *Health Physics.* **73:** 770-778.

BURWELL, R.D., WITTER, M.P. & AMARAL., D.G. (1995) Perirhinal and postrhinal cortices of the rat: a review of the neuroanatomical literature and comparison with findings from the monkey brain. *Hippocampus.* **5:** 390-408.

BUZSAKI, G., HAAS, H.L. & ANDERSON, E.G. (1987) Long-term potentiation induced by physiologically relevant stimulus patterns. *Brain Research.* **435:** 331-333.

CARLEN, P.L., SKINNER, F., ZHANG, L., NAUS, C., KUSHNIR, M. & VELAZQUEZ, J.L.P. (2000) The role of gap junctions in seizures. *Brain Research Reviews.* **32:** 235-241.

CHAPMAN, C.A., PEREZ, Y. & LACAILLE, J.C. (1998) Effects of GABA(A) inhibition on the expression of long-term potentiation in CA1 pyramidal cells are dependent on tetanization parameters. *Hippocampus.* **8:** 289-298.

CHAVEZ-NORIEGA, L.E. & BLISS, T.V.P. (1991) Persistent modulation of neural excitability in the hippocampus: the role of EPSP-spike (E-S) potentiation. In: Glutamate, cell death and memory. (P. Ascher Ed) Springer-Verlag, Berlin. p 37-44.

CHOU, C.K., BASSEN, H., OSEPCHUK, J., BALZANO, Q., PETERSEN, R., MELTZ, M., CLEVELAND, R., LIN, J.C. & HEYNICK, L. (1996) Radio frequency electromagnetic exposure: tutorial review on experimental dosimetry. *Bioelectromagnetics.* **17:** 195-208.

CHOU, C.K., CHAN, K.W., MCDOUGALL, J.A. & GUY, A.W. (1999) Development of a rat head exposure system for simulating human exposure to RF fields from handheld wireless telephones. *Bioelectromagnetics.* **20:** 75-92.

Pages 179 - 187 are missing from volume

MINSON, J.B., LLEWELLYN-SMITH, I.J., ARNOLDA, L.F., PILOWSKY, P.M., OLIVER, J.R. & CHALMERS, J.P. (1994) Disinhibition of the rostral ventral medulla increases blood pressure and Fos expression in bulbospinal neurons. *Brain Research.* **646:** 44-52.

MOREHOUSE, C.A. & OWEN, R.D. (2000) Exposure to low-frequency electro-magnetic fields does not alter HSP70 expression or HSF-HSE binding in HL60 cells. *Radiation Research.* **153:** 658-662.

MORGAN, J.I., COHEN, D.R., HEMPSTEAD, J.L. & CURRAN, T. (1987) Mapping patterns of c-fos expression in the central nervous system after seizure. *Science.* **237:** 192-197.

MORGAN, S.L. & TEYLER, T.J. (1999) VDCCs and NMDARs underlie two forms of LTP in CA1 hippocampus in vivo. *Journal of Neurophysiology.* **82:** 736-740.

MORRIS, R.G.M., ANDERSON, E., LYNCH, G.S. & BAUDRY, M. (1986) Selective imparement of learning and blockade of long-term potentiation by an N-Methyl-D-aspartate receptor antagonist, AP5. *Nature.* **319:** 774-776.

MORRIS, R.G.M. & DAVIS, M. (1994) The role of NMDA receptors in learning and memory. In: The NMDA receptor. Eds: Collingridge, G.L. & Watkins, J.C. Oxford University Press, Oxford. UK 340-375.

MORRIS, R.G. & FREY, U. (1997) Hippocampal synaptic plasticity: role in spatial learning or the automated recording of attended experience? *Philosophical Transactions of the Royal Society of London.* **B352:** 1489-1503.

MOROS, E.G., STRAUBE, W.L. & PICKARD, W.F. (1999) Compact shielded exposure system for the simultaneous long-term UHF irradiation of forty small mammals. II. Dosimetry. *Bioelectromagnetics.* **20:** 81-93.

MOSER, E.I. (1995) Learning related changes in hippocampal field potentials. *Behavioural Brain Research.* **71:** 11-18.

MOULDER, J.E., ERDREICH, L.S., MALYAPA, R.S., MERRITT, J., PICKARD, W.F. & VIJAYALAXMI. (1999) Cell phones and cancer: what is the evidence for a connection? *Radiation Research.* **151:** 513-531.

NADLER, J.V., PERRY, B.W. & COTMAN, C.W. (1978) Intraventricular kainic acid preferentially destroys hippocampal pyramidal cells. Nature. 271: 676-677.

NOLTE, C.M., PITTMAN, D.W., KALEVITCH, B., HENDERSON, R. & SMITH, J.C. (1998) Magnetic field conditioned taste aversion in rats. *Physiol. Behav.* **63:** 683-688.

NOWAK, T.S., BOND, U. & SCHLESINGER, M.J. (1990) Heat shock RNA levels in brain and other tissues after hyperthermia and transient ischemia. *Journal of Neurochemistry.* **54:** 451-458.

NOWAK, T.S. (1993) Synthesis of heat shock / stress proteins during cellular injury. *Annals of the New York Academy of Science.* **679:** 142-156.

NRPB. (1993) Restrictions on human exposure to static and time-varying electromagnetic fields. *Documents of the NRPB* **4:** 7-63.

OGURI, T., TAKAHATA, I., KATSUTA, K., NOMURA, E., HIDAKA, M. & INAGAKI, N. (2002) Proteome analysis of rat hippocampal neurons by multiple large gel two-dimensional electrophoresis. *Proteomics.* **2:** 666-672.

PAIS, I., HORMUZDI, S.G., MOYNER, H., TRAUB, R.D., WOOD, I.C., BUHL, E.H., WHITTINGTON, M.A. & LEBEAU, E.N. (2002) Sharp wave-like activity in the hippocampus *in vitro* in mice lacking the gap junction protein connexin 36. *Journal of Neurophysiology.* **89:** 2046-2054.

PAKHOMOV, A.G., MATHUR, S.P., DOYLE, J., STUCK, B.E., KIEL, J.L. & MURPHY, M.R. (2000a) Comparative effects of extremely high power microwave pulses and a brief CW irradiation on pacemaker function in isolated frog heart slices. *Bioelectromagnetics.* **21:** 245-254.

PAKHOMOV, A.G., MATHUR, S.P., AKYEL, Y., KIEL, J.L. & MURPHY, M.R. (2000b) High-resolution microwave dosimetry in lossy media. In: Radio Frequency Radiation Dosimetry. (B.J. Klauenberg and D. Miklavcic eds.), Kluwer Academic Publishers, Netherlands. p 187-197.

PAKHOMOV, A.G., MATHUR, S.P.& MURPHY, M.R. (2003) High-resolution temperature and SAR measurement using different sensors. *25th Bioelectromagnetics Society Conference Abstracts (In press).*

PENNES, H.H. (1948) Analysis of tissue and arterial blood temperature in the resting human forearm. *Journal of Applied Physiology.* **1:** 93-122.

PHILIPPOVA, T.M., NOVOSELOV, V.I. & ALEKSEEV, S.I. (1994) Influence of microwaves on different types of receptors and the role of peroxidation of lipids on receptor-protein shedding. *Bioelectromagnetics.* **15:** 183-192.

PIPKIN, J.L., HINSON, W.G., YOUNG, J.F., ROWLAND, K.L., SHADDOCK, J.G., TOLLESON, W.H., DUFFY, P.H. & CASCIANO, D.A. (1999) Induction of stress proteins by electromagnetic fields in cultured HL-60 cells. *Bioelectromagnetics.* **20:** 347-357.

PLANAS, A.M., SORIANO, M.A., ESTRADA, A., SANZ, O., MARTIN, F. & FERRER, I. (1997) The heat shock stress response after brain lesions: induction of 72 kDa heat shock protein (cell types involved, axonal transport, transcriptional regulation) and protein synthesis inhibition. *Progress in Neurobiology.* **51:** 607-636.

PREECE, A.W., IWI, G., DAVIES-SMITH, A., WESNES, K., BUTLER, S., LIM, E. & VAREY, A. (1999) Effect of a 915-MHz simulated mobile phone signal on cognitive function in man. *International Journal of Radiation Biology.* **75:** 447- 456.

PRINGLE, A.K., IANOTTI, F., WILDE, G.J.C., CHAD, J.E., SEELEY, P.J. & SUNDSTRÖM, L.E. (1997) Neuroprotection by both NMDA and non-NMDA receptor antagonists in *in vitro* ischemia. *Brain Research.* **775:** 36-46.

PRINGLE, A.K., SELF, J., ESHAK, M. & IANOTTI, F. (2000) Reducing conditions significantly attenuate the neuroprotective efficacy of competitive, but not other NMDA receptor antagonists *in vitro*. *European Journal of Neuroscience*. **12:** 3833-3842.

RAISMAN, G., COWAN, W.M., & POWELL, T.P.S. (1965) The extrinsic afferent, commissural and association fibres of the hippocampus. *Brain*. **88:** 963-997.

RAMÓN Y CAJAL, S. (1893) The structure of Ammon's horn. Translated by L.M. Kraft (1968). Published by C.C. Thomas, Springfield, Illinois.

RAMÓN Y CAJAL, S. (1911) Histologie du systeme nerveux de l'Homme et des Vertebres. Volume II. Translated by L. Azoulay. Paris, Maloine.

RANG, H.P., DALE, M.M. & RITTER, J.M. (1999) Amino acid transmitters. In: Pharmacology. Fourth Edition. Churchill Livingstone, Edinburgh. p 471-482.

REPACHOLI, M.H. (1998) Low-level exposure to radiofrequency electromagnetic fields: health effects and research needs. *Bioelectromagnetics*. **19:** 1-19.

REPACHOLI, M.H. & GREENBAUM, B. (1999) Interaction of static and extremely low frequency electric and magnetic fields with living systems: health effects and research needs. *Bioelectromagnetics*. **20:** 133-160.

REPACHOLI, M.H. (2001) Health risks from the use of mobile phones. *Toxicology Letters*. **120:** 323-331.

RIBAK, C.E. & SERESS, L. (1983) Five types of basket cell in the hippocampal dentate gyrus: a combined Golgi and electron microscope study. *Journal of Neurocytology*. **12:** 577-597.

RIBAK C.E., SERESS, L. & AMARAL, D.G. (1985) The development, ultrastructure and synaptic connections of the mossy cells of the dentate gyrus. *Journal of Neurocytology*. **14:** 835-857.

ROSS, F.M. GWYN, P., SPANSWICK, D. & DAVIES, S.N. (2000) Carbenoxolone depresses spontaneous epileptiform activity in the CA1 region of rat hippocampal slices. *Neuroscience.* **100:** 789-796

ROYAL SOCIETY OF CANADA (1999) A review of the potential health risks of radiofrequency fields from wireless telecommunications devices. Expert panel report prepared by the Royal Society of Canada for Health Canada. Ottawa, Royal Society of Canada, RSC.EPR 99-1.

ROZENTAL, R., GIAUME, C. & SPRAY, D.C. (2000) Gap junctions in the nervous system. *Brain Research Reviews.* **32:** 11-15.

RUDICK, C.N. & WOOLLEY, C.S. (2000) Estradiol induces a phasic response in the hippocampal CA1 and CA3 regions of adult female rats. *Hippocampus.* **10:** 274-283.

SADGROVE, M.P. (1999) The effects of temperature in an organotypic rat hippocampal slice culture model of ischaemia. M.Sc. Thesis. University of Southampton.

SAMARAS, T., REGLI, P. & KUSTER, N. (2000) Electromagnetic and heat transfer computations for non-ionising radiation dosimetry. *Physics in Medicine and Biology.* **45:** 2233-2246.

SANZ, O., ESTRADA, A., FERRER, I. & PLANAS, A.M. (1997) Differential cellular distribution and dynamics of HSP70, cyclooxygenase-2 and c-FOS in the rat brain after transient focal ischaemia or kainic acid. *Neuroscience.* **80:** 221-232.

SCHARFMAN, H.E., KUNKEL, D.D. & SCHWARTZKROIN, P.A. (1990) Synaptic connections of dentate granule cells and hilar neurons: Results of paired intracellular recordings and intracellular horseradish peroxidase injections. *Neuroscience.* **37:** 693-707.

SEAMAN, R.L. & WACHTEL, H. (1978) Slow and rapid responses to CW and pulsed microwave radiation by individual Aplysia pacemakers. *Journal of Microwave Power and Electromagnetic Energy.* **13:** 77-86.

SHARP, F.R., MASSA, S.M. & SWANSON, R.A. (1999) Heat-shock protein protection. *Trends in Neurological Sciences.* **22:** 97-99.

SIENKIEWICZ, Z. (1998) Biological effects of electromagnetic fields and radiation. *Journal of Radiological Protection.* **18:** 185-193.

SIENKIEWICZ, Z.J., HAYLOCK, R.G. & SAUNDERS, R.D. (1998) Deficits in spatial learning after exposure to a 50 Hz magnetic field. *Bioelectromagnetics.* **19:** 79-84.

SKUTELLA, T. & NITSCH, R. (2001) New molecules for hippocampal development. *Trends in Neuroscience.* **24:** 107-113.

SLOVITIER, R.S. & LOWENSTEIN, D.H. (1992) Heat shock protein expression in vulnerable cells of the rat hippocampus as an indicator of excitation-induced neuronal stress. *Journal of Neuroscience.* **12:** 3003-3009.

SMYTHE, J.W. & COSTALL, B. (2003) Mobile phone use facilitates memory in male, but not female, subjects. *Neuroreport.* **14(2):** 243-246.

SNYDER, D.J., JAHNG, J.W., SMITH, J.C. & HOUPT, T.A. (2000) c-Fos induction in visceral and vestibular nuclei of the rat brain stem by a 9.4 T magnetic field. *Neuroreport.* **11:** 2681-2685.

STEVENS, C.F. (1998) A million dollar question: does LTP = memory? *Neuron* **20:** 1-2.

STOPPINI, L., BUCHS, P-A. & MULLER, D. (1991) A simple method for organotypic cultures of nervous tissue. *Journal of Neuroscience Methods.* **37:** 173-182.

STUCHLY, M.A. (1979) Interaction of radiofrequency and microwave radiation with living systems. A review of mechanisms. *Radiat. Environ. Biophys.* **16:** 1-14.

SWICORD, M., MORRISSEY, J., ZAKHARIA, D., BALLEN, M. & BALZANO, Q. (1999) Dosimetry in mice exposed to 1.6GHz microwaves in a carrousel irradiator. *Bioelectromagnetics.* **20:** 42-47.

TATTERSALL, J.E.H., BALDWIN, P.J., WOOD, S.J. & CRISP, G. (1996) A novel system for producing controlled exposures of brain slice preparations to radiofrequency radiation during electrophysiological recording. *Journal of Physiology.* **495:** 6P.

TATTERSALL, J.E.H. (1999) A study on the effects of 10.75GHz microwave radiation on nicotinic acetylcholine receptor ion channels. In: Electricity and Magnetism in Biology and Medicine. (F. Bersani ed.) Plenum, New York. p 577-580.

TATTERSALL, J.E.H., SCOTT, I.R., WOOD, S.J., NETTELL, J.J., BEVIR, M. K., WANG, Z., SOMASIRI, N.P. & CHEN, X. (2001) Effects of low intensity radiofrequency electromagnetic fields on electrical activity in rat hippocampal slices. *Brain Research.* **904:** 43-55.

TAY, R.Y.S., BALZANO, Q. & KUSTER, N. (1998). Dipole configurations with strongly improved radiation efficiency for hand held transceivers. *IEEE Transactions on Antennas and Propagation. 46:* 798-806.

TAYLOR, H.C., BURL, M. & HAND, J.W. (1997) Experimental verification of numerically predicted electric field distributions produced by a radiofrequency coil. *Physics in Medicine and Biology.* **42:** 1395-1402.

TEYLER, T.J. & DiSCENNA, P. (1987) Long-term potentiation. *Annual Review of Neuroscience.* **10:** 131-161.

TRAUB, R.D. JEFFERYS, J.G.R. & WHITTINGTON, M.A. (1996) Neuronal networks for induced '40 Hz' rhythms. *Trends in Neuroscience.* **19:** 202-208.

TRAUB, R.D., SPRUSTON, N., SOLTESZ, I., KONNERTH, A., WHITTINGTON, M.A. & JEFFERYS, J.G.R. (1998) Gamma-frequency oscillations: a neuronal population phenomenon, regulated by synaptic and intrinsic cellular processes, and inducing synaptic plasticity. *Progress in Neurobiology.* **55:** 563-575.

VALBERG, P.A. KAVET, R. & RAFFERTY, C.N. (1997) Can low-level 50/60 Hz electric and magnetic fields cause biological effects? *Radiation Research.* **148:** 2-21.

VAN LEEUWEN, G.M., LAGENDIJK, J.J., VAN LEERSUM, B.J., ZWAMBORN, A.P., HORNSLETH, S.N. & KOTTE, A.N. (1999) Calculation of change in brain temperatures due to exposure to a mobile phone. *Physics in Medicine and Biology.* **44:** 2367-2379.

VIZI, E.S. & KISS, J.P. (1998) Neurochemistry and pharmacology of the major hippocampal transmitter systems: synaptic and nonsynaptic interactions. *Hippocampus.* **8:** 566-607.

WAINWRIGHT, P. (2000) Thermal effects of radiation from cellular telephones. *Physics in Medicine and Biology.* **45:** 2363-2372.

WALTERS, T.J., MASON, P.A., SHERRY, C.J., STEFFEN, C. & MERRITT, J.H. (1995) No detectable bioeffects following acute exposure to high peak power ultra-wide band electromagnetic radiation in rats. (Abstract) *Aviat. Space Environm. Med.* **66:** 562-567.

WALTERS, T.J., RYAN, K.L., TEHRANY, M.R., JONES, M.B., PAULUS, L.A. & MASON, P.A. (1998) HSP70 expression in the CNS in response to exercise and heat stress in rats. *Journal of Applied Physiology.* **84:** 1269-1277.

WALTERS, T.J., MASON, P. .A., RYAN, K.L., NELSON, D.A. & HURT, W.D. (2000) A comparison of SAR values determined empirically and by FD-TD modelling. In: Radio Frequency Radiation Dosimetry. (B.J. Klauenberg and D. Miklavcic eds.) Kluwer Academic Publishers, Netherlands. p 207-216.

WALTERS, T.J., RYAN, K.L. & MASON, P.A. (2001) Regional distribution of HSP70 in the CNS of young and old food-restricted rats following hyperthermia. *Brain Research Bulletins.* **55:** 367-374.

WANG, Z., SOMASIRI, N.P. & CHEN, X. (2000) Numerical Modelling of TEM Cell. **R210-00:** 4-27. Microwave Consultants Ltd.

WANG, Z., SOMASIRI, N.P., CHEN, X., BEVIR, M.K., HOLDEN, S.J. & TATTERSALL, J.E.H. (2001) Calculation of specific absorption rates in slices of rat hippocampus exposed to 700MHz radiofrequency fields in a waveguide. *Biolectromagnetics Society Abstracts.* **23:** 193.

WANG, Z., SOMASIRI, N.P., CHEN, X. *et al* (2001) Numerical bioelectromagnetics Dosimetry in a stripline RF exposure system. In: *Proceedings of the European Microwave Conference*. London.

WIERASZKO, A. (2000) Dantrolene modulates the influence of steady magnetic fields on hippocampal evoked potentials *in vitro. Bioelectromagnetics.* **21:** 175-182.

WHEAL, H.V., BERNARD, C., CHAD, J.E. & CANNON, R.C. (1998) Pro-epileptic changes in synaptic function can be accompanied by pro-epileptic changes in neuronal excitability. *Trends in Neurological Sciences*. **21:** 167-174.

WILDE, G.J.C. (1997) An investigation into the role of tumour necrosis factor-a in ischaemic neuronal damage in vitro. Ph.D. Thesis. University of Southampton.

WITTER, M.P. (1993) Organization of the entorhinal-hippocampal system: a review of current anatomical data. *Hippocampus.* **3:** 33-44.

WITTER, M.P., WOUTERLOOD, F.G., NABER, P.A. & VAN HAEFTEN, T. (2000) Anatomical organization of the parahippocampal-hippocampal network. *Annals of the New York Academy of Science*. **911:** 1-24.

ZHOU, Q., ABE, H. & NOWAK, T.S. Jr. (1995) Immunocytochemical and in situ hybridisation approaches to the optimisation of brain slice preparations. *Journal of Neuroscience Methods*. **59:** 85-92.